

VOLUME 80

APRIL 22, 1976

NUMBER 9

JPCHAx

THE JOURNAL OF
PHYSICAL
CHEMISTRY



PUBLISHED BIWEEKLY BY THE AMERICAN CHEMICAL SOCIETY



THE JOURNAL OF PHYSICAL CHEMISTRY

BRYCE CRAWFORD, Jr., *Editor*
STEPHEN PRAGER, *Associate Editor*
ROBERT W. CARR, Jr., **FREDERIC A. VAN-CATLEDGE**, *Assistant Editors*

EDITORIAL BOARD: C. A. ANGELL (1973-1977), F. C. ANSON (1974-1978), V. A. BLOOMFIELD (1974-1978), J. R. BOLTON (1976-1980), L. M. DORFMAN (1974-1978), H. L. FRIEDMAN (1975-1979), H. L. FRISCH (1976-1980), W. A. GODDARD (1976-1980), E. J. HART (1975-1979), W. J. KAUFMANN (1974-1978), R. L. KAY (1972-1976), D. W. McCLURE (1974-1978), R. M. NOYES (1973-1977), W. B. PERSON (1976-1980), J. C. POLANYI (1976-1980), S. A. RICE (1976-1980), F. S. ROWLAND (1973-1977), R. L. SCOTT (1973-1977), W. A. STEELE (1976-1980), J. B. STOTHERS (1974-1978), W. A. ZISMAN (1972-1976)

Published by the
AMERICAN CHEMICAL SOCIETY
BOOKS AND JOURNALS DIVISION
D. H. Michael Bowen, Director

Editorial Department: Charles R. Bertsch,
Head; Marianne C. Brogan, Associate
Head; Celia B. McFarland, Joseph E.
Yurvati, Assistant Editors

Graphics and Production Department:
Bacil Guiley, Head

Research and Development Department:
Seldon W. Terrant, Head

Advertising Office: Centcom, Ltd., 50 W.
State St., Westport, Conn. 06880.

© Copyright, 1976, by the American
Chemical Society. No part of this publica-
tion may be reproduced in any form with-
out permission in writing from the Ameri-
can Chemical Society.

Published biweekly by the American
Chemical Society at 20th and Northamp-
ton Sts., Easton, Pennsylvania 18042. Sec-
ond class postage paid at Washington, D.C.
and at additional mailing offices.

Editorial Information

Instructions for authors are printed in
the first issue of each volume. Please con-
form to these instructions when submitting
manuscripts.

Manuscripts for publication should be
submitted to *The Journal of Physical
Chemistry*, Department of Chemistry, Uni-
versity of Minnesota, Minneapolis, Minn.
55455. Correspondence regarding **accepted
papers and proofs** should be directed to
the Editorial Department at the ACS East-
on address.

Page charges of \$60.00 per page are as-
sessed for papers published in this journal.
Ability to pay does not affect acceptance or
scheduling of papers.

Bulk reprints or photocopies of indi-
vidual articles are available. For informa-
tion write to Business Operations, Books
and Journals Division at the ACS Wash-
ington address.

Requests for **permission to reprint**
should be directed to Permissions, Books
and Journals Division at the ACS Wash-
ington address. The American Chemical
Society and its Editors assume no responsi-
bility for the statements and opinions ad-
vanced by contributors.

Subscription and Business Information

1976 Subscription rates—including sur-
face postage

	U.S.	PUAS	Canada, Foreign
Member	\$24.00	\$29.75	\$30.25
Nonmember	96.00	101.75	102.25
Supplementary material	15.00	19.00	20.00

Air mail and air freight rates are avail-
able from Membership & Subscription Ser-
vices, at the ACS Columbus address.

New and renewal subscriptions
should be sent with payment to the Office
of the Controller at the ACS Washington
address. **Changes of address** must include
both old and new addresses with ZIP code
and a recent mailing label. Send all address
changes to the ACS Columbus address. Please
allow six weeks for change to become effec-
tive. **Claims** for missing numbers
will not be allowed if loss was due to
failure of notice of change of address to be
received in the time specified; if claim is

dated (a) North America—more than 90
days beyond issue date, (b) all other for-
eign—more than 1 year beyond issue date;
or if the reason given is "missing from
files". Hard copy claims are handled at the
ACS Columbus address.

Microfiche subscriptions are available
at the same rates but are mailed first class
to U.S. subscribers, air mail to the rest of
the world. Direct all inquiries to Business
Operations, Books and Journals Division,
at the ACS Washington address or call
(202) 872-4444. **Single issues** in hard copy
and/or microfiche are available from Spe-
cial Issues Sales at the ACS Washington
address. Current year \$4.75. Back issue
rates available from Special Issues Sales.
Back volumes are available in hard copy
and/or microform. Write to Special Issues
Sales at the ACS Washington address for
further information. **Microfilm** editions of
ACS periodical publications are available
from volume 1 to the present. For further
information, contact Special Issues Sales at
the ACS Washington address. **Supplemen-
tary material** must be ordered directly
from Business Operations, Books and Jour-
nals Division, at the ACS Washington ad-
dress.

	U.S.	PUAS, Canada	Other Foreign
Microfiche			
Photocopy	\$2.50	\$3.00	\$3.50
1-7 pages	4.00	5.50	7.00
8-20 pages	5.00	6.50	8.00

Orders over 20 pages are available only on
microfiche, 4 × 6 in., 24X, negative, silver
halide. Orders must state photocopy or mi-
crofiche if both are available. Full biblio-
graphic citation including names of all au-
thors and prepayment are required. Prices
are subject to change.

American Chemical Society
1155 16th Street, N.W.
Washington, D.C. 20036
(202) 872-4600

Member & Subscription Services
American Chemical Society
P.O. Box 3337
Columbus, Ohio 43210
(614) 421-7230

Editorial Department
American Chemical Society
20th and Northampton Sts.
Easton, Pennsylvania 18042
(215) 258-9111

THE JOURNAL OF
PHYSICAL CHEMISTRY

Volume 80, Number 9 April 22, 1976

JPCHAx 80(9) 905-1030 (1976)

ISSN 0022-3654

Theory of the Kinetics of Micellar Equilibria and Quantitative Interpretation of Chemical Relaxation Studies of Micellar Solutions of Ionic Surfactants E. A. G. Aniansson, S. N. Wall, M. Almgren, H. Hoffmann,* J. Kielmann, W. Ulbricht, R. Zana,* J. Lang, and C. Tondre	905
Relative Roles of Ensemble Constraints vs. Cross Sections in Hydrogen Dissociation S. H. Bauer,* D. Hilden, and Peter Jeffers	922
Kinetics of the Thermal Decomposition of Bis(trifluoromethyl) Peroxide B. Descamps and W. Forst*	933
Pulse Radiolytic Investigations of Some Peroxyhydroxycyclohexadienyl Radicals O. I. Mičić* and M. T. Nenadović	940
Homologous <i>trans</i> -4-Ethoxy-4'-cycloalkanecarboxyloxyazobenzenes. Calorimetry Craig L. Hillemann and Gerald R. Van Hecke*	944
Substitutional Photochemistry of Some Monoazido, Thiocyanato, and Isothiocyanato Complexes of Cobalt(III) and Rhodium(III). Some Quandries and Alternatives for Models of Excited State Reactivity John F. Endicott* and Guillermo J. Ferraudi	949 ■
Application of the Polanyi Adsorption Potential Theory to Adsorption from Solution on Activated Carbon. VII. Competitive Adsorption of Solids from Water Solution Michael R. Rosene and Milton Manes*	953 ■
Effect of Chain Tacticity on Dye Binding to Polyelectrolytes V. Vitagliano,* L. Costantino, and R. Sartorio	959
Reaction Kinetics and Differential Thermal Analysis Ralph T. Yang* and Meyer Steinberg	965
Fluorescence Quantum Yield Determinations. 9,10-Diphenylanthracene as a Reference Standard in Different Solvents John V. Morris, Mary A. Mahaney, and J. Robert Huber*	969
Inter- and Intramolecular Quenching of Indole Fluorescence by Carbonyl Compounds Robert W. Ricci* and Joseph M. Nesta	974
Electronic Spectra of the Anion Radicals of Heterocyclic Amine <i>N</i> -Oxides and Related Substances Kiyoshi Ezumi, Tanekazu Kubota,* Hiroshi Miyazaki, and Masumi Yamakawa	980
2,3,7,8-Tetramethoxythianthrene. A Novel Ground State Triplet Dication, the Neutral Photogenerated Triplet, and the Radical Cation Ira B. Goldberg,* Harry R. Crowe, George S. Wilson, and Richard S. Glass	988
A Unified Theory for Molecular Charge Transfer Ying-Nan Chiu	992
Theoretical Derivation of Partition Coefficient from Solubility Parameters Shalom Srebrenik* and Sasson Cohen	996
The Influence of Solute Size on the Thermodynamic Parameter of Transfer of a Nonpolar Hydrophobic Solute from Gas to Water or from Light to Heavy Water M. Lucas* and R. Bury	999

Viscosities and Conductivities of the Liquid Salt Triethyl- <i>n</i> -hexylammonium Triethyl- <i>n</i> -hexylboride and Its Benzene Solutions	Warren T. Ford* and Donald J. Hart	1002
Effect of Association Complexes on the Glass Transition in Organic Halide Mixtures	Arnold V. Lesikar	1005
Reactions of Cation Radicals of EE Systems. IV. The Kinetics and Mechanism of the Homogeneous and the Electrocatalyzed Reaction of the Cation Radical of 9,10-Diphenylanthracene with Hydrogen Sulfide	John F. Evans and Henry N. Blount*	1011
Emission Spectra and Chemical Reactions of Fluorinated Benzene Derivatives in a High-Frequency Discharge	R. Gilbert and A. Théorêt*	1017
Dynamic Nuclear Magnetic Resonance in the Gas Phase. The Torsional Barrier in <i>N,N</i> -Dimethylthioformamide	Torbjörn Drakenberg	1023
Kinetics of the Thermal Decomposition of Tetrakis(dimethylamino)ethylene in the Vapor Phase	Chas. E. Waring* and Raymond A. Berard	1025

COMMUNICATIONS TO THE EDITOR

Evidence for Superficial Reduction of NH ₄ Y Zeolite Silicon upon Pyridine Adsorption at 150 °C	C. Defosse, P. Canesson,* and B. Delmon	1028
---	--	------

■ Supplementary material for this paper is available separately (consult the masthead page for ordering information); it will also appear following the paper in the microfilm edition of this journal.

* In papers with more than one author, the asterisk indicates the name of the author to whom inquiries about the paper should be addressed.

AUTHOR INDEX

Almgren, M., 905	Endicott, J. F., 949	Kielmann, J., 905	Sartorio, R., 959
Aniansson, E. A. G., 905	Evans, J. F., 1011	Kubota, T., 980	Srebrenik, S., 996
Bauer, S. H., 922	Ezumi, K., 980	Lang, J., 905	Steinberg, M., 965
Berard, R. A., 1025	Ferraudi, G. J., 949	Lesikar, A. V., 1005	Théorêt, A., 1017
Blount, H. N., 1011	Ford, W. T., 1002	Lucas, M., 999	Tondre, C., 905
Bury, R., 999	Forst, W., 933	Mahaney, M. A., 969	Ulbricht, W., 905
Canesson, P., 1028	Gilbert, R., 1017	Manes, M., 953	Van Hecke, G. R., 944
Chiu, Y.-N., 992	Glass, R. S., 988	Mičić, O. I., 940	Vitagliano, V., 959
Cohen, S., 996	Goldberg, I. B., 988	Miyazaki, H., 980	Wall, S. N., 905
Costantino, L., 959	Hart, D. J., 1002	Morris, J. V., 969	Waring, C. E., 1025
Crowe, H. R., 988	Hilden, D., 922	Nenadović, M. T., 940	Wilson, G. S., 988
Defosse, C., 1028	Hillemann, C. L., 944	Nesta, J. M., 974	Yamakawa, M., 980
Delmon, B., 1028	Hoffmann, H., 905	Ricci, R. W., 974	Yang, R. T., 965
Descamps, B., 933	Huber, J. R., 969	Rosene, M. R., 953	Zana, R., 905
Drakenberg, T., 1023	Jeffers, P., 922		

THE JOURNAL OF PHYSICAL CHEMISTRY

Registered in U. S. Patent Office © Copyright, 1976, by the American Chemical Society

VOLUME 80, NUMBER 9 APRIL 22, 1976

Theory of the Kinetics of Micellar Equilibria and Quantitative Interpretation of Chemical Relaxation Studies of Micellar Solutions of Ionic Surfactants

E. A. G. Aniansson, S. N. Wall, M. Almgren,

Department of Chemistry, University of Gothenburg, Fack, S-40220 Gothenburg, Sweden

H. Hoffmann,* I. Kielmann, W. Ulbricht,

Institut für Physical Chemistry, University of Erlangen-Nuremberg, Erlangen, West Germany

R. Zana,* J. Lang, and C. Tondre

C.R.M.-C.N.R.S., 67083 Strasbourg, Cedex, France (Received August 15, 1975)

Publication costs assisted by Universität Bayreuth

New developments of the theory of micellar kinetics are reported together with new experimental results obtained in the course of chemical relaxations (T-jump, p-jump, and shock tube) studies of micellar solutions of ionic surfactants. These results as well as those obtained in previous studies are quantitatively interpreted in terms of this theory. Several pieces of information thus far not available on micellar solutions have been obtained: (1) the rate constants k^+ and k^- for the association/dissociation reactions of one amphiphilic ion to/from micelles. The association reaction is very close to being diffusion controlled. The variation of the dissociation rate constant with the alkyl chain length is in quantitative agreement with what is expected from theory; (2) the width of the distribution curve of stable micelles is found to increase with chain length but the micelle polydispersity is small and decreases for increasing chain length; (3) an approximate value of the average number of amphiphilic ions in the micellar species at the minimum of the distribution curve; (4) the enthalpy and entropy changes associated with the incorporation of one amphiphilic ion into the most stable micelle and into the aggregate at the minimum of the distribution curve. The enthalpy changes for these two processes are of opposite signs. This explains why the overall heat of micellization is very small.

I. Introduction

In a recent report¹ was presented the first experimental evidence of the existence of two relaxation processes related to micellar equilibria in solution of ionic detergents, not taking into account the additional relaxation process detected by means of ultrasonic absorption in more concentrated solutions. These processes are characterized by the relaxation times τ_1 and τ_2 differing by as much as two to three orders of magnitude ($\tau_1 \ll \tau_2$). The fast process (τ_1), which has been detected by means of ultrasonic absorption, T-jump, and/or shock tube method, has been assigned to the association-dissociation (exchange) equilibrium of amphiphilic ion to/from micelles¹ (reaction 1 in ref 1). A large consensus has now been reached among workers concerning this attribution.²⁻⁶ The slow process (τ_2), which has

been detected by p-jump and/or T-jump, is attributed to the micellization-dissolution equilibrium¹ (reaction 2 in ref 1). This interpretation is in line with that given by several authors,³⁻⁵ but at variance with that recently postulated by Coleen.⁶ The reasons which clearly indicate that Coleen's interpretation must be discarded are given in the note following ref 6.

The dependence of the two relaxation processes on ionic strength, detergent chain length, and concentration was recently¹ accounted for on a purely qualitative basis. At about the same time, but without knowing about the new experimental evidence, Aniansson and Wall^{5a} have used a new approach from which they were able to derive analytical expressions of relaxation times characterizing the two processes. This approach is based on the analogy between

the rate equations for the series of bimolecular equilibria by which micelles are formed or dissolved, and heat conduction, or more generally, diffusion processes. It was pointed out that as far as kinetics are concerned, the micellar solution can be viewed as a system of "two large metal blocks" connected by a thin "wire", one "block" corresponding to the monomers and oligomers, the other to micelles of the most probable size, and the "wire" corresponding to the region in between. After an initial, short period of adjustment (fast relaxation process) the main process would be a pseudo-stationary flow from one "block" to the other, through the "wire" (slow relaxation process). Assuming that the aggregation number s can be dealt with as a continuous variable, the expressions for the relaxation times τ_1 and τ_2 for the fast and slow process, respectively, could be obtained. These calculations^{5a} first yielded an expression of τ_1 independent of the detergent concentration, in clear disagreement with the experimental results (see ref 1 and references therein). Since then a correction and improvement of the theory^{5b} have resulted in an expression of τ_1 which correctly predicts the main features of the fast relaxation process, as will be shown below.

Thus, a situation had developed in which both new experimental results and a detailed theory had been obtained independently from each other and were published at about the same time. When the authors of the two corresponding groups compared the counterpart with their work, they realized that results and theory agreed exceptionally well and that the theoretical expressions permitted the evaluation of several parameters, both kinetic and thermodynamic, that could not be obtained thus far. It was thus decided to write a joint publication making the fullest use of both theory and experiment and where we report: (1) new developments of the theoretical approach of micellar kinetics based on the analogy with diffusion.⁵ In particular a new expression has been obtained by the group in Sweden for the rate constant for the dissociation of one amphiphilic ion from the stable micelles; (2) new data concerning amphiphiles that had not been previously investigated together with extensions of previous measurements, obtained by the groups in Germany and France; (3) the interpretation of the available data in terms of the new theory of micellar kinetics. This last point has led to a number of conclusions which now gives very good insight into the phenomena involved in micelle formation and provide quantitative information not available thus far on micellar solutions.

II. Theory

1. *General Outline.* In all likelihood, the association and dissociation of the micelles proceed stepwise,⁹ i.e., one monomer at a time enters and leaves the micelle. The concentration of dimers, trimers, etc., is generally much lower than that of monomers so that only a much greater ease of their entrance into and exit from the micelles could make their contribution to the rate comparable with that of the monomers. From the treatment below of the details of the elementary process it seems to follow that rather the opposite is true. Anyhow, the contribution from nonunitary steps would be a relatively small one, the effect of which could be taken into account as a correction when the precision of the measurements and other evidence so requires.

For ionic surfactants we assume that the mobility of the counterions is so much larger than that of the somewhat bulky surfactant ions that they adjust almost instantly to

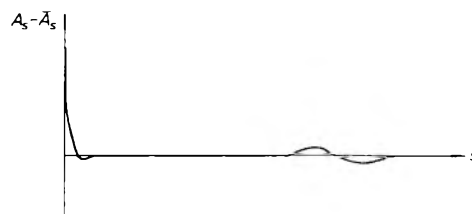
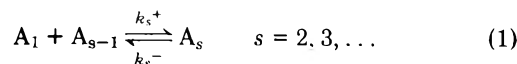


Figure 1. Sketch of a possible initial deviation from equilibrium, $A_s - \bar{A}_s$, as a function of aggregation number s .

the motion of the latter. The rearrangement of the counterions is, however, expected to show up as an independent process in ultrafast relaxation measurements and would be an interesting subject for separate study.

The individual steps (exchange processes) considered in the overall process are then the following:



where A_s denotes an aggregate containing s surfactant monomers.

At the beginning of a relaxation experiment (T-jump or p-jump, etc.) the deviation from equilibrium concentrations may typically be something like that shown in Figure 1. A_s denotes the concentration and \bar{A}_s its equilibrium value. In drawing the picture it has been assumed that aggregates occur in substantial amounts only in two regions, namely, in the region of proper micelles, around the mean aggregation number, and in the region of monomers, dimers, trimers, etc. (see Figure 1 in ref 5a).

In the attainment of equilibrium the excess population has to move from some regions of aggregation numbers to other ones. According to eq 1 this occurs in steps that are small compared to the distance in aggregation space generally covered. The process will, then, have the character of a flow.

It has indeed proved possible to write the kinetic equations in a form that closely resembles that of heat conduction, diffusion, etc.^{5a} By introduction of the relative deviation from equilibrium

$$\xi_s = \frac{A_s - \bar{A}_s}{\bar{A}_s} \quad (2)$$

and using the equilibrium relation

$$k_s^+ \bar{A}_1 \bar{A}_{s-1} = k_s^- \bar{A}_s \quad (3)$$

the kinetic equations can be written

$$\bar{A}_s (d\xi_s/dt) = -(J_{s+1} - J_s) \quad (4)$$

with

$$J_s = -k_s^- \bar{A}_s [\xi_s - \xi_{s-1} - \xi_1 (1 + \xi_{s-1})] \quad (5)$$

J_s is the net number of aggregates passing per unit time from $s-1$ to s . In eq 2-5 A_1 and \bar{A}_s refer to equilibrium concentrations.

The equations for diffusion in a tube of varying cross section $A(x)$, where x is the coordinate along the tube axis, and where the transverse dimensions are very small compared to the length of the tube, are

$$A(x) \frac{\delta c(x)}{\delta t} = - \frac{\delta J(x)}{\delta x} \quad (6)$$

and

$$J(x) = -D(x)A(x) \frac{\delta c(x)}{\delta x} \quad (7)$$

$J(x)$ is the total flow across $A(x)$, $D(x)$ is the diffusion constant that can vary with x , and $c(x)$ is the concentration. Equating now x with s , $J(x)$ with J_s , $D(x)$ with k_s^- , $A(x)$ with \bar{A}_s , $c(x)$ with ξ_s , and noting that the differences $\xi_s - \xi_{s-1}$ and $J_{s+1} - J_s$ are analogous to derivatives with respect to s , one finds that there is an almost complete analogy between eq 4 and 5 on one hand and eq 6 and 7 on the other. The difference is the term $\xi_1(1 + \xi_{s-1})$ within the square brackets of eq 5.

For small deviations from equilibrium the product $\xi_1 \xi_{s-1}$ can be neglected. Since the flow in ordinary diffusion is "driven" by the concentration gradient to which $\xi_s - \xi_{s-1}$ is analogous, our process is one where superimposed on that is a flow driven through the tube by the "force" ξ_1 , independent of the "coordinate" s but of course dependent on time. This introduces some peculiar characteristics which will be considered below but the main feature of the analogy used will remain valid and useful. For the further use of eq 4 and 5 and the diffusion analogy something must be assumed concerning the s dependence of \bar{A}_s and k_s^- .

The dependence of \bar{A}_s on s for micellar systems with low dispersion of micellar aggregation numbers is not at present experimentally known in any detail. The existence of dimers and trimers in noticeable amounts is still uncertain and the amount of larger aggregates between these and the proper micelles is most probably orders of magnitude lower than that of the proper micelles (at least at concentrations above the cmc). The width of the distribution of the proper micelles is generally about 20% of the mean aggregation number for the substances considered here, often called monodisperse since the ratio of weight to number average aggregation numbers is close to one. In agreement with these facts is the type of distribution curve given in Figure 1 of ref 5 and, obtained from statistical-thermodynamical arguments by Hoeve and Benson.⁷

The tube of the diffusion analogy is thus one with two thick ends connected by an extremely thin section. The diffusion from one end to the other can then be expected to be a much slower process than those of equalization of "concentration" within each of the thick ends. Only if the "diffusion constant" k_s^- were so much larger in the thin section than at the ends so that $k_s^- \bar{A}_s$ were of a similar order of magnitude in the thin section to that of the same product at the ends, only then could the diffusion through this section occur in a time of the same order of magnitude as the equalization at the ends. As will be shown further below this is quite improbable. However from the relation

$$-\ln \frac{k_s^-}{k_s^+ \bar{A}_1} = \ln \frac{\bar{A}_s}{\bar{A}_{s-1}} = \ln \bar{A}_s - \ln \bar{A}_{s-1} = \frac{d}{ds} \ln \bar{A}_s \quad (8)$$

obtained from eq 3 and also shown in Figure 1 of ref 5 it is clear that the ratio $k_s^-/k_s^+ \bar{A}_1$ varies little in the region in question. It is not probable that k_s^- and k_s^+ vary separately so strongly that an increase in k_s^- in the thin section could compensate for the low \bar{A}_s values there.

The process can then be separated into two parts. The first will be a rapid attainment of pseudo-equilibria in the thick ends followed by a pseudo-stationary flow from one end to the other. The calculation of the relaxation times for these two processes has been previously reported.⁵ We shall here dwell particularly on the physical meaning of the various quantities and assumptions involved in the calculations.

2. *Attainment of Pseudo-Equilibrium.* The processes in the two ends will be coupled to each other since in general

each one is accompanied by a net consumption or production of monomers which by eq 4 and 5 influences the rate in the other one. If the two processes have sufficiently different rates, however, they will be decoupled in the sense that the faster one can be treated alone since the slower one will be practically frozen, not consuming or producing monomers. The slower one can then be treated assuming internal equilibrium in the other end.

At present we shall assume that dimers, trimers, etc., are sufficiently rare so that their influence on the process in the region of proper micelles can be neglected.

Under these circumstances the kinetic equations have been solved^{5,10} for the case that (1) k_s^- and k_s^+ are independent of s in the region of proper micelles and equal to k^- and k^+ , (2) the micellar distribution is Gaussian, n being the average aggregation number and σ the distribution width, and (3) the latter is broad enough so that differences with good accuracy can be replaced by derivatives and referred to s irrespective of whether the difference is between s and $s - 1$ or between $s + 1$ and s . In accordance therewith ξ_{s-1} in the last inner bracket of eq 5 is replaced by ξ_s .

After some algebra, one obtains

$$\xi_1(t) = -ac_0(t) - \sqrt{2} \frac{\sigma}{n} ac_1(t) \quad (9)$$

where $c_0(t)$ and $c_1(t)$ are the first two time-dependent coefficients in the expansion of $\xi(s,t)$ in terms of Hermite polynomials, and a is given by

$$a = (A_{\text{tot}} - \bar{A}_1)/\bar{A}_1 \quad (10)$$

where A_{tot} is the total detergent concentration.

In deriving eq 9 the sums over s have been replaced by integrals over s , formally extended to $-\infty$ despite the fact that in the sums $s > 1$. It introduces a negligible error but allows the use of the orthogonality properties of Hermite polynomials.

With the aid of the known properties of Hermite polynomials and after some algebra both sides of eq 4 were rewritten as sums over these polynomials whereupon identification of their coefficients on both sides yielded first order differential equations for the $c_i(t)$'s. These could consecutively be solved in a straightforward way. Since in experiments one normally determines the time dependence of A_1 or an equivalent quantity, eq 9 shows that the interest is limited to c_0 and c_1 for which there resulted

$$c_0(t) = c_0(0) \quad (11)$$

and

$$c_1(t) = (c_1(0) + B) \exp \left[-\frac{t}{\tau_1} \right] - B \quad (12)$$

where

$$B = \frac{a \frac{\sigma}{\sqrt{2}} c_0(1 + c_0)}{1 + \frac{\sigma^2}{n} a(1 + c_0)} \quad (13)$$

and

$$\frac{1}{\tau_1} = \frac{k^-}{\sigma^2} + \frac{k^-}{n} a(1 + c_0) \quad (14)$$

Equation 11 expresses the fact that during the process under consideration the number of micelles remains constant. It can be easily shown that

$$c_0 = \frac{\sum \xi_s \bar{A}_s}{\sum \bar{A}_s} \quad (15)$$

Thus c_0 is the average relative deviation from equilibrium among the micelles, a quantity that in most relaxation experiments is of the order of 1% or less. Under these circumstances c_0 can be neglected compared with unity. Under these assumptions, the time dependence of the monomer concentration will be characterized by a single relaxation time constant. The concentration dependence of τ_1^{-1} will reside almost completely in the factor a since for a symmetric micelle distribution, of which the Gaussian is a special case, σ is concentration independent and since for $\sigma/n \ll 1$, n varies very slowly with concentration.⁵ It is further inherent in the above assumptions that k^- and k^+ are concentration independent. When n is large \bar{A}_1 will be practically concentration independent above the cmc and equal to the latter.

τ_1^{-1} will therefore be a linear function of the total concentration from the slope of which k^-/n is obtained. Since n can be obtained from light scattering or other measurements k^- can be calculated. The intercept gives k^-/σ^2 and thus also σ would, for the first time, be experimentally obtainable.

It is interesting to note that the first term, k^-/σ^2 , in the expression for τ_1^{-1} is well compatible with the diffusion analogy. The time for diffusional equalization over a distance l in a tube of approximately constant cross sectional area is of the order of l^2/D where D is the diffusion constant (see eq 7) so that with the correspondence of D to k^- and l to σ the analogy is clear. The second, concentration dependent term, is due to the occurrence of ξ_1 in the flow expression 4. It will be made intuitively understandable below that its effect is an accelerating one that increases with total concentration.

3. *Pseudo-Stationary Flow in the Case of Small Perturbations.* The calculation of the relaxation time associated with this process has been already presented in detail in a previous report.⁵ We shall here only insist on the analogy between diffusion in the "narrow passage" and the kinetics of the process.

When the "narrow" passage is "thin" enough the flow J from one end to the other will be so small that at each instant there will be ample time in each of the thick ends for an almost complete adjustment toward internal equilibrium. This is equivalent to setting J_s equal to zero in eq 4 for s values corresponding to the thick part.

On the other hand, in the narrow passage the \bar{A}_s 's on the left-hand side of eq 5 are so small that any sizable difference between J_s and J_{s+1} would cause large changes in ξ_s . However the pseudo-stationary flow is characterized by very slow changes of all "concentrations" in the diffusion analogy so one concludes that in the narrow passage

$$J_s = J = \text{constant} \quad (16)$$

From eq 5 it is seen that this assumption is equivalent with the usual Bodenstein stationarity hypothesis made in kinetics for species of very small concentrations.

With this assumption the following expressions were obtained for the flow J in the narrow passage and the relaxation time τ_2 characterizing this process

$$J = \frac{\bar{n}_1^2 c_1 + \bar{n}_3^2 c_3}{R c_3 \bar{n}_3} \xi_1 \quad (17)$$

$$\frac{1}{\tau_2} = \frac{1}{R c_3} \frac{\bar{n}_1^2 c_1 + \bar{n}_3^2 c_3}{\bar{n}_1^2 c_1 + \sigma^2 c_3} \quad (18)$$

with

$$\begin{aligned} c_1 &= \sum_{s=1}^{s_1} \bar{A}_s & c_3 &= \sum_{s>s_2} \bar{A}_s \\ \bar{n}_1^2 &= \frac{1}{c_1} \sum_{s=1}^{s_1} s^2 \bar{A}_s & \bar{n}_3^2 &= \frac{1}{c_3} \sum_{s>s_2} s^2 \bar{A}_s \\ \bar{n}_3 &= \frac{1}{c_3} \sum_{s>s_2} s \bar{A}_s & \sigma^2 &= \bar{n}_3^2 - \bar{n}_3^2 \end{aligned} \quad (19)$$

and

$$R = \sum_{s_1+1}^{s_2} \frac{1}{k_s^- \bar{A}_s} \quad (20)$$

The characteristics of eq 18 are borne out more clearly when certain simplifications are introduced. First we shall assume that $\bar{n}_1^2 \approx 1$, i.e., that dimers, trimers, etc. occur only in negligible quantities. Then

$$\bar{n}_1^2 c_1 \approx \bar{A}_1 \quad (21)$$

and

$$\bar{n}_3 c_3 = A_{\text{tot}} - \bar{A}_1 = A_{\text{exc}} \quad (22)$$

so that

$$\bar{n}_3^2 c_3 = (\bar{n}_3^2 + \sigma^2) c_3 \approx \bar{n}_3^2 c_3 = \bar{n}_3 A_{\text{exc}} \quad (23)$$

If then A_{tot} is not very close to $\bar{A}_1 \approx \text{cmc}$

$$\bar{n}_3 A_{\text{exc}} \gg \bar{A}_1 \quad (24)$$

since \bar{n}_3 is of the order of 100.

Equation 18 now takes the form

$$\frac{1}{\tau_2} \approx \frac{n^2}{\bar{A}_1 R} \frac{1}{1 + \frac{\sigma^2}{n}} \quad (25)$$

where the previous notation n for \bar{n}_3 has been reintroduced.

As before, \bar{A}_1 , σ , and n vary very little with total concentration above the cmc.⁵ The last factor, then, introduces a hyperbolically decreasing factor, the rate of decrease being determined by the value of σ^2/n as is shown in Figure 2.

The concentration dependence of R^{-1} is governed by that of the \bar{A}_s term of eq 20 that gives the largest contribution to R as is shown in Figure 3.

The application of the mass action law to the exchange processes¹ yields

$$\bar{A}_s = K_s \bar{A}_1^s \text{ with } K_s = \prod_{i=2}^s \frac{k_i^+}{k_i^-} \quad (26)$$

Since for the proper micelles s is of the order of 100, even extremely small relative changes in \bar{A}_1 will produce major changes in the number of proper micelles. This is, incidentally, the reason for the approximative constancy of \bar{A}_1 once micelles have started to appear in nonnegligible amounts. The approximate constancy of σ and n results in

$$\bar{A}_s \propto a^{s/n} \quad (27)$$

The larger s is, the faster will \bar{A}_s increase with the total concentration A_{tot} . This is shown in Figure 5. The narrow passage will then in general change shape with increasing A_{tot} . It will widen quickly in the upper end and very slowly in the lower end. The relative changes are shown in Figure 4 for several values of a .

If the narrow passage is relatively short R can be approximated by

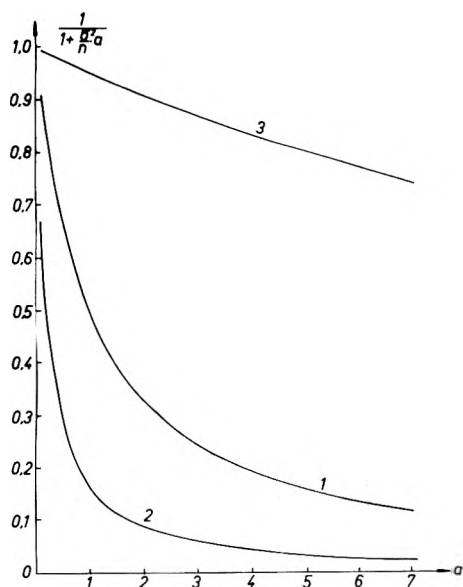


Figure 2. Plot of $[1 + (\sigma^2/n)a]^{-1}$ vs. a . Curves 1, 2 and 3 refer to values of σ^2/n equal to 1, 5, and 0.05, respectively.

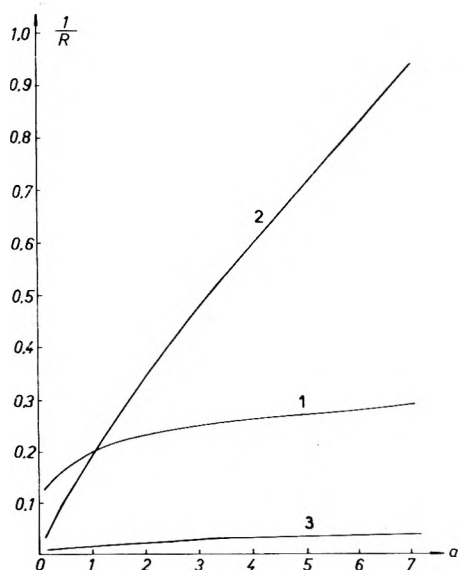


Figure 3. Plot of R^{-1} vs. a for a short narrow passage situated around $s = 20$ (curve 1); a short narrow passage situated around $s = 80$ (curve 2); and a long narrow passage between $s = 20$ and $s = 80$ (curve 3).

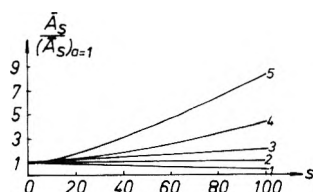


Figure 4. Variations of $\bar{A}_s / (\bar{A}_s)_{a=1}$ with s . Curves 1, 2, 3, 4, and 5 refer to values of a equal to 0.25, 1, 2, 4, and 8, respectively.

$$R \approx l/k_r \bar{A}_r \quad (28)$$

where l is the effective length of the narrow passage (expressed as a difference of two aggregation numbers) and r the value of s at the minimum of \bar{A}_s . If $l/r \ll 1$ there will

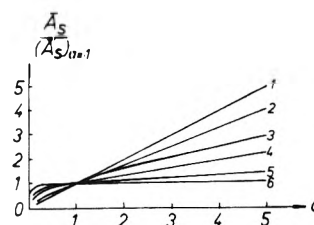


Figure 5. Variations of $\bar{A}_s / (\bar{A}_s)_{a=1}$ with a . Curves 1–6 refer to values of s/n equal to 1, 0.9, 0.666, 0.5, 0.25, and 0.05, respectively.

hold that r changes little with total concentration and the same will hold for l if the minimum in \bar{A}_s at $s = r$ is not too unsymmetric. In such a case

$$R \propto a^{-(r/n)} \quad (29)$$

and r would be obtainable from a plot of $\ln R$ vs. $\ln a$. Figure 3 shows the dependence of R^{-1} on total concentration for different narrow passages. Finally, Figure 6 shows the spectrum of concentration dependences of τ_2^{-1} that results from compounding the cases of Figures 2 and 3.

If the simplification leading to eq 25 is introduced already in eq 17 one obtains

$$J = \frac{n_3^2}{R n_3} \xi_1 \approx \frac{n \xi_1}{R} \quad (30)$$

The last step follows from eq 19 when one notices that $\sigma \ll n$. Equation 30 can be understood in the following way: when the amount of material in the proper micelle region is of the same order of magnitude or larger than in the monomer region the relative deviations in the former region must also be of the same order of magnitude or smaller than in the latter. The "driving force"

$$-(\xi_s - \xi_{s-1} - \xi_1) \quad (31)$$

in each step will, when summed from $s = 2$ to $s = n$, amount to

$$n \xi_1 - \xi_n \approx n \xi_1 \quad (32)$$

since ξ_n is of the same order of magnitude as ξ_1 whereas n is of the order of 100. The flow will then be the ratio between the total driving force, $n \xi_1$ and the resistance R as in eq 30. The same argument applied to eq 17 for $n_3 = n$ will confirm the result.

This result may also be expressed in the following way: since the free monomers are engaged in each step their deviation from equilibrium concentration will consistently influence each step in one direction, toward larger sizes, i.e., positive flow if $A_1 > \bar{A}_1$ ($\xi_1 > 0$) and vice-versa. The aggregate concentration will act in the opposite direction, but not consistently, since because of the conservation of matter it has to change from excess (positive ξ_s) in one end to deficit (negative ξ_s) in the other end. The net effect of the monomer deviation from equilibrium therefore overshadows that of the aggregates.

From eq 25 it is seen that τ_2^{-1} is proportional to $n_3^2 \approx n^2$. One of these factors n has its origin in the effect just described. The other has its root in the fact that the formation and disintegration of one proper micelle consumes or produces approximately n monomers a fact which also accelerates the process.

The factor \bar{A}_1^{-1} in eq 25 expresses the fact that the size of the reservoirs must affect τ_2 . Large reservoirs will in-

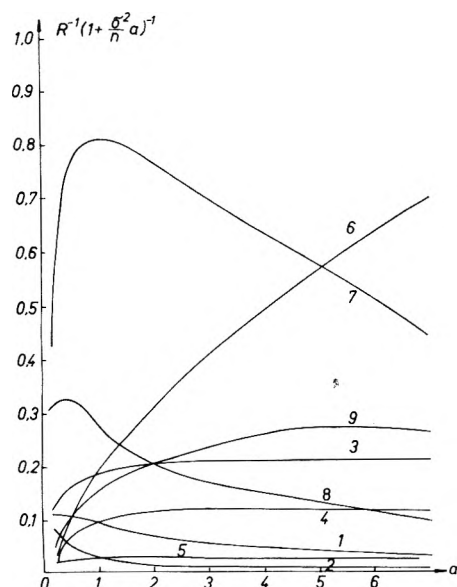


Figure 6. Variation of $R^{-1} [1 + (\sigma^2/n)a]^{-1}$ with a for a short narrow passage around $s = 20$ and values of σ^2/n equal to 1 (curve 1), 5 (curve 2), and 0.05 (curve 3); a short narrow passage around $s = 80$ and values of σ^2/n equal to 1 (curve 4), 5 (curve 5), and 0.05 (curve 6); and for a long narrow passage between $s = 20$ and $s = 80$ and values of σ^2/n equal to 1 (curve 7), 5 (curve 8), 0.05 (curve 9).

crease it since more material has to be transported through the given narrow passage.

The factor R^{-1} is self explanatory. The factor $(1 + \sigma^2 a/n)^{-1}$ is more elusive. It can however be understood qualitatively in the following way: for positive ξ_1 the micelle distribution will be shifted toward larger s values. This consumes monomers, ξ_1 will be reduced, and since it is the main driving force, τ_2 will be increased. The effect will be governed by the square of σ since both the average shift in s values and the amount of monomer consumed will be proportional to σ . For negative ξ_1 smaller s values will be enhanced, again reducing the absolute value of ξ_1 with the same effect.

The factor $(1 + \sigma^2 a/n)$ also enters expression 14 for τ_1 when c_0 is neglected, multiplying the expected value k^-/σ^2 . The explanation cannot be similar to the one given for τ_2 since it shortens instead of lengthens the time constant. A very qualitative explanation is the following one: the fast process is striving toward the equilibrium distribution. If, taking a neutral example, one assumes that at the start the ξ_s values are all similar, and further takes $\xi_1 > 0$ then, a movement of micelles toward larger s values will occur. Now, during the process there will be a consumption of monomers so that ξ_1 is reduced. However a lower ξ_1 value entails a smaller shift toward larger s values. The process is striving toward a goal but the goal is kind enough to meet the process half-way thereby reducing the time required. This acceleration of the fast process will increase with total concentration since then a larger number of monomers is consumed giving a faster reduction of ξ_1 .

The analogy with diffusion used above is equivalent with the concept of random walk. Such a view has independently been taken by Muller.³ He argued that the process of disintegration is one that requires as a net result n steps to the left. The characteristic time for such a process is the one for the single step multiplied by n^2 . Equation 25 is, however, completely at variance with this argument. The

reason seems to be that the argument requires equal probabilities for steps to the right and to the left. However close to equilibrium the ratio of these probabilities is

$$\frac{k_{s+1}^+ \bar{A}_1}{k_s^-} \approx \frac{k_s^+ \bar{A}_1}{k_s^-} \quad (33)$$

Between the proper micelle region and the narrow passage this ratio is larger than unity (see Figure 1 in ref 5a). Even if the ratio is not much larger than unity the cumulative effect of many steps will give a sizable effect. One may note that

$$\prod_{s=r}^{n-1} \frac{k_{s+1}^+ \bar{A}_1}{k_s^-} = \prod_{s=r}^{n-1} \frac{k_{s+1}^+ \bar{A}_s}{k_s^+ \bar{A}_{s-1}} = \frac{k_n^+ \bar{A}_{n-1}}{k_r^+ \bar{A}_{r-1}} = \frac{k_n^- \bar{A}_n}{k_r^- \bar{A}_r} \quad (34)$$

indicating why in a full treatment the equilibrium number of aggregates at the minimum is a decisive factor in the slow relaxation process.

4. *Theoretical Calculation of k_s^- and k_s^+ .* These quantities have recently been calculated¹² with the simplification and generalization of Kramers¹³ theory for reaction rates. Here we shall present a derivation of k_s^- based on a simple model¹⁴ that gives essentially the same result as the just mentioned one.

To begin with we shall treat the monomer as an essentially straight rod moving along its axis at right angles to the surface of the micelle. The motion will be a diffusional one characterized by a constant $D(x)$ which may vary with x , the length of the hydrophobic tail outside the micelle surface. Influencing the motion is also the hydrophobic bonding energy that tends to "pull" the hydrophobic tail into the micelle. For charged monomers the electrostatic interactions tend to pull it out of the micelle. The sum of these energies will be denoted by $V(x)$.

The hydrophobic bonding energy seems to be proportional to the chain length, i.e., to x .^{8,15} When the tip of the hydrophobic tail leaves the micelle surface there will be a drop in the free energy of the system due to the increased freedom of both the (now free) monomer and the remaining hydrophilic end groups in the micelle. In the description of Hoeve and Benson⁷ this drop, Δ , is

$$\Delta = -kT \ln \alpha \quad (35)$$

where

$$\alpha = \frac{1}{S_{(s-1)}} \frac{[S_{(s-1)} - (s-1)a_0 - a_1]^s \gamma_m}{[S_{(s-1)} - (s-1)a_0]^{s-1} \gamma_{\text{free}}} \quad (36)$$

Here $S_{(s-1)}$ is the surface area of a micelle of aggregation number $s-1$. a_0 and a_1 are the effective cross sectional areas of the hydrophilic head group and of the tail of the monomer. $\gamma_m/\gamma_{\text{free}}$ is the ratio of configurational freedoms of the monomer at the maximum of the energy $V(x)$ to that of the free monomer.

Neglecting the electrostatic energy, $V(x)$ would then schematically have the appearance of Figure 7, curve 1. In actual fact both the minimum and the maximum of V would of course be somewhat rounded out. The addition of the electrostatic energy would bring about a change to curve 2 in the same figure.

For an ensemble of such systems containing $c(x)$ monomers at x per unit length there will be a flow equation of the Einstein-Smoluchowski type

$$J = -D(x) \left[\frac{\delta c}{\delta x} + \frac{1}{kT} \frac{\delta V}{\delta x} c \right] \quad (37)$$

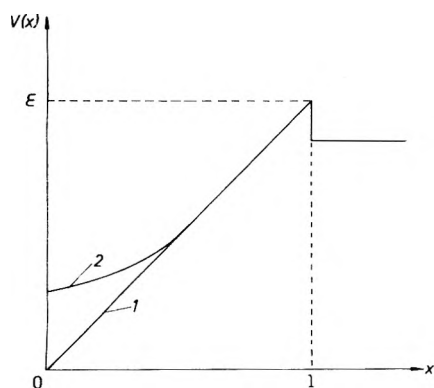


Figure 7. Plot of the free energy $V(x)$ for the dissociation of a monomer from the micelle as a function of the length x of the hydrophobic tail outside the micelle for the case of an uncharged surfactant (curve 1) and an ionic surfactant (curve 2).

where J is the number of systems that per unit time pass x in the positive, outgoing direction. The condition appropriate for a calculation is a stationary case with $c(0)$ kept at the value of undisturbed equilibrium and $c(l) = 0$, where l is the length of the hydrophobic tail. It corresponds to a situation where the freed monomers are continuously removed and new systems are continuously added to keep $c(0)$ at the prescribed value.

For such a system c will be independent of time and therefore, according to the continuity equation

$$\frac{\delta c}{\delta t} = -\frac{\delta J}{\delta x} \quad (38)$$

J will be independent of x .

Equation 37 can now be solved by noting that its bracket can be written

$$\exp(-V/kT) \frac{\delta}{\delta x} [c \exp(V/kT)] \quad (39)$$

so that

$$\frac{\delta}{\delta x} [c \exp(V/kT)] = -\frac{J}{D} \exp(V/kT) \quad (40)$$

Integration from $x = 0$ to $x = l$ and use of $c(l) = 0$ gives

$$c(0) = J \int_0^l \frac{1}{D(x)} \exp(V(x)/kT) dx \quad (41)$$

The main contribution to the integral will come from the region of maximal $V(x)$ since $D(x)$ will be a comparatively slowly varying function of x . Denoting V_{\max} by ϵ eq 41 can be rewritten as

$$c(0) = J \frac{l_b}{D_m} \exp(\epsilon/kT) \quad (42)$$

where D_m is the value of D in the region of maximal V and l_b is given by

$$l_b = \int_0^l \exp[(V(x) - \epsilon)/kT] dx \quad (43)$$

l_b is essentially the width of the barrier kT below its maximum. For a linear $V(x)$, it amounts to

$$l_b = \frac{kT}{\epsilon} l \quad (44)$$

For the actual rounded form it will be somewhat larger. $c(0)$ is obtained from the equilibrium distribution

$$c(x) = c(0) \exp[-V(x)/kT] \quad (45)$$

the integral of which will give the total number of monomers considered, $s\bar{A}_s$:

$$\begin{aligned} \int_0^l c(x) dx &= c(0) \int_0^l \exp[-V(x)/kT] dx \\ &= c(0)l_0 = s\bar{A}_s \end{aligned} \quad (46)$$

where

$$l_0 = \int_0^l \exp[-V(x)/kT] dx \quad (47)$$

For a linear $V(x)$

$$l_0 = l_b = \frac{kT}{\epsilon} l \quad (48)$$

but also here a rounded form of $V(x)$ will give a somewhat larger value. In the linear case, both l_0 and l_b are close to the 1.1 Å, i.e., slightly less than the projection of a C-C bond on the axis of the "zig-zag" alkyl chain. Inserting eq 46 into eq 42 we obtain

$$J = s\bar{A}_s \frac{D_m}{l_b l_0} \exp[-\epsilon/kT] \quad (49)$$

Since J is identical with $k_s^- \bar{A}_s$ the final result will be

$$k_s^- = s \frac{D_m}{l_b l_0} \exp[-\epsilon/kT] \quad (50)$$

This expression is readily understood intuitively by noting that l_b^2/D_m is the characteristic time for diffusional motion over the distance l_b and that $s(l_b/l_0) \exp[-\epsilon/kT]$ is the relative probability per micelle at equilibrium of finding a monomer in a region of length l_b around the maximum of V . Although the assumptions underlying eq 50 are not strictly true the main features of the actual process would be essentially the same. The hydrocarbon tails containing up to 22 carbon atoms are known¹⁵ not to be curled to an extent that influences the hydrophobic bonding energy. Note that even if the monomers were curled the dominant factor in eq 50, the exponential one, would not be influenced by this fact.

The restriction that the monomer moves only along a straight axis at right angles to the surface has of course to be relaxed. However the maximum in the free energy $V(x)$ would still be one where only one carbon is within the micelle. If this were not to be the terminal one the chain would have to be strongly bent at that point and would further require an extra crowding of the hydrophilic end groups of the other monomers in the micelle. Such configurations would therefore contribute little to the overall rate.

The configurations and motions of the exiting monomer for which the diffusion constant D_m has to be estimated are fairly similar to those of a free monomer in bulk solution except that the tip of the tail is in the micelle surface. After comparing the motions of the free monomer and of the leaving monomer one would expect D_m to be close to that of the free monomer.

In conclusion, one would then expect eq 50 to give at least the right order of magnitude for k_s^- and to be fairly useful in relating rate constants between different homologues, different ionic strengths of the solution, etc. Compared with the expression of the transition state theory eq 50 has a factor $D_m/l_b l_0$ instead of kT/h , where h is Planck's constant. The former is in our case much smaller than the latter reflecting the fact that the mean free path of the bulky monomer is much smaller than the width of the bar-

rier maximum. The assumption of the transition state theory that all systems reaching the "saddle point" from the reactant side pass on to the full product side is no longer valid.

The values obtained from the statistical-mechanical treatment are

$$k_s^- = \frac{D_m Q_{s-1} Q_1}{l_b Q_s} \alpha S_{(s-1)} \quad (51)$$

and

$$k_s^+ = \frac{D_m}{l_b} \alpha S_{(s-1)} \quad (52)$$

where Q_s is the partition function for a micelle of aggregation number s . For the proper micelles eq 50 and 51 are practically equal if the two D_m 's are properly defined.¹² From eq 52 it follows that k_s^+ is somewhat smaller than the ordinary "diffusion controlled" value since there is free energy barrier, Δ , to overcome before entering the micelle. However this barrier appears to be small.

III. Experimental Results

The measurements were carried out using the same p-jump, T-jump, and shock tube apparatuses as in previous studies.^{1,16} Sodium tetradecyl sulfate (STS) and sodium hexadecyl sulfate (SHS) were investigated for the first time. In addition our previous study on sodium dodecyl sulfate¹ (SDS) was extended to include the effect of added NaCl on the observed relaxation processes. These last measurements were mostly performed by means of a T-jump with spectrophotometric detection. Since SDS does not show any absorption spectrum in the range of wavelengths available on our equipment, acridine orange was added to the detergent solution and used to monitor the relaxation processes. As was shown elsewhere,¹⁷ the relaxation time obtained from the change of absorption or fluorescence of the dye + detergent solution with time is the same as for the micellar system in the absence of dye, when the ratio (detergent)/(dye) is large enough (i.e., 100 to 200 depending on the ionic strength, detergent concentration, etc.).

The experimental error on the measured relaxation times is expected to be less than 10%, except for the slow process of SHS where the error is about 20%. Indeed, owing to the limited solubility of this detergent, measurements had to be carried out at higher temperature, where the relaxation signals had a small amplitude and overlapped with the time constant of the equipment.

All surfactants investigated in this work were gifts from Henkel (Düsseldorf, West Germany). They were purified by successive recrystallizations in water or in mixtures of water and alcohol. The critical micelle concentrations (cmc) were measured by conductivity. Their values agreed well with the known cmc values.

In all instances, two well separated relaxation times, τ_1 and τ_2 with $\tau_1 \ll \tau_2$, have been detected, confirming our previous findings.^{1,16} The values of τ_1 and τ_2 for STS and SHS measured by means of the p-jump and shock-tube methods are given in Tables I and II. With these techniques the relaxation time τ_2 could be observed from the cmc up to about twice the cmc because the amplitude of the process became vanishingly small at higher concentrations. This, however, does not mean that the equilibrium responsible for τ_2 does not occur for these systems at higher concentration. Indeed the effect can be observed at such concentration when using a T-jump technique and moni-

toring the micelle concentration change with a dye, as described above. It is likely that the conductivity change brought about by a p-jump is simply too small to result in a significant relaxation effect. The relaxation times that were observed using the T-jump equipment for large detergent concentrations and solutions that had excess added NaCl are given in Table III. In a few cases, relaxation times could be observed under identical experimental conditions by means of T-jump and p-jump, thereby giving additional evidence that the different techniques are indeed observing the same process.

In Figure 8, the $1/\tau_1$ values for STS and SHS are plotted on a double logarithmic scale against the total detergent concentration (A_{tot}). Data from previous investigations on sodium hexyl sulfate and sodium heptyl sulfate by Rassing, Sams, and Wyn-Jones¹⁸ and on sodium dodecyl sulfate by Folger, Hoffmann, and Ulbricht¹⁶ are also shown. It is interesting to note that an almost linear plot results. The concentration dependence for a given detergent is so large that the $1/\tau_1$ values practically reach the beginning of the curve for the next shorter homologue when the concentration is increased up to and above the cmc of the shorter homologue. This situation however appears to be peculiar to the alkyl sulfates. Measurements on potassium alkyl carboxylates²⁰ were found to give different results.

It is apparent from Figure 8 that there are no data in the time range between 1 and 0.1 μ sec. This is due to the impossibility of carrying out relaxation experiments in this particular region with the techniques available in our laboratories. Because the $1/\tau_1$ values for the alkyl sulfates of intermediate chain length (C_9 - C_{11}) fell between 0.1 and 1 μ sec, the $1/\tau_1$ values at the cmc for these detergents should have been obtained by extrapolating data from far above the cmc. In view of the possible curvature of the plot of $1/\tau_1$ vs. A_{tot} this procedure may lead to substantial errors. For these reasons it was decided not to use the extrapolated values of the intercept at the cmc, in our calculations.

As predicted by eq 21 and as previously experimentally observed^{16,18,20} the $1/\tau_1$ values increase more or less linearly with A_{tot} from a finite value at the cmc. The rise is, however, slightly faster than linear as shown in Figures 9 and 10 for STS and SHS. The slight curvature seems also to be visible in some of the previous sound absorption measurements.¹⁸ No attention was previously paid to this deviation from a straight line but the effect seems significant enough to deserve some comments in the Discussion section.

The $1/\tau_2$ values are plotted in Figure 11 for STS and in Figure 12 for SDS. As predicted by eq 25 the $1/\tau_2$ values pass through a maximum with increasing A_{tot} . Addition of 0.01 M NaCl shifts the maximum away from the cmc and lowers the $1/\tau_2$ values. For larger concentrations of NaCl, the $1/\tau_2$ values increase with A_{tot} . At constant A_{tot} , $1/\tau_2$ goes through a minimum as c_{NaCl} is increased.

The slow relaxation time has recently been observed for sodium decyl sulfate (SDeS) by Yasunaga et al.³¹ Judging from the linear rise of $1/\tau_2$ with increasing A_{tot} the experimental values were probably affected by the presence of impurities. Preliminary studies on SDeS that were made in our laboratory indicate that τ_2 is much shorter than reported³¹ and that its concentration dependence is similar to that of SDS.

IV. Evaluation of Kinetic Parameters and Discussion

1. *The Fast Process.* Using eq 14 the parameters k^-/n and k^-/σ^2 can directly be determined from the slopes and

TABLE I: Relaxation Times τ_1 (μs) and τ_2 (ms) for STS at Different Temperatures and Total Concentrations

$10^3 A_{\text{tot}}$, M	15 °C		20 °C		25 °C		30 °C		35 °C		40 °C		45 °C	
	τ_1	τ_2	τ_1	τ_2	τ_1	τ_2	τ_1	τ_2	τ_1	τ_2	τ_1	τ_2	τ_1	τ_2
2.1			123	320	41	245	19	155	7			3.5		
2.2			87	290	33	220	13.5	148	5.6			3.3		
2.3		320	95	270	32	203	12	133	5.1	107		2.6		
2.4		298	85	210	32	175	12	131	4.8	108		2.5	87	
2.5		256	90		34		12		4.9			2.4		
2.6				183		133		100		85			73	
2.8		235	65		26		10		4.2			1.9		
3.0		250	70	125	34	88	12	73	5.1	60		2	60	
3.2		258	68		29		11		4.3			2		
3.4		212	55		33		11							
3.6			62		28									
4.0				71		57		43		36			26	
5.0				50		38		29		24			19	
7.5				30		20		14		10			7	
10				17		12		9		6				

TABLE II: Relaxation Times τ_1 (μs) and τ_2 (ms) for SHS at Different Temperatures and Total Concentrations

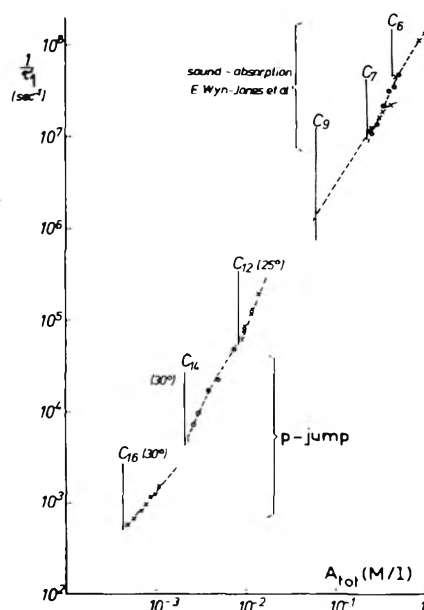
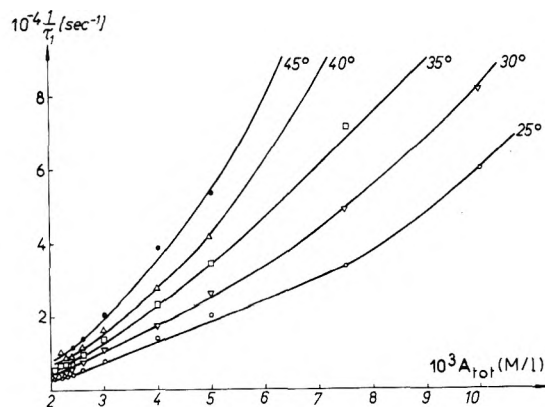
$10^4 A_{\text{tot}}$, M	30 °C		35 °C		40 °C		45 °C	
	τ_1	τ_2	τ_1	τ_2	τ_1	τ_2	τ_1	τ_2
4.6	1780							
5.0	1700		1340					
5.4	1520		1150		993			
5.8	1400		1120		945	58	807	34
6.2	1360		1030		950	40	735	29
6.6	1245		960		895	32	665	22
7.0	1135		870		780	28	603	22
8.0	937		740		673	29	613	
9.0	850	440	667	180	530	40	430	24
10	760	350	580	185	470	39	365	21
11	640	165	500	108	403	33	325	26
12			450	111	330	35		
20	280		200		143		114	
30	144		135		105		100	
50	90		70		53		38	

TABLE III: $1/\tau_2$ Values (s^{-1}) for SDS at 20 °C at Different Concentrations and Ionic Strengths (NaCl)

A_{tot} , M	c_{NaCl} , M				
	0	10^{-2}	6×10^{-2}	10^{-1}	2×10^{-1}
10^{-2}	550	23.8		0.89	4.27
2×10^{-2}	261	16.6		1.23	7.07
3×10^{-2}	104	8.8	0.89	1.58	10.7
5×10^{-2}	20	2.7	0.87	2.24	20

intercepts at the cmc of the curves of Figures 9 and 10. The values are summarized in Table IV. Included in the table are data from previous measurements that had been interpreted differently before. Values for k^-/n were obtained for these systems from the slopes of $1/\tau_1$ vs. A_{tot} plots, because the k^-/n values do not depend so critically on a small curvature. These values could be somewhat higher than would result if measurements close to the cmc had been available.

The values of n taken from the literature²² were used for the calculations of σ and k^- from k^-/n and k^-/σ^2 . The results of these calculations are listed in Table IV, together with the values of the recombination rate constant k^+ and of the cmc. k^+ values were obtained from k^- and the cmc using the approximate equation


Figure 8. Variation of $1/\tau_1$ with A_{tot} for a series of sodium alkyl sulfates.

Figure 9. Plot of $1/\tau_1$ vs. A_{tot} for STS at different temperatures

$$k^+/k^- = 1/\bar{A}_1 = 1/\text{cmc} \quad (53)$$

(a) Discussion of the k^+ Values. The rate constants k^+ in Table IV are all in the range expected for diffusion-con-

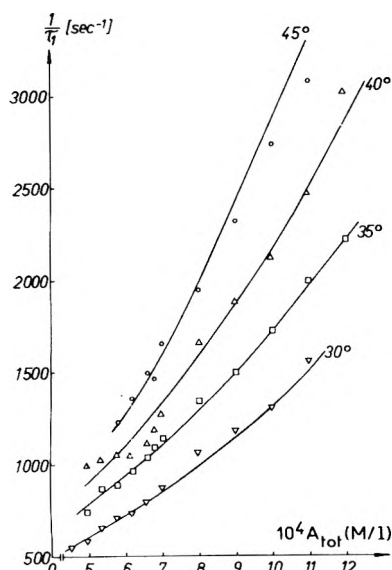


Figure 10. Plot of $1/\tau_1$ vs. A_{tot} for SHS at different temperatures

trolled association reactions. This indicates that the free energy of activation Δ (see section II4) must be small (1 to $2kT$) in agreement with the results of calculations based on approximate values of micellar radii and effective cross sectional area per charged head group. They nevertheless show a noteworthy decrease with increasing length of the alkyl group. Only a small fraction of this decrease can be accounted for by the decrease of the detergent ion diffusion coefficient with increasing chain length. Indeed the limiting equivalent conductivities λ_m^0 (which are proportional to the diffusion coefficients) of detergent ions increase²³ by a factor of less than 2 when the number of carbon atoms of the chain length is reduced from 16 to 6, while k^+ is increased by more than tenfold. It is likely that this increase is due in part to electrostatic effects. Indeed the k^+ values of the short chain detergents were obtained at higher ionic strength because of their larger cmc. This should allow a better shielding of the micellar charge and consequently result in a higher rate constant for the approach of the detergent ion to the micelle. The difference can also possibly be caused by a dependence on micelle size of the free energy barrier Δ (see end of section II4) that the hydrophobic tail of the approaching detergent ion must overcome before entering into the micelle. It seems reasonable to assume that this energy barrier increases with the size of the micelle owing to the tighter packing of larger micelles relative to small ones. In fact, approximate calculations support this assumption.

It is also worth noting that the k^+ values of Table IV are much larger than those obtained by Rassing, Sams, and Wyn-Jones¹⁸ from the interpretation that these authors gave to their ultrasonic absorption data on sodium alkyl sulfates. The difference is due to the fact that in their treatment of the fast process the slope of the plot of $1/\tau_1$ vs. A_{tot} gave directly k^+ , while with the theory given in section II the slope is k^+/n .

(b) *Discussion of the σ Values.* The σ values increase with the length of the hydrophobic tail up to STS. Surprisingly the value of σ for SHS is lower than for STS. The difference appears to be larger than the error limits. The reason for this behavior is unclear at present. It is however noteworthy that the σ/n values decrease with the number

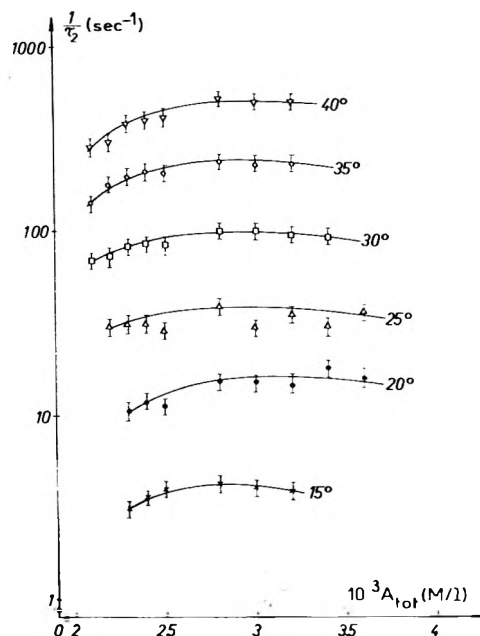


Figure 11. Semilog plot of $1/\tau_2$ vs. A_{tot} for STS at different temperatures.

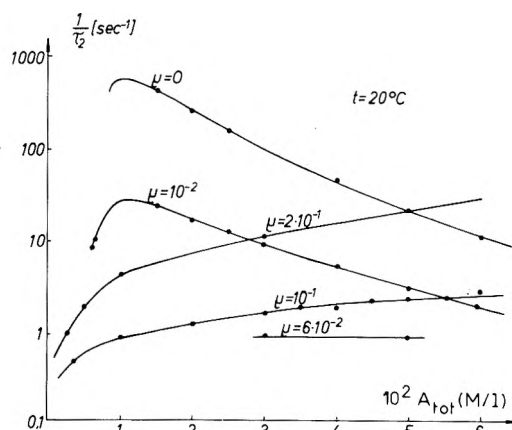
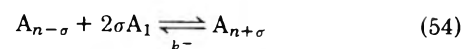


Figure 12. Semilog plot of $1/\tau_2$ vs. A_{tot} for SDS at 20 °C and different concentrations of added NaCl.

m of carbon atoms of the hydrophobic tail. Thus, the micelles appear to become more monodisperse with increasing m and size (n). It is interesting to note that the absolute values of σ agree fairly well with values that have been estimated from theoretical considerations by Tanford.⁸

It is also worth noting that the theory that was proposed by Graber and Zana^{20b} to explain sound absorption data for potassium alkyl carboxylate solutions gives the correct values of σ even though the model used by these authors was oversimplified in comparison to the one presented in this paper. The interpretation of the data was based on the reaction



for which the authors derived the following expression of the relaxation time:

$$\frac{1}{\tau_1} = k^- \left(1 + \frac{\sigma^2 A_{exc}}{n \bar{A}_1} \right) \quad (55)$$

TABLE IV: Values of the Kinetic Parameters, Aggregation Numbers, Distribution Widths, and cmc's for Sodium Alkyl Sulfates at 25 °C

Surfactant ^a	$k^-/n, s^{-1}$	$k^-/\sigma^2, s^{-1}$	\bar{n}	σ	cmc, M	k^-, s^{-1}	$k^+, M^{-1} s^{-1}$
NaC ₆ SO ₄ ^b	7.8×10^7	3.8×10^7	17	6	0.42	1.32×10^9	3.2×10^9
NaC ₇ SO ₄ ^b	3.3×10^7	6.9×10^6	22	10	0.22	7.3×10^8	3.3×10^9
NaC ₈ SO ₄ ^b	3.7×10^6		27		0.13	1.0×10^8	7.7×10^8
NaC ₉ SO ₄ ^b	4.2×10^6		33		6×10^{-2}	1.4×10^8	2.3×10^9
NaC ₁₀ SO ₄ ^b	2.2×10^6		41		3.3×10^{-2}	9×10^7	2.7×10^9
(40 °C)							
NaC ₁₁ SO ₄	8.2×10^5		52		1.6×10^{-2}	4×10^7	2.6×10^9
NaC ₁₂ SO ₄	1.65×10^5	6×10^4	64	13	8.2×10^{-3}	1.0×10^7	1.2×10^9
NaC ₁₄ SO ₄	1.2×10^4	2.8×10^3	80	16.5	2.05×10^{-3}	9.6×10^5	4.7×10^8
NaC ₁₆ SO ₄	6×10^2	5.5×10^2	100	11	4.5×10^{-4}	6×10^4	1.3×10^8
(30 °C)							

^a C_m refers to a hydrophobic tail C_mH_{2m+1} containing *m* carbon atoms. ^b The data relative to these detergents have been taken from ref 18 and 19 or calculated from the original data reported in these works.

Clearly this expression becomes identical with eq 14 when k^- is replaced by k^-/σ^2 . The concept that upon perturbation micelles of size $n + \sigma$ disappear and new ones of size $n - \sigma$ are formed is included in reaction 54. The shortcoming of this model was, of course, that this was formulated to happen in one step while it really occurs in about σ^2 steps.

For a given ionic surfactant, the dispersity broadens with increasing temperature as can be seen from Figure 13 where $[(1/\tau_1)/(k^-/\sigma^2)] - 1$ has been plotted against A_{exc}/A_1 . The slope of the curve gives directly σ^2/n . The reason for the increase of σ^2/n with temperature is not completely clear at present. It seems likely however that σ^2/n decreases with increasing surface charge density of the micelle. Indeed micelles with a lower surface charge density, such as, alkylpyridinium iodides where the iodide strongly interacts with the pyridinium ion, have larger σ^2/n values than the other ionic micelles where the charge transfer interaction is absent.²⁴ In the absence of charge effects the equilibrium constants for the successive steps (reactions 1) are probably very close. This results in a broader distribution curve than in the case where charge effects tend to minimize the equilibrium constants for small aggregates thereby resulting in a narrower distribution curve. These considerations make it understandable that any increase of interaction between the counterions and the ionic head groups by either special charge transfer effects or reduction of dielectric constant upon a temperature increase should have the same effect on σ^2/n .

With the available information on k^+ and σ that has been obtained for the most probable micelles it is also possible to obtain some information about micelles with intermediate aggregation numbers. Because the distribution curve is of considerable width it is clear that the ratio \bar{A}_n/\bar{A}_{n-1} which is equal to $K_n \bar{A}_1$, changes only slightly from unity for different aggregates at the distribution maximum. This means that the equilibrium constant K_n for the individual steps can also change no more than a few percent. Furthermore it is likely that the recombination rate constants k_s^+ for the different aggregates A_s are close to that for the most probable micelles because the incorporation of a monomer in the more loosely packed micelle cannot be more hindered than in the average size micelle that is more tightly packed. The consequence then would be that the k_s^- values also would have to be about the same for the intermediate micelles and the k_s^-/s values have to decrease as the number of monomers in the micelle increases. In other words, the lifetime of a monomer in a micelle de-

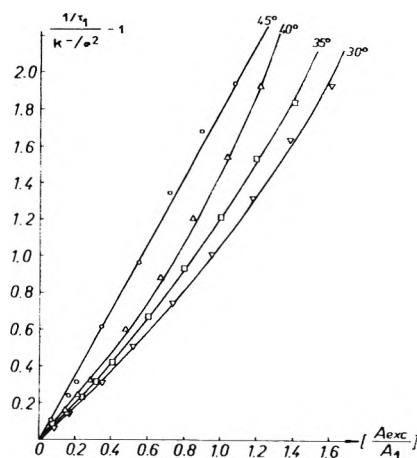


Figure 13. Plot of $[(1/\tau_1)/(k^-/\sigma^2)] - 1$ vs. a for SHS at different temperatures.

pends on the aggregation number s of the micelle. It increases linearly with s .

This behavior is exactly opposite to what has been assumed by Sams, Rassing, and Wyn-Jones¹⁹ in their interpretation of ultrasonic absorption data on sodium alkyl sulfates.

(c) Discussion of the k^-/n Values. The theoretical expression of k^-/n can readily be obtained from eq 50 where ϵ is the change in total free energy from a state where the monomer is in its lowest energy in the micelle, i.e., the hydrophobic tail is completely incorporated, to a state where the monomer is almost completely free. ϵ is the sum of a hydrophobic energy ϵ_H and an electrostatic energy ϵ_E . Several studies have shown that ϵ_H increases linearly with the number m of carbon atoms.¹⁵ On the other hand, Tanford's calculations⁸ indicate that ϵ_E depends on m but is small relative to ϵ_H . These conditions are close to those for having a potential free energy $V(x)$ varying linearly with x (see section II4) and thus l_b should be practically independent of m . On the other hand, it has been pointed out in the theoretical section that D_m is close to the diffusion coefficient of the free detergent ion. Thus, D_m is proportional to the limiting equivalent conductivity λ_m^0 of the detergent ion. Therefore a plot of $\log k^-/n\lambda_m^0$ vs. m should yield a straight line. Figure 14 shows that this prediction is fulfilled both for potassium alkylcarboxylates and sodium alkyl sulfates. The slope of this line is about 0.5. This value is very close to that which can be calculated by taking¹⁵

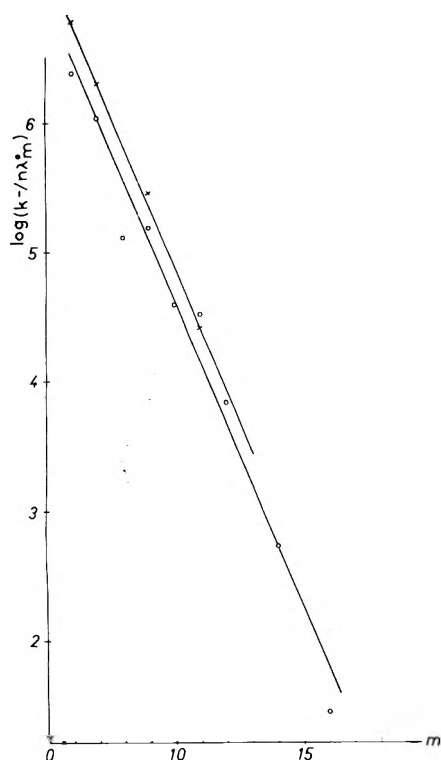


Figure 14. Plot of $\log(k^-/n\lambda_m^\circ)$ vs. the number m of carbon atoms of the hydrophobic tail for sodium alkyl sulfates (O) and potassium alkyl carboxylates (X). These last results are from the data reported in ref 20.

$$\epsilon \approx \epsilon_H = \text{constant} + 1.15kT(m - 1)$$

This result a posteriori confirms Tanford's calculations that

$$|\epsilon_H| \gg |\epsilon_E|$$

(d) *Thermodynamics of the Exchange Process.* The results presented in section IV1a have clearly shown that the exchange process is diffusion controlled. Therefore in Figure 7, the free energy of activation for the association reaction should essentially be due to the change of the viscosity of water with temperature, in addition to the free energy term Δ mentioned in section II4 and which has been found to be small.

Free Energy Change. The equilibrium constant for the exchange process, expressed in liter per mole of detergent, is given by

$$K = \frac{k^+}{k^-/n} \approx \frac{n}{A_1} \approx \frac{n}{\text{cmc}} \quad (56)$$

The factor n has been introduced to account for the fact that there are n possibilities for the dissociation of one detergent ion from the micelle of aggregation number n .

For neutral detergents, the rate constants k^+ and k^- are given by eq 50 and 52. In the case of a charged surfactant, eq 52 must be modified because the monomer has to overcome an electrostatic repulsion during its approach to the micellar surface. The rate constant k^+ can then be approximated by

$$k^+ = \frac{D_m}{l_b} \frac{N_A}{1000} \alpha S_{(s-1)} e^{-\epsilon_1/RT} \quad (57)$$

where ϵ_1 is the electrostatic free energy for the transfer of a monomer from infinite dilution to the surface of the mi-

celle (see Figure 7). The factor $N_A/1000$, where N_A is Avogadro's number, has been introduced to express k^+ in $\text{mol}^{-1} \text{s}^{-1}$. Note that eq 57 is strictly valid only for small concentrations. For higher concentrations, Debye-Hückel terms that account for the shielding of the micellar charge through ionic strength would have to be included.

From eq 50 and 57, with $s = n$ and assuming $l_0 = l_b$, one obtains

$$K = \frac{S_{(n-1)} l_b \alpha N_A}{1000} \exp[(\epsilon - \epsilon_1)/RT] \quad (58)$$

Thus, the total free energy change ΔG for the incorporation of one detergent ion is given by

$$\Delta G = -RT \ln K = -RT \ln \frac{S_{(n-1)} l_b \alpha N_A}{1000} - (\epsilon - \epsilon_1) \quad (59)$$

$S_{(n-1)}$ is the surface area of the micelle with the aggregation number $n - 1$. Calculations performed with the assumption that the radius of this micelle is close to the length l of the hydrophobic tail, and with $\alpha \approx 1$ and $l_b \approx 1.1 \text{ \AA}$ indicate that the first term on the right-hand side of eq 59 is small as compared to ΔG (see Table V). It is understood however that because the radius of the micelle depends on m , this term can change with chain length. The actual change appears to be not more than $2RT$ when m is increased from 6 to 16 (see Table V).

It is possible to determine $\epsilon_E + \epsilon_1$ from the difference between ΔG and ϵ_H for different m values. These values have been calculated and are given in Table V. They indicate an increase of $\epsilon_E + \epsilon_1$ from $m = 6$ to $m = 16$. It is likely that most of this energy is associated with ϵ_1 and that ϵ_E is rather small. The explanation for it may be that the average distance of the head group to the micelle center does not change much during the dissociation process. This can also be inferred from measurements on the effect of added NaCl on τ_1 . As seen from Figure 15 both k^-/σ^2 and k^-/n are affected only slightly by addition of 0.01 M NaCl to SDS solution, while the effect on the cmc and on k^+ seems to be more marked. Unpublished results on potassium decanoate show the same behavior.

Enthalpy Change. Expressing ϵ as

$$\epsilon = \Delta H - T\Delta S \quad (60)$$

and assuming for D_m an Arrhenius-type temperature dependence

$$D_m = D_m^\circ e^{-\Delta H_D/RT} \quad (61)$$

eq 50 becomes

$$\frac{k^-}{n} = \frac{D_m^\circ}{l_b^2} e^{\Delta S/R} e^{-(\Delta H + \Delta H_D)/RT} \quad (62)$$

This equation predicts a linear variation of $\ln(k^-/n)$ with $1/T$, as is experimentally found (see Figure 16). The slope of the lines in Figure 16 give the sum $(\Delta H + \Delta H_D)$. The value of ΔH_D can be determined independently from the temperature dependence of D_m and thus ΔH can be calculated. The values are given in Table VI. Strictly speaking the ΔH 's are activation enthalpies. However when considering the meaning given to ϵ it is clear that the ΔH 's also represent the enthalpy change for the transfer of a detergent molecule or ion from the micellar surface to the micellar interior. This quantity is very close to that for the transfer of the same molecule or ion from the bulk of the solution to the interior of the most stable micelle. It is noteworthy that the ΔH values are directly derived from

TABLE V: Thermodynamic Quantities (in kcal/mol of Monomer) for the Incorporation of a Monomer into Sodium Alkyl Sulfate Micelles

m	ΔG^a	$RT \ln S_{(s-1)}$	ϵ_H^c	$\epsilon_E + \epsilon_s$
		$\times l_b \alpha N_A^b$		
		10^3		
6	-2.2	-0.2	-5.5	3.1
8	-3.2	0.05	-6.9	3.75
10	-4.3	0.3	-8.3	4.3
12	-5.4	0.5	-9.7	4.8
14	-6.4	0.7	-11.1	5.4
16	-7.4	0.85	-12.5	5.95

^a Calculated according to eq 56 and 59. ^b Calculated with the assumption that $\alpha \cong 1$ and $l_b \cong 1.1$ Å. The surface area $S_{(s-1)}$ has been set equal to $4\pi l^2$, where the length l of the hydrophobic tail is given by l (Å) = $1.5 + 1.265m$ (see C. Tanford, *J. Phys. Chem.*, 76, 3020 (1972)). ^c Calculated according to eq 11 in C. Tanford, *J. Phys. Chem.*, 78, 2469 (1974). The positive sign is due to the fact that in the theory of section II4, ϵ corresponds to the free energy of dissociation while Tanford's equation gives the free energy of association.

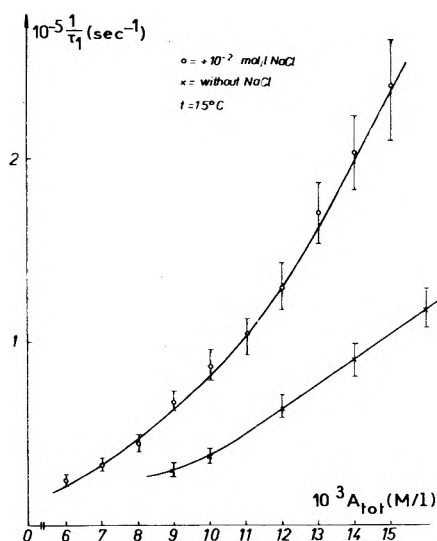


Figure 15. Plot of $1/\tau_1$ vs. A_{tot} for SDS at 15 °C with and without added NaCl.

k^-/n values that have been obtained experimentally. There is evidence that n changes with temperature^{25,26} but this change is already contained in the k^-/n values.

The ΔH values are composed of a hydrophobic and an electrostatic part. The results of Figure 14 indicate that the electrostatic contribution to ϵ is small and it is therefore likely that the electrostatic contribution (ΔH_E) to ΔH is small also, if not completely negligible. Therefore ΔH essentially represents the hydrophobic contribution to the heat of reaction for the incorporation of a detergent ion to a stable micelle. The results of Table VI show that ΔH increases linearly with m .

As seen from the Table VI, the incorporation process is exothermic which may, at first sight, look rather surprising because it is known²⁷ from calorimetric measurement that the heat of micelle formation (ΔH_M) for the overall process is small and sometimes even endothermic. Note however that ΔH_M is an average heat of formation, the averaging being done on the heat of each elementary step of association ΔH_s of one detergent ion to a micelle A_s . There is thus

TABLE VI: Thermodynamic Parameters (kcal/mol) for the Formation of the Nucleus (subscript N)^a and the Transfer of a Monomer from the Surface of the Micelle into the Micelle (no Subscript) for Sodium Alkyl Sulfates

m	ΔG_N^b	ΔH_N^c	$T\Delta S_N$	ϵ^d	ΔH^e	$T\Delta S$
8					-1.6 ^f	
12	-7.6	33	40.6	-7.5	-4.3	3.2
14	-11.2	33	44.2	-9.1	-5.2	3.9
16	-17.7	30.5	48.2	-10.9	-7.5	3.4

^a The values of the thermodynamic parameters for the nucleus formation are expressed in kilocalories per mole of nucleus. The nucleus contains about seven monomers for SDS and STS. The other quantities are in kilocalories per mole of monomer. ^b Calculated from $(\Delta G_N = -RT \ln \bar{A}_r/\bar{A}_r^r)$. The values of R are those determined in section IV2a. The values of \bar{A}_r are calculated according to eq 28 with $l \cong 1$ and $k_s^- \cong k^-$. It has also been assumed that $r = 7$ for SHS. ^c Calculated from the slope of the plot of $\ln(1/\tau_2)$ vs. $1/T$. ^d Calculated from eq 50 using the k^-/n values of Table IV and $l_0 \cong l_b \cong 1.1$ Å and $D_m = 2.66 \times 10^{-7} \lambda_m^0$ (R. A. Robinson and R. H. Stokes, "Electrolyte Solutions", 2nd ed, Butterworths, London, 1970, p 317). ^e Calculated from the slopes of the lines of Figure 16, and using the value $\Delta H_D = 4.2$ kcal/mol, obtained from the data listed by G. S. Kell, *Water, Compr. Treatise*, 1, 404 (1972). A correction of 0.6 kcal/mol has been made to the slopes to account for the fact that we have plotted $\log k^-/n$ instead of $\log k^-/nT$ vs. $1/T$ on Figure 16. ^f Value calculated from the ultrasonic absorption data in ref 19.

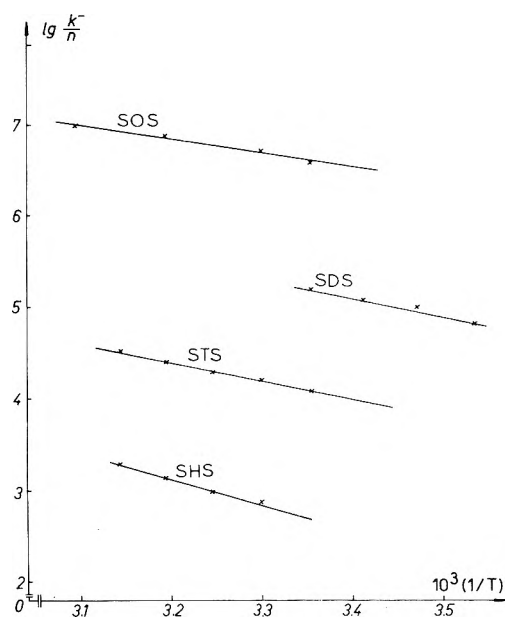


Figure 16. Plot of $\log(k^-/n)$ vs. $1/T$ for several sodium alkyl sulfates.

a basic difference between ΔH , as obtained in this work, and ΔH_M .

The question which then arises is that of the nature of the other processes with an endothermic heat of reaction, which balance the exothermic heat of reaction for the incorporation of a detergent ion into a stable micelle. Such processes cannot be due to counterion "binding" to the micelle surface. Indeed the electrostatic energy associated with this binding is largely compensated by that involved in the approach of a detergent ion to the micelle surface. One is thus led to assume that the value of ΔH must depend very much on s and can even change sign. In fact, as

will be shown below, the reaction of formation of very small aggregates is endothermic. It is then clear that the association reactions (1) are characterized by positive ΔH values that become smaller with increasing s and finally negative for the stable micelles. The average of all these individual contributions (ΔH_M) is close to zero, sometimes slightly positive or slightly negative, as indicated by the temperature dependence of the cmc.

Additional experimental evidence strongly supports our contention of the existence of fairly large ΔH 's for the association steps at the maximum and minimum of the distribution curve. This evidence is found in the fact that a T-jump can give rise to large perturbations of micellar equilibria. (In ref 1, results were reported showing that T-jumps as small as 0.1 °C still result in detectable relaxation signals). After recalling that a T-jump results in the perturbation of chemical equilibria only if those are accompanied by nonnegligible enthalpy changes, one is led to the conclusion that indeed sizable ΔH 's must be associated with micellar association steps.

The consequence of a negative ΔH and a small ΔH_E is that the equilibrium constant $K_s = k_s^+/(k_s^-/s)$ for a given s is decreasing with increasing temperature. From the temperature dependence of the cmc, on the other hand, we know that K/n changes very little. It must therefore be concluded that n decreases with increasing temperature, in agreement with previous results by other techniques.^{25,26}

2. *The Slow Process.* The slow relaxation process has been observed only with jump techniques and detergents with ten or more carbon atoms. In all sound absorption measurements only the fast process was detected. On the basis of the above theory and the experimental evidence for long chain detergents, the slow process must also be present for shorter detergents. This process may be more difficult to detect because its amplitude may be very small. Also for shorter detergents the relaxation times τ_1 and τ_2 may be much closer than for long chain detergents and it may become difficult to separate the two processes in the case of sound absorption data. The amplitude of the ultrasonic relaxation should show the same concentration dependence as p-jump relaxation amplitudes because for both methods the amplitudes are related to the volume change ΔV of the process. The relaxation amplitude as measured by the p-jump with a conductivity readout shows a sharp maximum at about 1.2–1.3 cmc, and the effect practically disappears at about twice the cmc. For this reason the sound absorption data should be carefully analyzed close to the cmc for the existence of a second relaxation process. Unfortunately, this is the concentration range where, for most of the systems, few measurements have been carried out. However, based on the available data for long chain detergents it is possible to extrapolate τ_2 values for short detergents from the $1/\tau_2$ plot against the number of carbon atoms m (see Figure 17).

(a) *Counterion Dependence of τ_2 .* As shown in Figure 18, the values of τ_2 are extremely sensitive to a change in added salt concentration. For both SDS and STS at a given A_{tot} a tenfold increase of τ_2 resulted from an addition of NaCl at a concentration c_{NaCl} equivalent to the cmc of the salt-free detergent. The fact that the change of τ_2 is not proportional to c_{NaCl} but rather to the ratio c_{NaCl}/cmc is indicative that the change of τ_2 is not directly a consequence of a salt effect in which a particular rate constant for charged particles is affected by the ionic strength. That the situation must be more complicated is also indicated by the

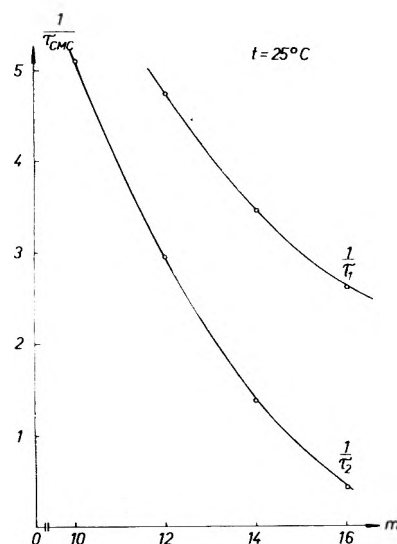


Figure 17. Plot of $\log(1/\tau_1)_{cmc}$ and $\log(1/\tau_2)_{cmc}$ vs. the number m of carbon atoms of the hydrophobic tail for several sodium alkyl sulfates at 25 °C.

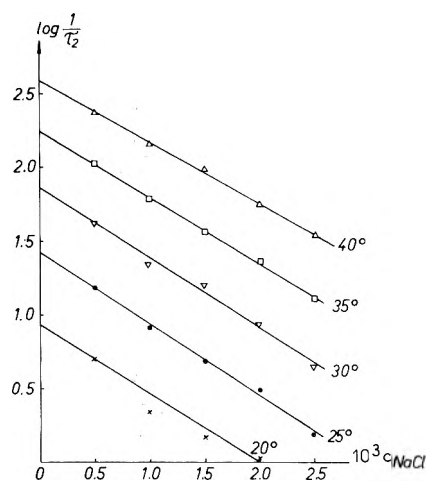


Figure 18. Plot of $\log 1/\tau_2$ vs. the concentration of added NaCl for STS with $A_{tot} = 2.3 \times 10^{-3}$ M at different temperatures.

large change in the relaxation times. Equation 25 can be rearranged to

$$\frac{1}{\tau_2} = \frac{n^2}{R \left[\bar{A}_1 \left(1 - \frac{\sigma^2}{n} \right) + \frac{\sigma^2}{n} A_{tot} \right]} \quad (63)$$

which clearly shows that the large change in $1/\tau_2$ for a given A_{tot} must find its origin in R . Indeed it is known²⁸ that n increases somewhat when c_{NaCl} is raised to 0.1 N. For small additions of NaCl of Figure 18 it can however be assumed that both n and σ^2/n remain approximately constant. Thus the increase of τ_2 can be totally attributed to an increase of R with c_{NaCl} . Seen from Figure 18 the added salt does not affect the temperature dependence of $1/\tau_2$, i.e., of R until the salt concentration reaches fairly high values (>0.05 N).

In addition to the high sensitivity of $1/\tau_2$ to ionic strength, and to A_{tot} and T (as is shown below) it has previously been observed^{1,16} that $1/\tau_2$ also changes drastically if small amounts of other surfactants and impurities are present into the solution. These changes can also be viewed as a change of R .

The results of Figure 18 make it possible to evaluate the average aggregation number r of the micellar species at the minimum of the distribution curve. Indeed, since n and σ^2/n are expected to change only little for the small additions of NaCl involved in Figure 18, one can write for the values of $1/\tau_2$ at two ionic strengths I and II (corresponding to $c_{\text{NaCl}} = 0$ and, e.g., $c_{\text{NaCl}} = 2 \times 10^{-3}$ M), at A_{tot} close to the cmc

$$\frac{(1/\tau_2)_I}{(1/\tau_2)_{II}} \simeq \frac{R_{II}(\bar{A}_1)_{II}}{R_I(\bar{A}_1)_I} \simeq \frac{(k_r^- \bar{A}_r)_I(\bar{A}_1)_{II}}{(k_r^- \bar{A}_r)_{II}(\bar{A}_1)_I} \quad (64)$$

where the last step follows from eq 28, assuming that the length of the narrow passage and the value of r do not depend on c_{NaCl} at the very low ionic strengths used in these experiments. For such very small changes of ionic strength one should also expect a negligible variation of k_r^- , because the dissociation rate constant does not show any extreme dependence on aggregation number (see end of section IV1b) or T . Therefore, to a first approximation one has $(k_r^-)_I = (k_r^-)_{II}$. It is thus clear that the sensitivity of τ_2 on c_{NaCl} results from that of \bar{A}_r . On the other hand, since all reaction steps such as reaction 1 obey the mass action law, one can write

$$\bar{A}_r = \frac{f_1^r}{f_r} \bar{A}_1^r \prod_{i=2}^r K_i^* \quad (65)$$

where $\prod_{i=2}^r K_i^*$ is the overall equilibrium constant at zero ionic strength and f_1 and f_r the activity coefficients of A_1 and A_r . The equation makes it clear that every effect that changes \bar{A}_1 causes a change in \bar{A}_r that is proportional to the i th power of the change of \bar{A}_1 . The large change of τ_2 with the added NaCl can thus be simply explained. The combination of eq 64 and 65 results in

$$\frac{(1/\tau_2)_I}{(1/\tau_2)_{II}} = \frac{(\bar{A}_1^{r-1})_I (f_1^r/f_r)_I}{(\bar{A}_1^{r-1})_{II} (f_1^r/f_r)_{II}} \quad (66)$$

The activity coefficients can be calculated using the extended Debye-Hückel or Fuoss equations. However, for a rough estimation of r and small c_{NaCl} the activity coefficients may be set equal to 1 so that eq 66 yields

$$r - 1 = \frac{\log [(1/\tau_2)_I / (1/\tau_2)_{II}]}{\log [(\bar{A}_1)_I / (\bar{A}_1)_{II}]} \quad (67)$$

The values of $1/\tau_2$ at the chosen ionic strengths I and II can be taken from the results of Figure 18. On the other hand, the logarithm of the cmc is known²⁹ to vary linearly with the logarithm of the counterion concentration, and thus $\bar{A}_1 \simeq \text{cmc}$ can be obtained at any value of the ionic strength. For SDS and STS, using data at $c_{\text{NaCl}} = 0$ and $c_{\text{NaCl}} = 2 \times 10^{-3}$ M, we found $r \simeq 7$.

(b) *Concentration Dependence of τ_2* . Using the values of σ and n from Table IV, the "resistance" R can be determined from the τ_2 values for various concentrations using eq 68 obtained from eq 18, assuming that only monomers are present in region 1.

$$\frac{1}{\tau_2} \simeq \frac{1}{Rc_3} \frac{\bar{A}_1 + n^2c_3}{\bar{A}_1 + \sigma^2c_3} \quad (68)$$

The values of R for SDS are given in Tables VII and VIII. R is not constant but first decreases and then increases with increasing A_{tot} . Thus, the $1/\tau_2$ values fall off faster with A_{tot} than they would for a constant R . It could of course be argued that the falloff is really caused by an increase of σ . This is unlikely, however, because σ would have to increase unrealistically much to account for the

data. The σ^2/n values depend only slightly on A_{tot} as we have seen from τ_1 . This leaves no doubt that R really is increasing with A_{tot} . This increase can be understood in the same manner as the change of R with ionic strength. When A_{tot} is increased above the cmc, micelles are formed from which counterions are partially dissociated. As a consequence the concentration of Na^+ ions increases with A_{tot} which in turn lowers the cmc, increases R and reduces $1/\tau_2$.

The data would make it possible to calculate cmc values and hence \bar{A}_1 values for different A_{tot} values above the cmc. This effect causes $1/\tau_1$ to rise faster than expected from eq 14 and thus may explain the deviation from a straight line in the $1/\tau_1$ vs. A_{tot} plots. The conclusion that \bar{A}_1 is decreasing above the cmc with A_{tot} has already been proposed by other workers from other evidence.³⁰ Nevertheless, the fact is not commonly accepted. Very recently, Tanford⁸ in a detailed theoretical treatment of the micelle formation assumed an increase of \bar{A}_1 with A_{tot} . Our data provide convincing evidence that the reverse is true.

(c) *Temperature Dependence of τ_2 , and Thermodynamics of the Micellization-Dissolution Process*. The temperature dependence of τ_2 was found to be unusually strong for a relatively fast process, and to be practically independent of A_{tot} . This appears to indicate that it arises from R . Actually, the sensitivity of R to temperature is even somewhat higher than expressed by τ_2^{-1} , because at A_{tot} close to the cmc, eq 63 yields

$$R = n^2/\bar{A}_1\tau_2^{-1} \quad (69)$$

and n^2/\bar{A}_1 decreases with increasing temperature at least for SDS.²⁵ The temperature dependence of R and thus of τ_2^{-1} can easily be explained. Indeed, when using the approximate expression 28 for R and expression 65 for \bar{A}_r , it becomes clear that only modest temperature dependences of the individual K values are required to lead to a dramatic change of \bar{A}_r , even when \bar{A}_1 is kept constant. The use of eq 28 and 65 also shows that the temperature dependence of τ_2^{-1} gives a quantity which is close to the total heat of formation of the aggregate A_r at the minimum of the distribution curve. This aggregate can be called the nucleus for micelle formation because, kinetically speaking, it is the first one that is large enough to have a better chance to grow than to dissociate back into monomers. The equilibrium constants for aggregates smaller than the nucleus are smaller than K_r at the nucleus, which is equal to $1/\text{cmc}$. The equilibrium constants increase rather rapidly with T and shall successively reach the values of $1/\text{cmc}$ which is also increasing with T but not as fast. It follows therefore, that the critical size of the nucleus is decreasing with increasing T . In the extreme, the size of the nucleus can only be reduced to two monomers. This state is probably being approached for high temperatures. At each temperature where the nucleus becomes smaller, the heat of reaction and hence the temperature dependence of $1/\tau_2$ should decrease. Unpublished measurements do indeed show that the temperature dependence for high temperatures is lowered in comparison to low temperatures. When the size of the nucleus is reduced, the A_{tot} dependence for a given temperature is also affected.

The thermodynamic quantities that have been evaluated for the studied systems are listed in Table VI. The values of the enthalpy of formation of the nucleus, ΔH_N , are large because they correspond to a reaction which involve several ($r = 7$) detergent ions. The most striking fact however is

TABLE VII: Values of R for SDS as Determined from the Relaxation Times τ_2 Assuming $n = 64$, $\sigma = 13$, and $\text{cmc} = 8.3 \times 10^{-3} \text{ M}$ at 20°C

$10^2 A_{\text{tot}}, \text{M}$	0.9	1	1.2	1.4	2	2.5	3	4	7
$R, \text{s M}^{-1}$	960	630	470	400	400	525	570	990	3430
$10^5 c_3, \text{M}$	1.1	2.65	5.8	8.9	18.7	26	34	49.5	96

TABLE VIII: Values of R for SDS ($A_{\text{tot}} = 1.2 \times 10^{-2} \text{ M}$) for Different Temperatures

$t, ^\circ \text{C}$	25	20	15	10	5
$R, \text{s M}^{-1}$	180	470	1190	3640	9850
$R, \text{s M}^{-1}$	165	470	1280	4450	13100

^a Assuming constant n and σ values. ^b Assuming n and σ values that change somewhat with temperature.

that the ΔH_N values are all positive. We realize that the calculations which have led to these values are only semi-quantitative but the approximations involved do not affect the sign of the calculated values. On the other hand, it is likely that these values do not change abruptly in sign and magnitude when aggregates larger than the nucleus are considered. It is therefore realistic to assume that the further steps of growth of the nucleus are also endothermic. On the other hand, we have obtained negative enthalpy of association (ΔH) of a monomer to the stable micelles. The results therefore indicate that aggregation starts with positive enthalpy of association that becomes smaller with increasing size of the aggregates. At intermediate aggregation number the enthalpies of association are close to zero and finally for the stable micelles the enthalpies of association are negative. As a consequence the total heat of reaction for micellization is rather small as shown by calorimetric measurements.¹⁵ At the present time we can offer no quantitative explanation of the change of ΔH with aggregate size. It is likely, however, that the decrease of the surface to volume ratio upon growth of the aggregate, and changes in the packing of solvent and solute molecules as the aggregate grows, must be involved in this change.¹⁶

(d) *Change of $1/\tau_2$ at High Concentration of NaCl.* For sodium alkyl sulfates, at a given A_{tot} , $1/\tau_2$ was always found to decrease with increasing c_{NaCl} , as long as $c_{\text{NaCl}} < 0.03 \text{ M}$. For higher c_{NaCl} , $1/\tau_2$ starts rising again. Two antagonistic effects are probably responsible for this behavior. The decrease of $1/\tau_2$ can be explained by a lowering of the cmc with increasing c_{NaCl} . Indeed, one has

$$\frac{1}{\tau_2} \propto \frac{1}{R \bar{A}_1} \propto \bar{A}_1^{r-1} \quad (70)$$

However, the cmc keeps decreasing with increasing c_{NaCl} when $1/\tau_2$ is already increasing. The first effect must therefore be overcompensated by a second one at higher c_{NaCl} . The upward trend of $1/\tau_2$ could be thought of as being caused by the increase of n with c_{NaCl} .³⁰ However in the case of SDS, the values of n that have been determined for different c_{NaCl} do not permit a quantitative prediction of the increase of $1/\tau_2$ and this explanation must be discarded. A more likely explanation is that micelles are formed via a different type of nucleus at high c_{NaCl} . Indeed at low salt concentration the nucleus is probably completely dissociated. As the salt concentration is increased, it becomes likely that the charge of the nucleus will be partly compensated by the binding of counterions. At the same time the size of the nucleus may change from r to r' . The concentration of this new nucleus $A_{r'}$ in R is given by

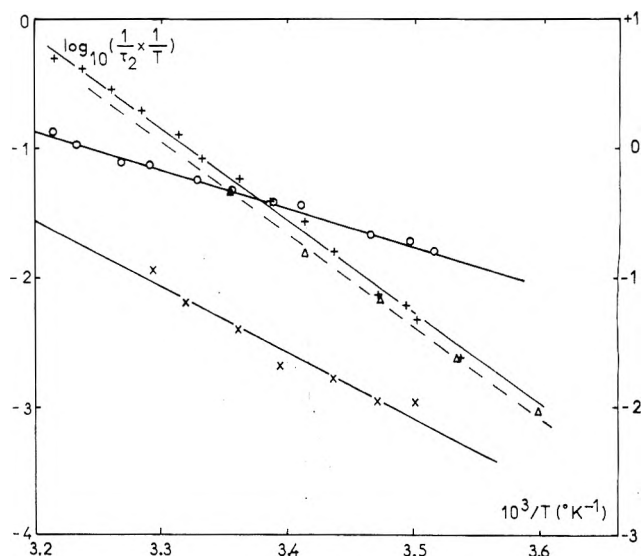


Figure 19. Plot of $\log [(1/\tau_2)(1/T)]$ vs. $1/T$ for SDS in the absence of NaCl, (Δ) $A_{\text{tot}} = 1.4 \times 10^{-2} \text{ M}$, and (+) $7 \times 10^{-2} \text{ M}$; (X) at ionic strength 0.06 M NaCl ($A_{\text{tot}} = 0.025 \text{ M}$); and (O) at ionic strength 0.2 M NaCl ($A_{\text{tot}} = 0.025 \text{ M}$). The relaxation times are in s^{-1} . The right ordinate scale is relative to the results in the absence of NaCl and $A_{\text{tot}} = 1.4 \times 10^{-2} \text{ M}$, and which have been obtained by p-jump. All other results have been obtained by T-jump.

$$\bar{A}_{r'} = K_{r'} \bar{A}_1^{r'} c_{\text{Na}}^\beta \quad (71)$$

where β is the number of counterions bound on the nucleus $\bar{A}_{r'}$ and $K_{r'}$ is the equilibrium constant for the association reaction of r' monomers and β counterions. The increase of c_{Na} may easily overcompensate the decrease of \bar{A}_1 upon increasing c_{NaCl} .

The temperature dependence of τ_2^{-1} has been investigated for SDS at various ionic strengths (see Figure 19). The value of ΔH_N was thus found to decrease from 33 kcal/mol in the absence of NaCl to 13 kcal/mol at $c_{\text{NaCl}} = 0.2 \text{ M}$. In view of this result, it is likely that the size of the nucleus is reduced upon increasing c_{NaCl} .

(e) *Ratio of the Two Relaxation Times at the cmc.* Equations 14 and 18 now become

$$(1/\tau_1)_{\text{cmc}} = k^-/\sigma^2$$

and

$$(1/\tau_2)_{\text{cmc}} = 1/Rc_3 \quad (72)$$

Using eq 22 and the approximate equation

$$R = 1/k^- \bar{A}_r$$

with

$$\bar{A}_r = A_0 e^{-\frac{(n-r)^2}{2\sigma^2}}$$

and

$$A_0 = \frac{A_{\text{exc}}}{n} \frac{1}{\sqrt{2\pi}\sigma}$$

one obtains

$$\left[\frac{1/\tau_1}{1/\tau_2} \right]_{\text{cmc}} = \frac{\sqrt{2\pi}}{\sigma} \exp \frac{(n-r)^2}{2\sigma^2} \quad (73)$$

For a given chain length the ratio of the two reciprocal relaxation times can decrease or increase with increasing temperature, depending on the change of $(n-r)/\sigma$ with T .

On the other hand, Figure 17 shows that $(1/\tau_1)/(1/\tau_2)$ increases with chain length which indicates according to eq 73 that $(n-r)/\sigma$ increases with chain length. In a first approximation this may be taken as indicating that r does not drastically change with chain length.

Conclusions

The complex concentration, temperature, hydrophobic tail length, and counterion dependence of the two relaxation times that have been observed in micellar solutions of sodium alkyl sulfates can be quantitatively understood on the basis of the theory developed by Aniansson and Wall. The theory has been used to obtain kinetic and thermodynamic information that were thus far not available and could not be obtained by other methods.

The following parameters have been determined for several systems; n/k^- , the lifetime of a surfactant molecule in the micelle; σ , characteristic width of the micellar distribution curve; ΔH , ΔS , reaction enthalpy and entropy for the incorporation of a monomer from the aqueous phase into the stable micelles; r , the aggregation number of the aggregate at the distribution minimum; \bar{A}_r , the concentration at the distribution minimum; $\Delta G_N, \Delta S_N, \Delta H_N$, thermodynamic quantities for the formation of the aggregate at the minimum of the distribution curve (nucleus of the micelle).

Acknowledgments. H.H., I.K., and W.U. thank the Deutschen Forschungsgemeinschaft (DFG) for a research grant in support of this work and the Fa. Henkel and Cie GmbH, Düsseldorf, for the donation of the surfactants used in this investigation. R.Z., J.L., and C.T. thank the DRME for its financial support of part of this work.

Appendix I. List of Symbols

cmc	critical micellization concentration
A_1	free surfactant molecule or ion (monomer); A_1 , concentration of free surfactant.
A_s	aggregate or micelle containing s surfactant molecules or ions; A_s , molar concentration of this aggregate
A_{tot}	$(= A_1 + \sum s A_s)$ total surfactant concentration expressed in mole of surfactant per liter
A_{exc}	$(= A_{\text{tot}} - \bar{A}_1)$ concentration of micellized surfactant in mole of surfactant per liter
a	$(A_{\text{exc}}/\bar{A}_1)$
ξ_s	relative deviation from equilibrium for the concentration of aggregate A_s , following a perturbation
s, j	aggregation number
$n = \bar{n}_3$	average aggregation number
r	value of s at the minimum of the distribution curve
σ	width of the micellar distribution curve
k_s^+	association rate constant of a surfactant molecule to aggregate A_{s-1}

k_s^-	dissociation rate constant of a surfactant molecule from the aggregate A_s
k^+, k^-	association and dissociation rate constants in the region of proper micelle (independent of s)
J_s	net number of aggregate passing per unit time from aggregation number $s-1$ to s
D	diffusion constant
l	length of the narrow passage (eq 23); total length of the hydrophobic tail of the surfactant molecule (sections II4 and IV)
x	coordinate along the tube of the diffusion analog of the slow process; length of the hydrophobic tail outside the micelle (section II4)
Δ	free energy decrease per monomer due to the increased freedom of a monomer dissociating from the micelle and of the remaining hydrophilic head groups in the micelle
$V(x)$	free energy involved in the dissociation of a monomer from the micelle
ϵ	maximum value of $V(x)$: $\epsilon = V(x)_{x=l}$
ϵ_H, ϵ_E	contributions of hydrophobic and electrostatic interactions to ϵ
ϵ_1	free energy for the transfer of a monomer from infinite distance to the micelle, to a state where the tip of its hydrophobic tail is in contact with the micellar surface
ΔG	total free energy for the incorporation of one detergent ion to the most stable micelle
$\Delta H, \Delta S$	enthalpy and entropy changes for the incorporation of one detergent ion to the most stable micelle
$\Delta G_N, \Delta H_N, \Delta S_N$	analog quantities for the formation of the aggregate at the minimum of the distribution curve (nucleus). These quantities are expressed in kcal/mol of nucleus
l_b	width of the free energy barrier for the dissociation process kT below its maximum value ϵ
D_m	diffusion coefficient of a dissociating monomer. Its value is very close to that of a free monomer and thus proportional to the equivalent conductivity λ_m° of the free monomer.
m	number of carbon atoms of the hydrophobic tail
τ_1, τ_2	relaxation times associated with the fast process and the slow process

References and Notes

- J. Lang, C. Tondre, R. Zana, R. Bauer, H. Hoffmann, and W. Ulbricht, *J. Phys. Chem.*, **79**, 276 (1975).
- E. Wyn-Jones, Ed., "Chemical and Biological Applications of Relaxation Spectrometry", D. Reidel, Dordrecht, Boston, 1975, pp 133-264.
- N. Muller, *J. Phys. Chem.*, **76**, 3017 (1972); E. Cordes, Ed., "Reaction Kinetics in Micelles", Plenum Press, New York, N.Y., 1973.
- T. Nakagawa, *Colloid Polym. Sci.*, **252**, 56 (1974).
- (a) E. A. G. Aniansson and S. Wall, *J. Phys. Chem.*, **78**, 1024 (1974); (b) *ibid.*, **79**, 857 (1975).
- A. Coleen, *J. Phys. Chem.*, **78**, 1676 (1974). This author assigns the slow process to the "reaction of an aggregate A_i , containing i units of the monomer A with an aggregate A_j , containing j units to form the aggregate A_n where $n = i + j$, n being the average aggregation number". Such a reaction is extremely unlikely however because of (i) the strong electrostatic repulsions between the highly charged particles A_i and A_j ; (ii) the very small concentrations at which these intermediate micelles

- are present within the solution⁷⁻⁸ which would result in negligible relaxation signals; (iii) the very complex reorganization of amphiphilic ions which would be involved in the association of two such intermediates. Note also that the main purpose of Coleen's model was the fitting of the data reported by Krescheck et al.⁹ on laurylpyridinium iodide in the whole concentration range. We have since shown that these data should be reexamined.¹ For all of these reasons we reasonably think that Coleen's interpretation should be discarded.
- (7) C. A. Hoeve and G. C. Benson, *J. Phys. Chem.*, **61**, 1149 (1957).
 - (8) C. Tanford, *Proc. Natl. Acad. Sci. U.S.A.*, **71**, 1811 (1974); *J. Phys. Chem.*, **78**, 2469 (1974); **76**, 3020 (1972).
 - (9) G. C. Krescheck, E. Hamori, G. Davenport, and H. A. Scheraga, *J. Am. Chem. Soc.*, **88**, 246 (1966).
 - (10) E. A. G. Aniansson and S. Wall in ref 2, p 223.
 - (11) G. Arfken, "Mathematical Methods for Physicists", Academic Press, New York, N.Y., 1966.
 - (12) E. A. G. Aniansson, M. Almgren, and S. Wall in ref 2, p 239, and E. A. G. Aniansson in ref 2, p 245.
 - (13) H. A. Kramers, *Physica*, **VII**, 284 (1940).
 - (14) E. A. G. Aniansson, M. Almgren, and S. Wall, unpublished calculations.
 - (15) C. Tanford, "The Hydrophobic Effect", Wiley-Interscience, New York, N.Y., 1973.
 - (16) R. Folger, H. Hoffmann, and W. Ulbricht, *Ber. Bunsenges. Phys. Chem.*, **78**, 986 (1974).
 - (17) C. Tondre, J. Lang, and R. Zana, *J. Colloid Interface Sci.*, **52**, 372 (1975).
 - (18) J. Rassing, P. Sams, and E. Wyn-Jones, *J. Chem. Soc., Faraday Trans. 2*, **70**, 1247 (1974).
 - (19) P. Sams, E. Wyn-Jones, and J. Rassing, *Chem. Phys. Lett.*, **13**, 233 (1972); J. Rassing, P. Sams, and E. Wyn-Jones, *J. Chem. Soc., Faraday Trans. 2*, **69**, 180 (1973).
 - (20) (a) E. Graber, J. Lang, and R. Zana, *Kolloid. Z. Z. Polym.*, **238**, 470 (1970); (b) E. Graber and R. Zana, *ibid.*, **238**, 479 (1970).
 - (21) H. Hoffmann et al., unpublished results.
 - (22) H. Tartar, *J. Colloid. Sci.*, **14**, 115 (1959).
 - (23) A. Campbell and G. R. Laksha-Minarayanan, *Can. J. Chem.*, **43**, 1729 (1965); J. Clunie, J. Goodman, and P. Symons, *Trans. Faraday Soc.*, **63**, 754 (1967); M. Mc Dowell and C. Kraus, *J. Am. Chem. Soc.*, **73**, 2170 (1951).
 - (24) P. Mukerjee and A. Ray, *J. Phys. Chem.*, **70**, 2138, 2144, 2150 (1966).
 - (25) T. Nakagawa and K. Shinoda, "Colloidal Surfactants", Hutchinson and Van Rysselberghe, Ed., Academic Press, New York, N.Y., 1963, p 124.
 - (26) P. Debye, *Ann. N.Y. Acad. Sci.*, **51**, 575 (1949).
 - (27) See ref 25, pp 30-32.
 - (28) K. J. Mysels and L. Princen, *J. Phys. Chem.*, **63**, 1699 (1959).
 - (29) See ref 25, pp 58-62.
 - (30) K. Shirahama, *Bull. Chem. Soc. Jpn.*, **47**, 3165 (1974), and references therein; T. Sasaki, M. Hattori, J. Sasaki, and K. Nukima, *Bull. Chem. Soc. Jpn.*, **48**, 1397 (1975); R. Hautala, private communication.
 - (31) K. Takeda and T. Yasunaga, *J. Colloid Interface Sci.*, **45**, 406 (1973).

Relative Roles of Ensemble Constraints vs. Cross Sections in Hydrogen Dissociation

S. H. Bauer,* D. Hilden,

Department of Chemistry, Cornell University, Ithaca, New York 14853

and Peter Jeffers

Department of Chemistry, State University of New York, Cortland, New York 13045 (Received April 14, 1975; Revised Manuscript Received January 19, 1976)

By extrapolation, values for the *initial* dissociation rate constants of hydrogen, infinitely diluted in inert gases, are now available; a preliminary value for D₂ (in Ar) has also been reported. These results provide idealized cases for computer modeling of the dissociation of a diatomic species in the strictly bimolecular regime, catalyzed by a single collider species and uncomplicated by extraneous reactions. Extrapolated results for pure hydrogen, again at very low levels of dissociation, permit one to inquire whether *v-v* energy transfer rates play a significant role in the currently well-documented discrepancies between the experimental activation energies (*E_a*) and the magnitude of the dissociation energy (*D₀*) as determined from spectroscopic data. We summarized our results in the form of answers to eight specific questions, supported by suitably selected plots which clearly show the evolution of state populations, and the relations between the three time regimes which characterize the drift of a suddenly perturbed system to its equilibrium condition. The following points, although not new to this analysis, are of particular interest: (i) the distinction between the total unidirectional flux coefficient (*κ_d*) and *k_d* is clearly demonstrated; (ii) the system does obey the conventional phenomenological rate equation; (iii) the so called "depletion" of the upper vibrational state populations solely does not account for *E_a* < *D₀*; (iv) the high value reported for *E_a* (H₂ + H₂ → 2H + H₂) provides a supporting argument for the importance of rotation-vibration coupling in the dissociation of highly energized molecules.

Introduction

Conceptually, the simplest collision induced dissociation is that of H₂ via encounters with a zero group element. The rates, at very low extent of dissociation, for hydrogen highly diluted in Ar have been carefully measured by Breshears and Bird,¹ and preliminary values for the dissociation of deuterium are also available.² The reported rate constants are, respectively

$$k_d^{\text{Ar}}(\text{H}_2) = 9.35 \times 10^{13} \exp(-88\,900/RT) \text{ cm}^3 \text{ mol}^{-1} \text{ s}^{-1} \quad (1a)$$

$$k_d^{\text{Ar}}(\text{D}_2) = 1.45 \times 10^{14} \exp(-93\,400/RT) \text{ cm}^3 \text{ mol}^{-1} \text{ s}^{-1} \quad (1b)$$

In both experiments shock tube techniques were utilized, covering the temperature range 2000-8000 K, but different diagnostics were used to measure progress of the reaction. The dependence of the overall rate on the H₂/Ar ratio and

on the extent of dissociation permitted the partition of the measured rate¹ into contributions due to Ar, H₂, and H as colliders. The following conclusions are consistent with these data. (a) For any collider, the rate is adequately represented by the phenomenological rate expression

$$-\frac{d[\text{H}_2]}{dt} = k_d^X[\text{X}] \left[[\text{H}_2] - \frac{[\text{H}]^2}{K_{\text{eq}}} \right] \quad (2)$$

over the time periods explored in these experiments (≈ 4 – $100 \mu\text{s}$). (b) For a mixed batch of collision partners the contribution of each to the net rate is linearly additive (mole fraction χ): $k_{d,\text{net}} = \sum \chi k_d^X$. (c) The activation energy [in this discussion E_a refers exclusively to the experimentally derived quantity: $-R \ln k_d/d(1/T)$] is approximately 89 kcal/mol for H₂ when the collision partners are atoms (H, Ar, Xr), and ≈ 105 kcal/mol for H₂ when the collision partner is another molecule of hydrogen; for D₂, $E_a \approx 93$ kcal/mol with Ar as a collision partner;² $D_0^\circ(\text{H}_2) = 103.24$ and $D_0^\circ(\text{D}_2) = 105.02$ kcal/mol.

Direct measurement of the inverse three-body recombination rates ($\text{H} + \text{H} + \text{X} \rightarrow \text{H}_2 + \text{X}$) with $\text{X} = \text{Ar}, \text{H}_2, \text{SF}_6$, etc. have been reported by Kaufman et al.³ over the temperature range 300–77 K; a few values are also available for $\text{D} + \text{D} + \text{D}_2 \rightarrow 2\text{D}_2$. The rate constants were found to increase with decreasing temperature (approximately as $T^{-0.8}$ for Ar and $T^{-0.60}$ for H₂), and can be connected to those derived from the dissociation rate constants measured in the shock tube experiments¹ via an extension of Keck's phase-space theory.⁴

Development of a theory for this simple kinetic process proved to be both difficult and involved. As do all chemical kinetic problems this one consists of three distinct parts: (i) calculation of the three-dimensional potential energy surface for $\text{H}_2 + \text{X}$; (ii) computation of the collision dynamics, preferably the quantum mechanical cross section $\sigma(g, b, v, J; \epsilon_p)$; that is, the cross section for dissociation from a specified initial set of states, to produce $2\text{H} + \text{X}$ in specified states (designated by ϵ_p); and (iii) solution of the master equation for the time evolution of the state populations in the ensemble. Only recently has an attempt been made to consider in some detail steps (i) and (ii) for $\text{H}_2 + \text{He} \rightarrow 2\text{H} + \text{He}$,⁵ and for the inverse process $\text{H} + \text{H} + \text{H} \rightarrow \text{H}_2 + \text{H}$.⁶ The published treatments of (iii)⁷ are encumbered by computational difficulties; the approximations generally introduced do not permit one to assess the sensitivity of the overall system to the individual features of the models proposed. We note that the lowest upper-bound estimates provided by Keck's formulation for three-body recombinations have been corrected by Shui, Appleton, and Keck⁸ to allow for the more probable redissociation of diatoms generated in the upper vibrational states, and for departure of vibrational level populations from Boltzmann distributions. We undertook a computer analysis to answer some clearly posed questions which depend on the time evolution of populations, taking for granted that the cross sections were derived from other sources. Some but not all of these questions have been treated in the large number of discussions published to date on collision induced dissociations of diatomics; reference to these will be indicated. The reader is also directed to earlier papers and to a number of recent ones.^{9–14}

To focus attention on the critical ensemble features we list the following questions (some of these were explicitly, others implicitly, discussed previously).⁷

(I) At what stage in the statistical evolution of the popu-

lations of the vibrational states does the phenomenological rate equation become valid? How large are the differences between the measured rate constants and the unidirectional flux coefficients, for the forward and reverse processes, defined as

$$\langle \kappa \rangle_d \equiv \frac{\sum_v \kappa_{v,d} [\text{H}_2^v][\text{Ar}]}{\sum_v [\text{H}_2^v][\text{Ar}]}; \quad \langle \kappa \rangle_a \equiv \frac{\sum_v \kappa_{v,a} [\text{H}_2^v][\text{Ar}]}{[\text{H}]^2[\text{Ar}]} \quad (3)$$

Thus $\langle \kappa \rangle_d$ is a measure of the average (over v) cross section for dissociation (unidirectional), while $\langle \kappa \rangle_a$ is the corresponding quantity for the unidirectional association to the various vibrational states.

(II) How large are the induced departures from a Boltzmann distribution over vibrational state populations, at a time when depopulation of vibrational states via dissociation becomes comparable to the repopulation of states via collisional vibrational energy transfer?

(III) At what stage of the approach of the system to equilibrium does the reverse flux attain a significant level, e.g., 10% of the dissociation flux, and over what time regime is a steady state condition approximately valid? Since various criteria have been proposed for the steady state condition, we may: (a) apply that term to any species individually, when the net rate of change of its mole fraction is small compared with the one-way flux rates for its production and destruction; (b) use that term in a purely mathematical context; i.e., to specify that the solutions for a set of coupled differential equations, obtained by setting to zero the net rates of change of selected species, are acceptably close to the correct solutions; (c) specify a criterion for the ensemble as a whole; that is, require that there be a time τ_0 such that for any $t > \tau_0$ the ratio $[n_v(t) - n_v(\infty)]/[n_w(t) - n_w(\infty)]$ remains constant for all v, w .

(IV) Are the observed $E_a < D_0$ for $\text{X} = \text{atoms}$ and $E_a \approx D_0$ for $\text{X} = \text{H}_2$ solely the consequence of depletion of the populations in the upper states, and therefore should have been fully predicted from the proper solution of the master equation?

(V) Must one also insert a functional constraint on the temperature dependence of the three-body recombination cross sections to account for the available rate data?

(VI) Does rotation–vibration coupling, particularly for the high energy states, account for $E_a < D_0$, with no added assumptions regarding the temperature dependence of the recombination cross sections?

(VII) Does a model which satisfactorily accounts for the dissociation of H₂ by Ar also account, without further adjustment of parameters, for the dissociation rate of D₂?

(VIII) Does a model which is satisfactory for the dissociation of hydrogen infinitely diluted in argon, and extended to incorporate (v, v) energy transfers, also account for observations on pure hydrogen without additional ad hoc features?

From the multitude of published discussions we found it difficult to extract clear cut answers to the above questions. We therefore set out to find such answers by the brute-force solution of the master equation for the simplest model which incorporates the essential features of such ensembles, given assigned values for the various cross sections.

Definition of Parameters

The model is best defined by the master equation for a

sample of hydrogen infinitely dilute in argon, suddenly raised to a high temperature and maintained thereafter at constant volume. We write for the instantaneous population of the v th vibrational state

$$\begin{aligned} d[\text{H}_2^v]/dt = & \kappa_{v-1,v}[\text{Ar}][\text{H}_2^{v-1}] + \kappa_{v+1,v}[\text{Ar}][\text{H}_2^{v+1}] \\ & - \kappa_{v,v-1}[\text{Ar}][\text{H}_2^v] - \kappa_{v,v+1}[\text{Ar}][\text{H}_2^v] \\ & + \kappa_{a,v}[\text{Ar}][\text{H}]^2 - \kappa_{d,v}[\text{Ar}][\text{H}_2^v] \quad (4) \end{aligned}$$

Note that there are three pumping processes and an equal number of depleting processes. The assumptions implied in eq 4 are: (A) only adjacent level transitions ($\Delta v = \pm 1$) are induced by collisions with the ambient gas; (B) dissociation may take place from any level to the continuum, and similarly for the reverse process, but not necessarily with equal a priori probabilities; (C) the corresponding cross sections are "partially integrated" quantities: for example

$$\begin{aligned} \kappa_{v,v-1} = \sigma_{v,v-1} = & \int \dots \int \sigma(g, b, v, J; v-1, J') \\ & \times P_1(g) dg \, 2\pi b \, db \, P_2(J, J') dJ dJ' \quad (5) \end{aligned}$$

(similarly for $\kappa_{d,v}$). Hence these κ 's are dependent on the distribution functions $P_1(g)$ and $P_2(J, J')$; that is, on the translational and rotational temperatures. We shall assume that these remain Boltzmannian, which is not valid for hydrogen at room temperature or below, where rotational relaxation times are substantial. The role of rotational energy transfers on the reaction cross sections was not specifically inserted in eq 4. Three distinct effects (which should not be confused) arise from vibration-rotation interaction. These will be discussed below.

Equation 4 was integrated under the following conditions. Every molecular event satisfies microscopic reversibility; i.e., for every reaction the inverse reaction was inserted. Progress along the integration routine was checked for conservation of total atomic species. The calculations were carried out over the total kinetic period, starting within 10^{-10} s after the imposed temperature step function, to full equilibrium (at approximately 10^{-2} s). Then

$$\lim_{t \rightarrow \infty} [\langle x \rangle_d / \langle x \rangle_a] = K_{\text{eq}}^{(c)} = k_d/k_a \quad (6)$$

Equation 6 follows from eq 2 and 3; note

$$\lim_{t \rightarrow \infty} [\langle x \rangle_d / \langle x \rangle_a] = \frac{\left(\sum_v \kappa_{v,d} [\text{H}_2^v]_{\text{eq}} [\text{Ar}] \right)}{\left(\sum_v \kappa_{v,a} [\text{H}]_{\text{eq}}^2 [\text{Ar}] \right)} \frac{[\text{H}]_{\text{eq}}^2}{\sum_v [\text{H}_2^v]_{\text{eq}}} \quad (7)$$

and the quantity in the bracket is equal to unity. Since there are two types of cross sections in the master equation, to obtain a meaningful representation of the statistical behavior of the ensemble these must be properly scaled. Therefore we inserted additional constraints; the $\kappa_{v,v-1}$'s should reproduce the observed (v, T) relaxation times¹⁵ while the $\kappa_{d,v}$ and $\kappa_{a,v}$ should be scaled so that the net computed rate approximately equals the measured rate at one selected temperature (4500 K).

For the various cases described below we followed a uniform procedure. Each sample, at $t = 0$, was assumed to be at a specified translation-rotation temperature (3500, 4500, or 5500 K) but with a vibrational Boltzmann distribution which corresponds to 300 K. The evolution of the vibrational state populations and the H atom concentrations were then calculated by integration of the simultaneous first-order non-linear differential equations⁴ from $t = 10^{-10}$ s, and on toward equilibrium. Depending on the magnitudes of the κ 's, the differential equations became "stiff"

at various stages in the integration routine. Two computational methods were used to solve this problem; the first was a Runge-Kutta-Merson numerical integration technique for the early times, which automatically shifted for any one species to an algebraic routine, written by Keneshea,¹⁶ when the rates of production and destruction approached equality. The Keneshea technique proved adequate for the $\text{H}_2 + \text{Ar}$ case, although some loss of mass balance did appear in the solution of the algebraic equations. However, when we incorporated the (v, v) energy transfer terms to model the $\text{H}_2 + \text{H}_2$ problem, these uncertainties increased to a point where the method was not acceptable. We then replaced that integration routine by a procedure developed by Gear.¹⁷ This maintained excellent mass balance while allowing the integration to proceed at an acceptable rate. Agreement between the two methods was good for the $\text{H}_2 + \text{Ar}$ calculations. Because the cross sections are "integrated" over the rotational state distributions (eq 5), a slightly different effective potential is implied for each temperature. The consequences of this unrealistic simplification are discussed below. Fifteen levels, with appropriate anharmonicity, were inserted for hydrogen and 20 levels for deuterium. Microscopic reversibility requires

$$\kappa_{v,v-1} = \kappa_{v-1,v} \exp[\beta(E_v - E_{v-1})] \quad \beta \equiv 1/kT_{\text{transl}} \quad (8)$$

$$\kappa_{d,v} = K_v^{(c)} \kappa_{a,v} \quad \text{where } K_v^{(c)} \equiv [\text{H}]_{\text{eq}}^2 / [\text{H}_2^v]_{\text{eq}} \quad (9)$$

Note that $[K^{(c)}]^{-1} = \sum_v [K_v^{(c)}]^{-1}$, and

$$K_v^{(c)} = \left(\frac{1}{RT} \right) \frac{4Q_{\text{tr}}^2(\text{H})}{Q_{\text{tr}}(\text{H}_2)Q_{\text{rot}}(\text{H}_2)} \exp[-\beta(D_0 - E_v)] \quad (10)$$

where the Q 's are the indicated standard partition functions at unit atmosphere.

For pure hydrogen additional terms which incorporate (v, v) transfer steps were included:

$$\begin{aligned} + \sum_w \kappa_{v+1,v}^{w,w+1} [\text{H}_2^w][\text{H}_2^{v+1}] + \sum_w \kappa_{v-1,v}^{w,w-1} [\text{H}_2^w][\text{H}_2^{v-1}] \\ - \sum_w \kappa_{v,v-1}^{w,w+1} [\text{H}_2^w][\text{H}_2^v] - \sum_w \kappa_{v,v+1}^{w,w-1} [\text{H}_2^w][\text{H}_2^v] \quad (11) \end{aligned}$$

$$\begin{aligned} \kappa_{v,v-1}^{w,w+1} = \kappa_{v-1,v}^{w+1,w} \exp[\beta(E_v - E_{v-1} + E_w - E_{w+1})] \quad (12) \end{aligned}$$

For a simple harmonic oscillator the $\kappa_{v,v \pm 1}$ cross sections are directly related to $\kappa_{1,0}$, which in turn is given by the measured (v, T) relaxation time¹⁵ [$\kappa_{v,v-1} = v \kappa_{1,0}$]. For an anharmonic case, write

$$\kappa_{v,v-1} = \kappa_{1,0} g(v); \quad \kappa_{1,0} = \frac{RT}{P\tau} \{1 - \exp[-\beta(E_1 - E_0)]\}^{-1} \quad (13)$$

The form of $g(v)$ is an aspect of the model which we explored; for the range of functions tested it appears to be of little consequence with respect to the $E_a < D_0$ problem. The function of significance which characterizes the model is the expression for $\kappa_{a,v}$. Were the dynamics of the association step simply a termolecular encounter between hard spheres, the magnitude of $\kappa_{a,v}$ would be given by classical kinetic theory. Clearly atoms and molecules do not behave like little balls. Hence, substantive questions remain relative to the characteristic efficiencies of third bodies, and the temperature dependence of the reactive cross sections for collisions which populate specific vibrational states. To explore this feature of the model we followed an empirical procedure. The useful formats are:

$$\kappa_{a,v} = ZT^n f_n(v) \quad (14a)$$

and

$$\kappa_{a,v} = ZT^m f_m(v, T) \quad (14b)$$

wherein Z is a collection of molecular parameters and constants that appear in the expression for the termolecular collision rate, exclusive of the translational temperature. To ensure that the relative magnitudes of $\kappa_{v,v-1}$ and $\kappa_{a,v}$ correctly represent the case of hydrogen, the absolute value of Z was adjusted so that the calculated net dissociation rate was close (but not necessarily equal) to that observed¹ at 4500 K, 10^{-5} s after shock initiation.

In the early discussions of diatom dissociations Rice¹⁰ and others assumed that those molecules dissociate which are within a band of width (kT) below the dissociation limit. This was also the assumption made by Kiefer.¹² On the other hand, Johnston and Birks¹¹ concluded that for collisions with sufficient relative kinetic energy all vibrational states dissociated with equal a priori probability. Treanor¹⁸ took an intermediate position; he used eq 14b with an exponential dependence: $f_m(v, T) \propto \exp[-\beta(D_0 - E_v)/\alpha]$; α is a small positive integer, and $m = 0$ or $+1/2$. Treanor's net temperature dependence of $\kappa_{a,v}$ is positive, with a large slope for small v , and a smaller one for large v ; also the slope is greater for small α than for large α . This is illustrated in Figure 1. However, trajectory calculations^{6a} as well as experimental recombination rates at low temperatures³ show a net negative temperature dependence for $\kappa_{a,v}$; this can be incorporated in eq 12 by assigning a small negative value to n or a larger one to m . The specific v dependence for various α 's and T 's are shown in Figure 2.

Specific Cases

The following is the first successful case we developed for H₂/Ar mixtures, though it was not the first tested. It will be discussed in detail so that the consequences of modifying its features may be summarized succinctly. The system is isothermal (3500 or 5500 K): (i) $0 \leq v \leq 14$ with anharmonicity. In eq 13, insert¹²

$$Pr = 1.4\{3.9 \times 10^{-10} \exp[100T^{-1/3}]\} \quad (15)$$

(ii) $g(v) = U_{rn}^2/U_{01}^2$, where U_{rn} is the matrix element for the $r \rightarrow n$ vibrational transition.¹⁹ (iii) $\kappa_{v+1,v}^{w,w+1} = 0$ for all v, w [i.e., no (v, v) transfers included, to simulate H₂ infinitely dilute in Ar]. (iv) $[H_2]_{\text{initial}} = 2.935 \times 10^{17}$; $[Ar] = 5.57 \times 10^{19}$ molecules cm⁻³, at 3500 K and $[H_2]_{\text{initial}} = 3.047 \times 10^{16}$; $[Ar] = 5.78 \times 10^{17}$ molecules cm⁻³, at 5500 K.

$$\kappa_{a,v} = ZT_{\text{transl}}^{-1} \exp[-\beta_r(D_0 - E_v)/8]; \beta_r = 1/k(4500) \quad (16)$$

It is instructive to consider the evolution of the vibrational state populations (Figure 3a,b) for this model. When $T_{\text{transl}} = 3500$ K, these populations do not attain their final values until the system nearly reaches chemical equilibrium. This "depletion effect" was noted previously, and is obvious for the upper states; it is a direct consequence of the relative magnitudes of $\kappa_{v,v-1}$ and $\kappa_{a,v}$ in eq 4. The surprising result appears in Figure 3b. Our model indicates an "overshoot" of the vibrational state populations for $T_{\text{transl}} = 5500$ K, for $5 \times 10^{-6} \leq t \leq 5 \times 10^{-4}$ s. However, individual level populations are not suitably scaled indicators of the system; better measures are the corresponding mole fractions (Figure 4a,b), or the equivalent vibrational temperatures (Figure 4c) defined by

$$T_v = \frac{E_v}{k \ln(n_0/n_v)}$$

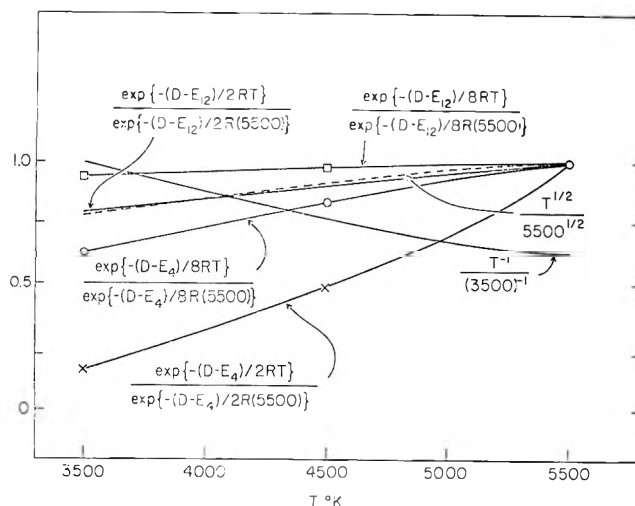


Figure 1. Temperature dependence of various functions tested, for use in eq 14; normalized.

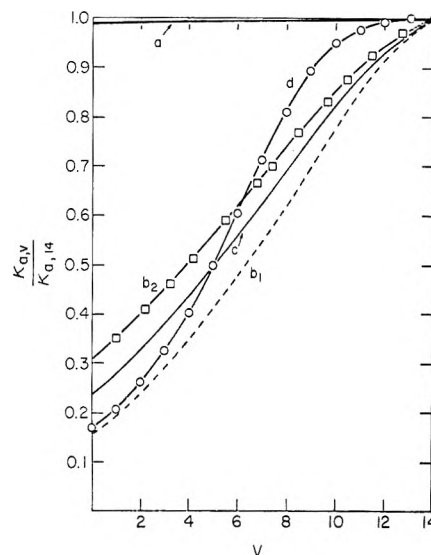


Figure 2. Ratio of κ 's [$v = 14$ as a reference] for $f(v)$, in eq (14): (a) $f_m(v)$ with $\alpha = 1600$; (b₁, b₂) $f_m(v)$ with $\alpha = 8$; $m = -1$ (b₁ 3500 K, b₂ 5500 K); (c) $\kappa_{a,v}$ given by eq 16; (d) $f_n(v)$ arbitrarily set to values shown in the graph, and $n = -1$.

The level populations in Figure 3a,b have thus been replotted. Whereas the system never attains a steady state [definition c in question III], there are time domains when the lower v states obey $(dT_v/dt) \approx 0$; and, as expected this occurs more predominantly at lower temperatures [definition a, question III]. It will be shown that for $t \approx 10^{-4}$ s dissociation and association fluxes become comparable; nevertheless, the T_v 's do not approximate a Boltzmann distribution until $\approx 5 \times 10^{-3}$ s [answers question II]. Finally, note the criss-crossing of the T_v curves in Figure 4; in particular, the positions of $v(10-14)$ relative to $v(5)$ for $t \geq 10^{-4}$ s, at $T = 5500$ K. This is due to the finite time required for deexcitation of the newly associated molecules. We thus conclude that the "depletion effect" cannot be solely blamed for $E_a < D_0$ (questions IV; more below). For the diatomics investigated thus far it is not meaningful to test a model in which a Boltzmann distribution is artificially maintained. However, one may speculate over the fate of strange molecular species which have cross sections for (v, T) energy transfers

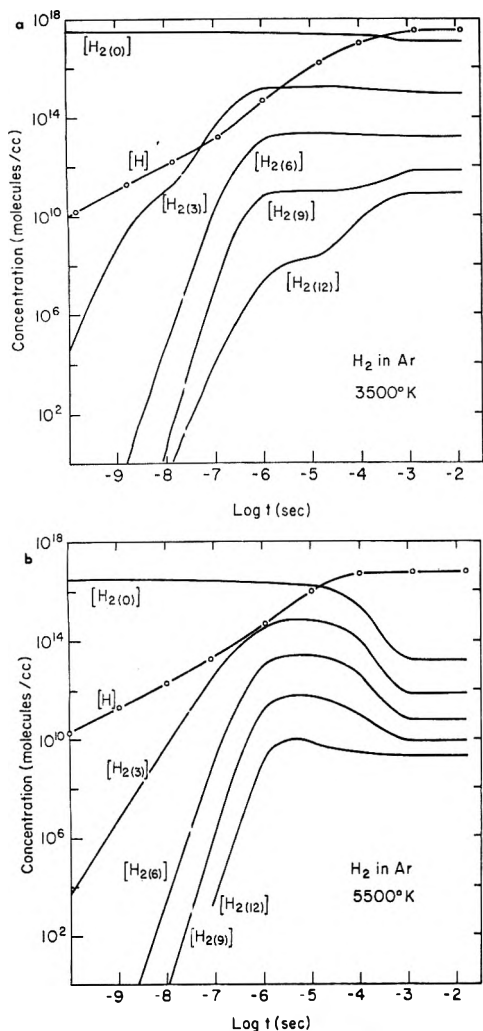


Figure 3. Computed concentrations of H₂^(v) and H for the initial conditions listed in the text: (a) 3500 K; (b) 5500 K. In comparing (a) with (b) superpose the two figures so that the initial [H₂] densities match.

comparable to (*J*, *T*) rates. Then the vibrational populations would remain close to Boltzmannian. Given $x_{a,v} = ZT^n f_n(v)$, it follows, after some manipulation, that

$$E_a = D_0 + \left(n + \frac{1}{2} \right) kT - h\nu \left[\frac{e^{-\theta/T}}{1 - e^{-\theta/T}} \right] \quad \theta \equiv h\nu/k \quad (17)$$

Plots of the total unidirectional fluxes, $\Sigma_v d[H_2^v]/dt$ _{diss} and $\Sigma_v d[H_2^v]/dt$ _{assoc}, are presented in Figure 5. These show that since termolecular events are considerably less probable than bimolecular events, even when the density of H atoms becomes comparable to that of H₂, the total association flux remains small compared to the total dissociation flux until the ensemble gets close to equilibrium (question III). An expected feature appears in Figure 5b (5500 K), between 10⁻⁶ and 10⁻⁴ s, when there is an overshoot in the dissociation flux; of course, this corresponds to the overshoot in the upper vibrational state populations. The unidirectional dissociation flux gives no hint of upper state "depletions", measured via mole fractions (Figure 4a,b). The most interesting results are demonstrated in Figure 6, for the time evolution of $\langle x \rangle_d$ and $\langle x \rangle_a$. While the dissociation flux coefficients are clearly time dependent, the limiting ratio at 3500 K, $\langle x \rangle_d / \langle x \rangle_a$ (at *t* = 0.1 s) = 7.2 × 10¹⁷, compared with the equilibrium constant, $K_{3500}^{(c)} = 7.2 \times 10^{17}$ molecules/cm³. Similarly, at 5500 K, $\langle x \rangle_d / \langle x \rangle_a$ (at 0.1 s) = 1.5 × 10²⁰; $K_{5500}^{(c)} = 1.51 \times 10^{20}$ (confirming eq 6). One may ascribe the sharp rise in $\langle x \rangle_d$ at about 10⁻⁶ s to

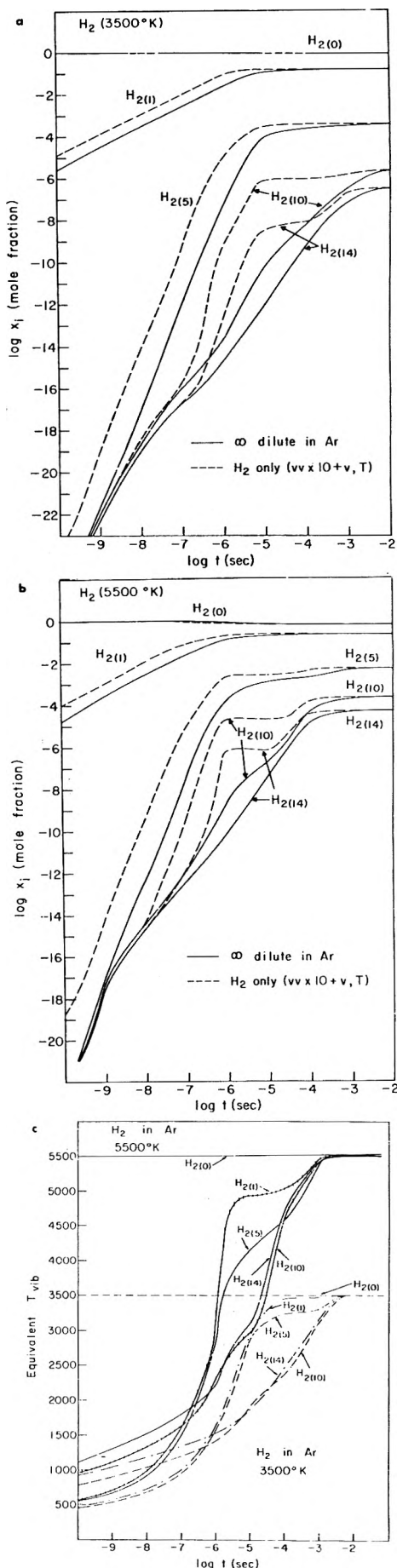


Figure 4. Plots of vibrational state populations (shown in Figure 3a,b) in terms of equivalent vibrational temperatures (c), and in units of mole fraction, (a) and (b). Note the acceleration of vibrational relaxation by v-v energy transfer.

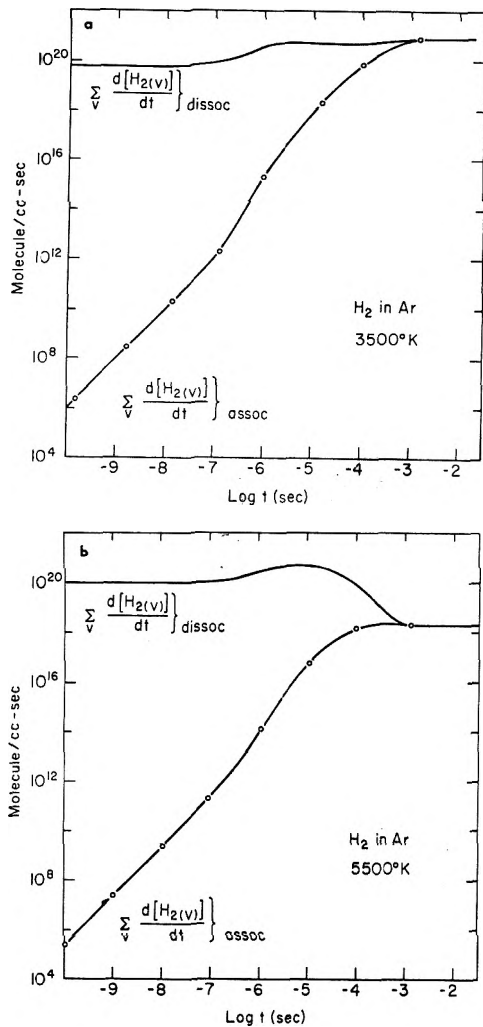


Figure 5. Unidirectional total fluxes at two temperatures.

the (ν, T) relaxation time for H₂-Ar collisions, but this is not solely a $P\tau_\nu$ effect since the break occurs earlier at 3500 K than at 5500 K. The second sharp rise in $\langle x \rangle_d$ at about 3×10^{-4} s may be ascribed to the substantial repopulation of the upper vibrational levels by the reverse reaction from which dissociations take place; refer to Figure 5.

To obtain the computer's equivalent of k_d , the net rates of dissociation of H₂ [i.e., the differences between $\sum_\nu d[H_2(\nu)]/dt|_{\text{dissoc}}$ and $\sum_\nu d[H_2(\nu)]/dt|_{\text{assoc}}$] were fitted to eq 2, using the corresponding thermodynamic equilibrium constant. For times greater than $\approx 5 \times 10^{-6}$ s, the k_d 's so derived were also plotted in Figure 6. It is evident that $\langle x \rangle_d \approx k_d$ only for the interval $10^{-5} < t < 10^{-4}$ s. As pointed out by several authors²⁰ there is no justification for equating $\langle x \rangle_d$'s (calculated for assumed Boltzmann distributions over $x_{d,\nu}$'s, such as are derived by sampling trajectories) to the measured k_d 's, notwithstanding claims for "agreement" between calculated flux coefficients and experimentally determined rate constants. The present calculations clearly demonstrate that a phenomenological rate equation does apply to this type of a bimolecular process for $t > 5 \times 10^{-5}$ s, and we have answered question I; this is consistent with the observation made in ref 13b, p 7701. On the basis of the k_d 's so obtained, the computer's value for the activation energy is $E^* = 89.4$ kcal/mol, compared with Breshears and Bird's value¹ $E_a = 88.9$ kcal/mol (Table I, our calculations no. 17, 18). Variations in the shape of the $f_n(\nu)$ function, that is, a change from a Gaussian to a Lorentzian, shown in Figure 2, gave an insignificantly better fit, $E^* = 89.2$ kcal/

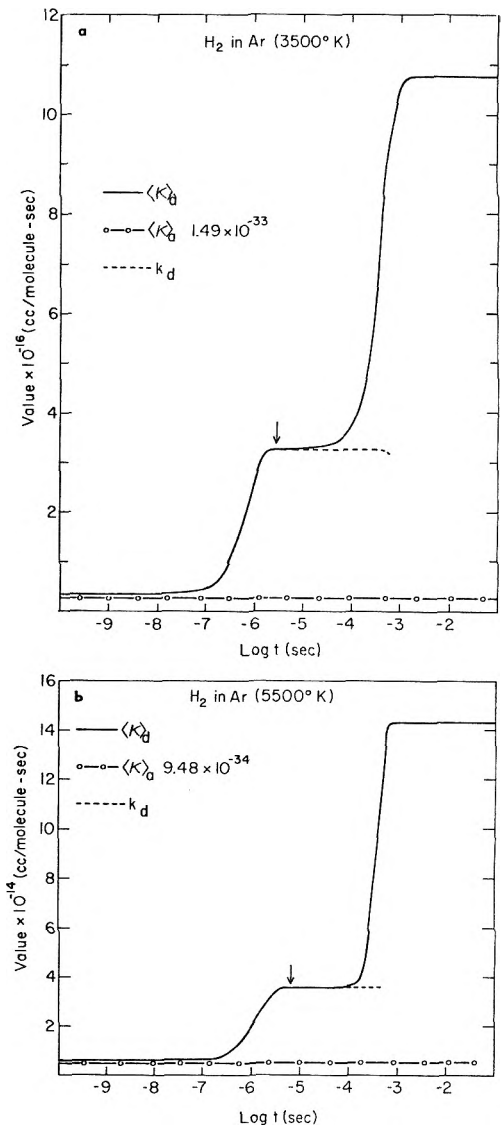


Figure 6. Unidirectional flux coefficients, and the corresponding phenomenological rate constants.

mol (runs 19, 20), but a somewhat lower absolute magnitude (Figure 7).

It is essential that this model be tested with respect to its sensitivity to the parameters inserted in the computer program. First, are the values shown in Figure 6 dependent on the initial concentration of the H₂? They should not if the model is set up correctly, since the infinitely dilute condition was simulated by considering only H₂-Ar collisions. This question was resolved early in our investigations by calculating curves for several concentrations but for the same set of parameters. The resulting curves for 0.5, 5, and 15% hydrogen in argon, exclusive of (ν, ν) transfer, superposed to well within the round-off errors of the computation. Thereafter only 5% mixtures were tested. Another feature to which the model is insensitive is the $g(\nu)$ function of eq 13. This measures the augmented (ν, T) energy transfer rate due to anharmonicity. Whether $g(\nu) = \nu^2$, or is set equal to the ratio of the corresponding matrix elements, as proposed by Rapp and Sharp,¹⁹ had no significant effect on E^* ; this is consistent with ref 13b and 21. However, we did not test the effect of varying (ν, T) rates by an order of magnitude.

A somewhat more sensitive, but still not a crucial parameter is the shape of the $f_n(\nu)$ function in eq 14. In our early tests we used exclusively Treanor's format, wherein the ν

TABLE I: $\kappa_{a,v} = cAT^m \exp [-(D_0^0 - E_v)/kU]$

Run no.	$\nu(\max)$	c	m	U	3500 K			5500 K			E^*
					$[H_2]_i$	$[Ar]$	$k_d(\text{at } 10^{-5} \text{ s})$	$[H_2]_i$	$[Ar]$	$k_d(\text{at } 10^{-5} \text{ s})$	
1	13-H ₂	1	1/2	8T				3×10^{16}	6×10^{17}	3.0×10^{-14}	
2;6	13-H ₂	3	1/2	8T	3×10^{17}	5.6×10^{18}	2.4×10^{-16}	3×10^{16}	6×10^{17}	6.0×10^{-14}	106
3	13-H ₂	3	1/2	8T				9×10^{16}	5×10^{17}	6.1×10^{-14}	
4	13-H ₂	3	1/2	8T				3×10^{15}	6×10^{17}	6.0×10^{-14}	
5;7	13-H ₂	3	1/2	1600T	3×10^{17}	5.6×10^{18}	4.1×10^{-16}	3×10^{16}	6×10^{17}	8.0×10^{-14}	101
8;9	13-H ₂	α			3×10^{17}	5.6×10^{18}	1.1×10^{-16}	3×10^{16}	6×10^{17}	4.0×10^{-14}	114
11;12	15-H ₂	3	1/2	8T	3×10^{17}	5.6×10^{18}	2.0×10^{-16}	3×10^{16}	6×10^{17}	5.2×10^{-14}	106
13;14	15-H ₂	3	1/2	1600T	3×10^{17}	5.6×10^{18}	3.7×10^{-16}	3×10^{16}	6×10^{17}	6.9×10^{-14}	100
15;16	15-H ₂	3	-1	8T	3×10^{17}	5.6×10^{18}	2.7×10^{-16}	3×10^{16}	6×10^{17}	4.0×10^{-14}	96
17;18	15-H ₂	0.5	-1	8×4500	3×10^{17}	5.6×10^{18}	3.3×10^{-16}	3×10^{16}	6×10^{17}	3.5×10^{-14}	89.4
19;20	15-H ₂		b		3×10^{17}	5.6×10^{18}	3.0×10^{-16}	3×10^{16}	6×10^{17}	3.2×10^{-14}	89.2
21;22	15-H ₂	3	-1	8×4500	3×10^{17}	3×10^{17}	1.3×10^{-15}	3×10^{17}	3×10^{17}	1.2×10^{-13}	86.5
23;24	20-D ₂	3	-1	8×4500	3×10^{17}	3×10^{17}	1.1×10^{-15}	3×10^{17}	3×10^{17}	1.1×10^{-13}	87.9
25;26	20-D ₂	1	-1	8×4500	3×10^{17}	3×10^{17}	4.6×10^{-15}	3×10^{17}	3×10^{17}	5.0×10^{-14}	89.5

^a $\kappa_{a,13}$ as in runs 2-4, but other $\kappa_{a,v}$'s scaled according to a Lorentzian form. ^b $\kappa_{a,15}$ as in runs 17,18, but other $\kappa_{a,v}$'s scaled according to a Lorentzian form.

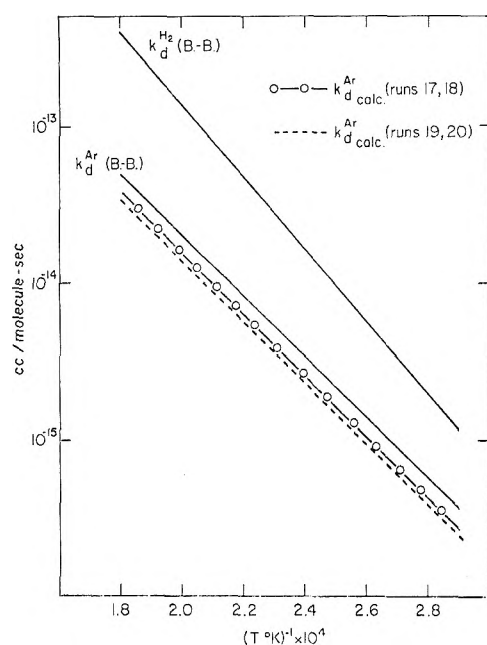


Figure 7. Reported (Breshears and Bird) vs. computed k_d 's for H₂-Ar and H₂-H₂.

and T dependences are coupled in the exponential, with a multiplicative T^m factor; this proved confusing. Reference to Table I and Figure 2 shows that varying α from 8 to 1600, with $m = 1/2$, reduced E^* from 106 to 101 kcal/mol. For $\alpha = 8$, when m was reduced from $+1/2$ to -1 , E^* decreased to 96 kcal/mol (runs 15; 16). Even so, the net $\kappa_{a,v}$ dependence has an unrealistic positive temperature coefficient. We then shifted to the $\{T^{-n} f_n(\nu)\}$ format. For $n = -1$, changing from a Gaussian $\{f_n(\nu) = \exp[-(D - E_v)/8k \cdot 4500]\}$ to a Lorentzian, as shown in Figure 2, had practically no effect.

After numerous computer runs covering a wide range of parameters, it became evident that for this model a sub-

stantial reduction in E^* below D_0 can be achieved *only* by inserting an inverse temperature dependence for $\kappa_{a,v}$, the termolecular association rate coefficients (question V). This is entirely consistent with both experimental observations on $H + H + X \rightarrow H_2 + X$ recombination rates³ and trajectory calculations.^{6a} Whether other features not incorporated in this model are significant (i.e., is this model unique?) cannot be ascertained from a mere comparison of computed with experimental results. For example, we did not investigate the effect of the restriction $\Delta v = \pm 1$. Wengle²² proposed that large increments in vibrational state quantum numbers should be considered. In our opinion, $\Delta v = \pm 1$ is not a crucial assumption (in agreement with ref 13b and 21) because lifting it merely provides additional channels for more rapid transfer of populations between vibration states. As shown below for the H₂-H₂ trial runs, the much more rapid redistribution of populations introduced by (ν, ν) transfer changed E^* by a few kilocalories per mole only.

Finally, the above calculations demonstrate that previously proposed models, wherein the $E^* < D_0$ discrepancy was ascribed solely to depletion of the upper vibrational level populations and/or the assumption that α is very large, are questionable since these authors failed to distinguish between $\langle \kappa \rangle_d$ and k_d . Because the former is time dependent, fortuitous selection of t 's at which the $\langle \kappa \rangle_d$'s are computed for the upper and lower temperatures can lead to a wide range of inferred E^* 's.

Isotope Effects

To check whether we incorporated in the model the essential features to which E^* is sensitive, we applied it to the dissociation of D₂ via Ar collisions, without introducing additional ad hoc assumptions. For this isotopic pair: $D_0^0(D_2) = D_0^0(H_2) + 1.8$ kcal; $\nu_{\max}(D_2) = 20$ whereas $\nu_{\max}(H_2) = 15$; the heavier isotopic species has a longer vibrational relaxation time¹⁵ (a factor of 3 at 1500 K; 1.8 at 5500 K) even though its levels are more closely spaced. At the high temperatures considered in this study, there are no directly

TABLE II: Representative Rate Coefficients^a

	H ₂	D ₂		H ₂	D ₂
$\kappa_{1,0}$	2.44×10^{-12}	1.72×10^{-12}	$\kappa_{0,1}$	1.00×10^{-12}	
$\kappa_{14,13}$	4.36×10^{-10}		$\kappa_{13,14}$	3.50×10^{-10}	
$\kappa_{19,18}$		4.29×10^{-10}			
$\kappa_{a,0}$	1.35×10^{-34}	1.23×10^{-34}	$\kappa_{d,0}$	3.13×10^{-14}	3.00×10^{-14}
$\kappa_{a,14}$	5.68×10^{-34}		$\kappa_{d,14}$	1.61×10^{-9}	
$\kappa_{a,19}$		5.30×10^{-34}	$\kappa_{d,19}$		1.83×10^{-9}

^a [$T = 5500$ K; H₂(or D₂) with Ar], [Ar] = 3.05×10^{17} ; units in molecules cm⁻³, $\nu_{\max}(\text{H}_2) = 15$, $\nu_{\max}(\text{D}_2) = 20$.

measured values for k_a 's for (D + D + Ar), relative to (H + H + Ar). Below 300 K, the rate for the former is approximately 0.7 that for the latter.^{3b} One may argue that since the $g(\nu)$ and $f(\nu)$ functions have little effect on E^* , if one accepts $f_n^D(E_\nu) = f_n^H(E_\nu)$ [i.e., identical recombination dependence on ν , but based on an energy scale], one should anticipate nearly equal E^* 's, but that for D₂ may be somewhat larger than for H₂, because of the larger number of vibrational states and its longer P_{τ_ν} . When the calculations were carried out in detail we found $E^*(\text{D}_2) = E^*(\text{H}_2)$ plus ≈ 1 kcal/mol (Table I; runs 21–24), in essential agreement with the experimental values,^{1,2} although the two sets of measurements are not strictly comparable. This answers question VII.

In the last test for the (D₂ + Ar) system we explored the effect of scaling the $\kappa_{\nu,\nu-1}$'s vs. $\kappa_{a,\nu}$. If one arbitrarily multiplies the latter by 3, E^* for D₂ is reduced from 89.5 to 87.9 kcal/mol; for H₂, from 89.4 to 86.5 kcal/mol. Representative magnitudes for the rate constants are listed in Table II.

H₂ as a Collision Partner

Solution of the master equation for an ensemble of pure hydrogen at high temperatures, even if one artificially restricts the program to H₂ as the only collision partner (experimentally obtained by partitioning rates, as did Breshers and Bird¹), is considerably more time consuming than the cases described in the previous section, because of the presence of (ν, ν) energy transfer processes. Note that the (ν, T) rate for the transfer of energy into the vibrational manifold is still limited; i.e., $\kappa_{0,1}(\text{H}_2 + \text{H}_2)$ is only three times as large as $\kappa_{0,1}(\text{H}_2 + \text{Ar})$. However, $\kappa_{\nu,\nu-1}^{\omega,\omega+1}$ provides many channels for the more rapid intravibrational energy redistribution.

The (ν, ν) cross sections were calculated via the Rapp and Englander-Golden theory,^{19c} as coded by Fisher.²³ Some of the σ 's, estimated in this manner, exceeded the hard-sphere values, particularly at 5500 K. In the program these were truncated so that none was larger than the kinetic theory cross section. As indicated previously, microscopic reversibility and strict mass were maintained. Even with the Gear integration routine runs which incorporated vibration–vibration energy transfers required 45–120 min of computer time on a Burroughs B3500.

Inclusion of the (ν, ν) transfer terms in the master equation did have the expected effect of speeding vibrational relaxation (Figure 8a,b); the overshoot at 5500 K is somewhat less marked. However, a Boltzmann population distribution was not attained until $t \rightarrow 10^{-2}$ s. This is illustrated in plots of T_ν 's vs. time (Figure 9 for H₂–H₂ at 3500 and 5500 K). Due to the more rapid redistribution of vibrational energy, nearby all states show two regimes for which $(dT_\nu/dt) \approx 0$: soon after translation \rightarrow vibration pumping significantly heated the reactant, and later when the association

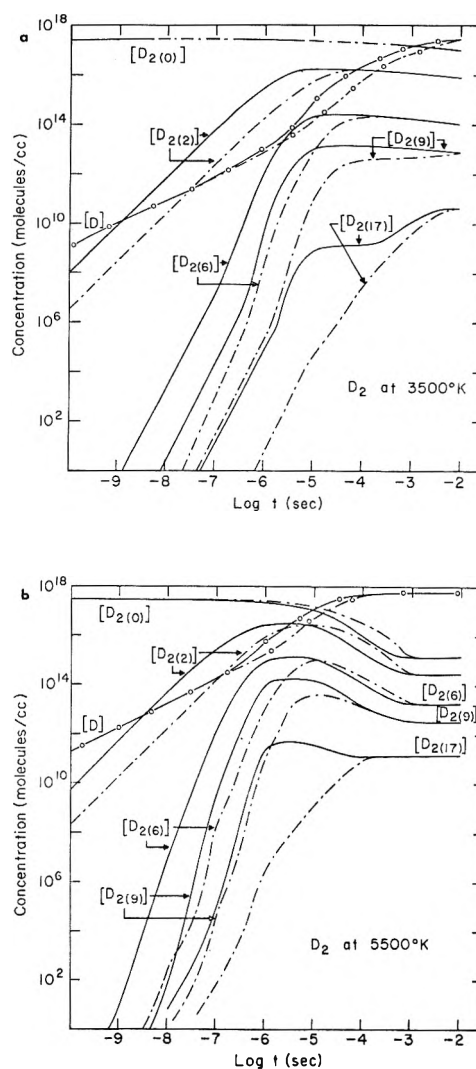


Figure 8. The evolution of vibrational state populations for D₂–D₂, showing the effect of (ν, ν) energy transfers: - - - - (ν, T) only; — (ν, T) + (ν, ν) terms.

flux became comparable to the dissociation flux. The “depletion” of the vibrational state populations now follows an ordinal sequence, a consequence of the more rapid intravibrational energy transfers. Returning to the D₂–D₂ example, over the interval $10^{-5} < t < 10^{-2.5}$, (ν, ν) processes increase the phenomenological rate constant (Figure 10a,b). Also, without adjusting the $\kappa_{a,\nu}$'s, the derived magnitude of $k_d^{\text{H}_2}$ at 5500 K is about three times as large as that for k_d^{Ar} ; this ratio is $1/3$ of the experimental value¹ (Figure 7)

$$k_d^{\text{H}_2} = 3.30 \times 10^{15} \exp(-105\,300/RT) \text{ cm}^3 \text{ mol}^{-1} \text{ s}^{-1} \quad (18)$$

TABLE III: $\kappa_{a,v} = cAT^{-1} \exp[-(D_0^\circ - E_v)/4500k]$

Run no.	$\nu(\max)$	$\kappa(\nu\nu)^a$	c	3500 K		5500 K		E^\bullet
				$[H_2]_i$	$k_d(\text{at } 10^{-5} \text{ s})$	$[H_2]_i$	$k_d(\text{at } 10^{-5} \text{ s})$	
26;27	H ₂ -15	$\times 0.1$	3	3.0×10^{17}	1.89×10^{-15}	3.0×10^{17}	1.89×10^{-13}	88.0
28;29	H ₂ -15	$\times 10$	3	3.0×10^{17}	2.86×10^{-15}	3.0×10^{17}	2.14×10^{-13}	82.5
26;29	H ₂ -15	$\times 0.1-10$	3	3.0×10^{17}	1.89×10^{-15}	3.0×10^{17}	2.14×10^{-13}	90.3
30;31	D ₂ -20	$\times 1$	1	3.0×10^{17}	9.0×10^{-16}	3.0×10^{16}	9.7×10^{-14}	89.5

^a $\nu\nu$ term calculated via Rapp-Englander-Golden theory,¹⁸ times a factor of 0.1, 1, or 10 as indicated, but always \leq kinetic theory collision number.

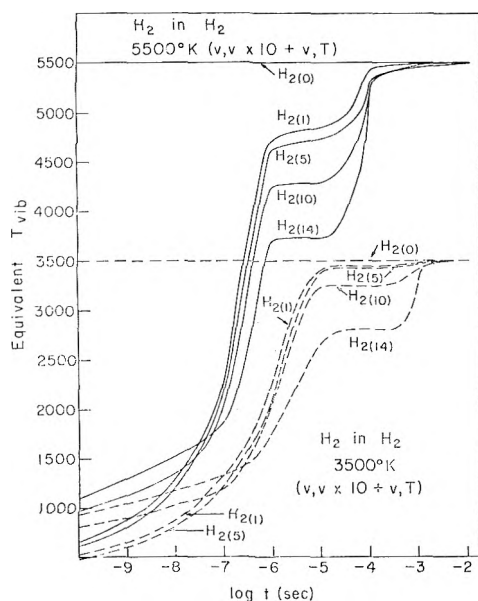


Figure 9. Equivalent vibrational temperatures for H₂-H₂. These correspond to the $(\nu, \nu) + (\nu, T)$ curves in Figure 4c. Note also the dashed curves in Figure 4a,b.

We had imposed the condition $\kappa_{a,v}(H_2) \approx \kappa_{a,v}(Ar)$. However, it is possible that at these high temperatures the former is larger than the latter even if they are within about 10% at room temperature.³ Note, however, that E^\bullet evaluated with (ν, ν) differed insignificantly from that in which only (ν, T) was allowed (Table III). Since the magnitudes of the (ν, ν) terms and their temperature dependence did affect the value of k_d , by arbitrarily increasing these cross sections we could obtain E^\bullet 's in the range 88-90 kcal/mol, compared with 86 kcal/mol when (ν, ν) transfers were omitted (Figure 11a,b). This brings us to the inescapable conclusion that adjusting such cross sections over a factor of 10, and thus manipulating the rates with which the vibrational levels are filled, has only a small effect on the deduced E^\bullet (question IV). Thus, maintaining an inverse temperature dependence for $\kappa_{a,v}$ of order -1 does not permit an E^\bullet in the range of 105 kcal/mol, as reported for the H₂-H₂ system¹ (Question VIII); another factor seems to be involved, i.e., rotation-vibration coupling with the collision orbit.

We conclude that for $H_2 + M \rightleftharpoons 2H + M$, with $M = Ar, Xe, H$, the significant factor is the temperature coefficient of the third-body collision efficiency at high temperatures. At low temperatures a range of values for the T exponent (in eq 14) was reported by Kaufman and coworkers.^{3b} They found for the sequence H₂, He, Ar, N₂, CH₄, CO₂, SF₆, the following magnitudes for $-n$: 0.60, 0.40, 0.81, 1.33, 1.2, 2.27, and 1.8.

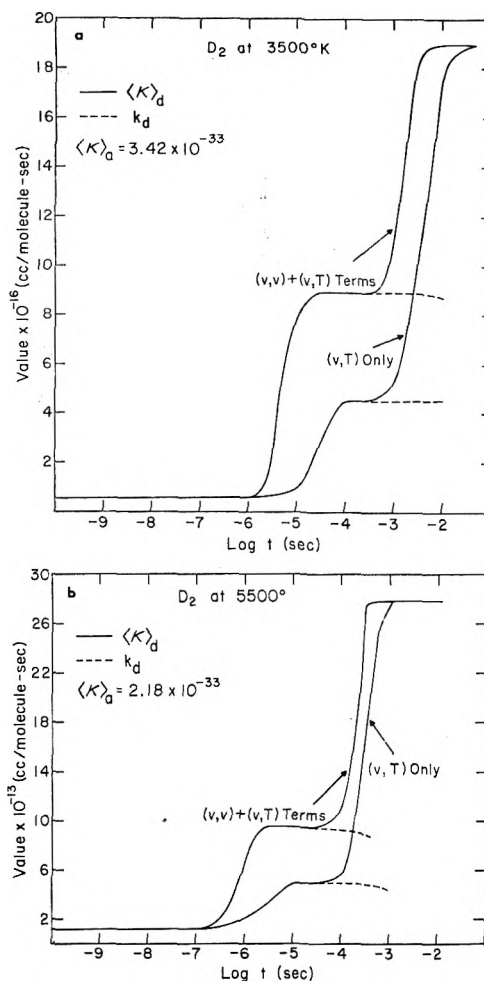


Figure 10. The total unidirectional flux coefficients and the corresponding phenomenological rate constants deduced for D₂-D₂, again with and without (ν, ν) transfer. (State populations shown in Figure 8).

The Role of Rotational States and Extension to Polyatomic Molecules

In formulating the above model we used "partially integrated" cross sections over the reactant and product rotational states $[P_2(J, J')]$ of eq 5, so that the mean effective potential for dissociation is temperature dependent:

$$\langle \varphi_{\text{eff}}(R) \rangle = \varphi(R)_{J=0}$$

$$+ \frac{\hbar^2}{2\mu R^2} \iint P_2(J, J') J(J+1) J'(J'+1) dJ dJ' \quad (19)$$

We now restate question VI. Were one to allow for the specific dependence of the recombination flux coefficient on

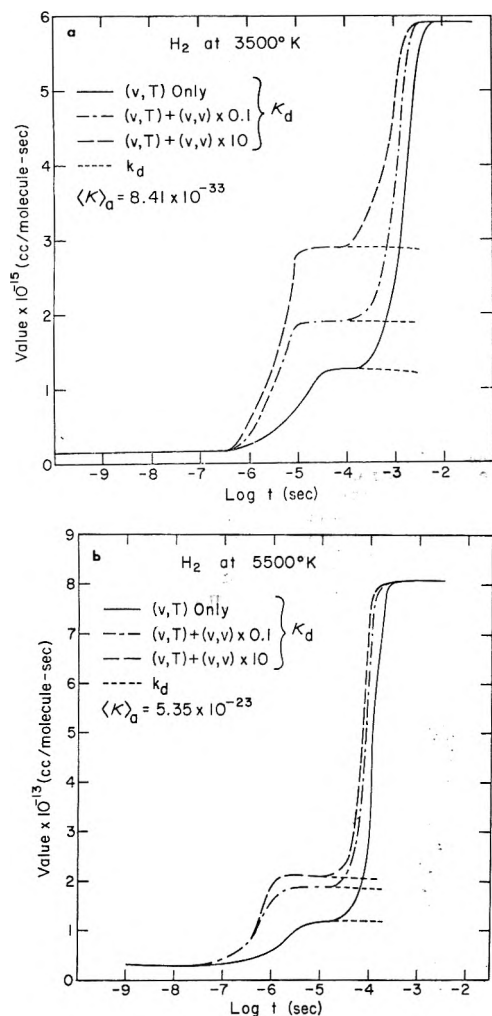


Figure 11. $\langle k_d \rangle$ and k_d for H₂-H₂. These show the effect of changing the relative magnitudes of the (v, v) cross sections: (---) $\times 10$, (- - -) $\times 0.1$, over the Rapp et al. rates.

the impact parameter [i.e., $\alpha_{a,v,g}$], would E_* be affected? The answer is yes. A second consequence^{15b} of allowing for rotation is implicit in eq 19. For any Morse-type potential the number of vibrational states is determined by the magnitude of J , and there is an upper bound to the number of rotational states.²⁴ When these limits are considered in calculating the vibrational and rotational partition functions the total number of states is diminished; in turn, this reduces the slope of the rate constant for dissociation, with increasing temperature.²⁵

The third factor introduced by incorporating rotation in the model is the constraint imposed by the rotational barrier on dissociation. As illustrated in Figure 12, the higher the rotational state of the diatom, the larger must be its energy content (measured above $v = 0; J = 0$) before it can break apart. For the same total energy (such as regions α and β) those with large J (region β) must pick up more energy to dissociate than those with small J (region α). Note also that at the lower temperatures there are proportionately more molecules with low J than there are at higher temperatures. Thus, the dissociation at high T is depressed below the magnitude extrapolated from lower T measurements.²⁶

A concurrent opposite effect, which increases the rate and E_* is also illustrated in Figure 12; unfortunately this is

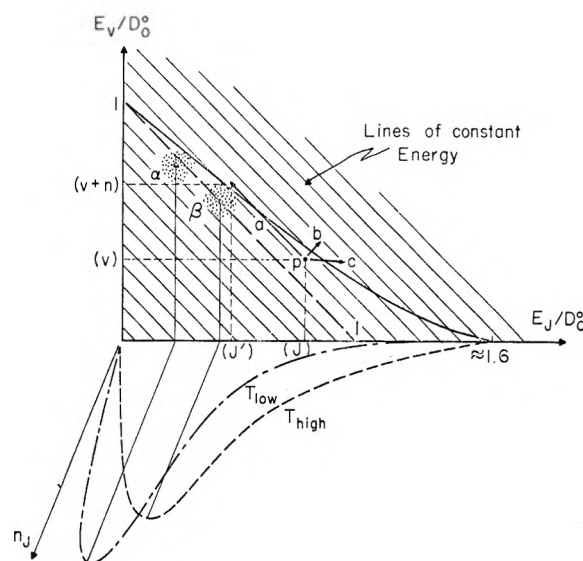
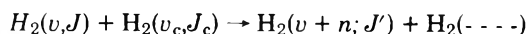


Figure 12. Plot of E_v/D_0^0 vs. E_J/D_0^0 required for dissociation of a diatom (heavy line that connects 1 to 1.6). (E_v/D_0^0 vs. E_J/D_0^0 graph suggested by Professor B. Widom.)

difficult to quantify but it may account for the distinctive E_a reported when the collision partner is molecular hydrogen.¹ That distant, and therefore numerous, collisions may trigger the dissociation of diatoms from higher rotational states was pointed out by Bauer in 1958.²⁷ Consider a diatom with energy partitioned as at point P. To dissociate, the largest energy increment is required for path c, when $\Delta v = 0$ coupled to a substantial increase in rotational quantum number. Less energy must be pumped into the molecule for path b, wherein both v and J increase. However, an encounter, even with a large impact parameter, which strongly couples this (v, J) state to the angular momentum of the collision orbit so as to conserve total angular momentum, i.e., $\Delta J \ll 0$, while $\Delta v > 0$ (path a) takes the molecule above its dissociation limit with no net energy transfer. In general collisions represented by motion along nearly constant energy lines are very efficient;²⁸ they should be particularly effective for the near resonant case:



$\Delta E \approx 0$; \vec{p} coupled to collision orbit. The reduction of the dissociation rate by the rotational barrier is thus circumvented and the effective activation energy approaches D_0 . In the absence of extensive trajectory calculations on a realistic potential energy surface we have insufficient information to assess the relative roles of the negative temperature dependence of $\alpha_{a,v}$ and the above rotational-vibration coupling.

Our final comment concerns the dissociation of polyatomic molecules. For large molecules, the E_a 's measured at the high pressure limits have been traditionally equated to the corresponding bond dissociation energies. On the basis of the preceding arguments this is legitimate provided: (i) the recombination rate constants for the corresponding fragments have no significant temperature dependence. This is indeed the case even for relatively small radicals ($\approx CH_3$);²⁹ and, (ii) for the molecules undergoing unimolecular decomposition only a few collisions (less than 10) are required for (v, T) relaxation. Typical values for $Z_{1,0}$'s were summarized by Lambert;³⁰ unsymmetric molecules with five or more atoms generally satisfy this criterion.

By extension, one may anticipate that there are molecules, in particular triatomics (CO_2 , SO_2 , O_3 , H_2), some tetraatomics (H_2CO , NF_3), and larger symmetric species (such as, CH_4 , CF_4 , SF_6 , etc.) which constitute an intermediate class. These have been discussed at length by Troe.^{14,31} Generally, such dissociations are investigated in their falloff regimes; then, extrapolation of the measured activation energies to either their high or low pressure limits should be undertaken only with the aid of a reliable theory. We anticipate that exploitation of the laser-schlieren technique for measuring density gradients at shock fronts^{15a} will provide E_a 's at the bimolecular limits, for very low degrees of dissociation. Preliminary data on CH_4 ³² show that for this case $E_a \ll D_0(\text{H}_3\text{C}-\text{H})$. As a consequence one may predict that recombination rate constants for the association of atoms with small radicals have negative temperature coefficients.

Acknowledgment. We benefited greatly from numerous discussions with Professor B. Widom, and appreciate critical comments from Professors J. H. Kiefer and H. O. Pritchard. We thank our colleagues for providing us with prepublication reports. This work was supported by the U.S. Air Force Office of Scientific Research under Contract No. AF49(638)-1448.

References and Notes

- (1) W. D. Breshears and P. F. Bird, *Symp. (Int.) Combust., [Proc.]*, 14th, (1972) [LA-DC-72-369 report].
- (2) D. Appel and J. P. Appleton, *Symp. (Int.) Combust., [Proc.]*, 15th, 701 (1975).
- (3) (a) D. W. Trainor, D. O. Ham, and F. Kaufman, *J. Chem. Phys.*, **58**, 4599 (1973); (b) L. P. Walkauskis and F. Kaufman, *Symp. (Int.) Combust., [Proc.]*, 15th, 691 (1975).
- (4) V. H. Shui and J. P. Appleton, *J. Chem. Phys.*, **55**, 3126 (1971).
- (5) N. J. Brown and R. J. Munn, *J. Chem. Phys.*, **56**, 1983 (1972).
- (6) (a) P. A. Whitlock, J. T. Muckerman, and R. E. Roberts, *J. Chem. Phys.*, **60**, 3658 (1974); (b) A. Jones and J. L. J. Rosenfeld, *Proc. R. Soc. London, Ser. A*, **333**, 419 (1973); (c) R. E. Roberts and R. B. Bernstein, *Chem. Phys. Lett.*, **6**, 282 (1970); (d) R. E. Roberts, R. B. Bernstein, and C. F. Curtiss, *J. Chem. Phys.*, **50**, 5163 (1969).
- (7) For a review and an exhaustive compilation of literature references: H. O. Pritchard, "Reaction Kinetics", Vol. 1, Specialist Periodical Reports, The Chemical Society, London, 1975, pp 243-290.
- (8) V. H. Shui, J. P. Appleton, and J. C. Keck, *J. Chem. Phys.*, **56**, 4266 (1972).
- (9) B. Widom, *J. Chem. Phys.*, **31**, 1027 (1959).
- (10) O. K. Rice, *J. Phys. Chem.*, **67**, 6 (1963).
- (11) H. S. Johnston and J. Birks, *Acc. Chem. Res.*, **5**, 327 (1972).
- (12) (a) J. H. Kiefer, *J. Chem. Phys.*, **57**, 1938 (1972); (b) J. H. Kiefer, H. P. G. Joosten, and W. D. Breshears, prepublication report, 1974.
- (13) (a) D. L. S. McElwain and H. O. Pritchard, *Symp. (Int.) Combust., [Proc.]*, 13th, 37 (1971); (b) *J. Am. Chem. Soc.*, **91**, 7693 (1969); (c) *ibid.*, **92**, 5027 (1970).
- (14) J. Troe and H. Gg. Wagner, "Physical Chemistry of Fast Reactions," Vol. 1, B. P. Levitt, Ed., Plenum Press, London, 1973, Chapter 1.
- (15) (a) J. Kiefer and R. W. Lutz, *J. Chem. Phys.*, **44**, 658, 668 (1965). (b) One of the three effects which arises from vibration-rotation coupling is a reduction in the measured vibration relaxation time, compared to a nonrotating sho. However, this does not affect the present calculations since we inserted the measured τ_{vib} . H. O. Pritchard and N. I. Labib (prepublication manuscript) have presented a detailed interpretation of rot-vib relaxation times as measured by various techniques. Note J. E. Dove, D. G. Jones, and H. Teitelbaum, *Symp. (Int.) Combust., [Proc.]*, 14th, 177 (1973), and, in particular, their Figure 5. Also refer to the analysis by H. Rabitz and G. Zarur, *J. Chem. Phys.*, **62**, 1425 (1975). (c) J. Lukasik and J. Ducuing, *Chem. Phys. Lett.*, **27**, 203 (1974).
- (16) We are indebted to Professor E. R. Fisher, Wayne State University, Research Institute for Engineering Science, for a copy of his program, described in his report to AFOSR (June 1972); T. J. Keneshea, "A Technique for Solving General Rate Equations . . .", Report No. ATR-70 (8107)-1, Aerospace Corporation, El Segundo, Calif., 1967.
- (17) (a) C. W. Gear, "Numerical Initial Value Problems in Ordinary Differential Equations", Prentice-Hall, Englewood Cliffs, N.J., (b) D. Edelson, *J. Comp. Sci.*, **11**, 455 (1973).
- (18) C. E. Treanor, AIAA, Paper No. 65-29 (Jan 1965).
- (19) (a) T. E. Sharp and D. Rapp, *J. Chem. Phys.*, **43**, 1233 (1965); (b) A. C. Hindmarsh, Report UCID-30001, Rev. 1, Lawrence Livermore Laboratory, Berkeley, Calif., 1972; (c) D. Rapp and P. Englander-Golden, *J. Chem. Phys.*, **40**, 573, 3120 (1964).
- (20) (a) B. Widom, *Science*, **148**, 1555 (1965); (b) N. S. Snider, *J. Chem. Phys.*, **42**, 548 (1965); (c) C. W. Pyun and J. Ross, *ibid.*, **40**, 2572 (1964); (d) E. Donoghue, Ph.D. Dissertation, Cornell University, Ithaca, N.Y., 1973; (e) J. T. Bartsis and B. Widom, prepublication report (*Physica*, in press).
- (21) J. E. Dove and D. G. Jones, *J. Chem. Phys.*, **55**, 1531 (1971).
- (22) H. Wengle, "Recent Developments in Shock Tube Research", D. Bershader and W. Griffith, Ed., Stanford University Press, Stanford, Calif., 1973, p 206.
- (23) E. R. Fisher, private communication.
- (24) S. H. Bauer and S. C. Tsang, *Phys. Fluids*, **6**, 182 (1963).
- (25) (a) G. W. Tregay, W. G. Valance, and D. I. MacLean, *J. Chem. Phys.*, **59**, 1634 (1973); (b) J. E. Dove and D. G. Jones, *Chem. Phys. Lett.*, **17**, 134 (1972).
- (26) (a) H. O. Pritchard, *Can. J. Chem.*, **51**, 3152 (1973); (b) *Acc. Chem. Res.*, in press.
- (27) S. H. Bauer, Presented at the 133d National Meeting of the American Chemical Society, San Francisco, Calif., April 1958, p 8Q, Abstracts.
- (28) This has been confirmed by trajectory calculations, for $\text{Br}_2 \rightleftharpoons 2 \text{Br}$: R. K. Boyd, G. Burns, D. T. Chang, R. G. Macdonald and W. H. Wong, *Symp. (Int.) Combust., [Proc.]*, 15th, 731 (1975).
- (29) S. W. Benson, "Thermochemical Kinetics", Wiley, New York, N.Y., 1968, Table 3.13.
- (30) J. D. Lambert, *J. Chem. Soc., Faraday Trans. 2*, **68**, 364 (1972).
- (31) J. Troe, prepublication manuscript, Ecole Polytechnique Fédérale, Lausanne.
- (32) J. A. Miller and S. H. Bauer, unpublished results.

Kinetics of the Thermal Decomposition of Bis(trifluoromethyl) Peroxide

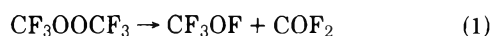
B. Descamps and W. Forst*

Molecular Dynamics Group, Department of Chemistry, Université Laval, Québec G1K 7P4, Canada (Received July 21, 1975; Revised Manuscript Received January 23, 1976)

The pyrolysis of CF₃OOCF₃ (BTMP) was studied in the gas phase from 1 to 200 Torr pressure and between 236 and 272 °C in a nickel reactor by the static method. Decomposition was limited to 5% to avoid complications. The reaction proceeds according to the overall stoichiometry BTMP → CF₃OF + COF₂, as determined by analysis of the products. The reaction is self-inhibited by COF₂ and accelerated by the addition of inert gases N₂, CO₂, and C₂F₆. Addition of 1–400 Torr of C₂F₆ was studied at 232 and 260 °C. A mechanism is proposed that accounts for the initial rate. Its main features are: (1) steady-state concentration of CF₃O radicals maintained by the equilibrium BTMP \xrightleftharpoons{K} 2CF₃O; (2) the rate-determining step is the unimolecular decomposition of the CF₃O radical which is pressure dependent and reversible: CF₃O (+M) $\xrightleftharpoons{K_2}$ COF₂ + F (+M); this also accounts for the inhibition by COF₂. The expression for initial rate is $v = k_2[(k_1/k_5) [\text{BTMP}]]^{1/2}$, with k_2 pressure dependent. The observed experimental activation energy of 49.7 kcal/mol therefore corresponds to $E_2 + \frac{1}{2}(E_1 - E_5)$.

Introduction

It is now generally agreed that bis(trifluoromethyl) peroxide (CF₃OOCF₃, BTMP) decomposes thermally according to the overall stoichiometry



and that between 200 and 300 °C the reaction reaches equilibrium well before all the peroxide has decomposed.¹ This work concerns the kinetics of reaction 1 (the "forward" reaction) in a thermal system, of which several studies have appeared previously.^{2–4} It largely confirms the experimental results of the most recent work, that of Kennedy and Levy,⁴ but examines in more detail the effect of inert gases, and consequently offers a somewhat different interpretation. A preliminary account of our findings has been given some time ago.⁵

Experimental Section

Materials. BTMP and CF₃OF were both purchased from Peninsular ChemResearch, Gainesville, Fla. As received, BTMP contained a small amount of COF₂ which was removed by pumping at –130 °C; CF₃OF contained as impurities CF₄, COF₂, and BTMP. The CF₄ impurity in CF₃OF was removed by pumping at liquid nitrogen temperature (with some loss of CF₃OF). The COF₂ impurity was difficult to remove by pumping, presumably because of formation of an azeotropic mixture⁶ with CF₃OF. The COF₂ was therefore first converted to CO₂ on a column of silica gel, and the CF₃OF was then distilled off at –196 °C, leaving BTMP and CO₂ behind in the residue.

COF₂, CF₄, and C₂F₆ were purchased from the Matheson Co. and were used without further purification.

Apparatus. Experiments were done in a static system consisting of a 442-ml cylindrical reactor fabricated from metal and placed inside a large thermostated oven with a heavy aluminum core to increase its thermal inertia. Dead space was 11 ml. Three different reactor materials were used: stainless steel 18/8, monel, and nickel 200 (a commercial grade of pure nickel), all argon-welded. Temperature was measured with a chromel–alumel thermocouple placed between the reactor and oven core. A conventional vacuum

system was used for the preparation of gas mixtures, except that parts exposed to CF₃OF and COF₂ at room temperature were made of copper, Monel, or stainless steel; the rest was made of glass.

Analysis. The analytical problem was to determine small amounts of CF₃OF and COF₂ in the presence of a large excess of BTMP. Positive ion mass spectrometry is of little help because of the similarity of the mass spectra.⁷ Infrared spectroscopy is of limited usefulness since it permits the determination of COF₂, but not of CF₃OF, in the presence of BTMP. Infrared was used occasionally to provide an independent check on COF₂. The best method was found to be gas chromatography, with a GOW-MAC gas density detector, nitrogen carrier gas, and a silica gel column^{8,9} (Davidson, 40/50 mesh), 30 cm long and 0.32 cm o.d. This column separates, in order of elution, air, CF₄, CF₃OF, C₂F₆, CO₂, and BTMP within about 15 min at 26 °C. We have confirmed by infrared analysis that this column transforms COF₂ quantitatively into CO₂ which is eluted. No reaction products other than COF₂ and CF₃OF were found, except that at high conversion (~50%) a trace of CF₄ appeared. The detector response was calibrated for COF₂, CF₃OF, and BTMP, and all three calibrations were linear.

Procedure. BTMP, either pure or in a suitable mixture, was introduced into the reactor by expansion from a reference volume, giving (measured) initial pressure P_0 . The ensuing pressure increase inside the reactor was followed manometrically by a differential pressure transducer (Pace, Model KP 15). All runs used for the determination of reaction rates were allowed to proceed to no more than 5% decomposition of BTMP to avoid complications due to the back reaction. A small initial portion of each pressure–time recording, representing the first 1% decomposition, was unusable, generally because of a pressure disturbance in the system following admission of the gases into the reactor. Only the portion of the recording between 1 and 5% decomposition was used for rate measurements. The pressure in the reactor at 1% decomposition is called $P_{1\%}$ and the corresponding rate is called the "initial" rate $v_{1\%}$; this was deemed preferable to obtaining the actual initial rate by extrapolation back to time zero. Reaction was stopped by expanding the contents of the reactor into a liquid nitrogen

trap; after a suitable warm-up period, an aliquot of the mixture was injected into the gas chromatograph for analysis, or, occasionally, into an infrared cell with NaCl windows for analysis by infrared.

Preliminary Results

No consistent results could be obtained in the stainless steel reactor, presumably due to surface effects, and it was therefore discarded.

The monel reactor was first cleaned and polished with nitric acid and then conditioned with fluorine gas¹⁰ at about 600 Torr for 17 days at 380 °C. Immediately following such conditioning, fairly good reproducible results on the pyrolysis of BTMP were obtained, but after a few runs reproducibility deteriorated and analysis showed that the reaction yielded an appreciable excess of COF₂ relative to CF₃OF. Since the stoichiometry of reaction 1 requires the two products to be formed in equal amounts, the results in the monel reactor indicate substantial (<50%) heterogeneous decomposition of the originally formed CF₃OF into COF₂ (plus, presumably, F₂, adsorbed or in the gas phase); this was confirmed by pyrolyzing CF₃OF alone at 230 °C. The decomposition of CF₃OF appears to be a very sensitive indicator of the catalytic activity of the surface. The catalysis is probably due to the copper fluoride into which some of the copper in the monel was undoubtedly converted by the pretreatment with fluorine gas. In fact Cady¹¹ has found that several metal fluorides, e.g., silver fluoride among others, are catalysts for the reverse reaction $\text{COF}_2 + \text{F}_2 \rightarrow \text{CF}_3\text{OF}$.

The nickel 200 reactor was first cleaned and polished by a mixture of nitric, sulfuric, orthophosphoric, and acetic acids.¹² This reactor behaved somewhat like the monel reactor, but the amount of CF₃OF catalytically decomposed to COF₂ was very much less. Conditioning of the nickel reactor with 5–6 Torr of BTMP for several minutes immediately prior to every run further reduced the catalytic decomposition of CF₃OF to a negligible value. Under such conditions the products of BTMP pyrolysis contained equimolar amounts of CF₃OF and COF₂ (within experimental error, cf. Table I), and therefore the reaction may be considered to be substantially free of surface effects. The pretreatment with BTMP was used in all kinetic runs reported in this paper, and the reactor so treated will be referred to as a "clean" nickel reactor.

We have next made a check to see if the recorded pressure increase in the "clean" nickel reactor (ΔP , corrected for dead space by the method of Allen¹³) was an actual measure of the progress of reaction as determined by analysis. Results of several runs, carried to higher conversion than usual for better precision, are given in Table I, and they show that ΔP is indeed a direct measure of either COF₂ or CF₃OF formed, or indirectly, of BTMP reacted.

Results

All results reported here refer to the "clean" nickel reactor and were obtained from pressure–time recordings taken during a run.

Reaction Order. Figure 1 shows a logarithmic plot of v_{in} vs. P_{in} at several temperatures. The slope α gives the order with respect to concentration^{14a} and is seen to be roughly unity. However if we consider a single run and determine the order with respect to time,^{14a} it is found¹⁵ that this order increases, i.e., the rate falls off more rapidly than

TABLE I: Results of BTMP Pyrolysis in "Clean" Nickel Reactor^a

from pressure increase in reactor, ΔP , Torr	Amount of BTMP reacted as determined	
	from product analysis, Torr CF ₃ OF	COF ₂
2.55	2.62	2.71
5.00	5.05	4.89
7.55	7.45	7.34
10.0	9.84	10.0
12.5	12.4	12.6

^a $T = 286$ °C, initial pressure of BTMP = 20 Torr. All pressures refer to reactor temperature.

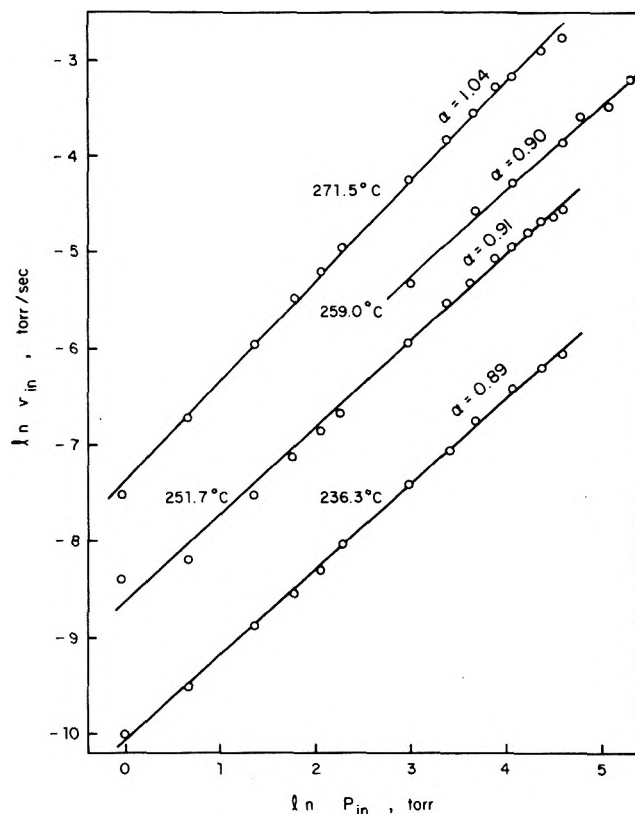


Figure 1. Order with respect to concentration. Logarithmic plot of initial rate (v_{in}) vs. initial pressure of BTMP (P_{in}) at four temperatures. The slope α gives the order with respect to concentration.

would be expected for a first-order reaction, suggesting self-inhibition, perhaps by one of the products.

Inhibition. The effect on v_{in} of the addition of up to 2 Torr of CF₃OF, F₂, and COF₂ was tested at fixed initial concentration of BTMP. Addition of F₂ and of CF₃OF had little effect on v_{in} , whereas COF₂ showed a pronounced inhibiting influence. To make sure that all the self-inhibition observed in the course of BTMP pyrolysis could be attributed entirely to COF₂, several pyrolyses of BTMP with and without initially added COF₂ were run to 5% decomposition. The results, shown in Figure 2, indicate that there is no difference between the inhibiting effect of COF₂ added initially or produced normally in the course of a pyrolysis, confirming that COF₂ is the sole agent responsible for inhibition, and that the degree of inhibition is related to the absolute amount of inhibitor present.

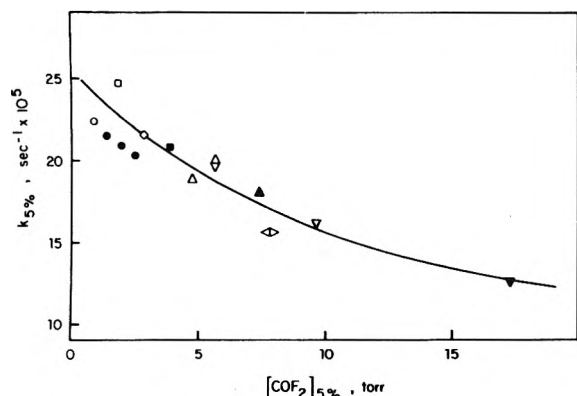


Figure 2. Inhibition by COF_2 . Ordinate is first-order rate constant calculated at 5% decomposition. Abscissa is total amount of COF_2 present at 5% decomposition, which is the sum of COF_2 produced from BTMP in the course of the pyrolysis, plus any COF_2 added initially: $T = 259^\circ\text{C}$; open symbols, no COF_2 added initially (pyrolysis of pure BTMP); full symbols, COF_2 added initially (pyrolysis of BTMP + COF_2): initial pressure of BTMP P_0 (Torr) = 20 (O), 40 (□), 60 (◇), 100 (Δ), 120 (◊), 160 (◈), 200 (▽).

First-order dependence of v_{in} on P_{in} and self-inhibition by COF_2 are also the main features of the reaction determined by Kennedy and Levy⁴ at comparable pressures of BTMP. At BTMP pressures higher than those used by us, they found a half-order dependence of v_{in} on P_{in} ; this point is taken up later in connection with eq 11 and 12. It should be noted that their results were obtained in an aluminum reactor, ours in a nickel reactor. Such basic agreement between studies done in the presence of two very different surfaces may be cited as further evidence for the absence of important surface effects in either study.

The form of the curve in Figure 2 suggests that the rate v can be written

$$v = \frac{C_1[\text{BTMP}]}{1 + C_2[\text{COF}_2]} \quad (2)$$

where C_1 and C_2 are constants and square brackets represent concentrations. Since v_{in} corresponds to $[\text{COF}_2] \sim 0$, we have $v_{\text{in}} = C_1[\text{BTMP}]_{\text{in}}$, i.e., first-order dependence on $[\text{BTMP}]$, in accordance with the results of Figure 1.

Inert Gas Effect. Three inert gases were used as additive: N_2 , CO_2 , and C_2F_6 . All three increase the rate, although to a different degree, as shown in Figure 3. We have confirmed by analysis that these gases are truly inert, i.e., do not change the nature or the proportion of the products in the pyrolysis of BTMP. To take into account the accelerating effect of inert gases we have to write for the initial rate

$$v_{\text{in}} = C_1[\text{BTMP}]_{\text{in}}^m [\text{M}]_{\text{in}}^n \quad (3)$$

where $m + n = \alpha$, m and n being partial orders with respect to BTMP and M, respectively, and $[\text{M}]$ is the concentration of inert gas defined below.

The inert gas effect indicates that the BTMP pyrolysis probably involves an energy transfer stage, in which BTMP itself very likely acts as an energy transfer agent, i.e., as an inert gas. It is therefore necessary to interpret $[\text{M}]$ more generally as a weighted sum of the concentrations of all inert gases present in the reaction system,¹⁶ including, in principle, the products. The problem becomes simplified in the absence of products, i.e., at the beginning of the reaction; then in the presence of one foreign inert gas X we have

$$[\text{M}]_{\text{in}} = [\text{BTMP}]_{\text{in}} + a[\text{X}]$$

where a is the relative energy transfer efficiency of X relative to BTMP. Equation 3 thus becomes

$$v_{\text{in}} = C_1[\text{BTMP}]_{\text{in}}^m \{[\text{BTMP}]_{\text{in}} + a[\text{X}]\}^n \quad (4)$$

If $[\text{BTMP}]_{\text{in}}$ is kept constant, eq 4 can be written

$$v_{\text{in}}^{1/n} = \text{constant} \times \{[\text{BTMP}]_{\text{in}} + a[\text{X}]\} \quad (5)$$

which is an equation of a straight line, but containing two

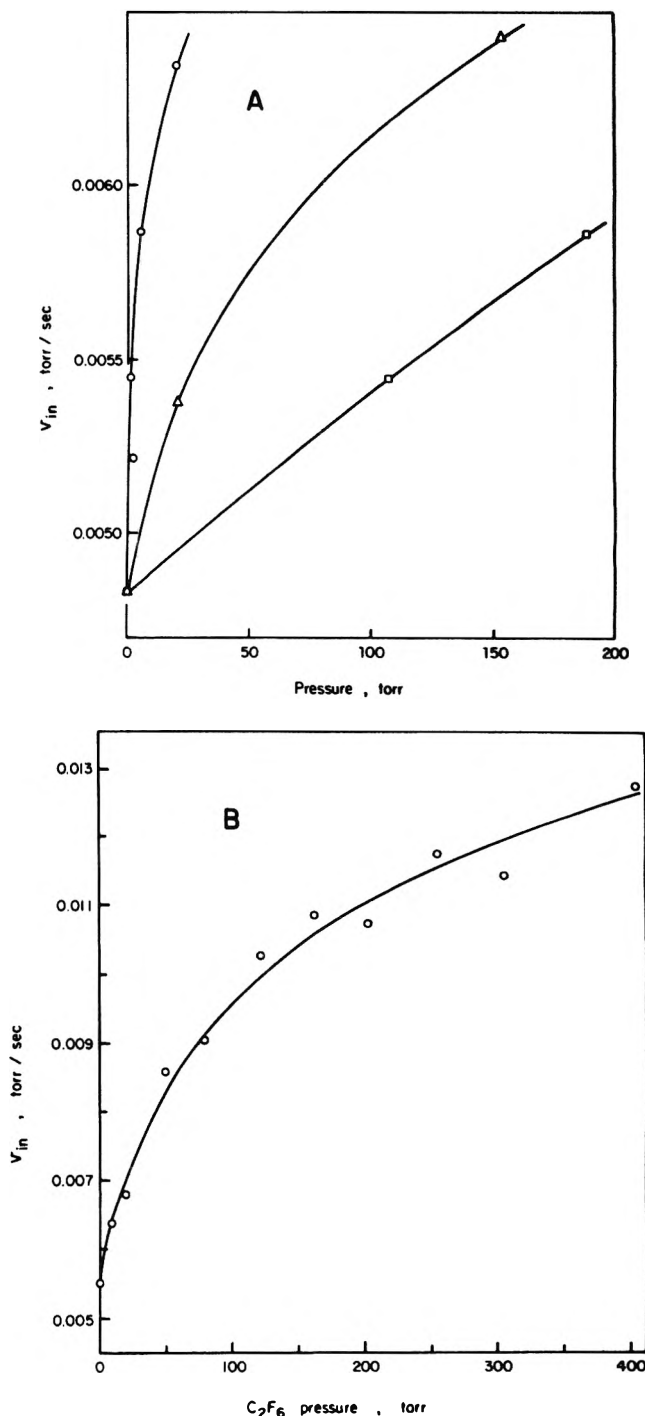


Figure 3. Example of inert gas effect. Initial rate v_{in} as a function of inert gas pressure. Initial pressure of BTMP constant at 20 Torr. (A) Low pressure results: N_2 (□); CO_2 (Δ); C_2F_6 (O), $T = 258.9^\circ\text{C}$. (B) High pressure results for C_2F_6 (O), $T = 259.7^\circ\text{C}$.

unknowns, n and a . Taking experimental results for $X = C_2F_6$, in which $[C_2F_6]$ was varied between 0 and 400 Torr and $[BTMP]_{in}$ kept constant, n in eq 5 was first adjusted until a "best" straight line was obtained by maximizing the correlation coefficient. Then the "constant" and a were obtained from the intercept and slope, respectively. The result¹⁵ for $X = C_2F_6$ was $n = 0.33 \pm 0.11$, $a = 0.70 \pm 0.33$, as determined over the temperature range 232–260 °C. A few runs over the same temperature range with $X = CO_2$ yielded $n = 0.31$ and $a = 0.12$, showing that n is independent of X , as it should be, and that CO_2 is a much less efficient energy transfer agent than C_2F_6 , which is what one would expect.

Substituting the results for $X = C_2F_6$ into eq 4 and taking logarithms we get

$$\ln \frac{v_{in}}{[BTMP]_{in} + 0.70[C_2F_6]^{0.33}} = \ln C_1 + m \ln [BTMP]_{in} \quad (6)$$

With constant $[C_2F_6]$ and variable $[BTMP]_{in}$ this is the equation of a straight line of slope m . Experimental results treated in accordance with eq 6 yield¹⁵ $m = 0.55 \pm 0.09$, again over the range 232–260 °C. The total order of v_{in} is $m + n = (0.33 \pm 0.11) + (0.55 \pm 0.09)$, which has been determined previously as $\alpha = 0.93 \pm 0.07$; thus the partial orders m and n determined from inert gas experiments are consistent, within experimental error, with the total order determined in the absence of foreign inert gas.

Initial rates give only information about the numerator of eq 2. It now remains to be determined if the denominator of eq 2 is also dependent on the concentration of inert gas. Experimental data obtained between 232 and 260 °C with $X = C_2F_6$ were used to calculate C_1 and C_2 from eq 2, and it turns out¹⁵ that C_1 is a constant independent of $[C_2F_6]$, as we already know, but C_2 increases with $[C_2F_6]$, although it is independent of $[BTMP]$. This suggests that C_2 should be written

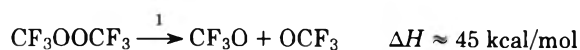
$$C_2 = C_2' \frac{[M]}{[BTMP]}$$

where C_2' is a (true) constant independent of pressure. Thus to fully account for the effect of inert gas, eq 2 should be written in the form

$$v = \frac{C_1 [BTMP]^{0.55} [M]^{0.33}}{1 + C_2' \frac{[M][COF_2]}{[BTMP]}} \quad (7)$$

Discussion

Initial Reaction Steps. The objective is to find first a mechanism that would account for the empirical rate equation (eq 2). From Table II we see that $D(CF_3OOCF_3) > D(CF_3O-OCF_3)$, so that the pyrolysis must start by O–O rupture:



In the pyrolysis of dialkyl peroxides the initial O–O rupture is followed by²² hydrogen abstraction by CH_3O to form CH_3OH , a reaction which is exothermic and requires an activation energy of about²³ 10 kcal/mol. The analogous reaction of perfluorinated compounds, however, is endothermic by about 80 kcal/mol (Table II), and therefore is very unlikely in a thermal system. The reason for the dissimilarity between the perfluorinated and perhydrogenated systems

TABLE II: Bond Dissociation Energies (kcal/mol)

	Y = H	Ref	Y = F	Ref
$D(CY_3O-OCY_3)$	36.1	17	46.2	36
$D(CY_3-OOCY_3)$	71	1	65	1
$D(Y-CY_2OY)$	92	18	120	19
$D(CY_3O-Y)$	102	20	43.5	21
$D(Y-CY_2OOCY_3)$	~92	a	≤106	19

^a Assuming that $D(H-CH_2OOCCH_3) \sim D(H-CH_2OH)$.

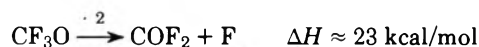
TABLE III: Standard Enthalpies of Formation

Substance	$H_{298 K}$, kcal/mol	Ref
F	+18.9 ± 0.4	a
COF ₂	-152.7 ± 0.4	a
CF ₄	-223.04 ± 0.3	a
CF ₃ OF	-182.8 ± 0.3	a
CF ₃	-112.4 ± 1	a
CF ₃ OOCF ₃	-360.2 ± 3	1
CF ₃ O	-156.8 ± 2	4

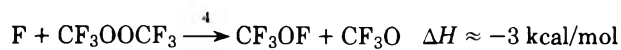
^a "JANAF Thermochemical Tables", *Natl. Stand. Ref. Data Ser., Natl. Bur. Stand., No. 37*, (1971).

is the very weak O–F bond in CF_3OF compared with the O–H bond in CH_3OH (Table II).

The only plausible alternative in the perfluorinated system seems to be



which is endothermic to about 23 kcal/mol, if we use enthalpies of formation given in Table III. At low conversion, the most abundant species is BTMP, so that the most likely subsequent step is

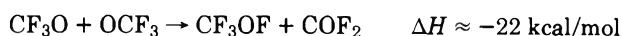


which is slightly exothermic (Table II). Since CF_3O is thus regenerated, reactions 2 and 4 constitute a short chain.

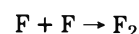
Chain Termination. Plausible chain-terminating reactions are



which are both exothermic. The disproportionation reaction



appears to be very slow compared with reaction 5, even with photolytically generated^{24–26} CF_3O , although a similar reaction is one of the major reactions producing CH_3OH in the pyrolysis of dimethyl peroxide.²³ The reason for the dissimilarity between the perfluorinated and perhydrogenated systems seems to be again the weak O–F bond in CF_3OF . Another possible chain-terminating step



must be eliminated because molecular fluorine is not a product of the pyrolysis. In fact addition of a small pressure of molecular fluorine is without any marked effect on

the pyrolysis (see Results) and this is consistent with the mechanism above which involves fluorine atoms but not F₂. It can be deduced from the data of Lloyd²⁷ that the equilibrium constant for the thermal dissociation F₂ ⇌ 2F is about 10⁻¹⁴ mol/cm³ at 250 °C, the temperature of our experiments, so that the thermal dissociation of fluorine could provide significant amounts of fluorine atoms only at substantially higher fluorine pressures than those we have used. Rough calculations in support of this are given below in connection with eq 17.

Inhibition. The mechanism proposed so far does not account for the observed inhibition by COF₂. The most likely candidate for inhibition is the reverse of reaction 2



a reaction that has been invoked previously^{28,29} in the system COF₂ + CF₃OF and which Aymonino³⁰ has observed in the photolysis of F₂ in the presence of COF₂. (However recently Schumacher et al.³¹ have speculated that in a photochemical system the reaction might be F + COF₂ → CF₂OF.)

Mechanism I. Reactions 1–6, but excluding reaction 6, will be called Mechanism I. This mechanism can be solved exactly in the usual steady-state approximation, yielding

$$v = -\frac{d[BTMP]}{dt} = \frac{k_2(k_1/k_5)^{1/2}[BTMP]^{1/2}}{1 + k_3[COF_2]/k_4[BTMP]} \quad (8)$$

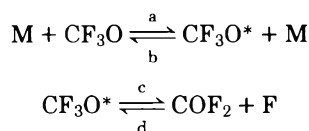
which is an expression fairly close to the empirical eq 7, except for the inert gas effect which has not yet been considered.

Equation 8 is also strongly reminiscent of the well-known rate expression for formation of HBr in the H₂ + Br₂ reaction,^{14b} with which mechanism I shares the principal characteristics (corresponding features of the H₂ + Br₂ reaction in parentheses): the equilibrium BTMP ⇌ 2CF₃O (Br₂ ⇌ 2 Br) furnishes the steady-state concentration of CF₃O (Br) radicals, and the rate-determining step is reversible, CF₃O ⇌ COF₂ + F (H₂ + Br ⇌ HBr + H), which leads to a very efficient inhibition of the reaction by COF₂ (HBr). Thus the numerator of the rate expression (8) contains the rate constant for the rate-determining step, k₂, multiplied by the square root of the equilibrium constant for the chain-initiating reaction, (k₁/k₅)^{1/2}; the denominator contains the ratio of rate constants for inhibition, k₃, and chain propagation, k₄.

Insofar as the pressure dependence of inert gases is concerned, reactions 1, 5, and 4 are unlikely to be in their pressure-dependent region at the pressures used in this work because they involve BTMP, a large molecule.

Reaction 2 is the unimolecular decomposition of a small radical originally formed in the strongly endothermic reaction 1. As formed in reaction 1, the radical CF₃O is almost certainly "cold", i.e., without sufficient internal energy to decompose further, unless it acquires additional energy by collision. Examples of such behavior are numerous.^{32–35}

Assuming a strong-collision (Lindemann) mechanism for the collisional activation of CF₃O, reactions 2 and 3 become



where the asterisk represents internal excitation energy sufficient for decomposition. Introducing this refinement

into mechanism I results in the replacement of k₂ by k_{uni}, where

$$k_{uni} = \frac{k_a k_c [M]}{k_b [M] + k_c} \quad (9)$$

is the pseudounimolecular rate constant in the usual sense for the forward dissociation CF₃O → COF₂ + F, and the replacement of k₃ by k_{bi}, where

$$k_{bi} = \frac{k_d k_b [M]}{k_b [M] + k_c} \quad (10)$$

can be looked upon as the pseudobimolecular rate constant for the reverse reaction COF₂ + F → CF₃O. Equation 8 thus becomes

$$v = \frac{k_{uni}(k_1/k_5)^{1/2}[BTMP]^{1/2}}{1 + k_{bi}[COF_2]/k_4[BTMP]} \quad (11)$$

Comparing constants between the numerators of eq 7 and 11 we find

$$C_1[M]^{0.33} = k_{uni}(k_1/k_5)^{1/2} \quad (12)$$

Comparing denominators between eq 7 and 11 we find C₂'[M] = k_{bi}/k₄.

The pseudoconstant k_{uni} depends on pressure roughly as [M]^q, where 0 ≤ q ≤ 1, so that the 0.33 order with respect to [M] = C₂F₆ found experimentally is entirely what one would expect for a unimolecular decomposition in the pressure-dependent region. Due to the size of the BTMP molecule, we can expect it to be an efficient energy transfer agent, so that when [M] = BTMP (i.e., in the absence of inert gas), it would very likely take only moderately high (~1 atm) pressure for k_{uni} to become of zero order with respect to [M], i.e., v_{in} to become proportional to [BTMP]^{1/2}. This is precisely what has been found by Kennedy and Levy⁴ at BTMP pressures above about 200 Torr. The size of BTMP will also cause the first-order region of k_{uni} (i.e., the 3/2-order region of v_{in}) to be located at pressures (~< 0.1 Torr) well below the lowest BTMP pressure used by us or by Kennedy and Levy.⁴

Mechanism I thus appears to account quite satisfactorily for the main features of the pyrolysis, even though the chain termination via reaction 6 has not been considered. This reaction cannot be dismissed because it was found²⁹ to be the rate-determining step in the inverse reaction CF₃OF + COF₂ → BTMP, and therefore must intervene in the forward reaction as well.

The complete mechanism comprising all the reactions 1–6 cannot be solved in closed form, but we can solve the mechanism consisting of reactions 1–4 and 6, but excluding reaction 5. It is sufficient to examine only the expression for v_{in}. Application of the steady-state hypothesis leads to

$$v_{in} \sim (k_1 k_2 k_4 / k_6)^{1/2} [BTMP]_{in}$$

At pressures below ~100 Torr, k₂ and k₆ will be both pressure dependent, but since v_{in} depends only on the ratio k₂/k₆, v_{in} will be substantially independent of [M], contrary to experiment. Hence this mechanism cannot be the principal mechanism. This is not to suggest that reaction 6 does not occur, but merely that under our experimental conditions (low conversion) reaction 6 is relatively unimportant. At low conversion, the principal constituent of the reaction mixture is BTMP, and under such conditions most fluorine atoms would be expected to disappear via reaction 4 rather than reaction 6.

Evaluation of Constants. We now return to mechanism I

and proceed to evaluate the numerical values of the constants in the rate expression. To this end we rewrite the empirical eq 7 in the form

$$v = \frac{c_1[\text{BTMP}]^{0.5}}{1 + c_2[\text{COF}_2]} \quad (13)$$

The new constants c_1 and c_2 are different from the old set C_1 and C_2 because they contain the inert gas effect. Since k_{uni} , and therefore c_1 , are pressure dependent, it is convenient to extrapolate c_1 to infinite pressure. Extrapolation of k_{uni} yields k_∞ , and therefore

$$\lim_{[M] \rightarrow \infty} c_1 = c_{1\infty} = k_\infty(k_1/k_5)^{1/2} \quad (14)$$

This is shown in Figure 4 as a plot of $1/c_1$ vs. $1/P_0$. Arrhenius plot for $c_{1\infty}$ yields the result

$$c_{1\infty} = (1.2 \pm 0.1)10^{18} \exp[-(49\,700 \pm 3\,700)/RT] \text{ Torr}^{1/2} \text{ s}^{-1} \quad (15)$$

The activation energy corresponding to $c_{1\infty}$ is thus $E_a = 49.7$ kcal/mol; recall this refers to the "clean" nickel reactor. It may be of interest that in the monel reactor, $E_a \sim 40$ kcal/mol, a substantially lower value, indicating appreciable heterogeneous contribution. From eq 14 we see that E_a corresponds to

$$E_a = E_\infty + \frac{1}{2}(E_1 - E_5) \quad (16)$$

If we take³⁶ $E_1 = 46.2$ kcal/mol and assume that $E_5 \sim 0$, as one would expect for the recombination of two radicals, eq 16 yields $E_\infty \sim 26.6$ kcal/mol. This appears to be in line with the estimate made by Benson³⁷ that a unimolecular chain-propagating step cannot have an activation energy larger than ~ 64 cal/mol deg, which works out to 35.5 kcal/mol at 250 °C. We have found previously that $\Delta H \sim 23$ kcal/mol for reaction 2; when combined with the above value of E_∞ , this yields $E_d \sim 3$ kcal/mol for the activation energy of the reverse reaction $F + \text{COF}_2 \rightarrow \text{CF}_3\text{O}$, which seems entirely plausible.

Extrapolation of c_2 vs. $1/P_0$ gives

$$c_{2\infty} = k_d/k_4 \quad (17)$$

Arrhenius plot for $c_{2\infty}$ yields the negative activation energy of ca. -17 kcal/mol. Thus $E_d - E_4 \sim -17$ kcal/mol which combined with the previous result for E_d gives $E_4 \sim 20$ kcal/mol. Such fairly high value for E_4 would suggest that reaction 4 does not occur as a concerted process, i.e., that as the fluorine atom is approaching the O-O bond in BTMP starts to break first and the O-F bond forms only after the O-O rupture is nearly complete.

The value of E_4 can be used to obtain an estimate of the steady-state concentration of fluorine atoms, $[F]_{\text{ss}}$, that can be expected on the basis of mechanism I according to which $[F]_{\text{ss}} = v/k_4[\text{BTMP}]$. If we take $k_4 \sim 10^{13} \exp(-E_4/RT) \text{ cm}^3 \text{ mol}^{-1} \text{ s}^{-1}$ and $[\text{BTMP}] \simeq 10 \text{ Torr}$, then $v \sim 9.1 \times 10^{-4} \text{ Torr s}^{-1}$ (Figure 1), from which $[F]_{\text{ss}} \sim 7 \times 10^{-2} \text{ Torr}$ at 250 °C. At the same temperature, the equilibrium pressure of F atoms generated from 2 Torr of F_2 by thermal dissociation is only about $8 \times 10^{-4} \text{ Torr}$, which explains why addition of 2 Torr of F_2 had no effect on the reaction (it would take ~ 200 atm of F_2 to produce $7 \times 10^{-2} \text{ Torr}$ of F atoms).

The result for $c_{1\infty}$ can also be used to obtain an estimate of the chain length based on mechanism I. Chain length l is usually defined as overall rate divided by the rate of the chain-initiating reaction. From mechanism I we have, ne-

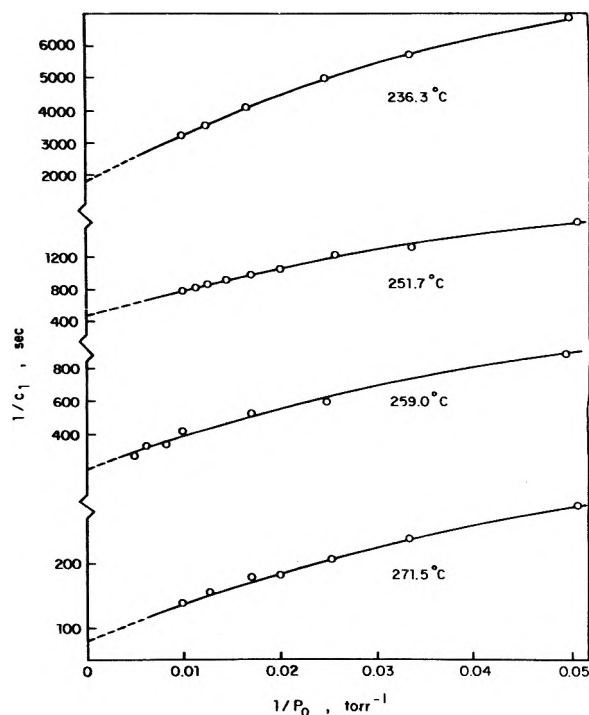


Figure 4. Extrapolation for $c_{1\infty}$ at four different temperatures. Plot of $1/c_1$ vs. $1/P_0$, where $c_1 = k_{\text{uni}}(k_1/k_5)^{1/2}$. Extrapolation to $1/P_0 \rightarrow 0$ yields $1/c_{1\infty}$.

glecting inhibition (i.e., in the early stages of the reaction)

$$l = \frac{c_{1\infty}[\text{BTMP}]^{1/2}}{k_1[\text{BTMP}]} \quad (18)$$

The chain length is thus inversely proportional to the square root of BTMP pressure. We know³⁶ that $k_1 = 10^{15.9} \exp(-46\,200/RT) \text{ s}^{-1}$, which combined with eq 15 gives, at 530 K

$$l = 5.44/[\text{BTMP}]^{1/2} \quad (19)$$

At 100 Torr of BTMP, $l = 0.5$, so that the chain length is already quite small at only moderate pressures of BTMP.

Mechanism II. In view of the very small chain length predicted by mechanism I, we have to examine the possibility that the mechanism of the pyrolysis of BTMP may not involve a chain. A possible nonchain reaction scheme would consist of reactions 1, 5, 2, 3, and 6. This reaction mechanism will be called mechanism II. It does not admit of an exact solution, but can be solved approximately if we look upon it as a variant of mechanism I, i.e., on the assumption (ignoring inert gas effect for the moment) that (1) the rate-determining step is reaction 2 so that

$$v = k_2[\text{CF}_3\text{O}] - k_3[\text{COF}_2][F]$$

(2) the steady-state concentration of CF_3O radicals is controlled by reaction 1 and its inverse, reaction 5; thus

$$[\text{CF}_3\text{O}] \approx (k_1/k_5)^{1/2}[\text{BTMP}]^{1/2}$$

With these assumptions we obtain

$$v \approx \frac{k_2(k_1/k_5)^{1/2}[\text{BTMP}]^{1/2}}{\frac{k_3[\text{COF}_2]}{k_6(k_1/k_5)[\text{BTMP}]^{1/2}} + 1} \quad (20)$$

This is again of the general form of eq 13, and in fact the empirical constant c_1 has the same interpretation in mech-

anisms I and II: inert gas effects result, as before, in the replacement of k_2 by k_{ini} (eq 9). Thus the same extrapolation procedure concerning c_1 applies, and mechanism II yields again eq 15 for $c_{1\infty}$.

The constant c_2 , on the other hand, though numerically the same, has a different interpretation in mechanism II:

$$c_2 = k_3/k_6(k_1/k_5)[\text{BTMP}]^{1/2} \quad (21)$$

Here once more inert gas effects cancel because they involve only k_3 and k_6 and the two constants appear only as a ratio. A plot of $1/c_2$ vs. $P^{1/2}$ gives fairly good straight lines of slope $(k_6/k_3)(k_1/k_5)^{1/2}$, and the Arrhenius plot of the slopes yields¹⁵

$$E_6 + \frac{1}{2}(E_1 - E_5) - E_3 = 16.4 \pm 5.7 \text{ kcal/mol} \quad (22)$$

Reactions 5 and 6 are radical recombinations, and therefore $E_5 = E_6 \sim 0$. If we make use of the previously determined $E_3 \sim E_d \sim 3 \text{ kcal/mol}$, and take $E_1 = 46.2 \text{ kcal/mol}$, we obtain

$$\frac{1}{2}E_1 - E_3 \approx 20 \text{ kcal/mol}$$

which is reasonably consistent with eq 22.

Mechanism II thus yields merely an alternative interpretation for the denominator of the rate expression 13, i.e., for rate after the start of the reaction. It will be noted that the fit of the data is reasonably good whether the denominator of eq 13 is interpreted in terms of mechanisms I or II; however, in either interpretation there is a fair amount of scatter in the data, suggesting that the maximum 5% conversion used in our work is not sufficient to probe accurately the fine detail of the reaction much beyond the initial rate.

Conclusions

It may seem somewhat surprising at first sight that mechanism I, a chain mechanism, and mechanism II, a nonchain mechanism, both give a reasonably good interpretation of the experimental results. We have seen, however, that the chain, if there is one, is in fact likely to be very short, and therefore the distinction between a chain mechanism and a nonchain mechanism becomes a very fine one, if not purely semantic. In addition, mechanism II was conceived at the outset as a variant of mechanism I of which it conserves the principal characteristics.

The principal characteristics of the initial stages of the pyrolysis of BTMP, insofar as we have been able to determine on the basis of our experimental results, and which are embodied in mechanisms I and II, are that after the initial split of BTMP into two CF₃O radicals (reaction 1), most radicals "do not do anything" except recombine to give back BTMP (reaction 5). A steady-state concentration of CF₃O is thus set up, but occasionally a CF₃O radical becomes sufficiently activated by collisions to decompose COF₂ and F (reaction 2). This is the rate-determining step, which, however, is reversible and leads to self-inhibition of the reaction by COF₂ (reaction 3) as this compound accumulates in the system. What happens next appears to be of little consequence, at least at the beginning of the reaction, and constitutes the main distinction between mechanisms I and II.

While we agree with Kennedy and Levy⁴ on the basic facts of the decomposition, our interpretation, which accounts satisfactorily for our own results as well as theirs, differs fundamentally in that they consider reaction 1 to be rate-determining at the beginning of the pyrolysis, while to us the rate-determining step is reaction 2. The reason for our different interpretation is the inert gas effect which they did not notice. We thus believe that the overall activation energy of 46.2 kcal/mol that they observed actually corresponds to the pressure falloff region of the reaction, while our value of 49.7 kcal/mol is the limiting high pressure activation energy.

Acknowledgments. The authors are grateful to Professors J. B. Levy and G. H. Cady for correspondence and preprints of their work, and to the National Research Council of Canada for financial support.

References and Notes

- (1) J. B. Levy and R. C. Kennedy, *J. Am. Chem. Soc.*, **94**, 3302 (1972).
- (2) H. L. Roberts, *J. Chem. Soc.*, 4538 (1964).
- (3) K. O. Christie and D. Pilipovich, *J. Am. Chem. Soc.*, **93**, 51 (1971).
- (4) R. C. Kennedy and J. B. Levy, *J. Phys. Chem.*, **76**, 3480 (1972).
- (5) B. Descamps and W. Forst, Presented at the 162nd National Meeting of the American Chemical Society, Division of Fluorine Chemistry, Washington, D.C. Sept 1971, Abstract No. 4.
- (6) K. B. Kellogg and G. H. Cady, *J. Am. Chem. Soc.*, **70**, 3986 (1948).
- (7) R. S. Porter and G. H. Cady, *J. Am. Chem. Soc.*, **79**, 5625 (1957).
- (8) S. A. Green and F. M. Wachi, *Anal. Chem.*, **35**, 928 (1963).
- (9) P. J. Aymonino, *J. Inorg. Nucl. Chem.*, **27**, 2675 (1965).
- (10) W. A. Cannon, S. K. Asummaa, W. D. English, and N. A. Tiner, *Trans. Met. Soc. AIME*, **242**, 1635 (1968).
- (11) G. H. Cady, *An. Asoc. Quim. Argent.*, **59**, 125 (1971); R. C. Kennedy and G. H. Cady, *J. Fluorine Chem.*, **3**, 41 (1973).
- (12) W. J. McG. Tegart, "Polissage électrolytique des métaux", Dunod, Paris, 1960.
- (13) A. O. Allen, *J. Am. Chem. Soc.*, **56**, 2053 (1934).
- (14) K. J. Laidler, "Chemical Kinetics", 2nd ed, McGraw-Hill, New York, N.Y., 1965: (a) p 16; (b) p 329.
- (15) For details see B. Descamps, Ph.D. Thesis, Université Laval, 1972. Microfiche available for \$2.00 from Canadian Theses Division, Cataloguing Branch, National Library of Canada, 395 Wellington St., Ottawa, Canada, K1A 0N4. Order no. 18946.
- (16) W. Forst, *Can. J. Chem.*, **36**, 1308 (1958).
- (17) P. L. Hanst and J. G. Calvert, *J. Phys. Chem.*, **63**, 104 (1959).
- (18) A. M. Tarr and E. Whittle, *Trans. Faraday Soc.*, **60**, 2039 (1964).
- (19) K. A. G. MacNeil and J. C. J. Thynne, *Int. J. Mass Spectrom. Ion Phys.*, **9**, 135 (1972).
- (20) R. Shaw and A. F. Trotman-Dickenson, *J. Chem. Soc.*, 3210 (1960).
- (21) J. Czarnowski, E. Castellano, and H. J. Schumacher, *Z. Phys. Chem. (Frankfurt am Main)*, **65**, 225 (1969); *Chem. Commun.*, **20**, 1255 (1968).
- (22) L. M. Toth and H. S. Johnston, *J. Am. Chem. Soc.*, **91**, 1276 (1969).
- (23) W. H. Richardson and H. E. O'Neil in "Comprehensive Chemical Kinetics", Vol. 5, C. H. Bamford and C. F. H. Tipper, Ed., Elsevier, Amsterdam, 1972, p 483 ff.
- (24) C. J. Schack and W. Maya, *J. Am. Chem. Soc.*, **91**, 2902 (1969).
- (25) C. T. Ratcliffe, C. V. Hardin, L. R. Anderson, and W. B. Fox, *J. Am. Chem. Soc.*, **93**, 3889 (1971).
- (26) L. C. Duncan, Ph.D. Thesis, University of Washington, 1964.
- (27) A. C. Lloyd, *Int. J. Chem. Kinet.*, **3**, 39 (1971).
- (28) R. S. Porter and G. H. Cady, *J. Am. Chem. Soc.*, **79**, 5628 (1957).
- (29) J. Czarnowski and H. J. Schumacher, *Z. Phys. Chem. (Frankfurt am Main)*, **73**, 68 (1970).
- (30) P. J. Aymonino, *Proc. Chem. Soc.*, 341 (1964).
- (31) M. I. Lopez, E. Castellano, and H. J. Schumacher, *J. Photochem.*, **3**, 97 (1974).
- (32) M. C. Lin and M. H. Back, *Can. J. Chem.*, **44**, 2357 (1966).
- (33) L. F. Loucks and K. J. Laidler, *Can. J. Chem.*, **45**, 2795 (1967).
- (34) D. L. Cox, R. A. Livermore, and L. Phillips, *J. Chem. Soc. B*, 245 (1966).
- (35) M. F. R. Mulcahy and D. J. Williams, *Aust. J. Chem.*, **17**, 1291 (1964).
- (36) B. Descamps and W. Forst, *Can. J. Chem.*, **53**, 1442 (1975).
- (37) S. W. Benson, "Thermochemical Kinetics", Wiley, New York, N.Y., 1968, p 122.

Pulse Radiolytic Investigations of Some Peroxyhydroxycyclohexadienyl Radicals

O. I. Mičić* and M. T. Nenadović

Boric Kidrič Institute of Nuclear Sciences, Vinča, Yugoslavia (Received September 29, 1975)

Publication costs assisted by the Petroleum Research Fund

The absorption spectra and decay kinetics of the peroxy OH and H adduct of phenol have been studied using the pulse radiolysis technique. Both peroxy radicals decompose by a first-order reaction. $O_2C_6H_5O\cdot H(OH)$ decomposes to HO_2 and a product which partly forms hydroquinone after some intramolecular rearrangement. In alkaline deaerated solutions of phenol disproportionation of phenoxyl radicals produces benzo-semiquinone radical anions. Formation of this transient is suppressed by the presence of O_2 . The reaction rate constants of $C_6H_5OH(OH)\cdot$, $C_6H_5OH(H)\cdot$, $C_6H_5O\cdot$, $C_6H_4(OH)_2(H)\cdot$, and $C_6H_4(OH)_2(OH)\cdot$ radicals with oxygen have been determined.

Introduction

The formation of hydroxycyclohexadienyl radicals by addition of hydroxyl radicals to aromatic rings or of H atoms to hydroxybenzenes has been studied in a number of cases.¹ Reaction rates of some hydroxycyclohexadienyl radicals with oxygen have been determined by pulse radiolysis.² No experimental evidence is, however, available about the peroxy radicals formed in these reactions, except for the study by Dorfman et al.,³ when the absorption spectrum of the peroxy radical was obtained in oxygenated solutions of benzene.

Many organic peroxy radicals decompose, directly or indirectly, to yield the perhydroxyl radical, thus creating a new experimental problem of identification and discrimination between their spectra.⁴⁻¹⁰ In the present work, we investigated oxygen reactions with mono- and dihydroxycyclohexadienyl radicals, formed in aqueous phenol solution. An attempt was made to obtain information about the formation of peroxy radicals and their subsequent reactions. Hydroquinone was used for comparison because of its capability to form isomeric radicals by reacting with H atoms.

In this work, pulse radiolysis was applied in the study of the spectral properties and kinetic behavior of the intermediates formed. In some cases, for complementary information steady state irradiations with a γ source were also performed.

Experimental Section

Solutions were prepared from analytical grade chemicals (BDH or Merck). Triply distilled water was used. The solution pH was adjusted with $HClO_4$, $NaOH$, or phosphate buffers. For neutral solutions the buffer concentration was only 6×10^{-5} M and the pH of the solution changed from 7.2 to 6.8 during the pulse. Higher buffer concentration could not be used since phosphate ions catalyze decomposition of the OH adduct of phenol.¹¹ Oxygen was removed by bubbling with argon or N_2O . Different oxygen concentrations were obtained by mixing appropriate volumes of N_2O and O_2 saturated solutions from two syringes.

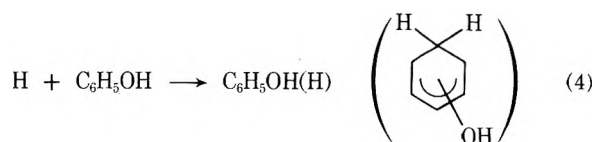
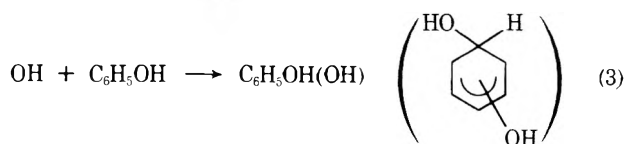
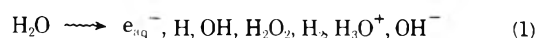
For pulse radiolysis a Febertron 707 (Field Emission Corp.) electron accelerator was used, and the operation conditions were similar to those in previous work.¹² The essential features of the pulse radiolysis set-up were a pulsed 450-W Xe lamp, all Suprasil silica glass optics, a double

monochromator OPTON MM 12, and a RCA 1P28 photomultiplier tube coupled directly to Tektronix 454 and 564B scopes. A photomultiplier tube 1P28 with seven dynodes and a risetime of $0.3 \mu s$ was used in most experiments. In some cases a system with five dynodes and a $50\text{-}\Omega$ load resistor was used and the risetime was 10 ns. Stability of the lamp was controlled during observation of the slow processes. The total light path through the cell was 5.1 cm. The absorbed doses were in the range 0.5–7 krad/pulse. The absorbed dose was measured by using a potassium ferrocyanide dosimeter,¹³ taking $\epsilon_{420nm}(Fe(CN)_6^{3-})$ as $1000 \text{ M}^{-1} \text{ cm}^{-1}$ and $G(Fe(CN)_6^{3-}) = 6.0$. The temperature was $19 \pm 1^\circ C$.

Steady state irradiations were performed with a ^{60}Co γ source. The total absorbed doses were in the range of 30–180 krads and the dose rate was $1.6 \text{ krads min}^{-1}$. The change in phenol concentration was measured using a simplified 4-aminoantipyrene method.¹⁴ Hydroquinone was determined directly by measuring absorbances of irradiated solutions at 305 nm ($\epsilon_{305nm} 680 \text{ M}^{-1} \text{ cm}^{-1}$). The total amount of hydroquinone and catechol was determined using *o*-phenantroline as a reagent.¹⁵

Results and Discussion

Spectrum and Decay of $O_2C_6H_5OH(OH)$ Radicals. An aqueous phenol solution is expected to undergo the following reactions after the pulse in the presence of N_2O :



About 90% of the total primary radicals should react with phenol to produce $C_6H_5OH(OH)$ radicals. Reaction 3 is very fast, $k_3 = 1.4 \times 10^{10} \text{ M}^{-1} \text{ s}^{-1}$.¹¹ The nature and ab-

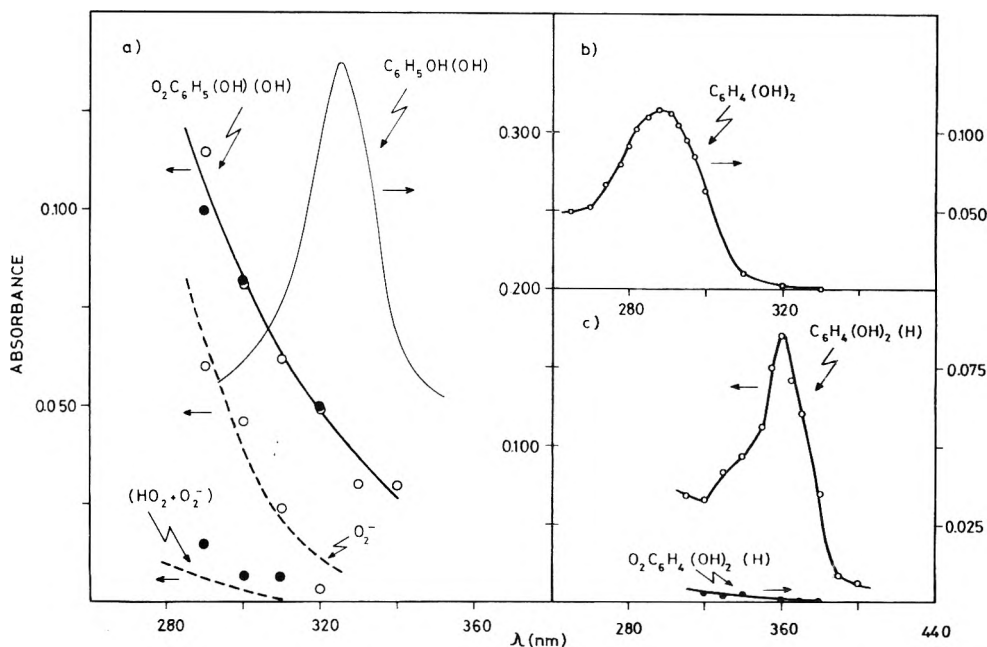
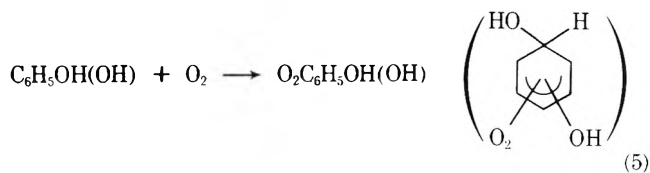


Figure 1. Absorption spectra of transients formed in phenol or hydroquinone aqueous solution, dose 3.5 \times rads. Each point is an average of three to six determinations. (a) 5×10^{-4} M phenol solution saturated with O_2 and N_2O (1:4): (O) pH 6.8 (6×10^{-5} M phosphate buffer); (●) pH 3.9 ($HClO_4$ solution). $C_6H_5OH(OH)$ radicals produced immediately ($< 1 \mu s$) after the pulse. $O_2C_6H_5OH(OH)$ formed after 10 μs . The dashed line represents the expected absorbances of O_2^- radicals calculated from ref 16; dots, the absorption measured after 400 μs . (b) 5×10^{-4} M phenol, pH 7, saturated with O_2 and N_2O (1:4), stable products. (c) $C_6H_4(OH)_2(H)$ formed immediately ($< 1 \mu s$) after the pulse in 5×10^{-4} M hydroquinone and 5×10^{-1} M *tert*-butyl alcohol solution, pH 1.3, argon saturated; $O_2C_6H_4(OH)_2(H)$ radical 250 μs after the pulse in 2×10^{-3} M hydroquinone, 2 M $HCOOH$, and 1.3×10^{-4} M O_2 solution, pH 1.

sorption spectrum of these radicals (λ_{max} 330 nm; ϵ_{330} 4400 $M^{-1} cm^{-1}$) has been established previously.¹¹ When O_2 is present, $C_6H_5OH(OH)$ radicals react according to

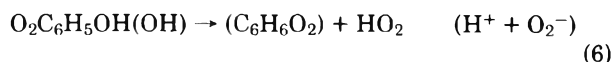


Both radicals, $C_6H_5OH(OH)$ and $O_2C_6H_5OH(OH)$, may exist in various ionized forms, because of the presence of an OH group and thus influence the rate of reaction 5 and also the mechanism of degradation of the peroxy radical. Since fast elimination of water from the $C_6H_5OH(OH)$ radical takes place already in slightly acid and alkaline solutions,¹¹ our observations were limited only to the solutions with pH 7 to 4.

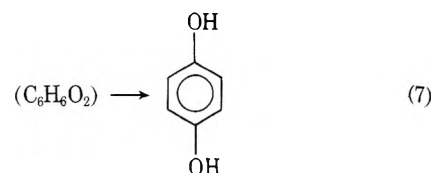
In the presence of O_2 a different absorption spectrum is observed. It is shown in Figure 1a, where the spectrum of the $C_6H_5OH(OH)$ radicals obtained under the same conditions is also presented. O_2^- radicals formed in the reaction of H atoms ($G = 0.6$) with oxygen contribute to the solid line spectrum ($O_2C_6H_5(OH)_2$), but not more than 6% with respect to molar absorptivity. The rate of reaction 5 was determined by monitoring the decay kinetics of the $C_6H_5OH(OH)$ radical at 330 nm, for different concentrations of O_2 (0.26–1.3 mM). An average value of $k_5 = (1.5 \pm 0.12) \times 10^9 M^{-1} s^{-1}$ was obtained. The previously published value, $k_5 = 4.9 \times 10^6 M^{-1} s^{-1}$,² obtained in a phenol solution saturated with oxygen is lower probably because of the recording of peroxy radical decomposition following reaction 5.

The first-order decay of $O_2C_6H_5(OH)$ absorption was followed at 290 nm and the rate constant calculated from an appropriate plot assuming the products were formed at the

same rate. No effect of phenol and oxygen concentrations on the decay rate was observed. The value $k_6 = (8.0 \pm 1.0) \times 10^3 s^{-1}$ was obtained for pH 6.8 and 3.9. The most probable reaction is unimolecular decomposition in which the long lived O_2^- radical is formed.



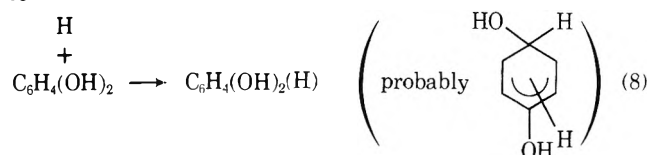
In Figure 1a, absorbances measured after 400 μs are presented by dots. The dashed line represents calculated absorbances based on the known absorption spectrum of the O_2^- radical,¹⁶ taking $G(O_2^-) = 6.0$. Calculated and experimental values are in good agreement. At pH 3.9 the absorption spectrum of the product is shifted toward the uv region, due to $HO_2 \rightleftharpoons H^+ + O_2^-$ equilibrium, $pK = 4.88$,¹⁶ while the spectrum of $O_2C_6H_5OH(OH)$ remains unchanged. It seems that contribution of the products, $C_6H_6O_2$, cannot be observed in the spectrum obtained after 400 μs in the wavelength region between 320 and 290 nm. Catechol, *o*-dihydroxybenzene, and resorcinol (*meta*) can contribute considerably only below 290 nm,¹⁷ where phenol itself also absorbs. Hydroquinone (*para*) is not formed immediately in the decomposition process of $O_2C_6H_5OH(OH)$ (reaction 6), but after some intramolecular rearrangement.



Since hydroquinone has a λ_{max} of 290 nm, we were able to observe first-order formation of hydroquinone at 290 nm and obtained $k_7 = 26.7 s^{-1}$. The absorption spectrum of stable product is presented in Figure 1b. Besides hydroqui-

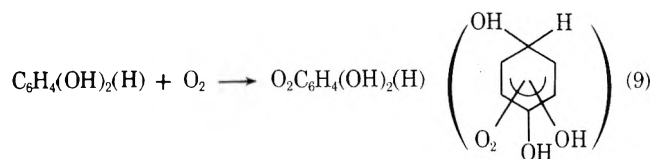
none catechol and probably resorcinol are also formed. In order to complete information on the stable product yield, steady state irradiations with a γ source were used. We determined G (hydroquinone), G (catechol), and G (-phenol) for phenol solution saturated with a mixture of $N_2O:O_2$ (4:1), and obtained the values 2.8, 1.6, and 5.4, respectively. The missing product with the yield of about 1 is probably resorcinol though this value is somewhat higher than the 0.3 reported previously.¹⁸ Dose rate difference between pulse and steady state conditions does not appear to affect the yield of stable products, since reactions 6 and 7 are first order.

The isomeric intermediate of the OH adduct of phenol is formed by addition of H atom to hydroquinone, according to



with a rate of $1.3 \times 10^9 M^{-1} s^{-1}$.¹⁹ The transient absorption spectrum of $C_6H_4(OH)_2(H)$ radicals (Figure 1c), hitherto unknown, has been obtained. *tert*-Butyl alcohol ($5 \times 10^{-1} M$) was added to scavenge OH radicals and the absorption of its radical did not overlap the measured spectrum up to 300 nm. This spectrum, with a λ_{max} of 360 nm and an ϵ_{360} of $3000 M^{-1} cm^{-1}$, is quite different from that for the $C_6H_5O-H(OH)$ radical (Figure 1a). Elimination of water from the $C_6H_4(OH)_2(H)$ radicals is a slow process; at pH 1 the rate constant is $\leq 10^2 s^{-1}$, while for the OH adduct of phenol the rate constant is $> 10^6 s^{-1}$ under the same conditions.

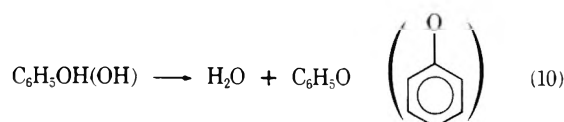
The rate constant for the reaction of $C_6H_4(OH)_2(H)$ with O_2



was measured in acid (pH 1) hydroquinone solution at 360 nm and $k_9 = (1.2 \pm 0.2) \times 10^8 s^{-1}$ was obtained. $HCOO^-$ ions were added to this solution to react with OH radicals and to suppress the formation of the OH adduct of hydroquinone having strong absorption in the observed wavelength region.²⁰ Besides, $HCOO^-$ ions are suitable scavengers since they do not form peroxy radicals but transfer the electron immediately to O_2 .¹⁶

After 250 μs when the reaction 9 has been completed, only weak absorption was observed in the wavelength region 310–450 nm (Figure 1c). Since hydroquinone itself absorbs below 310 nm, it was not possible to determine whether peroxy radicals form in reaction 9 or decompose instantaneously.

Reaction of C_6H_5O Radicals. Pulse radiolysis experiments¹¹ have shown that in absence of oxygen, $C_6H_5O-H(OH)$ radicals eliminate water and produce phenoxyl radicals.



This elimination is a first-order process, catalyzed by H^+ , OH^- , and phosphate ions.¹¹ In oxygen-containing solutions

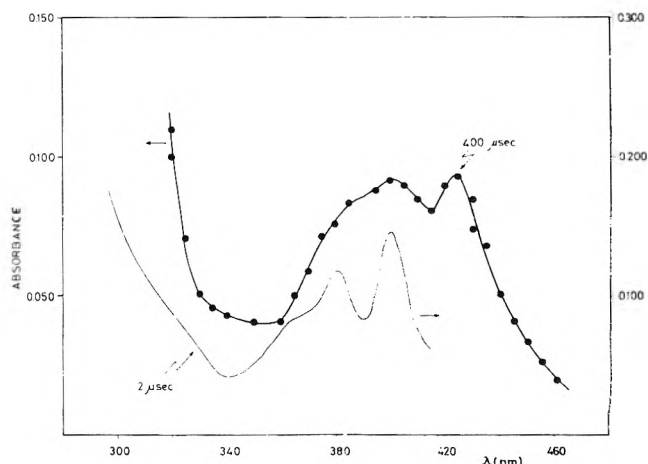
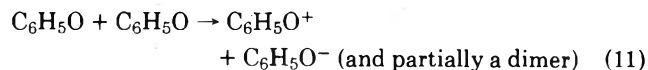


Figure 2. Absorption spectra obtained in N_2O saturated $5 \times 10^{-4} M$ phenol solution, pH 10, 3.5 krad; lower curve corresponds to C_6H_5O radicals formed 2 μs after the pulse and the upper one to transient species produced after 400 μs .

the formation of C_6H_5O radicals is dependent on competition between reactions 5 and 10. The absorption of C_6H_5O radicals observed at 400 nm is reduced only by about 10% in oxygenated solution of phenol ($2.5 \times 10^{-3} M$) and H_2O_2 ($1 \times 10^{-1} M$) at pH 2.3. Under the experimental conditions used (dose ≤ 2 krad) disappearance of C_6H_5O radicals is faster than in an air free solution. The rate curve was analyzed by a linearizing method based on successive approximations²¹ taking into account the competition between



and



From the results obtained $k_{12} = (1.4 \pm 0.2) \times 10^7 M^{-1} s^{-1}$ and $2k_{11} = (1.3 \pm 0.1) \times 10^9 M^{-1} s^{-1}$ were calculated.

We know very little about the products of reaction 11. Disproportionation of phenoxyl radicals through electron transfer by the formation of positive and negative ions has been assumed early.²² In the absence of oxygen, in N_2O saturated phenol solution at pH 2, we obtained by γ radiolysis a value of 2.2 for G (-phenol) which can be considered to indicate phenol re-formation in reaction 11. Besides dihydrobenzenes,²³ some stable product with broad optical absorption spectrum between 280 and 450 nm also formed in this reaction. As has been assumed previously²⁴ the spectrum observed could probably be attributed to dimer or polymer formed.

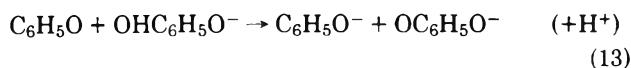
In alkaline deaerated solutions (pH 8.5–14) decay kinetics of phenoxyl radicals and subsequent formation of transients are quite different from those in neutral and acid medium. Absorption spectra registered in phenol solution at pH 10 are presented in Figure 2. The spectrum observed 2 μs after the pulse (lower curve) is essentially identical with that of C_6H_5O radicals in neutral solution.¹¹ Formation of the second transient, after 400 μs , is independent of both phenol concentration and the nature of e_{aq}^- scavengers (N_2O or H_2O_2), but strongly depends on pH and the amount of the product present in the solution. Its absorbance increases with increasing solution pH, and also with repeated irradiations of the same solution. Neta and Fessenden²² observed by steady-state ESR experiments in al-

TABLE I: Formation and Decay Rate Constants of Peroxy Radicals

Solute	pH	Reacting species	Radical formed, R	k_{R+O_2} , $M^{-1} s^{-1}$	Decay of RO_2 , s^{-1}
Phenol	3-7	OH	$C_6H_5OH(OH)$	$(1.5 \pm 0.12) \times 10^9$	$(8 \pm 1) \times 10^3$
Phenol	1	H	$C_6H_5OH(H)$	$(2.65 \pm 0.3) \times 10^9$	$(2.2 \pm 0.2) \times 10^4$
Phenol	1-6	OH^a	C_6H_5O	$(1.4 \pm 0.2) \times 10^7$	
Hydroquinone	1	OH	$C_6H_4(OH)_2(OH)$	6.1×10^8 ^b	
Hydroquinone	1	H	$C_6H_4(OH)_2(H)$	$(1.2 \pm 0.2) \times 10^8$	

^a Followed by unimolecular elimination of water. ^b Rate constant was determined by using competition between reactions $C_6H_4(OH)_2(OH) + O_2 \rightarrow O_2C_6H_4(OH)_2(OH)$ and $C_6H_4(OH)_2(OH) \rightarrow H_2O + OC_6H_4OH$ ($k = 4.6 \times 10^4 s^{-1}$), in hydroquinone solution (0.5 mM) in the presence of O_2 (0.1-1 mM) and N_2O (2-20 mM) at pH 7.

kaline phenol solution three different radicals, i.e., phenoxyl, and *o*- and *p*-semiquinone anion radicals. They assumed the semiquinone radicals to be formed in the second reaction of OH radicals with accumulated hydroquinone and catechol. Under our experimental conditions OH radicals react only with phenol whereas phenoxyl radicals, besides reaction 11, may partly react with the products, probably dissociated dihydroxybenzene to form semiquinone anion radicals by electron transfer.



The features of the second transient spectrum, between 400 and 450 nm, are very similar to those of the spectrum of the *p*-semiquinone radical²⁰ (Figure 2), although contribution from underlying absorption of the stable products or other transients is not excluded.

In oxygenated alkaline solutions, formation of semiquinone radicals is suppressed due to the reaction of phenoxyl radicals with oxygen which occurs here at the same rate as in acid solutions.

$O_2C_6H_5OH(H)$ Radicals. In acid phenol solutions H atoms react according to reaction 4. Since there is no reported spectrum for this radical, although its characteristics λ_{max} of 330 nm and ϵ_{330} of $3800 M^{-1} cm^{-1}$ had previously been determined,¹¹ the absorption spectrum of $C_6H_5OH(H)$ is presented in Figure 3. The decay rate of $C_6H_5OH(H)$ radicals in the presence of O_2 (0.3-1.3 mM) was measured at 330 nm and $k_{1\epsilon} = (2.65 \pm 0.3) \times 10^9 M^{-1} s^{-1}$ was obtained.

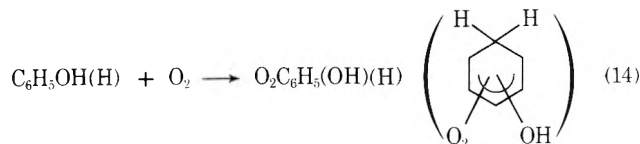


Figure 3 also shows the transient spectrum of $O_2C_6H_5OH(H)$ radicals. The $O_2C_6H_5OH(H)$ decay was followed at 290 nm and the first-order rate constant $k = (2.0 \pm 0.2) \times 10^4 s^{-1}$ was obtained. The difference in the kinetic behavior of this and the isomeric radical $O_2C_6H_6(OH)$, formed in oxygenated benzene solution, is due to slower reaction of the OH adduct of benzene with oxygen, the rate constant of which is $5 \times 10^8 M^{-1} s^{-1}$, and to decomposition by second-order reaction³ of the peroxy radical formed.

Reactivity toward Oxygen. The formation and decay rates of peroxy radicals are summarized in Table I. The results for phenol show that both OH and H adducts react very fast with oxygen forming peroxy transients, which then decompose further by first-order reaction. We were able to follow consecutive reactions of decomposition of the peroxy OH adduct of phenol. Peroxy radical $O_2C_6H_5O-$

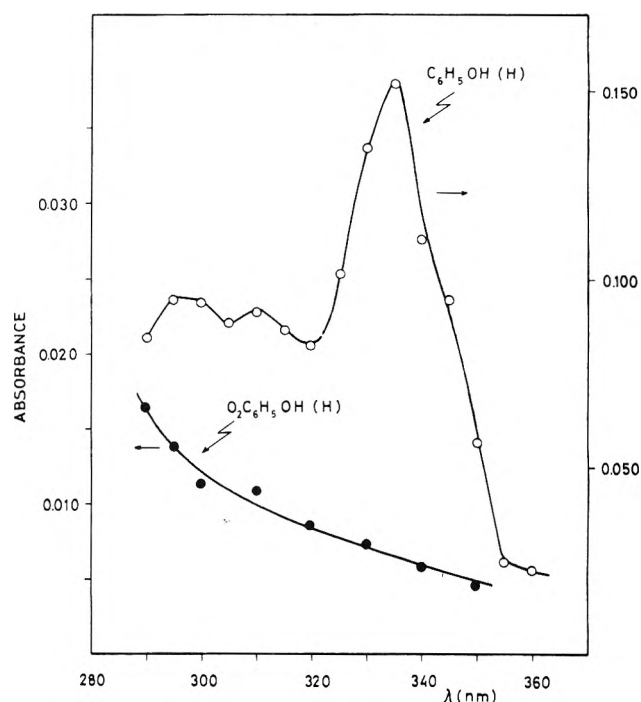


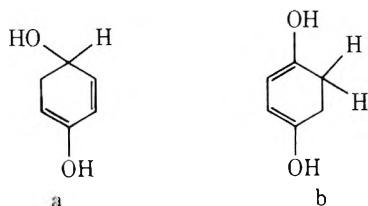
Figure 3. Absorption spectra of $C_6H_5OH(H)$ in argon saturated $5 \times 10^{-4} M$ phenol solution and $5 \times 10^{-4} M$ *tert*-butyl alcohol, pH 1, and $O_2C_6H_5OH(H)$ formed 20 μs after the pulse in $2.5 \times 10^{-3} M$ phenol, 2 M HCOOH, and $1.3 \times 10^{-4} M$ C_2 solution, pH 1. Pulse 2 krad.

$H(OH)$ decomposes ($k = 8 \times 10^3 s^{-1}$) to produce the O_2^- radical in equivalent extent. The other product formed in this reaction does not have the absorption spectrum in the observed wavelength region and decomposes to yield hydroquinone, the formation of which we were able to follow ($k = 26.7 s^{-1}$).

In its reactions with OH or H, phenol does not form one type of radical but probably a mixture of isomers.²³ Land and Ebert¹¹ found different rates of elimination of water from the OH adduct of phenol (reaction 10) which they ascribed to existence of isomers. In this study there was no indication of different kinetic behavior of isomers toward oxygen. No significant alternations of the decay rate of radicals in the reaction with O_2 at different wavelengths were detected in the test performed. On the other hand, results presented here show that $O_2C_6H_5OH(OH)$ radicals decompose to produce about 50% hydroquinone (para), 30% catechol (ortho), and 20% probably resorcinol (meta). However, these results are not a support for the existence of isomers of the OH adduct of phenol since O_2^- radicals are formed in an extent equivalent to the decomposition of peroxy radicals in reaction 6.

The behavior of $C_6H_4(OH)_2(H)$, the isomer radical

formed in hydroquinone solution, is quite different. The two possible structural isomers for this radical are (a) in which the H atom attaches directly to a carbon carrying one OH group, and (b) presented by the 1,2,4 structures.



The fact that the absorption maximum of the H adduct of hydroquinone (360 nm) is different from that of the OH adduct of phenol (330 nm) and that these two isomers have quite different rate constants with oxygen, and even different rates of water elimination, implies that the H atom adds to a carbon at positions other than that at which the OH is attached.

It can be seen in Table I that the reaction with oxygen is slightly hindered for both OH and H adducts of hydroquinone. This is most likely due to the existence of one more OH groups in the hydroquinone radicals as compared to the corresponding phenol adducts.

The more resonance stabilized phenoxyl radical, C_6H_5O , reacts about two orders of magnitude slower with O_2 than its precursor, the OH adduct of phenol. This is even more pronounced for the *p*-semiquinone radical formed by elimination of water from the OH adduct of hydroquinone. The *p*-semiquinone radical does not react with oxygen at all, and can even be produced in the reverse reaction of the O_2^- radical with benzoquinone.

Acknowledgment. We thank Mrs. M. Marović for technical assistance. This work was partly supported by International Atomic Energy Agency, Research Contract No. 1527/RB.

References and Notes

- (1) For a summary of work on this subject, see E. J. Fendler and J. H. Fendler, *Prog. Phys. Org. Chem.*, **7**, 267 (1970).
- (2) B. Cercek, *J. Phys. Chem.*, **72**, 3832 (1968).
- (3) L. M. Dorfman, I. A. Taub, and R. E. Büfler, *J. Chem. Phys.*, **36**, 3051 (1962).
- (4) G. Czapski, *Annu. Rev. Phys. Chem.*, **22**, 171 (1971).
- (5) K. Stockhausen, A. Fojtik, and A. Henglein, *Ber. Bunsenges. Phys. Chem.*, **74**, 34 (1970).
- (6) E. Hayon and M. Simić, *J. Am. Chem. Soc.*, **95**, 6681 (1973).
- (7) T. Eriksen, A. Henglein, and K. Stockhausen, *Trans. Faraday Soc.*, **69**, 337 (1973).
- (8) M. T. Downes and H. C. Sutton, *Trans. Faraday Soc.*, **69**, 263 (1973).
- (9) J. Rabani, M. Pick, and M. Simić, *J. Phys. Chem.*, **78**, 1049 (1974).
- (10) J. Rabani, D. Klug-Roth, and A. Henglein, *J. Phys. Chem.*, **78**, 2089 (1974).
- (11) E. J. Land and M. Ebert, *Trans. Faraday Soc.*, **63**, 1181 (1967).
- (12) V. Marković, D. Nikolić, and O. I. Mičić, *Int. J. Radiat. Chem.*, **6**, 227 (1974).
- (13) J. Rabani and M. S. Matheson, *J. Phys. Chem.*, **70**, 761 (1966).
- (14) "Standard Methods for the Examination of Water and Waste Water", XIII ed, American Public Health Association, Washington, D.C., 1971, p 501.
- (15) R. Belcher and W. J. Stephen, *Analyst*, **76**, 45 (1951).
- (16) D. Behar, G. Czapski, J. Rabani, L. M. Dorfman, and H. A. Schwarz, *J. Phys. Chem.*, **74**, 3209 (1970).
- (17) "International Critical Tables of Numerical Data in Physics, Chemistry and Technology", Vol. V, McGraw-Hill, New York, N.Y., 1929, p 360.
- (18) P. I. Dolin, V. N. Shubin, and S. A. Brusentseva, "Radiation Purification of Water", *Izdatel'stvo Nauka, Moscow*, 1973 (in Russian).
- (19) O. I. Mičić and M. T. Nenadović, unpublished results.
- (20) G. E. Adams and B. D. Michael, *Trans. Faraday Soc.*, **63**, 1171 (1967).
- (21) M. S. Matheson and Z. M. Dorfman, "Pulse Radiolysis", M.I.T. Press, Cambridge, Mass., 1969, p 125.
- (22) P. Neta and R. W. Fessenden, *J. Phys. Chem.*, **78**, 523 (1974).
- (23) G. Stein and J. Weiss, *J. Chem. Soc.*, 3265 (1951).
- (24) M. Fiti, *Rev. Roum. Chim.*, **19**, 1083 (1974).

Homologous *trans*-4-Ethoxy-4'-cycloalkanecarbonyloxyazobenzenes. Calorimetry

Craig L. Hillemann and Gerald R. Van Hecke*

Harvey Mudd College, Department of Chemistry, Claremont, California 91711 (Received October 6, 1975)

Calorimetric data are presented for the nematogenic homologous *trans*-4-ethoxy-4'-cycloalkanecarbonyloxyazobenzenes from cyclopropane to cycloundecane and the nematic-isotropic transition temperature, enthalpy, and entropy trends are discussed within the framework of current theories. A correlation of physical properties with the size of the terminal cycloalkane ring is observed. An extensive solid state polymorphism is noted.

1. Introduction

Since the discovery of liquid crystalline mesophases manifesting molecular and orientational order, considerable synthetic effort has been expended using various substituents as structural probes to help elucidate the molecular properties required for the existence of mesophases.¹ Many, though not all, materials forming thermotropic liquid crystalline mesophases contain roughly rodlike molecules possessing a highly polarizable, usually conjugated, central link and various types of terminal substituents.

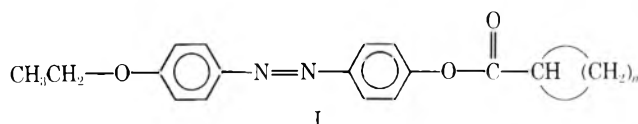
Other than common functional groups such as halogens and cyanide, the most frequently used substituent is a terminal normal alkane. Many studies have reported various physical properties for a homologous series of mesomorphic compounds based on the variation in length of a terminal alkane chain.² Our work with the homologous series of 4-ethoxy-4'-*n*-alkanoyloxyazobenzenes lead to use of *p*-(*p*'-ethoxyphenylazo)phenol as a convenient compound bearing azobenzene as the central link to which we could add various ester substituents. In particular we have prepared a

TABLE I: Transition Temperatures and Derived Entropies for 4-Ethoxy-4'-cycloalkanecarboxyloxyazobenzenes and Certain Analogous Esters

Cycloalkane carboxylate ester	Transition ^a	Temp, K	Temp ref ^b	$\Delta\bar{H}$, kJ mol ⁻¹	$\Delta\bar{S}$, J mol ⁻¹ K ⁻¹
Cyclopropane	K _{II} → I ^c	381.30 ± 0.24		25.9 ± 1.0	68 ± 3
	K _I → I ^d	394.23 ± 0.29		31.7 ± 1.3	80 ± 3
	N → I ^c	375.62 ± 0.19		0.69 ± 0.04	1.83 ± 0.12
Cyclobutane	K _{II} → N ^c	350.0 ± 0.8 ^e	T1		
	K _I → N	380.80 ± 0.15	T2	26.6 ± 0.9	70 ± 3
	N → I	403.25 ± 0.17	T3	0.76 ± 0.04	1.88 ± 0.10
Cyclopentane	K → N	397.05 ± 0.16	T2	30.8 ± 1.0	78 ± 2
	N → I	403.59 ± 0.16	T3	1.01 ± 0.05	2.51 ± 0.13
Cyclohexane	K _{II} → N ^c	393.5 ± 0.3 ^e	T1		
	K _I → N	400.72 ± 0.15	T2	29.6 ± 1.4	74 ± 4
	N → I	417.14 ± 0.23	T3	0.96 ± 0.05	2.29 ± 0.12
Cycloheptane	K _{II} → N ^c	351 ± 5 ^e	T1		
	K _I → N	379.20 ± 0.17	T2	24.0 ± 0.9	63 ± 2
	N → I	393.00 ± 0.16	T3	0.67 ± 0.03	1.68 ± 0.08
Cyclooctane	K _{III} → N ^c	349 ± 2 ^e			
	K _{II} → K _{III} ^c	336 ± 10 ^e			
	K _I → I	376.51 ± 0.15		26.7 ± 0.9	71 ± 3
Cyclononane	N → I ^c	375.03 ± 0.15		0.49 ± 0.04	1.30 ± 0.10
	K _{II} → K _I ^f	359.03 ± 0.29		3.9 ± 0.3	11.0 ± 0.7
	K _I → I ^g	362.94 ± 0.16		21.3 ± 0.8	59 ± 2
	N → I ^c	354.65 ± 0.15		0.32 ± 0.02	0.90 ± 0.06
Cyclodecane	K _I → I	352.82 ± 0.33		27.4 ± 1.2	78 ± 3
	N → I	<i>h</i>		<i>i</i>	
Cycloundecane	K _I → I	361.94 ± 0.38		29.0 ± 0.8	80 ± 2
	N → I	<i>j</i>		<i>i</i>	
Adamantane	K → I	447.9 ± 0.4		35.5 ± 1.0	79 ± 2
Benzene	K → N	445.1 ± 0.4		43.0 ± 1.2	97 ± 3
	N → I	474.0 ± 0.3		1.10 ± 0.05	2.32 ± 0.10

^a Notation of Verbit.⁵ K, crystal, N, nematic, I, isotropic. ^b Temp ref code refers to the transitions depicted in Figure 1b. T2 means the temperature at point 2 which refers to the K_I → N transition. ^c Monotropic. ^d K_{II} crystal previously fractured and allowed to stand 2 h at 315 K. ^e Estimation by microscopy; not resolvable by DSC. ^f Previously allowed to stand 24 h at 344 K. ^g Previously allowed to stand 15 min at 360 K. ^h Monotropic nematic phase that could only briefly be observed on rapid undercooling to $T < 333$ K. ⁱ Not observable by DSC. ^j Monotropic nematic that could only briefly be observed on rapid undercooling to $T < 331$ K.

new series of nematogenic compounds, trans-4-ethoxy-4'-cycloalkanecarboxyloxyazobenzenes (I), by varying the ali-



cyclic ring in the terminal position. We report here the results of calorimetric studies for this new homologous series for $n = 2$ to 10 and discuss and contrast the trends observed with the analogous normal alkane compounds.³

2. Experimental Section

Syntheses of Cycloalkanecarboxylate Esters. The esters were all prepared from the appropriate acyl chlorides and *p*-(*p*'-ethoxyphenylazo)phenol from Eastman Organic Chemicals and used without purification. The acyl chlorides were directly obtained from Aldrich Chemical Co. for the cyclopropane and cyclobutane carboxylate esters, while the other cycloalkyl acyl chlorides were obtained by treatment of the carboxylic acids with thionyl chloride. Description of typical syntheses of the acyl chlorides and esters was given previously.⁴ Complete synthetic details will be described in a forthcoming article.

Carboxylic Acids. The cyclooctane-, cyclononane-, cyclodecanecarboxylic acids were commercially unavailable. Cyclooctanecarboxylic acid was prepared by hydrobromination of cyclooctene and carbonation of the Grignard from the resulting bromocyclooctane. The cyclononane- and cyclodecanecarboxylic acids were respectively obtained from

cyclodecanone and cycloundecanone by Favorskii rearrangement of the corresponding 2-bromocycloalkanone intermediates.

Microscopy. The mesophases were identified and transition temperatures measured by the use of a Bausch and Lomb Dynoptic polarizing microscope equipped with a modified Koeffler hot stage. A particularly successful technique used to study the monotropic phases formed by these materials was to use an additional hot plate set at a temperature suitable to form the isotropic phase, heat a sample to form the isotropic phase, and then quickly place the sample on the microscope hot stage set to a desired temperature. This procedure generally allowed estimations of the transition temperatures for the difficult to observe monotropic phases.

Calorimetric Measurements. The calorimetric measurements were made with a Perkin-Elmer DSC-1B. Details were as described previously.⁴

3. Results

Cycloalkanecarboxylate Esters. The cycloalkanecarboxylate esters from cyclopropane to cycloundecane were prepared and studied by means of differential scanning calorimetry as previously mentioned. The results of the calorimetric studies are presented in Table I. All of the cycloalkanecarboxylate esters exhibit nematic mesophases, but the carboxylate esters of cyclopropane, cyclooctane, cyclononane, cyclodecane, and cycloundecane are monotropic rather than enantiotropic. The esters also exhibit considerable solid state polymorphism, much of which is monotropic.

ic and, with the exception of the cyclopropane-, cyclooctane-, and cyclononancarboxylate esters, not detectable by means of differential scanning calorimetry.

The phase behavior of these compounds can be summarized in Figure 1 with just a few comments. Cyclopropanecarboxylate ester exhibits a monotropic nematic phase as well as a monotropic crystalline phase called here K_{II} . Figure 1a presents the idealized free energy-temperature diagram unique to the cyclopropanecarboxylate. The phase behavior of the cyclobutane-, cyclohexane-, and cycloheptanecarboxylate esters is presented in Figure 1b as all of these compounds exhibit an enantiotropic nematic phase and two crystal forms, one of which is monotropic. The temperatures are of course different and can be determined from Table I. The cyclopentane ester is unique in that it exhibits only one crystal form and an enantiotropic nematic phase. Figure 1b is appropriate if the line for K_{II} is ignored. Cyclooctanecarboxylate ester exhibits the greatest polymorphism observed in this series, showing three crystalline modifications two of which are monotropic with respect to the stable room temperature crystal but enantiotropic with respect to each other. Further the nematic phase is monotropic. Figure 1c presents the phase diagram unique to the cyclooctane ester. The last member of the series to exhibit a characterizable nematic phase is the cyclononane carboxylate ester; Figure 1d presents its pertinent phase diagram showing a monotropic nematic phase and two enantiotropic crystalline forms.

4-Ethoxy-4'-cyclodecanecarboxyloxyazobenzene (Cyclodecanecarboxylate). This ester exhibits a nematic phase, but the phase is so unstable that only fleeting studies could be performed. The only successful way to achieve the N phase was to quickly cool the sample from isotropic to temperatures lower than $\sim 57^\circ\text{C}$. This could be reproducibly done by taking the microscope slide from a hot plate with $T > 82.5^\circ\text{C}$ ($K \rightarrow I$ transition) and placing the slide on a hot stage 57°C or cooler. The nematic phase could be readily discerned as crystallization proceeded rapidly. It was not possible to establish an equilibrium nematic-isotropic temperature. Further the nematic phase could not be observed with DSC techniques (though sometimes complex cooling exotherms which might include the $I \rightarrow N$ transition were observed). This ester exhibits at least two crystal forms one of which is monotropic, but, given the transient nature of the nematic phase, determination in detail of possible crystal modifications was not carried out.

4-Ethoxy-4'-cycloundecanecarboxyloxyazobenzene (Cycloundecanecarboxylate). The phases and properties of this ester are very similar to those of the cyclodecane in that a nematic phase forms but only on quick undercooling. The nematic phase formed by cycloundecane appears to be qualitatively more stable than the cyclodecane analogue in that a nematic-isotropic equilibrium could almost be achieved. This ester also exhibits at least two crystal forms but complete characterization was not carried out.

4-Ethoxy-4'-(1-adamantanecarbonyl)oxyazobenzene (1-Adamantanecarboxylate). Differential scanning calorimetry and microscopy reveal that this ester melts into the isotropic at 176°C and freezes at about 162°C without the formation of a nematic phase. Moreover, microscopic examination reveals that the crystal formed initially obtained from this crystallization spontaneously and almost instantaneously converts to yet another crystal form which appears to be thermodynamically or at least kinetically stable down to below room temperature.

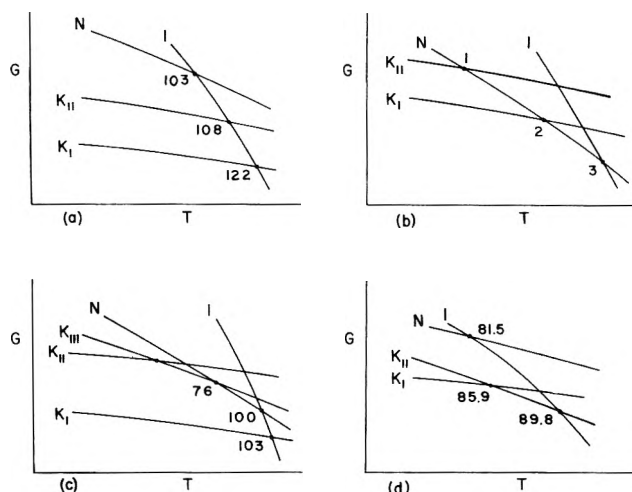


Figure 1. Idealized free energy-temperature diagrams. Temperatures noted are in degrees Celsius and slope differences are in some instances exaggerated for clarity: (a) cyclopropanecarboxylate ester; (b) cyclobutane-, cyclohexane-, cycloheptanecarboxylate esters; (c) cyclooctanecarboxylate ester; (d) cyclononancarboxylate ester.

4-Ethoxy-4'-benzoyloxyazobenzene (Benzoate). Examination by differential scanning calorimetry discloses that this ester melts at 174°C into what microscopy confirms is the nematic phase. The nematic to isotropic transition occurs at 194°C , by far the highest temperature known for esters of *p*(*p'*-ethoxyphenylazo)phenol.

4. Discussion

Trends in Nematic to Isotropic Properties. The alicyclic homologous series exhibits definite trends in nematic to isotropic transition temperature, enthalpy, and entropy. The nematic to isotropic transition temperature is seen in Figure 2a to monotonically rise from cyclopropanecarboxylate to cyclohexanecarboxylate and then, again monotonically, decline almost linearly. Although the melting point behavior is similar, except for the decline from cyclopropane- to cyclobutanecarboxylate, its fluctuation is more moderate in magnitude so that the nematic phase becomes monotropic for the cyclopropane and all the esters past cycloheptane.

The nematic to isotropic transition enthalpy is depicted in Figure 2b. The entropy results parallel the enthalpy closely and are similar to the transition temperature trend with one surprising exception. The nematic to isotropic transition temperature reaches a maximum for the cyclohexanecarboxylate ester, while the maximum in the transition enthalpy and entropy is reached with the cyclopentanecarboxylate ester.

The enthalpy and entropy, as noted above, do not completely follow the transition temperature trend and furthermore exhibit much larger percentage variations. Indeed if the marginally nematogenic cyclodecane- and cycloundecanecarboxylates are ignored, the nematic-isotropic transition enthalpy and entropy decline 68 and 64%, respectively, from the highest to the lowest values exhibited by this homologous series, while the transition temperature declines only 15% when similarly considered on an absolute scale. Thus although there are large percentage changes in the transition enthalpy and entropy, the ratio results in a much smaller variation in transition temperature.

Steric Properties of Substituent Cycloalkanes. Gray

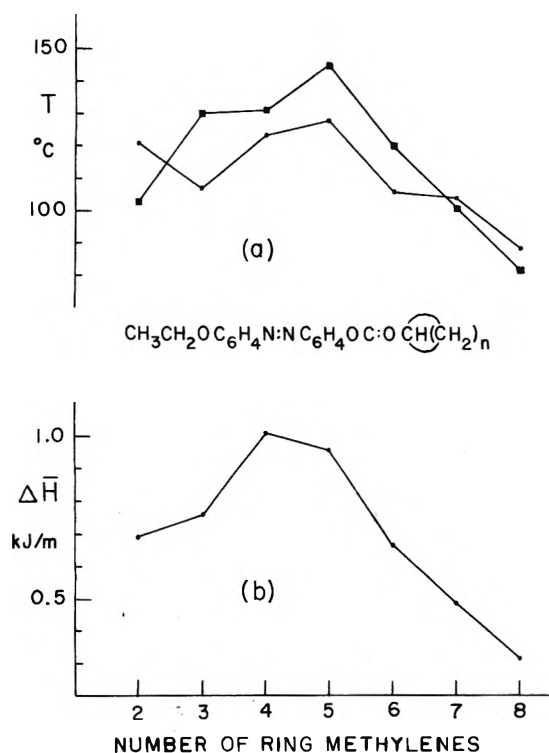


Figure 2. Physical properties as a function of the number of carbons in the terminal cycloalkane ring for the homologous *trans*-4-ethoxy-4'-cycloalkanecarboxyloxyazobenzenes: (a) transition temperatures (●) $K \leftrightarrow N$, (■) $N \leftrightarrow I$. In the case of solid state polymorphism the $K \rightarrow N$ temperature shown is for the room temperature stable crystal melting to nematic. (b) Enthalpies for the nematic-isotropic transition.

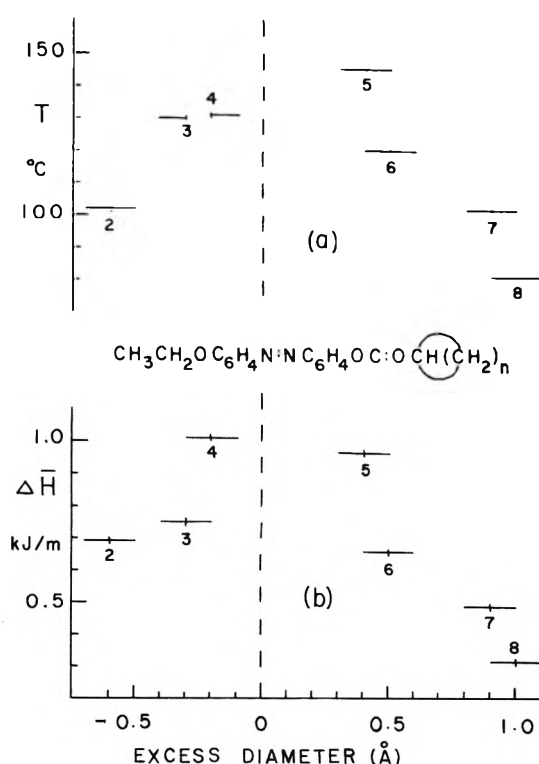


Figure 3. Physical properties as a function of the cylindrical diameter of cycloalkane in excess of that of remainder of ester for the homologous *trans*-4-ethoxy-4'-cycloalkanecarboxyloxyazobenzenes: (a) nematic-isotropic transition temperatures; (b) enthalpies of the nematic-isotropic transition. The numbers beside each point indicate the number of methylene carbons in the terminal cycloalkane ring.

studied the effect of molecular diameter on mesophase formation by preparing a number of 3'-substituted derivatives of 4'-*n*-alkoxybiphenyl-4-carboxylic acids.¹ In particular plots of the nematic to isotropic transition temperature T_{NI} of the 4'-*n*-octyloxybiphenyl-4-carboxylic acids vs. molecular diameter, the diameter of the narrowest cylinder through which the molecule could pass, show a decreasing T_{NI} for an increasing molecular diameter.⁶ Since the substituents included hydrogen, methyl, halogens, and nitro groups, changes in molecular dipole moment seem to be of little importance. The stability of the nematic phase formed by the above series decreases as the substituents force the highly polarizable phenyl rings apart. However, the substituents themselves add to the total polarizability in rough proportion to their size, thus separate assessment of the size and polarizability effects is difficult.

Our structural probe, the increasing size of the alicyclic ring in a terminal position, would first simply add to the total polarizability of the molecule without significantly increasing the lateral distance between the highly polarizable azobenzene centers of neighboring molecules. The small cycloalkane polarizability contribution would result in somewhat increased nematic stability. When the ring size reaches a point where it does contribute to the molecular diameter, the azobenzene centers would be forced far enough apart to cause a reduction in internal forces despite the small cycloalkane polarizability addition, and hence a decline in nematic stability. Use of terminal alicyclic rings should give a minimal change in dipole moment and total dipole, leaving any resulting effect ascribable to steric and, to a lesser extent, polarizability factors.

We assume that a molecule in the nematic phase will adopt a conformation minimizing the cylindrical diameter and hence maximizing the lateral intermolecular dispersion attractions. In particular, this means that the larger alicyclic rings which naturally exist in effectively elliptical conformations will preferentially adopt a ring conformation with the long axis of the ellipse as colinear as possible with the long axis of the remainder of the molecule. The cylindrical diameters for the cyclopentane to cyclononane substituents were determined from molecular models while the diameters for the cyclopropane and cyclobutane were estimated from molar volume data.⁷ We believe the estimates good to $\pm 0.1 \text{ \AA}$.

The nematic to isotropic transition temperature as a function of the disparity between substituent cylindrical diameter and the cylindrical diameter of the remainder of the molecule (6.0 \AA) is shown in Figure 3a, while similar correlations for transition enthalpy appear in Figure 3b. The esters appear on the abscissa in the same order as seen in Figures 2a and b, but they are no longer evenly spaced. The transition temperature and enthalpy (and entropy, not shown) reach a maximum at an alicyclic ring cylindrical diameter approximating that of the remainder of the molecule. That the enthalpy should behave so is not unexpected, since one would anticipate that the maximum lateral intermolecular dispersion attraction present in the nematic phase would be reached when the substituent group possesses the maximum ring size without sterically forcing the polarizable azobenzene portions of neighboring molecules apart.

Evidently the nematic to isotropic entropy change increases as the intermolecular ordering forces become stronger. From simple Maier-Saupe theory, if the densities of these compounds do not vary much, the entropy of the nematic to isotropic transition should vary as A/T_{NI} , where A is a complex parameter that mainly reflects the intermolecular forces in the mean-field approximation.⁸ Since both ΔS_{NI} and T_{NI} increase with stronger intermolecular ordering dispersion forces, the Maier-Saupe A parameter must also increase. Whether the change in ΔS_{NI} , T_{NI} , and A can be correlated with changing molar volume for this series is a question of interest under study. Finally we note that since the transition entropy does not generally change as rapidly as the transition enthalpy with change in strength of the ordering dispersion forces, the temperature of transition also tends to follow the trend in transition enthalpy and entropy.

Comparison with the Nematic-Isotropic Thermodynamic Observables of Other Cyclic Substituent Esters. One might expect that increasing the polarizability of a substituent as well as decreasing the cylindrical diameter disparity would increase the N \rightarrow I transition temperature, enthalpy, and entropy. The benzoate ester (cylindrical diameter deviation only +0.1 Å) predictably possess a much higher nematic to isotropic transition temperature (194 °C) than observed for the alicyclic series. The enthalpy and entropy for both the K \rightarrow N and the N \rightarrow I transitions are significantly higher than the cyclohexane homolog or, indeed, the other cycloalkanes. The large polarizability increase accompanying the addition of the benzene ring as opposed to a saturated alkane ring must greatly increase the intermolecular forces responsible not only for crystal packing but also those giving rise to nematic order.

The 1-adamantanecarboxylate ester (cylindrical diameter deviation +0.6 Å) would be expected to show a relatively low N \rightarrow I temperature in the vicinity of 110 °C. In fact, it melts into the isotropic at 176 °C and freezes after undercooling at 162 °C without exhibition of a nematic phase. This is the first reported example of a *p*-(*p'*-ethoxyphenylazo)phenyl ester in which a relatively high melting point prevents the expression of a nematic phase.

Comparison of Nematic-Isotropic Trends with Those of the n-Alkanecarboxylates. The *trans*-4-ethoxy-4'-*n*-alkanoxyazobenzenes have been found by Hillemann et al.⁴ to also exhibit distinct N \rightarrow I transition temperature, enthalpy, and entropy trends. For the pentanoate through tetradecanoate esters studied, the transition temperature tends to decline with increase in chain length, with a slight even-odd alternation superimposed on this trend. However, the transition enthalpy and entropy both tend to increase with a superimposed even-odd alternation. Again the percentage changes in transition enthalpy and entropy are much larger than that of the resultant transition temperature.

Since the alkyl chain does not increase the cylindrical diameter of the molecule and adds to its polarizability, it is not surprising that the transition enthalpy and entropy increase with alkyl chain length. However, that the transition entropy rises faster than transition enthalpy, in contradistinction to the alicyclic series, may be a reflection that a flexible alkyl chain may tend to adopt a greater number of conformations in the isotropic phase than in the nematic. We note with others^{4,9} that the increment of ΔS_{NI} with chain length is much less than the $R \ln 3$ predicted on the basis of a single conformation in the nematic and an infinite number of conformations in the isotropic. This suggests that the number of probable conformations in the isotropic phase is not much larger than that in the nematic.

Melting Point Trends. One notes from Table I and Figure 3 that the melting point generally follows the nematic to isotropic transition temperature trends, reaching a maximum at cyclohexanecarboxylate and declining thereafter. This suggests that the same properties of a terminal substituent which lend high thermal stability to the nematic phase, that is a size adding to the polarizability of the molecule without increasing the cylindrical diameter, also tends to result in high lattice energies. However, the decline in melting point from cyclopropane- to cyclobutanecarboxylate, the considerable variation in the transition enthalpies and entropies, and the widely different melting temperatures, enthalpies, and entropies for different crystal modifications of a given ester serve to caution one that lattice stability is dependent upon lattice packing arrangement as well.

Acknowledgments. The authors wish to thank Messrs. R. Loft, B. Santarsiero, and B. Williams for assistance in some of the aspects of this work. Financial assistance of the Cal Biochem Foundation and the Harvey Mudd College Research Committee is gratefully acknowledged.

References and Notes

- (1) G. W. Gray, *Mol. Cryst.*, **1**, 333 (1966).
- (2) G. H. Brown, J. W. Doane, and V. D. Neff, "A Review of the Structure and Physical Properties of Liquid Crystals", Chemical Rubber Publishing Co., Cleveland, Ohio, 1971.
- (3) Rather than always using the systematic name we will call the compounds by just the ester portion. Thus in I the compound for $n = 5$ is the cyclopentanecarboxylate ester.
- (4) C. L. Hillemann, G. R. Van Hecke, S. R. Peak, J. B. Winther, M. A. Rudat, D. A. Kalman, and M. L. White, *J. Phys. Chem.*, **79**, 1566 (1975).
- (5) L. Verbit, *Mol. Cryst. Liq. Cryst.*, **15**, 89 (1971).
- (6) G. W. Gray and B. M. Worrall, *J. Chem. Soc.*, 1545 (1959).
- (7) Models used were Stuart and Briegler space filling type based on a correlation of 0.629 Å/cm. Density data from G. Harris, Ed., "Dictionary of Organic Compounds", Vol. 2, 4th ed, Oxford University Press, New York, N.Y., 1965, and Beilstein, "Der Organischen Chemie", Suppl. 2, Vol. 5, 3, J. W. Edwards, Ed., Ann Arbor, Mich., 1944.
- (8) W. Maier and A. Saupe, *Z. Naturforsch. A*, **14**, 882 (1959); **15**, 287 (1960).
- (9) W. R. Young, I. Haller, and A. Aviram, *IBM J. Res. Develop.*, **15**, 41 (1971).

Substitutional Photochemistry of Some Monoazido, Thiocyanato, and Isothiocyanato Complexes of Cobalt(III) and Rhodium(III). Some Quandries and Alternatives for Models of Excited State Reactivity¹

John F. Endicott* and Guillermo J. Ferraudi

Department of Chemistry, Wayne State University, Detroit, Michigan 48202 (Received October 16, 1975)

Publication costs assisted by the National Science Foundation

Ligand field excitations of $\text{Rh}(\text{NH}_3)_5\text{X}^{2+}$ and $\text{Co}(\text{CN})_5\text{X}^{3-}$ ($\text{X} = \text{N}_3, -\text{NCS}, \text{and } -\text{SCN}$) lead to aquation of X with very small (10^{-2} to 10^{-4}) quantum yields for the rhodium(III) complexes and appreciable yields (0.03–0.2) for the cobalt(III) complexes. As is generally observed for these families of complexes, these yields are largely independent of excitation wavelength through the ligand field absorption region. In contrast the quantum yields of products from ligand field excitations of the analogous $\text{Co}(\text{NH}_3)_5\text{X}^{2+}$ complexes are strongly wavelength dependent. It is found that numerical values of quantum yields vary with conditions of the medium (e.g., viscosity), are not correlated to simple crystal field parameters. It is observed that the lowest energy electronic excited states of all complexes which exhibit wavelength independent photosubstitutional quantum yields occur at energies greatly in excess of the minimum energy for substitution into the ground state, while for the $\text{Co}(\text{NH}_3)_5\text{X}^{2+}$ complexes the lowest excited states lie at energies equal to or less than the minimum energy for substitutional decomposition of the ground state. As an alternative to various excited state models, it is proposed that electronic relaxation of the ligand field excited states may populate high energy ground state vibrational levels whose decay trajectories can lead to various product distributions depending on the configurational coordinates at the crossing point and on the energy and nature of the vibrational modes excited.

Introduction

Some remarks by Zink² a few years ago led us to examine the ligand field photochemistry of $\text{Co}(\text{NH}_3)_5\text{X}^{2+}$ ($\text{X} = \text{N}_3, -\text{NCS}$)³, $\text{Co}(\text{CN})_5\text{Y}^{3-}$,³ and $\text{Rh}(\text{NH}_3)_5\text{Y}^{2+}$ ($\text{Y} = \text{N}_3$,^{3b,4-7} $-\text{NCS}$, and $-\text{SCN}$). Continued interest in the ligand field photochemistry of coordination complexes⁸ has prompted this report on the results of our studies. We have been particularly interested in the continued efforts to correlate relative quantum yields with spectroscopic parameters and with the remarkable claims made for those correlations,⁹ and in other attempts to infer patterns of excited state reactivity from variations in quantum yields.^{10,11} Not only do our results not fit neatly into these postulated reactivity patterns, but we believe there is evidence accumulating that these attempts to relate photoproducts and/or their yields to intrinsic reactivities of ligand field excited states suffer from some basic philosophical flaws. Our major concern has been that most of the proposed models deal with structural or static properties of transition metal excited states, while the formation of products must necessarily involve some dynamic properties of the excited system. Even if we always attribute product formation to the lowest energy state of a given multiplicity⁹ or to some other thermally equilibrated excited state of the system,^{10,11} the dynamic behavior of the system can affect product yields either (a) through variations from complex to complex in the rate of nonreactive relaxation to the ground state, and/or (b) through variations in the rate of product formation from the excited system. Ford¹² has nicely articulated some of the concerns relating to the former. In this report, we wish to comment on aspects of the latter.

Experimental Section

The thiocyanato and isothiocyanato complexes were prepared using procedures described in the literature.¹³⁻¹⁶

Products of irradiations of $\text{M}(\text{NH}_3)_5\text{X}^{2+}$ ($\text{X} = -\text{NCS}$ or $-\text{SCN}$) were separated by ion-exchange chromatography and analyzed using procedures described elsewhere.^{3b} For analysis of NCS^- in photolyzed solutions of $\text{Co}(\text{CN})_5\text{X}^{3-}$ the following procedure was used: 3 ml of photolyte and 2 ml of 0.5 M $\text{Fe}(\text{NO}_3)_3$ in 0.5 M HNO_3 were diluted to 10 ml, absorbance at 460 nm vs. a similarly treated unphotolyzed blank was determined, and $[\text{NCS}^-]$ was obtained from a calibration curve constructed for that specific complex concentration.

Substrate concentrations were chosen to produce total light absorption in a 1-cm optical path. Irradiations were carried out to less than 5% conversion to product. Other details of photolysis procedures are described elsewhere.³

Results

The results of our photolyses of $\text{Rh}(\text{NH}_3)_5\text{X}^{2+}$ and $\text{Co}(\text{CN})_5\text{X}^{3-}$ ($\text{X} = -\text{NCS}, -\text{SCN}$) may be found in Table II.¹⁷ The limit of $\phi_{\text{NH}_3} < 4 \times 10^{-4}$ for the former complexes is based on our failure to detect any observable changes in pH (initial pH's 4.0 to 4.3). We also found no spectroscopic evidence for linkage isomerization following irradiations of any of these four complexes in their low energy ligand field absorption bands; irradiations of the rhodium complexes at 254 nm did produce some evidence of linkage isomerization. Photosubstitution in $\text{Co}(\text{CN})_5\text{NCS}^{3-}$ and $\text{Co}(\text{CN})_5\text{SCN}^{3-}$ was found to be partially quenched by glycerol and that of $\text{Co}(\text{CN})_5\text{SCN}^{3-}$ by $\text{H}_2\text{Ni}(\text{EDTA})$.

Discussion

The results of this study, together with the previous reports on $\text{Co}(\text{NH}_3)_5\text{N}_3^{2+}$, $\text{Co}(\text{NH}_3)_5\text{NCS}^{2+}$, $\text{Rh}(\text{NH}_3)_5\text{N}_3^{2+}$, and $\text{Co}(\text{CN})_5\text{N}_3^{3-}$, do present some striking contrasts with popular generalizations about the "photoreactivity of ligand field excited states": (1) the rhodium(III) complexes

TABLE I: Comparisons of Photosubstitution Yields with Estimated Crystal Field and Activation Parameters for Several d⁶ Complexes

Complex	Dt' , ^a kK	ϕ_s ^b	${}^3E^0 - \Delta H^{\ddagger}({}^1A_1)$, ^c kK	$\sim \Delta H^{\ddagger}(\epsilon E)$, kK ^d	$\psi_3(X)/\psi_3(L)$ ^e	ϕ_X/ϕ_L ^f
Co(NH ₃) ₆ ³⁺	0	$<5 \times 10^{-3}$ (11e, 18)	~ 0	5		
Co(NH ₃) ₅ NCS ²⁺	0.08	<0.01 (3c, 11e)	-1	4, 5		
Co(NH ₃) ₅ F ²⁺	0.18	2.4×10^{-3} (11e)			0.72	0.29
Co(NH ₃) ₅ Cl ²⁺	0.23	<0.02 (11e)	~ 0	3.3, 5	0.683	<0.34
Co(NH ₃) ₅ Br ²⁺	0.32	<0.07 ^h (11e; 19)	~ 0	3.3, 5	0.72	>1
<i>trans</i> -Co(en) ₂ (NCS)Cl ⁺		$<4.4 \times 10^{-3}$ (20)			1.19	>0.16
Co(NH ₃) ₅ N ₃ ²⁺	0.40	<0.3 (3c)	-5	4.5, 5	0.867	<0.01
Co(CN) ₃ ³⁻	0	0.31 (21)				
Co(CN) ₅ NH ₃ ²⁻	0.35	0.35 (22)				
Co(CN) ₅ NCS ³⁻	0.51	0.19	~ 8	4		
Co(CN) ₅ Cl ³⁻	0.75	0.07 (23)	~ 7 ⁱ			
Co(CN) ₅ Br ³⁻	0.78	0.2 (23)	~ 7 ⁱ			
Co(CN) ₅ N ₃ ³⁻	0.93	0.03 (24)	6			
Co(CN) ₅ I ³⁻	1.04	0.17 (26)	7			
Rh(NH ₃) ₆ ³⁺	0	0.075 (27)	~ 8 ^j	4.6		
Rh(NH ₃) ₅ NCS ²⁺	0.19	1.8×10^{-3}	~ 10	3, 4.6		
Rh(NH ₃) ₅ OH ₂ ³⁺	0.19	0.43 (28)				
Rh(NH ₃) ₅ Cl ²⁺	0.59	0.14 (29a)	10	2.7, 4.6		
Rh(NH ₃) ₅ N ₃ ²⁺	0.75	<0.01 (4-7)	84.4,	4.4, 4.6		
Rh(NH ₃) ₅ SCN ²⁺	0.8	7×10^{-4}				
Rh(NH ₃) ₅ Br ²⁺	1.02	0.20 (29a)	8	4.2, 4.6		
Rh(NH ₃) ₅ I ²⁺	1.09	0.87 (29)	8	4.6, 4.6		

^a Estimated using $Dt' = -4/35[W - (10Dq - C)_{xy}]$; see ref 32. Assignments for Rh(NH₃)₅X are based on ref 33; for Co(CN)₅X on ref 25. ^b Total photosolvation yield ($\phi_L + \phi_X$). Upper limits only are included for the wavelength dependent yields of cobalt(III)-ammine complexes; these correspond to near-uv excitations and ϕ_s generally becomes orders of magnitude smaller for long wavelength excitations. References are indicated in parentheses; no reference indicates this work. ^c Difference in energy estimated for the thermally equilibrated ³E state and the activation energy for substitution in the ¹A₁ ground state (see ref 30). Differences listed are for X ligand hydrolysis in M^{III}L₅X complexes. ³E⁰ energies are estimated as about 3 kK smaller than the absorption maximum observed³¹ in Co^{III}(NH₃)₅X (X = NH₃, Cl, Br) or estimated from crystal field arguments³² for Co^{III}(NH₃)₅X' (X' = NCS, N₃);^{3c} ³E⁰ energies of the rhodium(III)-ammines are based on Thomas and Crosby;³³ ³E⁰ energies for³³ Co(CN)₅X³⁻ (X = Cl, Br, I, N₃) are based on Fujita and Shimura³⁴ or estimated from crystal field arguments³² (X = NCS). We would estimate [³E⁰ - H[†](¹A₁)] to be about 2-5 kK more negative for ammine substitution than for X ligand substitution in M(NH₃)₅X complexes. ^d Estimated activation barrier for replacement of X in the equilibrated ³E state of ML₅X complexes. Estimated as $\Delta H^{\ddagger}(\epsilon E) \sim \frac{1}{2}[\Delta H^{\ddagger}({}^1A_1) - 14(Dt - Dt')] + \frac{21}{4}(Dt - Dt') = \frac{1}{2}\Delta H^{\ddagger}({}^1A_1) - \frac{7}{4}(Dt - Dt')$, where Dt' is the splitting parameter estimated for a square pyramidal ML₅, or ML₄X complex. First value listed is for X ligand substitution; second for substitution of L. Since configuration interaction is omitted, the numerical values only serve to illustrate that single electron excitation does not necessarily lead to a loss of crystal field stabilization energy in the ³E⁰ states. ^e From ref 9b, Table I. ^f Data from ref 8a, 11e, 11a, 19, and 20. ^g Irradiations of the ¹A₁ → ¹T₁ band only. ^h This limit on the quantum yield of Br⁻ aquation is based on ref 11e. Adamson^{11f} has recently revised downward many of the quantum yields for the longer wavelength excitations of Co(NH₃)₅Br²⁺. The ammonia aquation process claimed for this complex in ref 9b has not been verified in the published literature (see ref 3c, 8, 11e, 11f, and 19). ⁱ ΔH^{\ddagger} for halide aquation in Co(CN)₅Cl³⁻ and Co(CN)₅Br³⁻ based on the value determined for Co(CN)₅I³⁻ and the differences in rate constants.³⁰ ^j Since values of ΔH^{\ddagger} are about 1 kK smaller for rhodium(III)-ammines than for cobalt(III)-ammines,³⁰ we would estimate $\Delta H^{\ddagger} \sim 12$ kK/mol for Rh(NH₃)₆³⁺.

are not very photolabile and (2) Co(NH₃)₅N₃²⁺ is more photolabile than Rh(NH₃)₅N₃²⁺. However some caution must be exercised in the latter comparisons as *the product quantum yields (and product ratios) from ligand field excitations of the cobalt(III)-ammines are very strongly dependent on the excitation energy*. In fact, this is but one of several important features of the ligand field photochemistry of d⁶ metals which is exemplified in the complexes being considered here.

(a) The product quantum yields for "pure" ligand field excitations of cobalt(III)-ammines are generally very small (Co(NH₃)₅N₃²⁺ is a partial exception) and *very strongly wavelength dependent*.

(b) The product quantum yields for excitations of the pentacyanocobaltates and rhodium(III)-ammines are nearly wavelength independent through the ligand field region.

(c) Those complexes which exhibit *nearly wavelength independent* photosubstitutional chemistry have their low-

est energy ligand field excited states at energies large compared to the activation energy for ligand substitution.

(d) There is some evidence for correlations between non-radiative relaxation rates and photosubstitutional quantum yields³⁵ in a homologous series of rhodium(III) complexes. More generally photoreactivity does not appear to increase with excited state lifetimes; e.g., it appears that the photoactive chromium(III) quartet states may be several orders of magnitude shorter lived³⁶ than the "photoinert" cobalt(III)-ammine ligand field excited states.³⁷

(e) The numerical values of product quantum yields are sometimes functions of medium conditions.^{38,39}

Despite Zink's several optimistic statements⁹ we see little hope of rationalizing the known photochemistry of d⁶ complexes in terms of any single simple model. Certainly Table I demonstrates the lack of correlation between the crystal field tetragonality parameters, Dt ,⁴⁰ and observed quantum yields. In addition to the assertion that the crys-

tal field model could predict relative quantum yields,^{9d} there have been several attempts to use crystal field arguments in a qualitative way to rationalize the products formed.⁸⁻¹⁰ While these latter arguments are frequently helpful, the attempt to make them quantitative does not seem to have been very useful: e.g., the overlap populations reputed^{9b} to discriminate between L and X substitution in ML_5X excited states are far less sensitive to the nature of X (ratios of M-X and M-L overlap populations average 0.75 ± 0.05 for the four $Co(NH_3)_5X$ complexes listed in ref 9b) than are the quantum yields (ϕ_X/ϕ_L varies over a range in excess of 10^2 for the same four complexes). Furthermore, the ratio ϕ_X/ϕ_L appears to vary with excitation wavelength for many cobalt complexes,⁸ and for at least one complex, $Co(NH_3)_5Cl^{2+}$, ammonia aquation predominates for $^1A_1 \rightarrow ^1E$ excitation^{11e} while chloride aquation predominates for $^1A_1 \rightarrow ^3E$ excitation.⁴¹ It should be kept in mind that the quantum yields for products of ligand field excitations of most cobalt(III)-ammines, excepting in part $Co(NH_3)_5N_3^{2+}$, are extremely small (10^{-3} to 10^{-6}).

Simple mechanical models seem intrinsically incapable of providing useful insights into the nature of these complex systems. We know of no definitive evidence that the observed photoreactions are the result of chemical reactions of excited state species. Further, we find it difficult to understand how a system which appears to be efficiently thermally equilibrated, apparently remaining intact during the dissipation of large amounts of electronic and vibrational excitation energy while "cooling" to the lowest energy excited state, can find the apparently significant energy to promote thermal dissociation during its very transient lifetime after it has "cooled". Given that cage recombination of product fragments appears to be an important factor in many systems exhibiting nearly wavelength independent quantum yields (this work and ref 38), and that a photodissociative state should exhibit excitation energy recombination effects,⁴² the observed wavelength independence of quantum yields seems most consistent with vibrational and electronic relaxation within a bound state. Furthermore, there is no reason to believe that promotion of a single electron from a nonbonding to an antibonding orbital should break the chemical bond or destroy the crystal field stabilization energy^{8a,30a,43} (e.g., see Table I and Appendix I⁷). There are alternative approaches to the problems of ligand field photochemistry. An approach which we believe should be given serious consideration is that the role of the "photoactive excited state" is to provide a stereospecific distortion which couples the "cooled" excited state to the ground state electronic manifold in such a way as to determine the regions of most probable entry into the ground state manifold, thus the configuration coordinates and the momentum in configuration space of the relaxing system.

The correlation (c) of a large energy gap between the lowest energy thermalized ligand field triplet state and the transition state for substitution into the ground state, with wavelength independent, frequently photoactive, systems is quite striking. The transition state for substitution into the ground state corresponds to the lowest energy channel for substitutional decomposition of the ground state. This channel corresponds to the substitution process which is thermally observed. Several other channels for substitutional decomposition of the ground state exist. In a six coordinate complex one ought to consider at least one channel for each ligand, although several of these possible channels may be degenerate due to symmetry; also it is

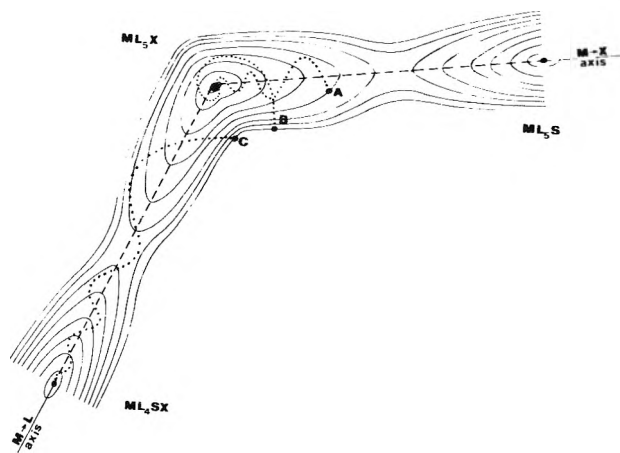


Figure 1. Qualitative representation of a free energy surface with two substitutional decomposition channels for the ground state of an ML_5X complex. Solid curves represent isoenergetic contours. Substitutions along the M-X and some M-L axis are indicated. Free energy minima occur for the substrate species, ML_5X , and the two substituted products, ML_5S and ML_4SX . Isoenergetic relaxation of an ML_5X excited state may occur by populating ground state vibrational modes which relax efficiently (A and B) to ML_5X or which relax predominantly along some reactive coordinate (C); dotted curves are hypothetical trajectories for possible relaxing systems. While the coordinates of the region of entry into the ground state may be generally important in determining the numerical values of quantum yields, the population of vibrational modes giving the relaxing system a significant component of momentum along an axis of dissociation is viewed as more critical; thus entry at a point which is not deeply imbedded in a reaction channel (C) may lead to reaction while entry at a point deeper in a reaction channel (B) may not, even if the energy requirements are met, if the former populates a vibrational mode with a significant momentum component along the dissociation axis while the latter does not.

probably most convenient to regard the continuous spectrum of transition states from limiting dissociative to limiting associative as corresponding to different configurational coordinates and energies within a single channel for substitution at a specific coordination site; i.e., the "system" being considered should include not just the coordination complex, but the surrounding solvent as well. The generation of different isomeric products from the substitution of a single ligand should be regarded as a consequence of branching of the reaction channel. Figure 1 is a qualitative representation of the ground state free energy surface, considering only two possible reaction channels.

Isoenergetic, nonradiative relaxation of an excited state species will populate very high energy vibrational modes of the ground state of the system. It is simplest for our purposes to assume that the lowest energy electronic excited state can be described by a similar free energy surface. If nested, the excited state and ground state surfaces would be weakly coupled. However, in the systems of interest here, population of an antibonding orbital will lead to distortion of the excited states with respect to the ground state; e.g., in Figure 1 we have postulated a lengthening of both the M-L and M-X axes. Such a situation would lead to regions where the excited and ground electronic state free energy surfaces are strongly coupled, the coordinates of the strongly coupled regions would be expected to be critical in determining the sequence of events following electronic relaxation. Coupling which populates vibrational modes critical to ground state substitutional decomposition would be expected to lead to production of solvated products if (1) those ground state vibrational modes are popu-

lated with an energy in excess of the threshold energy for the appropriate ground state substitutional process and if (2) the momentum of the vibrationally excited system has a major component along the critical configuration coordinate leading to product species; such a situation is represented qualitatively in point C of Figure 1. This may be characteristic of many $\text{Rh}^{\text{III}}(\text{NH}_3)_5\text{X}$ and most $\text{Co}^{\text{III}}(\text{CN})_5\text{X}$ complexes.

If neither of the above criteria are met, there will be little net substitutional chemistry in the relaxing system. Thus electronic relaxation which populates vibrational modes providing a major momentum component orthogonal or opposed to a critical (e.g., $\text{M} \rightarrow \text{X}$ or $\text{M} \rightarrow \text{L}$) coordinate axis will favor nonreactive vibrational relaxation; this may be the situation for the $\text{Rh}(\text{NH}_3)_5\text{Y}^{2+}$ ($\text{Y} = -\text{NCS}, -\text{SCN}, \text{N}_3$) complexes and is qualitatively represented by point B in Figure 1. Electronic relaxation which populates vibrational modes with energy below the threshold energy for ground state substitutional chemistry cannot induce much chemistry in the ground state unless the ground state manifold is entered above the dissociation threshold before the excited system has thermally equilibrated with the environment; this is quite likely the case for $\text{Co}^{\text{III}}(\text{NH}_3)_5\text{X}$ complexes and is qualitatively represented by point A in Figure 1.

In summary, we know of no compelling evidence for substitutional reactions of d^6 coordination complexes in their electronic excited states. In contrast, it is now evident that the complexes which exhibit wavelength independent photosubstitutional behavior have thermalized excited states with energies in excess of the threshold for substitutional decomposition of the ground state. The generation of substituted species following ligand field excitations of these systems seems a likely consequence of the relaxation trajectory described by the ground electronic state following its generation by electronic relaxation of higher states. Multiple products are possible owing to the possibility of population of distributions of vibrational modes, or configuration coordinates which bias the relaxing system along any of several channels for substitutional decomposition. Similarly, several competitive, nonradiative, nonreactive relaxation modes^{12,27-29,35} are possible in a single complex owing to detailed differences possible in the coupling (strong, weak, etc.) of each of the several excited state reaction channels with their ground state analogues. Since the excited state distortions determine the coordinates of regions of strong coupling between the excited and ground state free energy surfaces, the electronic parameters which effect different metal-ligand bonding interactions in the ground and excited state species⁸⁻¹⁰ should have some qualitative influence on the distribution of product species, although that influence must be modulated by the dynamics of relaxation across the product surface. Clearly definitive quantitative models for photosubstitutional chemistry in these systems require a reasonably detailed and complete knowledge of ground and excited state free energy surfaces.

Acknowledgment. The authors are grateful to Professors R. G. Linck, P. C. Ford, and G. P. Reck for helpful discussions.

Supplementary Material Available: Tabulated quantum yield data and Appendix I (4 pages). Ordering information is available on any current masthead page.

References and Notes

- (1) (a) Partial support of this research by the National Science Foundation (Grant No. MPS 72 0591A02) is gratefully acknowledged. (b) Further partial support of this research by means of a fellowship to G.J.F. from the Faculty of Sciences, the University of Chile, is also gratefully acknowledged. (c) Presented in part at the VIII International Conference on Photochemistry, Edmonton, Alberta, Canada, August 7-13, 1975; paper L5.
- (2) J. I. Zink, presented at the 164th National Meeting of the American Chemical Society, New York, N.Y., Sept 1972, INORG 069.
- (3) Reports of the photoredox chemistry of these complexes may be found elsewhere: (a) J. F. Endicott, M. Z. Hoffman, and L. S. Beres, *J. Phys. Chem.*, **74**, 1021 (1970); (b) G. J. Ferraudi and J. F. Endicott, *Inorg. Chem.*, **12**, 2389 (1973); (c) J. F. Endicott, G. J. Ferraudi, and J. R. Barber, *J. Am. Chem. Soc.*, **97**, 6406 (1975); (d) J. F. Endicott and G. J. Ferraudi, *Inorg. Chem.*, **14**, 3133 (1975).
- (4) The photochemistry of $\text{Rh}(\text{NH}_3)_5\text{N}_3^{2+}$ is complicated by a dominant pathway involving nitrene intermediates.⁵ A relatively less important pathway results in formation of $\text{Rh}(\text{NH}_3)_5\text{OH}_2^{3+}$; this product cannot arise from a redox pathway^{2b,6,7} and must be due either to a photosubstitutional pathway, to secondary photolysis, or to secondary thermal reactions, and is the basis for the yields quoted in Table I.
- (5) (a) J. L. Reed, F. Wang, and F. Basolo, *J. Am. Chem. Soc.*, **94**, 7173 (1972); (b) J. L. Reed, H. D. Ganey, and F. Basolo, *ibid.*, **96**, 1363 (1974).
- (6) J. Lilie, M. Simic, and J. F. Endicott, *Inorg. Chem.*, **14**, 2129 (1975).
- (7) J. F. Endicott, T. Inoue, and G. J. Ferraudi, manuscript in preparation.
- (8) For recent reviews see: (a) E. Zinato, Chapter 4 in "Concepts of Inorganic Photochemistry", A. W. Adamson and P. D. Fleischauer, Ed., Wiley, New York, N.Y., 1975, p 143; (b) P. C. Ford, R. E. Hintze, and J. D. Petersen, *ibid.*, Chapter 5, p 203; (c) P. C. Ford, J. D. Petersen, and R. E. Hintze, *Coord. Chem. Rev.*, **14**, 67 (1974); (d) C. H. Langford and N. A. P. Kane-Maguire, *MTP Int. Rev. Sci.: Inorg. Chem., Ser. Two*, **9**, 135 (1974); (e) V. Balzani and V. Carassiti, "Photochemistry of Coordination Compounds", Academic Press, London, 1970; (f) P. O. Fleischauer, A. W. Adamson, and G. Sartori, *Prog. Inorg. Chem.*, **17**, 11 (1972).
- (9) (a) J. I. Zink, *Mol. Photochem.*, **5**, 151 (1973); (b) *J. Am. Chem. Soc.*, **96**, 4464 (1974); (c) *Inorg. Chem.*, **12**, 1018 (1973); (d) M. J. Inorvia and J. I. Zink, *ibid.*, **13**, 2489 (1974).
- (10) M. Wrighton, H. B. Gray, and G. S. Hammond, *Mol. Photochem.*, **5**, 165 (1973).
- (11) (a) A. W. Adamson, *Discuss. Faraday Soc.*, **29**, 163 (1960); (b) *J. Phys. Chem.*, **71**, 798 (1967); (c) C. K. Kung and A. W. Adamson, *J. Am. Chem. Soc.*, **93**, 5581 (1971); (d) *Inorg. Chem.*, **12**, 1990 (1973); (e) R. A. Pribush, C. K. Poon, C. M. Bruce, and A. W. Adamson, *J. Am. Chem. Soc.*, **96**, 3027 (1974); (f) H. Ganey and A. W. Adamson, *Coord. Chem. Rev.*, **16**, 171 (1975).
- (12) P. C. Ford, *Inorg. Chem.*, **14**, 1440 (1975).
- (13) H. H. Schmidtke, *Z. Phys. Chem. (Frankfurt am Main)*, **45**, 305 (1965).
- (14) J. L. Burmeister, *Inorg. Chem.*, **3**, 919 (1964).
- (15) W. K. Wilmarth and A. Haim, *Inorg. Chem.*, **7**, 1250 (1968).
- (16) A. Werner and H. Muller, *Z. Anorg. Chem.*, **22**, 101 (1906).
- (17) Quantum yield data obtained for the present study are collected in Table II. See paragraph at end of paper regarding supplementary material.
- (18) M. F. Manfrin, G. Varani, L. Moggi, and V. Balzani, *Mol. Photochem.*, **1**, 387 (1969).
- (19) J. F. Endicott, G. J. Ferraudi, and J. R. Barber, *J. Phys. Chem.*, **79**, 630 (1975).
- (20) A. Vogler and A. W. Adamson, *J. Phys. Chem.*, **74**, 67 (1970).
- (21) L. Moggi, F. Bolletta, V. Balzani, and F. Scandola, *J. Inorg. Nucl. Chem.*, **28**, 2589 (1966).
- (22) R. Sriram and A. W. Adamson; private communication from Dr. Sriram.
- (23) (a) A. W. Adamson and A. W. Sporer, *J. Am. Chem. Soc.*, **80**, 3865 (1958); (b) *J. Inorg. Nucl. Chem.*, **8**, 209 (1958).
- (24) G. J. Ferraudi and J. F. Endicott, *J. Chem. Soc., Chem. Commun.*, 674 (1973).
- (25) (a) D. F. Gutterman and H. B. Gray, *J. Am. Chem. Soc.*, **93**, 3364 (1971); (b) V. M. Miskowski and H. B. Gray, *Inorg. Chem.*, **13**, 401 (1975).
- (26) A. W. Adamson, A. Chiang, and E. Zinato, *J. Am. Chem. Soc.*, **91**, 5467 (1969).
- (27) J. D. Petersen and P. C. Ford, *J. Phys. Chem.*, **78**, 1144 (1974).
- (28) P. C. Ford and J. D. Petersen, *Inorg. Chem.*, **14**, 404 (1975).
- (29) (a) T. L. Kelly and J. F. Endicott, *J. Phys. Chem.*, **76**, 1937 (1972); (b) *J. Am. Chem. Soc.*, **94**, 1797 (1972).
- (30) For appropriate reviews of ground state substitutional processes see (a) F. Basolo and R. G. Pearson, "Mechanisms of Inorganic Reactions", 2nd ed, Wiley, New York, N.Y., 1967; (b) C. H. Langford and V. S. Sastri, *MTP Int. Rev. Sci.: Inorg. Chem., Ser. One*, **9**, 203 (1972).
- (31) (a) M. Linhard and M. Weigle, *Z. Phys. Chem.*, **11**, 308 (1957); (b) C. J. Ballhausen, *Mol. Phys.*, **6**, 461 (1963).
- (32) R. A. D. Wentworth and T. S. Piper, *Inorg. Chem.*, **4**, 709 (1965).
- (33) T. R. Thomas and G. A. Crosby, *J. Mol. Spectrosc.*, **38**, 118 (1971).
- (34) J. Fujita and Y. Shimur, *Bull. Chem. Soc. Jpn.*, **36**, 1281 (1963).
- (35) J. D. Petersen, R. J. Watts, and P. C. Ford, submitted for publication (private communication from P.C.F.).
- (36) G. B. Porter, A. D. Kirk, and M. Windsor; comments of M.W. at the VIII International Conference on Photochemistry, Edmonton, Alberta, and private communication from G.B.P. to J.F.E.; A. D. Kirk, P. E. Hoggard, G. B. Porter, M. G. Rockley, and M. W. Windsor, *Chem. Phys. Lett.*, **37**, 199 (1976).
- (37) Although there has been no direct observation of $\text{Co}^{\text{III}}(\text{NH}_3)_5\text{X}$ ligand field excited states, photoinduced electron transfer reactions between

- Co(en)₃³⁺ and Fe(CN)₆⁴⁻ (N. A. P. Kane-Maguire, *J. Chem. Soc., Chem. Commun.*, 351 (1974)) and of biphonotic photoredox processes (K. G. Cunningham and J. F. Endicott, *ibid.*, 1024 (1974); K. G. Cunningham, R. Sriram, and J. F. Endicott, work in progress) have been interpreted as evidence that some excited state cobalt(III) species have lifetimes in the nanosecond range.
- (38) F. Scandola, M. A. Scandola, and C. Bartocci, *J. Am. Chem. Soc.*, **97**, 4757 (1975).
- (39) C. F. C. Wong and A. D. Kirk, *Can. J. Chem.*, **52**, 419 (1975).
- (40) Our estimates of Dt are simple first-order estimates. Corrections for off-diagonal terms could significantly alter some of the numerical values, especially for the rhodium complexes, but it is not likely that such second order corrections could result in a correlation of Dt with ϕ_s .
- (41) C. H. Langford and C. P. J. Vuik, VIII International Conference on Photochemistry, Edmonton, Alberta, Canada, Aug 7-13, 1975; paper L4.
- (42) (a) R. M. Noyes, *Prog. React. Kinet.*, **1**, 128 (1961); (b) J. P. Lorand, *Prog. Inorg. Chem.*, **17**, 207 (1972).
- (43) S. T. Spees, Jr., J. R. Perumareddi, and A. W. Adamson, *J. Am. Chem. Soc.*, **90**, 6626 (1968).

Application of the Polanyi Adsorption Potential Theory to Adsorption from Solution on Activated Carbon. VII. Competitive Adsorption of Solids from Water Solution

Michael R. Rosene and Milton Manes*

Chemistry Department, Kent State University, Kent, Ohio 44242 (Received November 21, 1975)

Publication costs assisted by Calgon Corporation

Equations have been derived for calculating the physical adsorption of solids from multicomponent solutions from the adsorption isotherms of the individual components. The method shows good agreement with experimental data on the adsorption from water solution onto activated carbon of the following binary systems: *p*-nitrophenol(PNP)-glucose; PNP-urea; PNP-benzoic acid; phthalide-glucose; phthalide-urea; and benzoic acid-glucose. It is well adapted for estimating the adsorption of traces of one component from high concentrations (up to near-saturation) of another.

Introduction

In earlier articles in this series the Polanyi adsorption potential theory has been applied to the adsorption onto activated carbon of: individual solids from a variety of solvents;^{1,2} organic liquids from water solution;^{3,4} mixed binary organic liquids;⁵ and some individual organic solids from water solution.⁶ In addition, there is some as yet unpublished work⁷ on the adsorption of a rather wide variety of individual solids from water solution, in which the Polanyi theory has been of considerable utility. We here consider the problem of estimating the individual adsorption of two or more solid solutes onto activated carbon from the isotherms of the individual components; we refer to this as competitive adsorption because the components tend to compete for the same adsorption sites.

The problem of competitive adsorption occurs in the use of adsorbents to purify a wide variety of compounds in solution; the adsorbent capacity depends on the adsorbability and concentrations of both substrate and impurity. It also occurs in chromatographic adsorption, where one would like to account for the relative order of the various chromatographic bands. We here develop a theory for competitive physical adsorption (or multisolute adsorption) that is based on the Polanyi model,⁸ and report verification of the theory on aqueous solutions of the following binary solute mixtures: *p*-nitrophenol(PNP)-glucose; PNP-urea; PNP-benzoic acid; phthalide-glucose; phthalide-urea; and benzoic acid-glucose. The theory is readily applicable to multi-

component solid solutes and to other solvents, and further work is continuing.

Theory

The Polanyi adsorption potential theory and its application to the adsorption of single solids from solution has been dealt with in an earlier publication.¹ We start with the assumption that the adsorption isotherms of a number of individual solids from a given solvent, when expressed in terms of volume adsorbed vs. adsorption potential per unit volume, give curves ("correlation curves") that are identical except for an abscissa scale factor. (We shall find this to be a reasonable assumption for a number of solids, when the adsorbate volume is appropriately calculated.) Our problem is to calculate the adsorption of each component at some temperature, given the individual concentrations and mutual solubilities.

Let ϵ_i represent the net molar adsorption potential of the i th solid in solution, i.e., the adsorption potential of the solid (as if it were adsorbing from vapor) minus a correction for the adsorption potential of the displaced solvent. Polanyi⁸ defines ϵ_{s1} by the equation:

$$\epsilon_{s1} = \epsilon_s - \epsilon_l V_s/V_l$$

where V_s and V_l are the respective molar volumes of solid and liquid and where we denote ϵ_{s1} as ϵ for convenience; he postulates that solid will precipitate in the adsorption space wherever

$$\epsilon \geq RT \ln c_s/c \quad (1)$$

where c_s and c are the saturation and equilibrium concentrations. The equality holds at the postulated equipotential surface at which solid and solution are at equilibrium. Elsewhere in the adsorption space the net driving force for adsorption, per mole of single adsorbate, is

$$-\Delta G_i = \epsilon_i - RT \ln (c_s/c)_i \quad (2)$$

where the first term on the right is the energy component and the second term the entropic component of the adsorptive driving force.

Let us now consider a number of solid solutes in solution, all of which are presumed to be adsorbable, i.e., to have higher values of ϵ/V than the solvent. We assume that the individual solutes are mutually insoluble as solids and therefore in the adsorbate, and we seek to determine which solid will be adsorbed in any given element of the adsorption space. (We anticipate that different solids may occupy different regions in the adsorption space.) Paralleling at this point the treatment of Hansen and Fackler⁹ we postulate that the adsorption of any solid in any element of volume occupied by another solid must take place with no net volume change, i.e., with displacement of an equal volume of the displaced solid; e.g., for the adsorption of dn_i moles of solid i and the displacement of dn_j moles of solid j

$$V_i dn_i + V_j dn_j = 0 \quad (3)$$

$$dn_j = -(V_i/V_j) dn_i \quad (4)$$

The condition that $dG \leq 0$ for adsorption leads back to eq 1 for the criterion of whether any solid can adsorb in a given element of adsorption space. If two or more solids can adsorb as single solutes, then for the displacement of any solid by any other, for example, of the j th by the i th component,

$$dG = \Delta G_i dn_i + \Delta G_j dn_j \leq 0 \quad (5)$$

Substitution of dn_j from eq 4 and ΔG_i and ΔG_j from eq 2 leads to the equation

$$\frac{dG}{dn_i} = -\frac{\epsilon_i}{V_i} + \frac{RT}{V_i} \ln \frac{c_{is}}{c_i} + \frac{\epsilon_j}{V_j} - \frac{RT}{V_j} \ln \frac{c_{js}}{c_j} \leq 0 \quad (6)$$

as the criterion for the displacement of component j by component i . If $dG/dn_i > 0$, then component j will displace component i (or be adsorbed in preference to component i). For any element of volume in the adsorption space, eq 6 leads to the expectation that the adsorbed solid will be the one with the highest value of $-\Delta G/V$. Although the concentration-dependent component of the adsorptive driving force per unit volume will be constant for a given set of equilibrium concentrations, each value of ϵ/V varies over the adsorption space. Consequently, different components may be adsorbed in different regions. The total volume of each component adsorbed may now be in principle calculated for a multicomponent system. Since however we here have data only for binary solutes we shall illustrate the calculation method for a two-solute system, in which case the criterion for competitive adsorption of component 2, assumed to have the higher value of ϵ/V , is

$$\frac{RT}{V_2} \ln \frac{c_{2s}}{c_2} \geq \frac{\epsilon_2}{V_2} - \frac{\epsilon_1}{V_1} + \frac{RT}{V_1} \ln \frac{c_{1s}}{c_1} \quad (7)$$

We now illustrate the graphic calculation of the adsorbed volumes of both components in Figures 1 (component 1

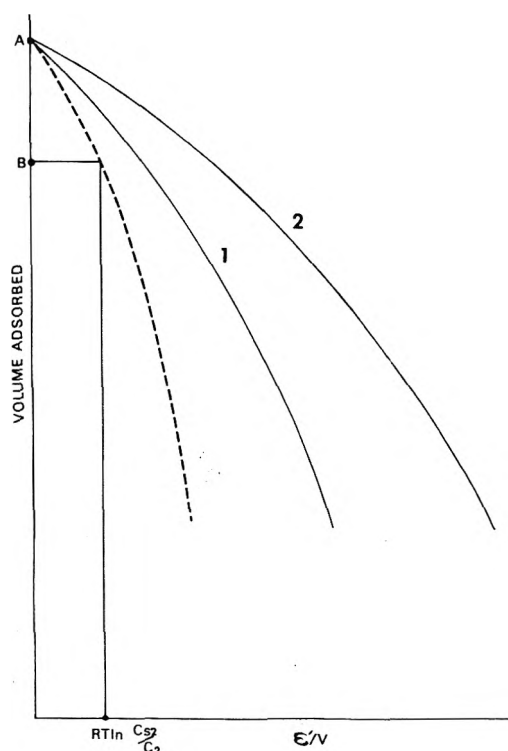


Figure 1. Schematic diagram showing the construction of the correlation curve for adsorption from a saturated solution of competitor. Curves 1 and 2 are the correlation curves for the pure compounds. The dotted curve is the correlation curve for adsorption of component 2 (adsorbate) from a saturated solution of component 1 (competitor); it is constructed by subtracting the abscissa of 1 from that of 2 for every value of the ordinate. Point B is an illustrative value for the volume of component 2 adsorbed corresponding to a given value of $RT \ln (c_{2s}/c_2)$.

saturated) and 2 (component 1 unsaturated). In Figure 1 the two solid curves (from left to right) are the correlation curves for components 1 and 2. We wish to determine the adsorbed volumes of both components. We first draw the dotted line so its abscissa scale factor is the difference between those for components 2 and 1. The dotted curve now gives $\epsilon_2/V_2 - \epsilon_1/V_1$ as a function of adsorbate volume. Since component 1 is saturated, eq 7 becomes

$$\frac{RT}{V_2} \ln \frac{c_{2s}}{c_2} \geq \frac{\epsilon_2}{V_2} - \frac{\epsilon_1}{V_1} \quad (8)$$

It states that component 2 will be adsorbed wherever the value of $(RT/V_2) \ln (c_{2s}/c_2)$ equals or exceeds the abscissa of the dotted curve. For any given value of c_2 (given the saturation value of c_{2s} in the presence of saturated component 1) we can calculate this value, enter it into the abscissa, and find the corresponding ordinate (B) on the dotted line. This ordinate gives the volume of component 2 adsorbed. The volume of component 1 adsorbed is $(A - B)$, i.e., the difference between the maximum adsorbate volume A (the volume where both correlation curves meet the vertical axis) and the volume (B) of adsorbed component 2. Since one component is saturated, the entire adsorption space is occupied.

When neither component is saturated the calculation is illustrated by Figure 2. Again the correlation curve on the right is for component 2. The curve on the left is the correlation curve for component 1, shifted to the left by a distance equal to $(RT/V_1) \ln (c_{1s}/c_1)$; we would need a new curve for each new value of c_1 . The shifted curve meets the

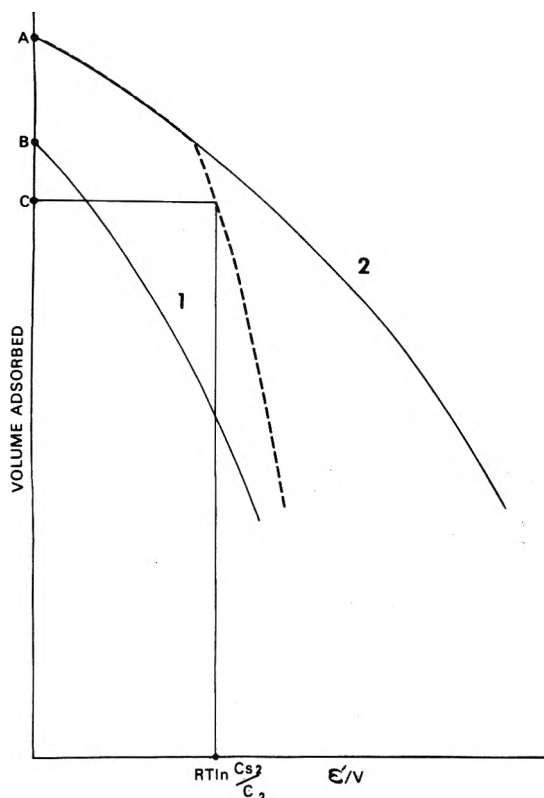


Figure 2. Schematic diagram showing the construction of the correlation curve for adsorption from an unsaturated solution of competitor. Curve 2 is the correlation curve for pure component 2 (adsorbate). Curve 1 is the correlation curve for pure component 1 (competitor), shifted to the left by $RT \ln (c_{1s}/c_1)$. The dotted curve is for adsorption of component 2 from component 1 at c_1 ; it is constructed by subtracting the abscissa of curve 1 from curve 2 for every ordinate point, and it coincides with curve 2 for all ordinate values larger than point B. The volume C is an illustrative volume of component 2 adsorbed at concentration c_2 of component 2.

vertical axis at point B, which represents the volume of pure component 1 that would be adsorbed at c_1 . The abscissa of this curve is now the value of $\epsilon_1/V_1 - (RT/V_1) \ln (c_{1s}/c_1)$, and the difference between the abscissas of the two curves (the dotted curve) now gives the value of the right side of eq 7. By eq 7, this curve now gives the values of $(RT/V_2) \ln (c_{2s}/c_2)$ above which component 2 will adsorb. Note that the dotted curve is a composite of two curves; the upper part is the original correlation curve without competition, whereas competition is effective over the lower part. To find the adsorption of both components at equilibrium concentrations c_1 and c_2 , we enter the abscissa with the value of $(RT/V_2) \ln (c_{2s}/c_2)$. The corresponding volume, at point C, is the volume of component 2 adsorbed. The volume of component 1 adsorbed is $B - C$, if $B \geq C$. If $C \geq B$, then only component 2 will be adsorbed. Figure 2 is especially interesting in that it predicts a kink in the correlation curve for component 2 adsorbing competitively. We shall see this kink later in our results.

Given the initial rather than the equilibrium concentrations, one can readily determine the equilibrium capacities and concentrations by successive approximations.

We now consider the possibility that the limiting adsorbate capacities are not equal by the conventional calculation of adsorbate mass divided by bulk density. The lower limiting capacity of solids relative to liquids and vapors has been observed by Manes and Hofer,¹ Chiou and Manes,⁶

and Ozcan,⁷ and has been ascribed to submaximal packing of the solid in the adsorption space for compounds that do not exhibit molecular sieving. The submaximal packing has been ascribed to packing anomalies between the solid crystal and the adsorbent pore structure, and to hydration of the adsorbate. We have assumed the true maximum adsorbate volume to be equal for all of the solutes, and used the observed small differences in limiting adsorbate volumes to calculate adsorbate densities that differ in some cases from the bulk densities. We have chosen to take one solid (PNP) as the tentative standard and to adjust the other densities downward to give the same limiting adsorbate volume for all. The adjustment also has consequence for the displacement. For example, if a spongy rather than a solid adsorbate is displaced, the energy required to displace it is thereby reduced. The derivation is adjusted by using V^* , the estimated relative adsorbate density rather than the bulk density V in the calculations. Thus the abscissa becomes $(RT/V^*) \ln c_s/c$ in the preceding calculation. Although the adjustment has not been large, in the sense that it has not been necessary for most of the experimental points, it does make a significant difference for the low capacity measurements, and we have used it in our calculations. We have been encouraged to use it by the findings that it results in correlation curves that superimpose well by the application of a single abscissa scale factor.

Experimental and Data Reduction

Materials. The activated carbon, a CAL grade carbon (200 × 325 mesh) from the Pittsburgh Activated Carbon Division of Calgon, Inc., came from the same batch (No. 2131) that has been the source of all of the carbon used in this series. It was oven-dried overnight at 110 °C.

The PNP, phthalide (α -hydroxy-*o*-toluic acid lactone), and benzoic acid (USP) came from commercial sources and were used without further purification. Adsorption isotherms of the PNP and phthalide were not detectably different from those reported by Chiou and Manes⁶ for samples recrystallized from the same starting material. The urea was ACS certified. Solutions of Matheson Coleman and Bell reagent grade glucose were treated prior to use with small amounts of activated carbon (about 1 g/l.) to remove uv-absorbing impurities.

Adsorption Experiments and Data. Competitive adsorption was determined by the shaker bath techniques described earlier,¹ using uv absorption spectrophotometry. The individual isotherms for PNP and phthalide were taken from Chiou and Manes,⁶ but with use of solid rather than liquid molar volumes in data reduction.

The individual isotherms for urea, glucose, and benzoic acid were determined by measuring the breakthrough volumes (with appropriate dead-space correction), of solutions of known concentration on small carbon columns (typically 200–500 mg), using techniques and apparatus common to liquid chromatography, e.g., a high-pressure pump, a 0.25-in. o.d. stainless steel column tube, and an effluent monitor. For benzoic acid we used an Altex Model 152 uv monitor; urea and glucose were detected by a Waters R-401 differential refractometer. This technique considerably improved capacity determinations at high equilibrium concentrations, and confirmed shaker-bath determinations at lower concentrations; it was particularly useful for urea and glucose at the higher capacities. The technique confirmed some of the earlier measurements of Ozcan⁷ and led to considerable improvement in others.

Bulk solid molar volumes (cm^3/mol) were calculated from literature values of the densities as follows: PNP, 94.0; phthalide, 95.7; benzoic acid, 96.5; glucose, 116; and urea, 45.5.

The urea solubility in water (based on total organic carbon determination of the saturated solution) was taken from Ozcan,⁷ and the PNP and phthalide solubilities from Chiou and Manes.⁶ Those of benzoic acid and of glucose were respectively determined by uv spectrophotometry and by stepwise addition of weighed solid to saturation. Competitive adsorption calculations required the solubilities of the measured adsorbates in the presence of relatively high concentrations of the competitors. These were determined by uv spectrophotometry; the absorption peaks of PNP and benzoic acid were sufficiently separated for the determination of PNP. The solubility data in water and in solutions are given in Table I.

Data Reduction. The individual isotherm data for all five adsorbates were first plotted (as previously) as volume adsorbed vs. $(T/V) \log(c_s/c)$ (Figure 3). The adsorbate densities were then adjusted to make all of the limiting capacities equal, in this case to the essentially equal limiting capacities of benzoic acid and PNP ($42 \text{ cm}^3/100 \text{ g}$). The respective adjustment factors for phthalide, glucose, and urea, i.e., 0.95, 0.88, and 0.90, were intended to correct for the presumed difference in packing anomalies. The data were replotted as volume adsorbed (using adjusted densities where required) vs. $(T/V^*) \log(c_s/c)$, where V^* is the molar volume calculated by use of the adjusted density, presumably the molar volume of the adsorbate. For benzoic acid and PNP, $V^* = V$.

The theoretical correlation curves for competitive adsorption were determined from those of the individual components, adjusted where necessary, by the method outlined in the theoretical section. Because we could go to lower capacities in competitive adsorption than in single solute adsorption, it was necessary to use extrapolated values for single-solute adsorption at low capacities. The extrapolation was facilitated by the observation that the single-solute correlation curves, when replotted on the basis of the adjusted adsorbate densities, could now be superimposed over their experimentally observed lengths by the application of a single abscissa scale factor in the same fashion as for vapor-phase isotherms.¹ The glucose curve, which had the widest observable capacity range, was used as the standard from which the others were generated by using the scale factor that best fit their experimental points. The observed closeness of fit over all of the experimental points was taken as justification for extrapolation of the single-component correlation curves beyond the directly observable range.

Results

The adsorption data for the individual solutes are given in Table II¹⁰ as cm^3 adsorbed per 100 g of carbon against $(T/V) \log(c_s/c)$, where the adsorbate and molar volumes are calculated from the bulk solid densities. The data may be readily converted to other units by use of the molar volumes and solubilities given here. The table contains both our original data and some from Chiou and Manes,⁶ which are recalculated on the basis of the bulk solid molar volume. The low concentration points for urea confirm those of Ozcan.⁷

The data for competitive adsorption are also given in

TABLE I: Solubilities of Adsorbates in Water and Competitor Solutions

Component 1 (adsorbate)	Component 2 (competitor)	Solubility, g/l.
Glucose	Water	750
Urea	Water	655 ^a
Benzoic acid	Water	3.5
Phthalide	Water	5.0 ^b
PNP	Water	16.0 ^b
PNP	95+% sat. urea	11.0
PNP	10% sat. urea	14.0
PNP	66% sat. glucose	11.4
PNP	10% sat. glucose	12.5
Phthalide	30% sat. glucose	4.28
Phthalide	5% sat. glucose	5.0
Benzoic acid	66% sat. glucose	2.61
Benzoic acid	10% sat. glucose	3.28
PNP	Sat. benzoic acid	15.1
Phthalide	10% sat. urea	5.0

^a Reference 7. ^b Reference 6.

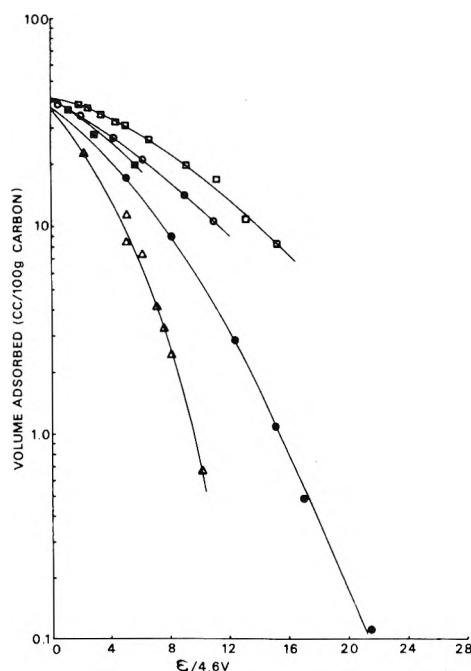


Figure 3. Correlation curve (volume adsorbed vs. $\epsilon/4.6V$) for the single solutes (left to right): glucose, urea, benzoic acid, phthalide, and PNP.

Table II.¹⁰ Here, however, the adjusted densities have been used in calculating the tabulated values.

The individual isotherm data plotted as (adjusted) volume adsorbed vs. $\epsilon/4.6V$ ($= (T/V^*) \log(c_s/c)$) are given in Figure 4. The differences resulting from the adjustment may be seen by comparison of Figures 3 and 4.

The competitive adsorption data are shown in Figures 5–9. We here report only the adsorption of the first-named component as a function of its concentration. The concentration of the second component was held constant within the uncertainty limits of the correlation; the relative magnitudes of its (high) concentration and the sample size precluded any appreciable concentration change resulting from adsorption, except for PNP–benzoic acid, where addi-

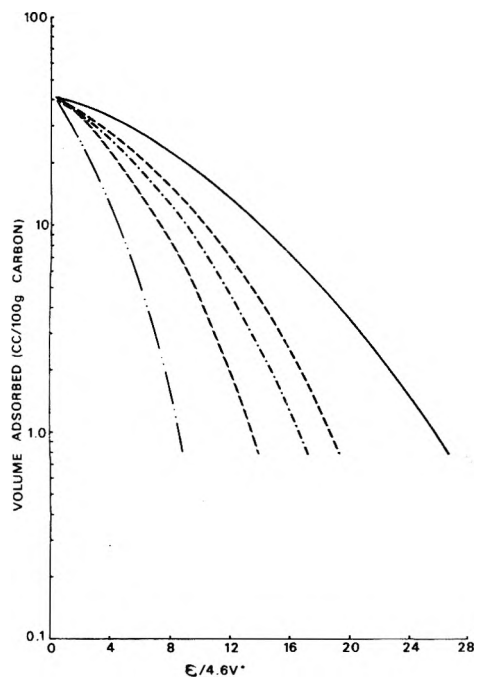


Figure 4. Shifted correlation curves using V^* for single solutes (left to right): glucose, urea, benzoic acid, phthalide, and PNP.

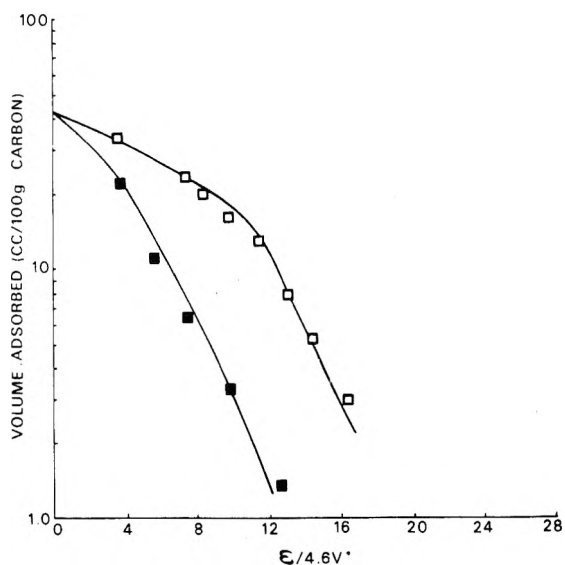


Figure 5. Correlation curves for the adsorption of PNP from urea solutions plotted as volume adsorbed vs. $\epsilon/4.6V^*$. Solid curves are calculated from theory. Left, PNP from 95+ % saturated urea; right, PNP from 10% saturated urea.

tional benzoic acid was added to maintain its equilibrium concentration.

Figure 5 shows two calculated curves for PNP in near-saturated (95+) and 10% saturated urea, together with experimental points. Figure 6 is for PNP in 66 and 10% saturated glucose. Figure 7 is for phthalide in 30 and 5% saturated glucose, and Figure 8 is for benzoic acid in 66 and 10% saturated glucose. Figure 9 is for phthalide from 10% saturated urea and for PNP from saturated benzoic acid; here the two curves are unrelated but presented together to save space.

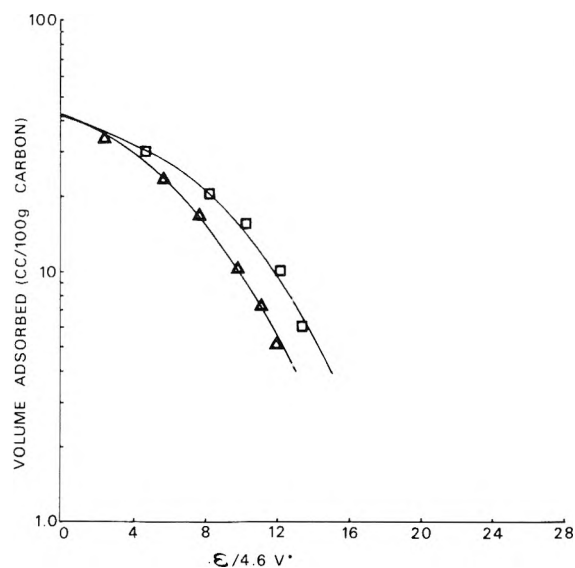


Figure 6. Correlation curves for the adsorption of PNP from glucose solutions. Plot same as Figure 5. Left, PNP from 66% saturated glucose; right, PNP from 10% saturated glucose.

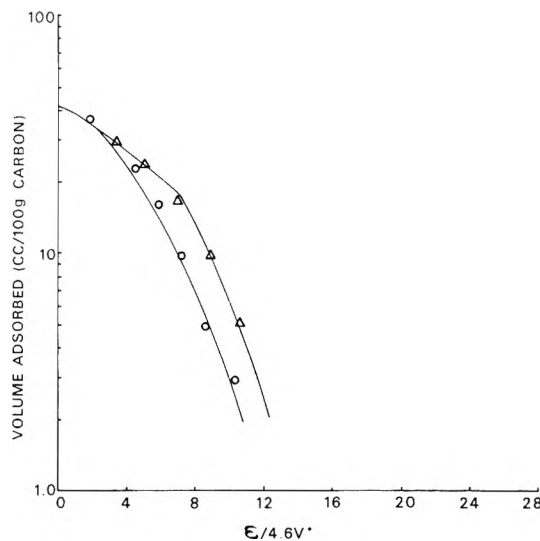


Figure 7. Correlation curves (volume adsorbed vs. $\epsilon/4.6V^*$) for the adsorption of phthalide from glucose solutions. Solid curves are calculated from theory. Right, phthalide from 30% saturated glucose; left, phthalide from 5% saturated glucose.

Discussion

We first consider the rationale for the choice of experiments. We knew from earlier work^{6,7} that PNP, phthalide, and benzoic acid had higher abscissa scale factors than either urea or glucose (the source of the differences will be discussed in a later publication), and should therefore be adsorbed at relatively low concentrations even from relatively concentrated solutions of urea or glucose. We also expected that PNP should be adsorbed from benzoic acid. The systems chosen had the added advantage of ease of analysis by spectrophotometry. Moreover, the relatively high solubilities of urea and glucose made it possible to vary their concentration range without concern for concentration changes from their own adsorption. Experiments with adsorbates requiring separation are reserved for later study. The use of near-saturated rather than saturated so-

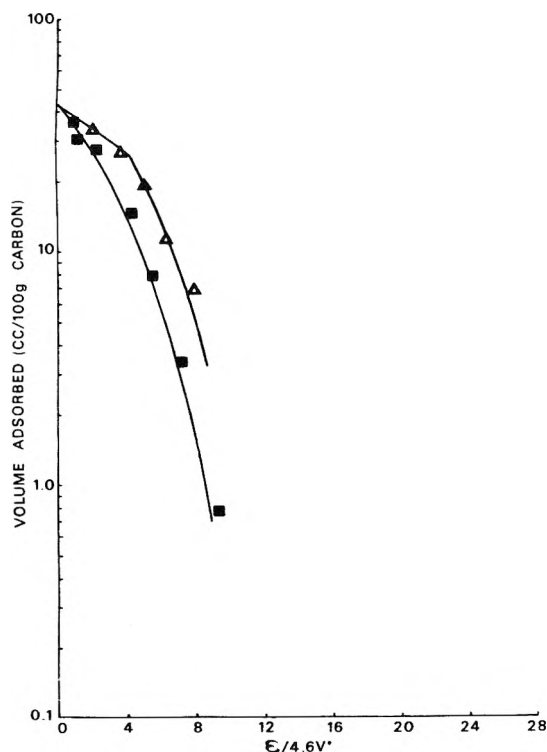


Figure 8. Correlation curves for benzoic acid from 66% saturated glucose (left) and benzoic acid from 10% saturated glucose (right). Plot same as Figure 7.

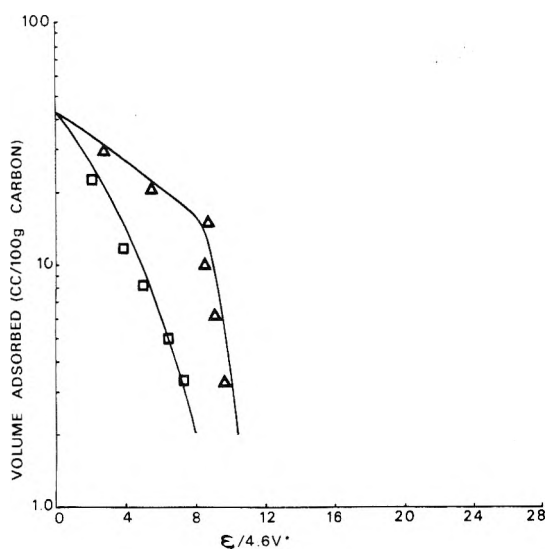


Figure 9. Correlation curves (volume adsorbed vs. $\epsilon/4.6V^*$) for the adsorption of PNP from saturated benzoic acid (left) and phthalide from 10% saturated urea (right). Solid curves are calculated from theory.

lutions was dictated by the necessity of allowing for displacement, for example, of urea by PNP; one would not expect displacement into an already saturated solution. In fact, experiments with PNP in saturated benzoic acid (in the presence of excess solid benzoic acid) led to somewhat low adsorption of PNP (see Figure 9) in the high capacity range; the anomaly disappears at low capacities. The choice of experimental conditions was influenced by our experience with PNP-benzoic acid, where the low solubility of benzoic acid gave problems in maintaining constant solu-

tion concentration. For systems containing glucose the original intent was to make the glucose solutions nearly saturated; however we later had to correct an earlier reported solubility for glucose. The experiments nevertheless served our purposes because we could achieve a reasonably wide concentration range for glucose.

The theoretical analysis had led, as noted earlier, to the expectation of composite (or kinked) correlation curves for what we shall refer to as the "adsorbates" (i.e., the determined component) at decidedly subsaturation concentrations of what we shall consider the "competitors" (e.g., the glucose in PNP-glucose). The competitor concentrations were chosen to best display the expected kinks. We do not report data for phthalide from near-saturated urea because the two appeared to react slowly in solution. At lower concentrations the reaction rate was sufficiently reduced for accurate adsorption determinations.

Finally, we have not here attempted to determine the adsorption of both components, partly to simplify analysis, partly because the determination of adsorption of a component present in high concentrations poses serious problems in precision, and partly because any failure of the proposed theory would make itself manifest with either component. Systems in which both components adsorb approximately equally are reserved for later study.

We now consider the data and its agreement with theory. The first feature of Figures 3-9 is the quite satisfying agreement of theory and experiment over a relatively wide range of capacities and competitor concentrations and an adsorbate concentration range of from four to five orders of magnitude. Indeed, the limitations of the observed agreement have been thus far set by the analytical sensitivity rather than by any concentration limitations of the theory.

A quite striking feature is the contrast between adsorption from near-saturated and unsaturated solutions of competitor. Whereas the correlation curve in near-saturated solutions differs only in its scale factor from single-solute isotherms, the corresponding curve at lower competitor concentrations is, as expected from theory, a composite of two curves. When they differ considerably in slope, e.g., in phthalide-urea and PNP-urea, the transition appears as a quite sharp kink in the correlation curve. This kink marks the theoretically expected transition between competition and noncompetition. In retrospect it seems quite natural to expect that a solid will not compete where it cannot adsorb. Finally, in all cases the kink occurred at capacities at which the correlation curves for the individual components were directly determined from experimental points; it cannot therefore be an artifact of the extrapolation.

Comparing the presented treatment with earlier approaches, we find that the method of Radke and Prausnitz¹¹ contains the assumption that the adsorbed phase forms an ideal solution. This does not appear to be a realistic assumption for solids that are not mutually soluble in bulk. Moreover, although Radke and Prausnitz¹¹ report some success for dilute aqueous solutions, their theory cannot handle concentrated solutions. By contrast, the data presented here include concentrated solutions of one or both components; indeed, there appears to be no loss of accuracy as one approaches saturation. The present approach is of particular advantage for estimating the removal of trace impurities from a concentrated substrate, a common application of adsorption. Jain and Snoeyink¹² apply a Langmuir model to account for binary adsorbates. Whereas they distinguish between regions of competitive and non-

competitive adsorption on the same carbon, their model is expected to be valid only when a fraction of the adsorption occurs without competition. No such restriction appears in our model. Moreover, Jain and Snoeyink reported difficulty in reconciling their data to their model. It seems reasonable on the basis of our data to consider the Polanyi-based approach to be an improvement on preexisting methods.

We now consider the expected generality and limitations of the present approach to competitive adsorption. We would expect it to be quite generally applicable to competing adsorbates that do not react, form solid solutions, or exhibit pronounced molecular sieving effects. We would, moreover, expect the effect of competitor concentration on adsorption to be rather accurately predictable. We assume that the method starts with correlation curves (or adsorption isotherms) of each component; the prediction of the individual scale factors from more fundamental considerations is left for a later publication. We have not yet examined systems in which both components have nearly equal abscissa scale factors, but expect to do so soon.

Acknowledgments. We thank the Calgon Corporation for

supporting this work. We also thank Dr. Bruce Roe for assistance with techniques in high-pressure chromatography.

Supplementary Material Available: Table II, data for competitive adsorption (2 pages). Ordering information is available on any current masthead page.

References and Notes

- (1) M. Manes and L. J. E. Hofer, *J. Phys. Chem.*, **73**, 584 (1969).
- (2) L. J. E. Hofer and M. Manes, *Chem. Eng. Prog.*, **65**, 84 (1969).
- (3) D. A. Wohleber and M. Manes, *J. Phys. Chem.*, **75**, 61 (1971).
- (4) D. A. Wohleber and M. Manes, *J. Phys. Chem.*, **75**, 3720 (1971).
- (5) T. W. Schenz and M. Manes, *J. Phys. Chem.*, **79**, 604 (1975).
- (6) C. C. T. Chiou and M. Manes, *J. Phys. Chem.*, **78**, 622 (1974).
- (7) M. Ozcan, Dissertation, Kent State University, 1972. (Some of the experimental data are being checked with improved equipment pending publication.)
- (8) M. Polanyi, *Z. Elektrochem.*, **26**, 370 (1920); *Z. Phys.*, **2**, 111 (1920).
- (9) R. S. Hansen and W. V. Fackler, *J. Phys. Chem.*, **57**, 634 (1953).
- (10) See paragraph at end of text regarding supplementary material.
- (11) C. J. Radke and J. M. Prausnitz, *AIChE J.*, **18**, 761 (1972).
- (12) S. Jain and V. L. Snoeyink, *J. Water Pollut. Control Fed.*, **45**, 2463 (1973).
- (13) Single solute data in Table II are calculated using the bulk molar volume V and competitive adsorption data are calculated using V^* , the adjusted adsorbate molar volume.

Effect of Chain Tacticity on Dye Binding to Polyelectrolytes¹

V. Vitagliano,* L. Costantino, and R. Sartorio

Istituto Chimico, Università di Napoli, Naples, Italy (Received April 14, 1975; Revised Manuscript Received September 22, 1975)

The interaction between isotactic polyelectrolytes and acridine orange has been studied in the case of poly(methacrylic acid) and poly(styrenesulfonic acid), and compared with the results previously obtained with the atactic polyacids. The dye binding strength is higher and its stacking coefficient is lower in the presence of isotactic polyelectrolytes. This result has been interpreted as due to the higher probability for the dye molecules to be located between couples of negative charged groups arranged in helical sequences, when bound to isotactic polymers.

The difference in the properties of solutions of polyelectrolytes with different tacticity has been widely recognized in the past, especially as regards the polyvinyl chain macroions. Solubility, viscosity, carboxylic groups ionization, and counterion binding are sensitive to the chain configuration.²⁻⁸

Most of the results suggest that isotactic polyelectrolytes have a higher charge density than syndiotactic ones; this was found for poly(2-vinylpyridine),³ poly(styrenesulfonic acid),⁷ and poly(methacrylic acid).⁴ It must be remembered, however, that in this last case results from our laboratory seem to suggest an opposite interpretation; sodium ion binding to isotactic polymethacrylate is in fact weaker than binding to atactic and syndiotactic polyelectrolyte,⁸ and the electrophoretic mobility of the former polyion is lower than that of the latter ones.⁹

Some results were also reported on the different behav-

ior of dye binding to polyelectrolytes of different tacticity.¹⁰⁻¹²

The relevant aspects of these studies can be summarized as follows. A number of cationic dye molecules bind to a polyacid matrix as monomeric species or they can interact each other through the π -electron system; in this case dye molecules bind as dimer or higher order aggregates.

Monomer, dimer, and higher order aggregate dye molecules can be distinguished because of their different optical absorption in the visible region (see Figure 5, graphs 1-4). The tendency of a given dye to aggregate, when bound along a polymeric matrix (stacking tendency), depends on the polyelectrolyte matrix species.¹²⁻¹⁴

It is the aim of this paper to present a spectrophotometric study of the binding of acridine orange to isotactic poly(styrenesulfonic acid) and to discuss the possible reasons for the marked differences observed with respect to

the dye behavior between atactic and isotactic polyelectrolytes. It is known that atactic polymers with a vinyl chain have mainly syndiotactic configurations.^{4,15}

Some results concerning isotactic and atactic polymethacrylic acids will also be presented.

Experimental Section

Acridine orange (AO) was purified as described elsewhere.¹³

Atactic poly(methacrylic acid) (a-PMA, commercial product) was purified by precipitation with ethyl ether from a methanol solution (light scattering $M_w = 160\,000$).

Isotactic poly(methacrylic acid) (i-PMA) was obtained by acid hydrolysis of a poly(methylmethacrylate) sample (degree of hydrolysis higher than 91%, $M_w \approx 200\,000$). The isotactic poly(methylmethacrylate) was obtained by polymerization of methylmethacrylate in toluene solution at -60°C using *n*-phenylmagnesium bromide as a catalyst.¹⁶

The AO absorption spectra in the presence of PMA, discussed here, were taken at a very high P/D ratio (polymer equivalent concentration to dye concentration) by using a Beckman DK2 apparatus. The dye concentration was 10^{-6} M, the polyacids were partially neutralized with NaOH at a pH ~ 7 and 0.001 M sodium cacodylate was added as a buffer.

Due to the very low dye concentration, the absorption data were not very accurate; in order to compare different runs it was found convenient to compute the ratios, R , between the optical density at 500 nm (maximum of monomer bound dye) and that at 465 nm (maximum of aggregate bound dye).¹⁴ In this way a set of self-consistent values was obtained which allowed comparing the behavior of the AO-a-PMA system to that of AO-i-PMA; the R data are shown in Figure 1.

An approximate value of the fractions X_1 of monomer bound dye at different values of the D/P ratio can be estimated from the graphs of Figure 1, as well as an approximate value of the bound AO stacking coefficients, q_1 .^{13,17}

Isotactic Polystyrene (i-PS). A sample of i-PS was kindly furnished by Professor E. Butta from the Applied Chemical Institute of Pisa University. Both ir¹⁸ and x-ray diffraction¹⁹ characterization gave a crystallinity degree of about 60–70%, corresponding to a highly pure isotacticity.

Isotactic poly(styrene sulfonic acid) (i-PSS) was prepared by sulfonation of the (i-PS) as described elsewhere,²⁰ degree of sulfonation $\sim 81\%$.

The i-PSS molecular weight was computed by measuring the limiting viscosity number of sodium salt at pH 7 in 2.5 M NaCl through the expression

$$[\eta] = 1.9M_v^{0.6} \quad (1)$$

obtained by interpolation of literature data:²¹ $M_v = 3 \times 10^6$.²²

Spectrophotometric data were recorded using a Cary 14 apparatus with a technique described in a previous paper.¹³ The experimental results were treated as those obtained for the atactic poly(styrenesulfonic acid) (a-PSS)-acridine orange system.¹³ The limiting extinction coefficient of the monomer (E_1) and aggregate bound dye (E_3) were evaluated by a proper extrapolation of experimental data at $P/D \rightarrow \infty$ and at $P/D = 1$ (see Figure 2). The dimer extinction coefficient (E_2) at 498 nm was assumed equal to that of aggregated dye, as done in the previous paper¹³ (see Table I). By using the data given in Table I and the experimental extinction coefficients at 485 and 498 nm, the fractions of mo-

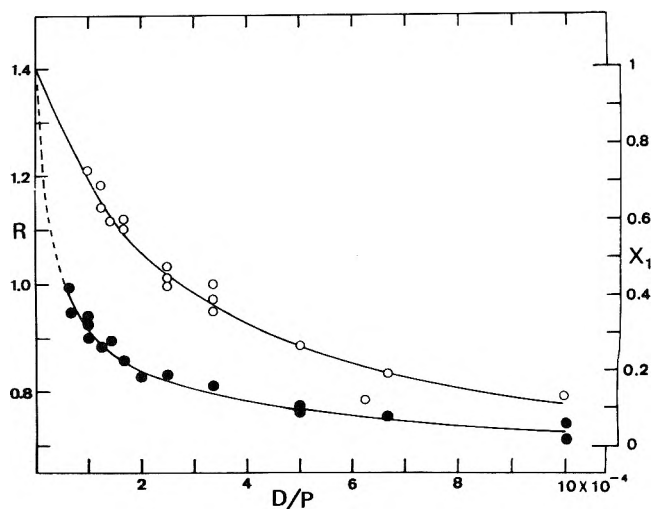


Figure 1. Poly(methacrylic acid)-acridine orange system, dye concentration 10^{-6} M, pH ≈ 7 , polyacid degree of neutralization ~ 0.5 : (O) isotactic PMA, (●) atactic PMA, $R =$ (optical density at 500 nm)/(optical density at 465 nm); $X_1 =$ approximate value of the fraction of dye bound as a monomer; D/P = ratio of dye to polymer equivalent concentration.

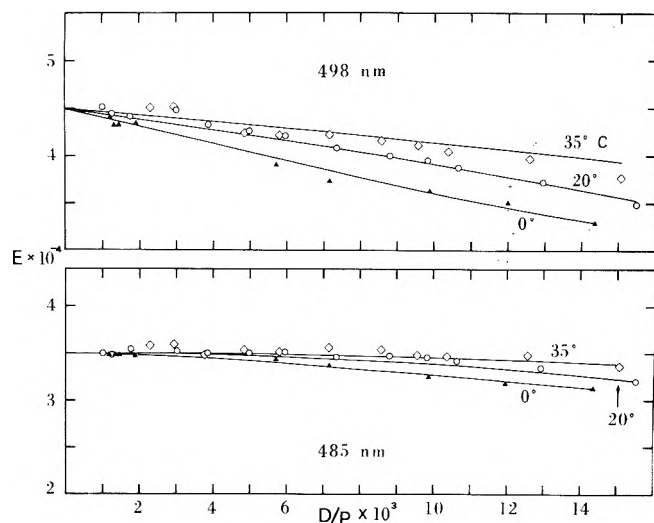


Figure 2. Extrapolation of experimental extinction coefficients at two wavelengths to obtain the monomer limiting extinction coefficients E_1 : acridine orange concentration, 10^{-5} M; 498 nm, maximum of monomer bound dye; 485 nm, isosbestic point of monomer-dimer bound dye.

TABLE I: Extinction Coefficients of Bound Dye

	λ , nm	E_1	E_2	E_3	E_1 (atactic)
(monomer max)	498	45 000	13 000	13 000	53 400 ^a
(monomer-dimer isosbestic)	485	35 000	35 000	17 500	
(monomer-dimer isosbestic)	482				36 000

^a From ref 13.

nomer (X_1), dimer (X_2), and aggregated bound dye (X_3) were computed at various P/D ratios.

The dye-polyelectrolyte complex was treated as an infinite linear sequence of empty sites A, and occupied sites B:

... AABBBAAAAABAABBBBBBAAAABBAAB ...

so that ... ABA ... corresponds to the dye monomer, ... ABBA ... to the dye dimer, and ... ABB ... BA ... to the dye aggregate. The dye distribution among the three different species was computed by accounting for first, second, and third neighbor interaction parameters, following the sequences generating function treatment suggested by Lifson.^{17,23} Accordingly the partition function of an infinite linear sequence of A and B sites can be obtained as the highest root of the equation

$$f(z) = 1 - U(z) V(z) = 0 \quad (2)$$

where $U(z)$ and $V(z)$ are series functions referring to the A and B sequences, respectively. If A and B represent empty sites and sites occupied by a dye molecule along the polyelectrolyte chain

$$U(z) = \sum_{i=1}^{\infty} q_0^i z^{-i} = q_0/(z - q_0) \quad (3)$$

and

$$V(z) = q_a \lambda_a z^{-1} + q_1 q_a^2 \lambda_a^2 z^{-2} + \dots + q_{m-1} \dots q_1^{m-1} (q_a \lambda_a)^m z^{-m} \times \sum_{j=1}^{\infty} (q_m q_{m-1} \dots q_1 q_a \lambda_a z^{-1})^{j-m} \quad (4)$$

where q_0 is the partition function of a desorbed state site; q_a is the partition function of a site in an adsorbed state, and λ_a is the absolute activity of the dye in solution. Furthermore, it is assumed that neighboring adsorbed molecules interact with each other such that a pair of first neighbors has a partition function of pairwise interaction q_1 (stacking coefficient), a pair of second neighbors has a partition function q_2 , and so on up to the m th order of neighborhood. Finally, interactions of bound molecules through an empty site are excluded.

It is possible to obtain informations about dye distribution along the polymer chain by appropriate derivations without actually solving eq 2:

$$D/P = (\partial f(z)/\partial \ln q_a \lambda_a) / (\partial f(z)/\partial \ln z^{-1}) \quad (5)$$

$$X_1 = U(z) q_a \lambda_a z^{-1} / (\partial f(z)/\partial \ln q_a \lambda_a) \quad (6)^{24}$$

$$X_2 = 2X_1 q_1 q_a \lambda_a z^{-1} \quad (7)$$

More detailed expressions are given in ref 12 and 13.²⁴

By using these expressions, the values of q_1 , q_2 , and q_3 were computed that gave the best fitting between experimental and computed X_1 and X_2 values ($q_m = 1$ for $m > 3$). Table II reports the values of the interaction parameters q_1 , q_2 , and q_3 .²²

Discussion

Two main effects can be attributed to the polyion tacticity, both in the case of PMA and PSS; a third one has to be mentioned in the PSS case.

(1) The dye binding strength is markedly enhanced in the case of isotactic polymers, as was already observed for PMA in the past.¹⁰

Figure 3 shows the titration of AO with i-PSS at 20 °C; the end point titration at $P/D = 1$ (SO_3^- groups concentration to dye concentration) is much sharper than the corresponding titration with a-PSS (ref 13, Figure 1) denoting a smaller amount of free dye in solution around the end point.

TABLE II: Interaction Parameters of Acridine Orange Bound to Isotactic PSS^c

$T, ^\circ\text{C}$	q_1	q_2	q_3	$\overline{\Delta X}_1^a$	$\overline{\Delta X}_2^a$	ΔX_3^a	q_1 (atactic) ^b
0	15.6	2.21	1.57	0.027	0.019	0.031	43.1
20	8.74	2.23	2.70	0.021	0.026	0.034	30.0
35	5.33	2.11	3.0	0.031	0.020	0.034	22.9

^a Mean square error on mole fractions of monomer, dimer, and aggregate bound dye. ^b From ref 13. ^c See footnote 22.

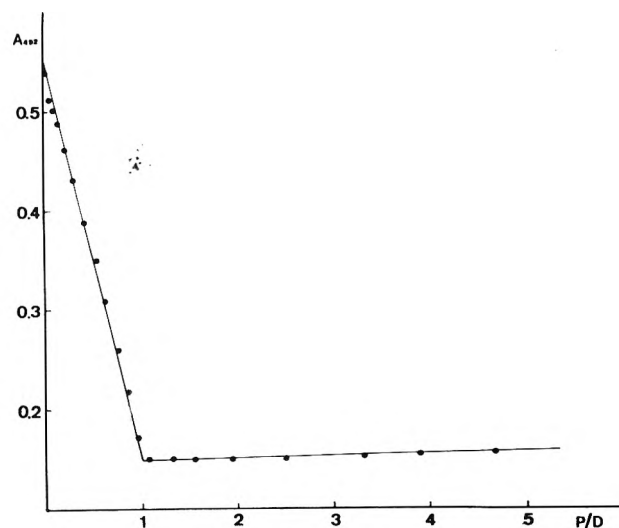


Figure 3. Acridine orange titration with isotactic PSS; dye concentration 10^{-5} M. The end point corresponds to the 1:1 ratio between dye concentration and polyelectrolyte equivalent (SO_3^- groups) concentration.

More direct evidence of this fact is shown in Figure 4 where the AO extinction coefficients of solutions at constant $P/D = 1.1$ and varying dye concentration are plotted as a function of $1/D$, both for atactic and isotactic PSS solutions at 35 °C. The terms $E - E^0$ (E^0 being the intercept) of such graphs measure the amount of free dye in solution at each $1/D$ value, as previously suggested.¹³ It can be seen that the amount of free AO in the presence of i-PSS at 35 °C is very small. No free dye could be detected by using this technique at 20 °C and at lower temperatures for the AO-i-PSS system, in contrast with the results obtained for the AO-a-PSS system.

(2) The bound dye stacking tendency is markedly lowered when bound to isotactic polymers, i.e., the dilution of the dye along (or within²⁵) the polymer chain is favored in the case of isotactic polyacids.

An approximate value of the q_1 stacking coefficient was estimated for the polymethacrylic acids from the slope at $D/P = 0$ of the graphs in Figure 1, by using the limiting expression (ref 13, eq 18)

$$X_1 = 1 - 2q_1(D/P) + \dots \quad (8)$$

$q_1 \approx 8000$ for a-PMA and $q_1 \approx 1600$ for i-PMA.

The q_1 values for a-PSS and i-PSS are collected in Table II. We may remember that the q_1 parameter corresponds to the dimerization constant of the dye bound along the polyelectrolyte chain (ref 13, eq 32).

(3) The optical absorption of monomer dye bound to i-PSS exhibits a marked hypochromicity with respect to

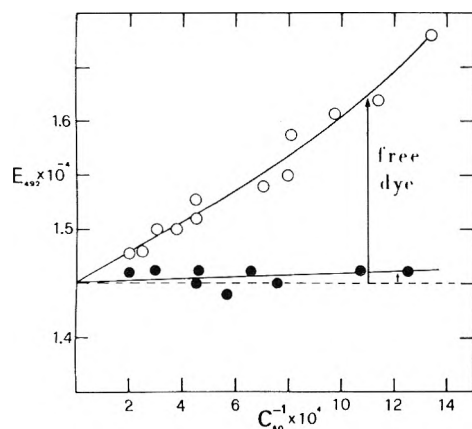


Figure 4. Extinction coefficients of solutions at constant $P/D = 1.1$ and varying total dye, and polymer, concentration. Comparison between the AO-a-PSS system (O) and the AO-i-PSS system (●), at 35 °C. It has been assumed that the extrapolated E^0 value at dye concentration $\rightarrow \infty$ ($C_{AO}^{-1} = 0$) corresponds to the extinction of bound dye. The difference $E - E^0$ corresponds, at any actual concentration, to the amount of free monomer dye.

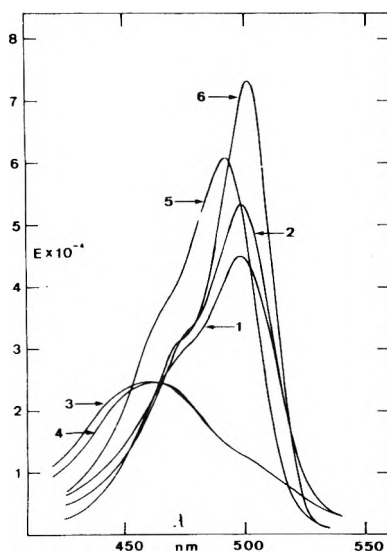


Figure 5. Limiting extinction coefficients of AO in various solutions: (1) AO-i-PSS monomer bound dye spectrum; (2) AO-a-PSS monomer bound dye spectrum; (3) AO-i-PSS aggregate bound dye spectrum; (4) AO-a-PSS aggregate bound dye spectrum; (5) monomer AO in water; (6) monomer AO bound to a-PMA at a polyacid degree of ionization lower than 0.2 (ref 25).

that bound to a-PSS; furthermore in both cases the extinction coefficients are lower than in water.

This effect is remarkable if compared with the behavior of the AO-polyacrylate and AO-polymethacrylate systems where the bound monomer dye exhibits the same extinction coefficient as in water or even a hyperchromic effect, in the presence of PMA at low degree of ionization, comparable to that shown in alcoholic solutions^{12,25} (some comparative spectra are shown in Figure 5).

Jordan et al.¹¹ mentioned a similar hypochromic effect for proflavine bound to i-PSS and to a-PSS, however, they found that by increasing temperature in the range 45–50 °C any difference between i-PSS and a-PSS disappear. On the contrary we found no appreciable changes in the absorption spectrum of a AO-i-PSS sample ($P/D = 200$, dye

concentration 10^{-5} M) up to 70 °C (under these conditions the AO is bound mainly in its monomeric state).

We already suggested, in the past, that the low stacking coefficient of dyes bound to PSS, as compared to that of dyes bound to other polyelectrolytes with a vinyl chain, might be due to specific interactions between the dye molecules and the benzene rings.^{12,13,26} These interactions could eventually favor some kind of partial intercalation similar to that described for the DNA-proflavine and DNA-AO systems.^{27,28} Also in the DNA case, in fact, the bound dye stacking tendency is very low, being lower for the native DNA than for denatured DNA.^{29–31}

It is known that both isotactic and syndiotactic configurations of polyvinyl chains may assume a relevant number of helical conformations in the crystalline state.^{32,33} Due to steric hinderance, the flexibility of isotactic chains is lower than that of the syndiotactic. So, while the syndiotactic chains may assume a zig-zag trans-planar conformation with the side groups spaced at about 5.2 Å, as found for the 1,2-polybutadiene³⁴ (see Figure 6A), such a conformation is not allowed for the isotactic chains because it would impose a 2.6 Å distance between side groups; such a distance is not even sufficient for locating the methyl groups of isotactic polypropylene.

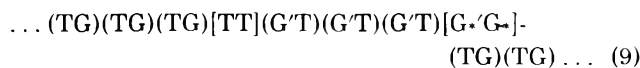
Figure 6B shows another possible helical conformation of syndiotactic chains^{33,35} with a spacing of about 7.3 Å between side groups. Figure 7A and 7B shows the ternary and quaternary helices of isotactic polystyrene and polystyrene derivatives,^{32,36,37} the phenyl groups spacing being 6.65 and 8.1 Å, respectively.

The best possibility for intercalation of an aromatic structure is offered by the quaternary helix of isotactic chains (Figure 7B). The syndiotactic helix shown in Figure 6B can also allow for some intercalation but steric hinderance is probably much more effective in this case.

Actually the polymer chain conformation in solution is not ordered and helical structures must be limited to short distances; however, the possibility of local conformations allowing for dye molecules intercalation shown by the polymer rigid crystalline structure can be preserved and, certainly, enhanced in solution.

It may be interesting to compute the probability of such local helical conformations both in the case of isotactic and syndiotactic chains. This can be easily done if we assume a very simple model for the chains, and neglect electrostatic interactions.

The isotactic chain can be realized by a sequence of $-(C-C)-$ bonds with internal rotation angles of 180° (trans, T) or 60 to 90° (G), ... (TG)(TG)(TG) ..., the side groups being included between the T and the G bonds.^{38,39} The sequence (180°, 60°)(180°, 60°) corresponds to the right-handed ternary helix (Figure 7A), while the $G = 90^\circ$ corresponds to the quaternary right-handed helix. The left-handed helices are generated by sequences ... (G'T)(G'T)(G'T) ..., G' being 300 (−60°) to 270° (−90°) (Figure 7B). Helix inversion can be achieved through a sequence (TT) (inversion right to left) and a sequence (G'G') (inversion left to right):⁴⁰



where (G'G') can be either (240°, 60°) or (300°, 120°).^{39,41}

The sequences (TG), (G'T), and (TT) can be assumed as all having the same energy, while the (G'G') sequence has

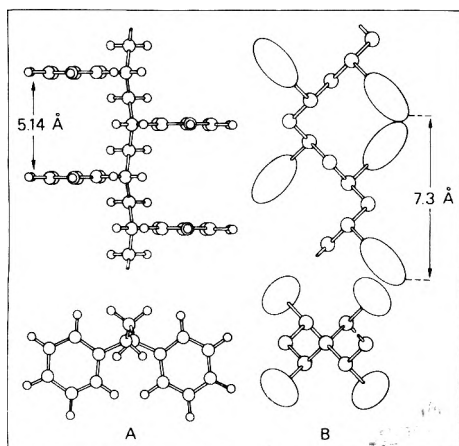


Figure 6. Possible helical conformations of syndiotactic vinyl chain polymers: (A) zig-zag trans-planar conformation (as found for 1,2-polybutadiene (ref 34)); (B) ... TTGGTTGGTTGG ... conformation (ref 33 and 35).

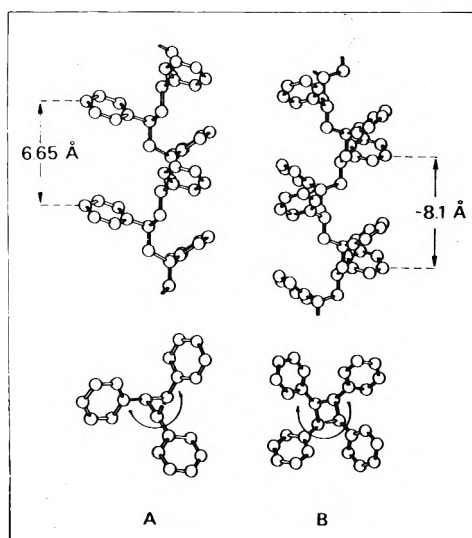


Figure 7. Helical conformations found for isotactic polystyrene and polystyrene derivatives: (A) ternary helix of i-PS (ref 36); B quaternary helix found for a number of PS derivatives, such as the poly- α -methylstyrene and the poly- α -vinyl-naphthalene (ref 37).

a higher energy content of about 3000 cal/mol (reasonable value for polystyrene).

The syndiotactic chain can be realized through the following sequences:³⁹

$$\dots (TT)_n(GG)(TT)_m(GG)(TT)_s(G'G')(TT)_p \dots \quad (10)$$

(180°, 180°), (60°, 60°), or (300°, 300°)

In this case the side groups are located between neighboring sequences (TT) and (XX), or (XX) and (TT). The sequence ... (TT)(TT)(TT) ... corresponds to the zig-zag trans-planar conformation shown in Figure 6A, while the helix shown in Figure 6B corresponds to the sequence ... (TT)(GG)(TT)(GG) ... All syndiotactic sequences have about the same energy content.³⁹

We may assume that a minimum of five (TG) or (G'T) sequences be required for a dye molecule intercalation along the isotactic PSS chain, and a minimum of five sequences (TT)(GG)(TT)(GG)(TT), or (G'G'), be required for syndiotactic PSS.

Lifson's algebra¹⁷ can be easily applied to compute the helical sequence length distribution in both cases.

(A) *Isotactic Chain Case.* Chain model

$$\dots AAABBABAAABBBBAAABAABA \dots$$

where A \rightarrow (TG), and B \rightarrow (G'T); each AB inversion includes a (TT) sequence and each BA inversion includes a (G'G') one.

Let us assign the U(z) function to the A sequences and the V(z) to the B:

$$U(z) = \sum_1^{\infty} u^i z^{-i} = \frac{uz^{-1}}{1 - uz^{-1}} \quad (11)$$

$$V(z) = \sum_1^{\infty} \epsilon u^i z^{-i} = \frac{\epsilon uz^{-1}}{1 - uz^{-1}} \quad (12)$$

$$f(z) = 1 - \epsilon \left[\frac{uz^{-1}}{1 - uz^{-1}} \right]^2 \quad (13)$$

u being the partition function of both A and B, while ϵ is the partition function of the BA joints;⁴⁰ a reasonable value for ϵ is

$$\epsilon = Z_0 \exp(-\Delta E/RT) = 2 \exp(-3000/RT) \quad (14)$$

at 20 °C $\epsilon = 0.0115$. The factor $Z_0 = 2$, in eq 14, accounts for the two isoenergetic possibilities (G'G') = (240°, 60°) and (300°, 120°).

The fraction of BA joints is obtained by solving the expression^{17,23}

$$[BA] = (\partial f(z)/\partial \ln \epsilon) / (\partial f(z)/\partial \ln z^{-1}) = \frac{1}{2}(1 - uz^{-1}) \quad (15)$$

By solving eq 2 one obtains the partition function z:

$$z^2 - 2uz + u^2(1 - \epsilon) = 0 \quad (16)$$

and by assuming $u = 1$:

$$z = u(1 + \sqrt{\epsilon}) = 1 + \sqrt{\epsilon} = 1.107 \quad (17)$$

$$[BA] = [AB] = 0.0484$$

$$[A] = [B] = 0.5 \quad (18)$$

$$[AA] = [A] - [BA] = 0.4516$$

By using these values it is possible to compute the fractional concentration of any desired sequence, through the following general expression:⁴²

$$\begin{aligned} [XYW \dots QRZ] &= [YW \dots QRZ][XYW \dots QR] / \\ & \quad [YW \dots QR] \\ &= [XY][YW] \dots [QR][RZ] / \\ & \quad [Y][W] \dots [Q][R] \quad (19) \end{aligned}$$

in particular

$$[A_n] = [AA]^{n-1} / [A]^{n-2} \quad (20)$$

and

$$[BA_n B] = [BA]^2 [AA]^{n-1} / [A]^n \quad (21)$$

where, actually

$$\sum_{n=1}^{\infty} n [BA_n B] = 0.5 \quad (22)$$

By using eq 20 the following fractions for some given sequences have been obtained: ($[A_5] + [B_5]$) = 66.6%, ($[A_{10}] + [B_{10}]$) = 40%, ($[A_{20}] + [B_{20}]$) = 14%. The fraction of A + B present as a monomer (BAB + ABA) plus dimer (BAAB + ABBA) plus, ..., up to the tetramer, which do not allow for intercalation, is about 7.7%; accordingly, it may be con-

cluded that about 92% of isotactic chains monomeric units are arranged in sequences allowing for intercalation.

(B) *Syndiotactic Chain Case*. Chain model



where $A \rightarrow (TT)$, $B \rightarrow (GG)$, and $B' \rightarrow (G'G')$:

$$U(z) = \sum_1^{\infty} u^i z^{-i} = \frac{uz^{-1}}{1 - uz^{-1}} \quad (23)$$

$$V(z) = vz^{-1} \quad \text{and} \quad V'(z) = v'z^{-1} \quad (24)$$

where $u = v = v' = 1$ because of the assumption that all sequences have the same energy content.

The generating functions $V(z)$ and $V'(z)$ have the only first term because only monomers ABA and AB'A are allowed.

$$f(z) = 1 - U(z)[V(z) + V'(z)] = 1 - (v + v') \frac{uz^{-1}}{1 - uz^{-1}} \quad (25)$$

$$[ABA] = [BA] = [B]$$

$$= (\partial f(z) / \partial \ln v) / (\partial f(z) / \partial \ln z^{-1}) = \frac{1}{2} \frac{1 - z^{-1}}{2 - z^{-1}} \quad (26)$$

$$z = 2 \text{ and } [B] = [B'] = 0.167.$$

The shortest sequence allowing for intercalation is ABABA, $[ABABA] + [AB'AB'A] = 0.0834$.

By adding the number of monomeric units participating in the helical sequences of any length greater than 5,⁴³ one obtains $\approx 35.4\%$. This value is much lower than the corresponding 92% value found for the isotactic chain; so we may conclude that the probability of dye intercalation in isotactic polymers is much higher than that in syndiotactic ones.

This higher probability must be responsible both for the higher binding strength exhibited by isotactic polyacids toward cationic dyes and for the higher tendency of the dye to dilute along the polymer chain, due to a lower stacking coefficient.

It may also be suggested that, in the special case of PSS, the π -electron interaction between the benzene rings and the partially intercalated AO molecule is also responsible for the observed hypochromic effect on the monomer dye absorption spectrum.

Finally it must be remembered that the computed chain sequences distribution cannot be quantitatively correlated to the experimental results; the assumed model is in fact oversimplified and it does not include electrostatic interactions. However it is interesting to have pointed out that isotactic helical sequences allow for partial intercalation, such possibility being interrupted only by defects (TT or G'G'), while a number of syndiotactic helical sequences, such as $\dots TTTT \dots$, do not.

Acknowledgment. The authors wish to thank Professor

G. Allegra and Professor P. Corradini for some useful discussions and suggestions.

References and Notes

- (1) This research was supported by the Italian C.N.R.
- (2) E. M. Loebel and J. J. O'Neill, *J. Polym. Sci.*, **45**, 538 (1960).
- (3) C. Loucheux and M. Rinfret, *J. Chim. Phys.*, **65**, 17 (1968).
- (4) M. Nagasawa, T. Murase, and K. Kondo, *J. Phys. Chem.*, **69**, 4005 (1965).
- (5) H. Morawetz and A. Y. Kandarian, *J. Phys. Chem.*, **70**, 2295 (1966).
- (6) J. J. O'Neill, E. M. Loebel, A. Y. Kandarian, and H. Morawetz, *J. Polym. Sci., Part A3*, 4201 (1965).
- (7) D. O. Jordan, T. Kurucsev, and M. L. Martin, *Trans. Faraday Soc.*, **65**, 598, 606 (1969).
- (8) L. Costantino, V. Crescenzi, F. Quadrioglio, and V. Vitagliano, *J. Polym. Sci., A2*, **5**, 771 (1967).
- (9) G. Anzuino, L. Costantino, R. Gallo, and V. Vitagliano, *Polym. Lett.*, **4**, 459 (1966).
- (10) V. Crescenzi, F. Quadrioglio, and V. Vitagliano, *J. Macromol. Sci. (Chem.)*, **A1**, 917 (1967).
- (11) D. O. Jordan, T. Kurucsev, and M. L. Martin, *Trans. Faraday Soc.*, **65**, 612 (1969).
- (12) V. Vitagliano, "Interaction between Cationic Dyes and Polyelectrolytes" in "Chemical and Biological Applications of Relaxation Spectrometry", E. Wyn-Jones, Ed., D. Reidel, Dordrecht, Holland, 1975, p 437.
- (13) V. Vitagliano, L. Costantino, and A. Zagari, *J. Phys. Chem.*, **77**, 204 (1973).
- (14) Extensive literature on this subject is given in ref 12, 13, and 25.
- (15) F. A. Bovey, *J. Polym. Sci., Part A1*, 843 (1963).
- (16) V. Crescenzi, M. D'Alagni, A. M. Liquori, L. Picozzi, and M. Savino, *Ric. Sci.*, **33** (II-A), 123 (1963).
- (17) S. Lifson, *J. Chem. Phys.*, **40**, 3507 (1964).
- (18) H. Utiyama, *J. Phys. Chem.*, **69**, 4138 (1965).
- (19) G. Natta, P. Corradini, and M. Cesari, *Atti Acad. Naz. Lincei*, **22**, 11 (1957).
- (20) R. Hart and T. Timmerman, *C. R. Congr. Int. Chim. Ind.*, **31** (1958); *Ind. Chim. Belge.*, **80**, 137 (1958); *Chem. Abstr.*, **54**, 8141f (1960).
- (21) A. Takahashi, T. Kato, and M. Nagasawa, *J. Phys. Chem.*, **71**, 2001 (1967).
- (22) Some spectrophotometric data were also recorded by using a sonicated i-PSS sample ($M_n \approx 500$ 000); no relevant effects due to molecular weight were observed.
- (23) D. F. Bradley and S. Lifson, "Molecular Association in Biology", B. Pullmann, Ed., Academic Press, New York, N.Y., 1968, p 261.
- (24) Equation 11 of ref 13 is not correct; in order to obtain a correct expression the second term must be divided by $f(x)$.
- (25) G. Barone, V. Crescenzi, F. Quadrioglio, and V. Vitagliano, *Ric. Sci.*, **36**, 503 (1966).
- (26) V. Vitagliano and L. Costantino, *J. Phys. Chem.*, **74**, 197 (1970); *Boll. Soc. Nat. Napoli*, **78**, 169 (1969).
- (27) L. S. Lerman, *Proc. Natl. Acad. Sci. U.S.A.*, **49**, 94 (1963).
- (28) J. P. Schreiber and P. M. Daune, *J. Mol. Biol.*, **83**, 487 (1974).
- (29) D. F. Bradley and M. K. Wolf, *Proc. Natl. Acad. Sci. U.S.A.*, **45**, 944 (1959).
- (30) D. F. Bradley and G. Felsenfeld, *Nature (London)*, **184**, 1920 (1959).
- (31) A. L. Stone and D. F. Bradley, *J. Am. Chem. Soc.*, **83**, 3627 (1961).
- (32) G. Natta and P. Corradini, *Nuovo Cimento, Suppl., Ser. X*, **15**, 9 (1960).
- (33) G. Natta, *Makromol. Chem.*, **35**, 94 (1960).
- (34) G. Natta and P. Corradini, *J. Polym. Sci.*, **20**, 251 (1956).
- (35) G. Natta and P. Corradini, *Makromol. Chem.*, **39**, 238 (1960).
- (36) G. Natta, P. Corradini, and I. W. Bassi, *Nuovo Cimento, Suppl., Ser. X*, **15**, 68 (1960).
- (37) P. Corradini and P. Ganis, *Nuovo Cimento, Suppl., Ser. X*, **15**, 96, 104 (1960).
- (38) P. Corradini, P. Ganis, and P. Oliverio, *Ann. Acad. Lincei*, **33**, 320 (1962).
- (39) G. Allegra, P. Ganis, and P. Corradini, *Makromol. Chem.*, **61**, 225 (1963).
- (40) Note that the defect sequences (TT) and (G'G') must always appear coupled!
- (41) P. Corradini and G. Allegra, *Ann. Acad. Lincei*, **30**, 516 (1961).
- (42) G. Schwarz, *Z. Elektrochem.*, **75**, 40 (1971).
- (43) We may assume that a given helical sequence of the type $\dots ABABA \dots$ can be interrupted in four different ways: $\dots E(AB)_n AE' \dots$, where E and E' can be either A and/or B'.

Reaction Kinetics and Differential Thermal Analysis

Ralph T. Yang* and Meyer Steinberg

Department of Applied Science, Brookhaven National Laboratory, Upton, New York 11973 (Received October 2, 1975)

Publication costs assisted by Brookhaven National Laboratory

Quantitative relationships between chemical kinetics and DTA curves are studied for the reactions which follow the general rate expression: $r = r_0 e^{-E/RT}(1-x)$. Both the frequency factor and the activation energy can be derived from a single DTA curve. From the known kinetic parameters, the DTA curve can also be predicted. The rather simple models developed in this work have been tested by the oxidation reaction of nuclear graphite with CO_2 and by data in the literature on the thermal dehydration of clays. The results are satisfactory considering the complexities involved in DTA.

Introduction

Considerable importance and interest exist in the study of reaction kinetics by differential thermal analysis (DTA). Since the classic work of Murray and White on clay dehydration kinetics,² DTA has been used to characterize complex chemical reactions, such as the thermal dehydration and decomposition of solid compounds³⁻⁷ and homogeneous reaction systems.⁸ The method of Borchardt and Daniels was later extended to heterogeneous reactions.⁹⁻¹¹ It has not been possible, however, to obtain both the activation energy and frequency factor from a single DTA curve for a heterogeneous gas-solid reaction, and to predict the DTA curve from the known kinetic parameters for the same reaction system.

Most of the previous work was concerned with the dehydration and decomposition of minerals with the reaction form: $\text{A (solid)} \rightarrow \text{B (solid)} + \text{C (gas)}$. The order of the reaction is defined as the exponent n in the following rate expression:

$$r = r_0 e^{-E/RT}(1-x)^n \quad (1)$$

Here r is the rate and is expressed as dx/dt ; t is the time; r_0 the frequency factor; E the activation energy; R the gas constant; T the absolute temperature; and x the fractional completion of the reaction.

For heterogeneous gas-solid reactions of the form $\text{A (solid)} + \text{B (gas)} \rightarrow \text{C (gas)}$, such as carbon oxidation reactions, the order of the reaction is conventionally related to the dependence of rate on the concentration of the gaseous reactant. The rate of a carbon oxidation reaction (r) is normally expressed as $-(1/m)(dm/dt)$, here m is the instantaneous mass of the solid. It can be shown that this expression is identical with $(dx/dt)(1-x)^{-1}$ by using the relation: $x = 1 - (m/m_0)$, here m_0 is the initial mass. When the rate is independent of the burn-off (x), the rate expression is identical with that of the "first order" reaction in the previous case (with the concentration of the gaseous reactant constant). It should be noted here that the quotation mark is used here to differentiate it from the conventional meaning of the order of a gas-solid reaction.

The scope of this work is to (1) calculate both frequency factor and the activation energy from a single DTA curve and (2) predict the DTA curve, or at least its shape, from known kinetic parameters. The type of reactions considered here is of the general form as in eq 1 with $n = 1$.

Theoretical Considerations

In a DTA curve, the temperature differential (ΔT) at any given instant can be approximated as being proportional to the instantaneous mass reacting rate:

$$\Delta T = k_1 y \quad (2)$$

Here y is the instantaneous mass rate ($=rm_0$) and k_1 is a constant. The equation is approximate because k_1 is affected by the heat and mass transport processes which do not remain strictly constant during the reaction (the term reaction is used to include all chemical changes). However, for the case in which only the instantaneous thermal effect is detected and there is no accumulation of the effect, k_1 is equal to the heat of reaction divided by the total heat capacity of the sample mass.

For the "first order" reactions

$$\Delta T = k_1 r_0 e^{-E/RT}(1-x)m_0 \quad (3)$$

The peak temperature of a DTA curve (T_m) is obtained by simply setting $d(\Delta T)/dT = 0$ and solving for T_m . The following relationship was obtained and tested satisfactorily by Murray and White:²

$$\frac{r_0}{k_2} e^{-E/RT_m} = \frac{E}{RT_m^2} \quad (4)$$

where k_2 is the heating rate.

The temperature at the inflection points (T_i), i.e., at the maximum and minimum slopes, can be obtained by setting $d^2(\Delta T)/dT^2 = 0$ and solving for T_i . The following relationship is obtained:

$$\frac{r_0}{k_2} e^{-E/RT_i} \left(\frac{3E}{RT_i^2} - \frac{r_0}{k_2} e^{-E/RT_i} \right) = \left(\frac{E}{RT_i^2} \right)^2 - \frac{2E}{RT_i^3} \quad (5)$$

In eq 5, there exist two solutions for T_i (T_{i1} and T_{i2}) which correspond to the two inflection points.

E and r_0 can be calculated by solving eq 4 and 5 simultaneously with T_m and either one of the T_i 's, or by solving eq 5 with T_{i1} and T_{i2} . The calculation is, however, quite tedious. In eq 5, approximation for T_{i1} (the first inflection point) can be made by dropping the second term in the left-hand side because it is normally quite small compared to the first term for T_{i1} . Thus, one obtains

$$3 \frac{r_0}{k_2} e^{-E/RT_i} = \frac{E}{RT_i^2} - \frac{2}{T_i} \quad (6)$$

T_i in eq 6 refers to T_{i1} only. By knowing T_m and T_{i1} , eq 4

and 6 can be easily solved simultaneously for E and r_0 . Examples will be provided of this method for the kinetics of C + CO₂ reaction and dehydration of kaolinite and halloysite.

To predict a DTA curve, one has to be able to express ΔT as a function of T . This can be achieved only when the functional form of $x(T)$ is established. We start with

$$\frac{dx}{dt} = r_0 e^{-E/RT}(1-x) \quad (1a)$$

or

$$\frac{dx}{1-x} = \frac{r_0}{k_2} e^{-E/RT} dT \quad (7)$$

Here t is the time.

Upon integration of eq 7, $x(T)$ can be obtained. However, because normally $E/RT \gg 1$, the integration of $\int e^{-E/RT} dT$ is the most troublesome task. This integration has been attempted, and the following substitution has been used:^{7,12}

$$\int_0^{T'} e^{-E/RT} dT = \frac{e^{-z}}{z} - \int_z^\infty \frac{e^{-u}}{u} du \quad (8)$$

Here $u = E/RT$. The function $\int_z^\infty (e^{-u}/u) du$ has been tabulated for $E = 10 - 66$ kcal/mol and $T = 100 - 430$ °C.⁷ An approximate solution for the same function was used by Murray and White² in their calculation of the percentage reaction at the peak DTA temperature. The approximate solution was taken as the first two terms of the Taylor series expansion of e^{-u}/u . The two terms involve the second and third powers of RT/E .

It is nevertheless, more desirable to obtain an analytical solution or approximation in a simpler form for it not only simplifies the calculation but also characterizes the actual processes. In order to achieve this, we adopt the "method of expanding the exponent" first suggested by Frank-Kamenetskii in developing his theory of combustion.¹³ The argument of the integrand is approximated as the following:

$$\frac{E}{RT} = \frac{E}{R(T_0 + \delta T)} = \frac{E}{RT_0} \frac{1}{1 + \frac{\delta T}{T_0}} \approx \frac{E}{RT_0} - \frac{E}{RT_0^2} \delta T \quad (9)$$

Here $\delta T = T - T_0$ and T_0 can be chosen arbitrarily, provided it is near the reaction range so that $\delta T/T_0$ is small. The approximation is better at higher temperature ranges and is in error by less than a few percent for all practical DTA measurements. Equation 7 can then be integrated conveniently with the boundary condition: $T = 0, x = 0$, and the solution substituted in eq 3. The following results are obtained:

$$1-x = e^{-k_4 [e^{(E/RT_0^2)T} - 1]} \quad (10)$$

$$\Delta T = k_1 r_0 m_0 \exp \left[-\frac{E}{RT} - k_4 e^{(E/RT_0^2)T} + k_4 \right] \quad (11)$$

Here

$$k_4 = \frac{r_0 RT_0^2}{k_2 E} e^{-2E/RT_0} \quad (12)$$

The lower integration limit of T was chosen to be zero to simplify the solutions. When T is small, the approximation in eq 9 is poor but since $E/R \gg T$, the integrands, both the original and the approximated, are negligibly small.

Equation 11 can be used to predict DTA curve. There

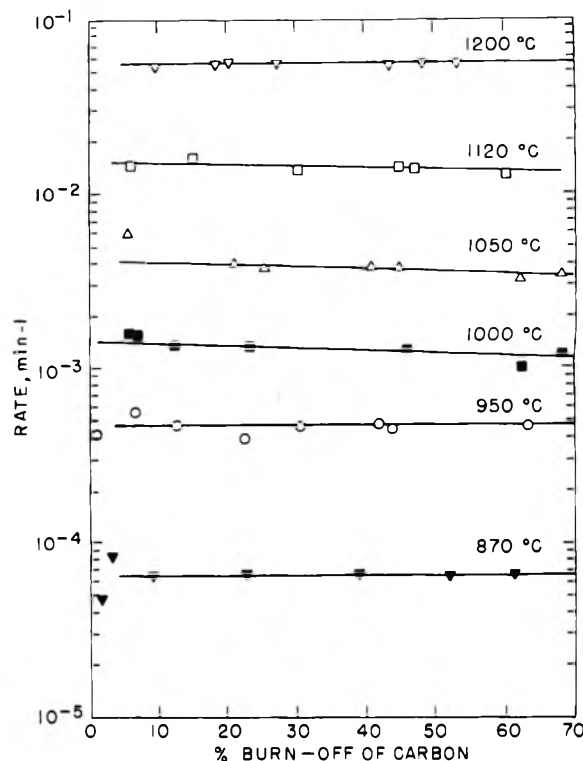


Figure 1. Reaction rate of nuclear graphite in CO₂.

are three factors in this equation: the first one is the Arrhenius factor; the second and third describe the decrease of the reacting material with the linearly increasing temperature. It is also interesting to note that eq 10 can be used to calculate E and r_0 with two sets of corresponding x and T values, which are obtained with the simultaneous DTA/TG apparatus. Applications of the method will be exemplified.

Experimental Section

The kinetics and DTA curve of the reaction $C + CO_2 \rightarrow 2CO$ were obtained by using a Mettler differential thermoanalyzer Model TA-1. Reaction rates were measured gravimetrically (TG), and are expressed as $-(1/m)(dm/dt)$ with the units of min^{-1} . Sensitivity of the balance was $\pm 3 \times 10^{-6}$ g.

The carbon sample used was pile-grade nuclear graphite. Ash content of the graphite was below 0.01% and its major constituents were less than 0.001% of Si, Ag, and Cu and less than 0.0001% of Mg as detected by emission spectroscopy. Particle size of the sample used in all the experiments was in the range 590–840 μm . The CO₂ and argon gases used were originally bone dry and prepurified grades, respectively, and were supplied by Liquid Carbonic Co. The gases were purified from traces of water and oxygen by passing through a train of silica gel, Mg(ClO₄)₂ (both at room temperature), and copper turnings held at 500 °C. Gas flow rate was maintained constant and was about three orders of magnitude greater than could be consumed at the maximum reaction rate. Same samples and flow conditions were employed in both TG and DTA measurements.

In the DTA curve measurement, 20 mg of graphite was mixed with alumina (grade A-10, Alcoa, -50 + 200 mesh) and diluted to 10%. The reference contained 200 mg of alumina. It is also noteworthy that the thermocouple wells were immersed in the centers of the materials so that any

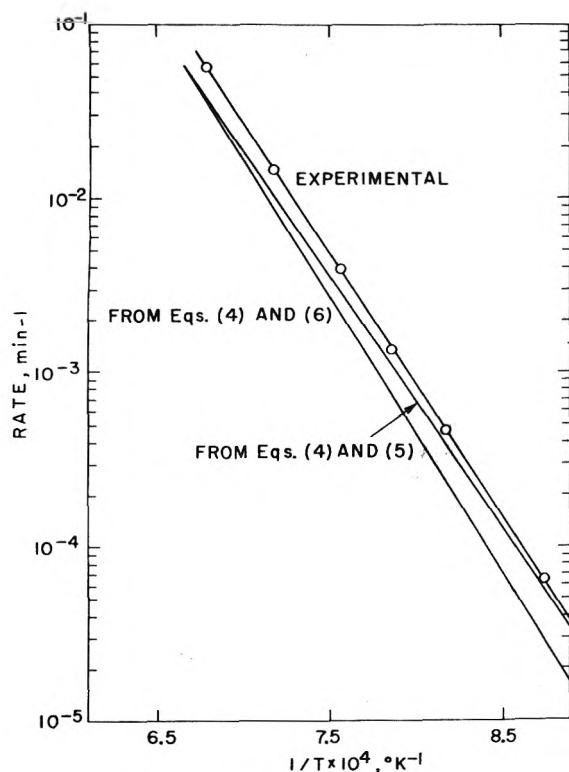
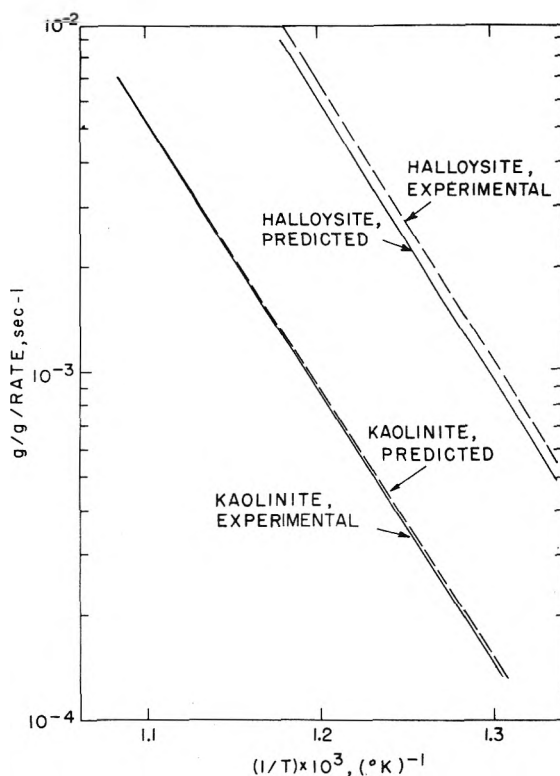
Figure 2. Arrhenius plot of C + CO₂.

Figure 3. Rates of dehydration of kaolinite and halloysite (from ref 3 and 4).

TABLE I: Kinetic Parameters for Some Reactions

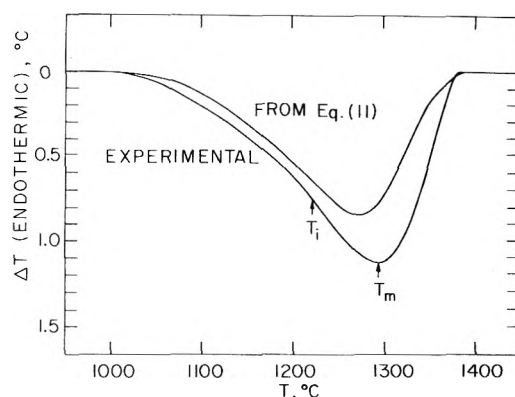
Reaction	Predicted from eq 4 and 6		Expt value		Source
	$E,^a$ kcal/ mol	$r_0, 1/s$	$E, kcal/mol$	$r_0, 1/s$	
C + CO ₂ → 2CO	72	3.25×10^7	71.16	3.32×10^7	This work
Dehydration of Georgia kaolinite	35	1.23×10^6	34.97	1.29×10^6	3, 4
Dehydration of Eureka halloysite	36	2.05×10^7	35.85	1.66×10^7	3, 4

^a Two significant figures are derived by considering the error limits of T_m and T_i of ± 0.5 °C.

thermal effect could be detected promptly. Platinum and platinum-10% rhodium thermocouples were used.

In a typical rate measurement, between 10 and 20 mg of graphite was used. The sample particles were spread into a layer of one to two particles thick on a flat disk sample holder made of alumina or platinum. The thermocouple joint was, in this case, underneath the disk and was in contact with its surface. The sample was heated to the desired reaction temperature in a stream of argon at a rate of 10 °C/min. The purified CO₂ was then introduced and reaction rates were calculated from the DTG curve (time derivative of the weight).

Reaction rates of nuclear graphite + CO₂ were measured at six temperatures ranging from 870 to 1200 °C. No difference was observed between the rates obtained with the

Figure 4. DTA curves of nuclear graphite in CO₂ (10 °C/min heating rate).

platinum and the alumina holders. The rate was plotted against burn-off of carbon and shown in Figure 1. As seen in this figure, the rate was quite constant throughout the reaction. One is then justified in assuming that the reaction is approximately "first order". An Arrhenius-type plot of the rates at 20% burn-off (Figure 2) shows that the reaction was within the chemical controlled region and diffusional effects were negligible.¹⁴ Also from Figure 2, the following values were calculated for the kinetic parameters: $r_0 = 3.32 \times 10^7 \text{ s}^{-1}$ and $E = 71.16 \text{ kcal/mol}$.

The DTA curve of nuclear graphite in CO₂ was measured at a heating rate of 10 °C/min and is shown in Figure 4. The temperature scale was enlarged by using fast chart speed so that more accurate readings of T_i 's and T_m could be obtained. The temperatures were 1221, 1293, and 1343 °C for T_{i1} , T_m , and T_{i2} , respectively.

Comparisons of Experimental Results with Theories

Equations 4 and 6 (or eq 4 and 5) are used to calculate the activation energy and frequency factor from a single DTA curve, based on our data on the C + CO₂ reaction and the well-known dehydration data of kaolinite and halloysite obtained from the literature. The examples were chosen because they are "first order" and they differ in a wide range of activation energies. Table I gives the comparison of the values of the two kinetic parameters calculated from eq 4 and 6 and the experimental data for the above reactions.

The peak and inflection temperatures of the reactions are: $T_{i1} = 1221$ °C and $T_m = 1293$ °C for C + CO₂ reaction; $T_{i1} = 555$ °C and $T_m = 600$ °C for kaolinite dehydration; $T_{i1} = 496$ °C and $T_m = 533$ °C for halloysite dehydration. The heating rate was 6°C/min for the two latter cases.

It should be noted that the values calculated from eq 4 and 6 are approximate. The cumbersome eq 4 and 5 would give exact solutions. A comparison was made in this respect for the C + CO₂ reaction. By using eq 4 and 5 the following values were obtained: $E = 66$ kcal/mol and $r_0 = 4.11 \times 10^6$ s⁻¹. The predicted rates calculated from the predicted E 's and r_0 's are also shown in Figure 2. These predicted values are lower than the experimental data determined isothermally. It is because the temperatures measured (T_i and T_m) were the reference temperatures and during the reaction, the sample temperature was lower than the reference and the heating rate was also lower before the peak temperature. Consequently, the kinetic parameters calculated are lower than the values determined isothermally. Correction in the calculations cannot be made at this point because the heating rate of the sample during the reaction is not a constant, being smaller than the reference heating rate before the peak temperature and greater after the peak. However, by reducing the peak height experimentally, closer values can be obtained.

Figure 3 gives the comparisons between the predicted rates from DTA and the experimental rates determined isothermally for kaolinite and halloysite. The results are surprisingly satisfactory considering the complexities involved in DTA. The lower rates predicted for halloysite can be again attributed to the lower temperature in the sample during the endothermic reaction.

To predict a DTA curve from the kinetic parameters, the reaction C + CO₂ is used as an example. From the isothermal TG data we obtained: $E = 71.16$ kcal/mol and $r_0 = 3.32 \times 10^7$ s⁻¹. The value of T_0 is chosen, with the knowledge of E and r_0 , to be 1500 K where the rate is appreciable. As discussed previously, the approximation in eq 9 is good as long as $\delta T/T_0$ is small. The initial mass of carbon m_0 was 20 mg. Substituting the above values into eq 11, we obtain

$$\Delta T = 6.64 \times 10^5 k_1 \exp \left[- \frac{35\,812.8}{T} - 2.2893 \times 10^{-11} e^{0.015\,92T} + 2.2893 \times 10^{-11} \right]$$

Here k_1 can be approximated as the heat of reaction divided by the total heat capacity of the sample; both change slightly with temperature. Now ΔT can be calculated as a function of T and is plotted in Figure 4. The DTA curve predicted in this fashion gives lower values of the ΔT than the experimental curve. This discrepancy indicates that heat transport is not fast enough and the thermal effect is partially accumulated.

In summary, from a single DTA curve, eq 4 and 6 can be used to estimate the two important parameters, namely, activation energy and frequency factor. Knowing the two kinetic parameters, eq 11 can be used to predict the DTA curve. Some examples are given in this work of such applications. Comparisons of predictions by the simple models with the experimental data are considered satisfactory in view of the complexities involved in DTA.

In general, the rates predicted from DTA are lower for the endothermic reactions and are higher for the exothermic reactions. This is because both the temperature and the heating rate are measured and controlled for the reference in all the commercial instruments. The DTA curve predicted by eq 11 gives somewhat smaller temperature differential than the experimental value because the heat transfer rate is not rapid enough and the thermal effects are partially accumulated.

Acknowledgments. Discussions with Drs. G. Adler and C. R. Krishna of Brookhaven National Laboratory were most helpful. Mr. R. Smol is acknowledged for his able technical assistance.

References and Notes

- (1) This work was performed under the auspices of the Office of Molecular Science, Division of Physical Research, U.S. Energy Research and Development Administration, Washington, D.C.
- (2) P. Murray and J. White, *Trans. Br. Ceram. Soc.*, **48**, 187 (1949); **54**, 137, 189, 204 (1955).
- (3) H. E. Kissinger, *J. Res. Natl. Bur. Stand.*, **57**, 217 (1956).
- (4) H. E. Kissinger, *Anal. Chem.*, **29**, 1702 (1957).
- (5) E. S. Freeman and B. Carroll, *J. Phys. Chem.*, **62**, 394 (1958).
- (6) G. O. Piloyan, I. D. Ryabchikov, and O. S. Novikova, *Nature (London)*, **212**, 1229 (1966).
- (7) J. Zsako, *J. Phys. Chem.*, **72**, 2406 (1968).
- (8) H. J. Borchardt and F. Daniels, *J. Am. Chem. Soc.*, **79**, 41 (1957).
- (9) A. A. Blumberg, *J. Phys. Chem.*, **63**, 1129 (1959).
- (10) H. J. Borchardt, *J. Am. Chem. Soc.*, **81**, 1529 (1959).
- (11) H. J. Borchardt, *J. Inorg. Nucl. Chem.*, **12**, 133 (1959); **12**, 252 (1960).
- (12) C. D. Doyle, *J. Appl. Polym. Sci.*, **15**, 285 (1961).
- (13) D. A. Frank-Kamenetskii, "Diffusion and Heat Transfer in Chemical Kinetics", 2nd ed, Plenum Press, New York, N.Y., 1969, Chapter VI.
- (14) P. L. Walker, Jr., F. Rusinko, Jr., L. G. Austin, *Adv. Catal.*, **11**, 133 (1959).

Fluorescence Quantum Yield Determinations. 9,10-Diphenylanthracene as a Reference Standard in Different Solvents

John V. Morris, Mary A. Mahaney, and J. Robert Huber*

Fachbereich Chemie, Universität Konstanz, D-775 Konstanz, Germany (Received August 29, 1975)

A controversy has arisen regarding the photophysical properties of 9,10-diphenylanthracene (DPA), a popular emission quantum yield standard. In order to elucidate the causes of the disagreement in the literature, fluorescence quantum yields, lifetimes, and oscillator strengths were measured for DPA in ethanol, 3-methylpentane, cyclohexane, and benzene solutions. The effects of high concentrations and self-absorption were dramatized by determining the measured lifetime for a series of concentrations of DPA in cyclohexane, demonstrating that the optical density in the 0-0 band must be kept below 0.05/cm in DPA to avoid reabsorption. It is proposed that these effects constitute a partial explanation for the discrepancies in the literature. In addition, the universal application in quantum yield measurements of the correction factor n_s^2/n_r^2 for differences between the index of refraction of the sample n_s and the reference n_r is questioned. By means of a variable slit arrangement, we have shown that the proper correction is a strong function of the geometry of the sample compartment. This effect suggests that wide utilization of the standard correction term may also provide a source of error. Taking these deficiencies into consideration the following fluorescence quantum yields and lifetimes of DPA at 293 K were determined: 0.95, 8.19 ns in ethanol; 0.93, 7.88 ns in 3-methylpentane; 0.86, 7.58 ns in cyclohexane; 0.82, 7.34 ns in benzene.

Introduction

Most emission quantum yield determinations found in the literature are relative measurements vs. a standard whose quantum efficiency has been accurately determined by absolute methods or is otherwise generally agreed upon. As a consequence of the difficult and time consuming nature of absolute methods, only a very small number of compounds have been investigated in this manner.^{1,2} The most popular of these substances for use as a standard is quinine bisulfate in aqueous 1.0 or 0.1 N H₂SO₄.^{3,4} Additionally, anthracene in ethanol is accepted as a standard because of the consistency of the results obtained by different authors.^{2,3,5} 9,10-Diphenylanthracene (DPA) has also been employed by several researchers,⁶⁻¹⁰ although it has several disadvantages with regard to its use as a fluorescence standard including a long lifetime (susceptibility to oxygen quenching), a large 0-0 band overlap (possibility of self-absorption), and a structured absorption spectrum. In spite of these drawbacks, its continued use is maintained largely due to its high quantum yield, the presence in the literature of values in a large number of solvents, and because it is one of the few emission standards available for work at 77 K. Unfortunately, a controversy has arisen between certain authors^{11,12} about the values themselves. In the time since the airing of this dispute in the literature, a pair of articles have appeared in an attempt to clear it up. Gusten and co-workers¹³ have compiled a large collection of literature values as well as presenting their own determinations. Birch and Imhof¹⁴ reported lifetimes of DPA in cyclohexane and benzene and observed that a solvent dependence is manifest in DPA which the disputants had not hitherto remarked upon. However, this difference was not sufficient to account for the discrepancies in the literature. These authors suggested high concentrations and resulting reabsorption as a possible explanation for the disparity.

The dramatic increase in apparent intensity which results from self-absorption with a solute such as DPA with both high fluorescence yield and strong overlap between ab-

sorption and emission has already been demonstrated by Melhuish.¹⁵ Still, some researchers prefer to work under conditions which allow all exciting light to be absorbed, obviating the necessity of correcting for differences in absorbance between sample and reference. Certain authors are under the impression that by observing front-face, they have eliminated any problem with reabsorption.¹² This is most definitely not the case, as Melhuish pointed out, stating that ca. 85% of the emission passes back into the solution where a part may be absorbed.¹⁵

The only additional major source of error involves the differences between the refractive index of the sample and reference solutions. Losses or amplifications, depending on the viewing geometry, in the observed intensity due to internal reflections are exacerbated as the index of refraction n increases. When comparing solutions with different refractive indices, very few authors account for the resultant differences in reflection errors. More important, however, is the correction for the spreading of the emission upon leaving the sample cell. The well-known n^2 factor has been recognized for a quarter century^{16,17} and is commonly used by most researchers, but many fail to report whether or not it has been applied. Moreover, some workers may have ignored the admonition by Hermans and Levinson¹⁷ to employ small slits when applying the n^2 correction term. Large slits and large viewing angles can lead to errors in the application of this factor, which might provide an explanation for some anomalies observed by Demas and Crosby.³ When these authors corrected quantum yield values found in the literature prior to the initial acceptance of the refractive index term, many of the results proved to be greater than unity. The possibility suggests itself that in these cases, the viewing geometry may not have been compatible with the n^2 correction factor.

We began this study in an attempt to determine the causes of the dispute as well as possibly settling it. To this end, we have measured the fluorescence quantum yields and lifetimes of DPA in the three main solvents in which literature values are reported (ethanol, cyclohexane, and

benzene) and in 3-methylpentane, because of the importance of this solvent in temperature dependent studies. In addition, the oscillator strengths were determined from the absorption spectra in each of these solvents to verify the correlation between the rate constants found from the ratio of quantum yields and lifetimes and those calculated from the oscillator strengths.

Experimental Section

Materials. Quinine bisulfate (Mallinckrodt Co.), anthracene (Merck, Schuchardt), and 9,10-diphenylanthracene (Aldrich) were purified by multiple recrystallizations (from water in the case of quinine bisulfate and from ethanol for anthracene and 9,10-diphenylanthracene). The melting points of these substances after purification were as follows: quinine bisulfate, 235 °C (lit. 235.2 °C¹⁸); anthracene, 216.2–216.4 °C (lit. 216.2 °C¹⁹); 9,10-diphenylanthracene, 250.6 °C (lit. 245–247 °C²⁰). Both benzene (Uvasol, fluorescence grade, Merck) and 3-methylpentane (purum, Fluka) contained traces of absorbing impurities. These were removed by frontal analysis chromatography employing a basic aluminum oxide column (activity level I, Merck).

Cyclohexane (Uvasol, fluorescence grade, Merck), absolute ethanol (analysis grade Merck), and aqueous 0.1 N H₂SO₄ (fluorescence grade, Merck) were used as received.

Apparatus and Techniques. A fully computerized spectrofluorimeter with a photon counting detection system which has been described elsewhere²¹ was utilized for most emission spectra; in addition, a series of measurements of DPA in ethanol has also been performed at Northeastern University with a system which has been previously described.²² A Cary 17 recording spectrometer was employed for all absorption measurements. The observed emission spectra were corrected for spectral response of the emission monochromator and photomultiplier. The sensitivity curve for this correction was derived by use of a 200-W standard tungsten-iodide lamp (ES-732, Eppley Laboratory, Newport, R.I.) which had been calibrated against U.S. National Bureau of Standards QM-111, QM-112, and EPI-1469 reference standards. The resulting correction function was checked by comparison of the spectra of several compounds with their published spectra.²³

The room temperature quantum yields of DPA were determined relative to fluorescent standards, with the possibility of correcting for differences between the refractive index of the reference n_r , and the sample solutions n_s using the expression

$$\phi_f(s) = \phi_f(r) \frac{\int I_s(\bar{\nu}) d\bar{\nu} D_r n_s^2}{\int I_r(\bar{\nu}) d\bar{\nu} D_s n_r^2} \quad (1)$$

Here the indices s and r , respectively, denote sample and reference. The integrals over I represent areas of the corrected emission spectra, and D is the optical density at the wavelength of excitation. Anthracene in ethanol ($\phi_f = 0.28$)^{3,5} and quinine bisulfate in aqueous 0.1 N H₂SO₄ ($\phi_f = 0.55$)^{3,4} were standards for DPA in ethanol. DPA in both benzene and 3-methylpentane was measured against DPA in ethanol using our value of 0.95 as well as against quinine bisulfate, whereas DPA in cyclohexane had only DPA in ethanol as a standard. Over 20 measurements were involved in determining each quantum yield. The excitation wavelengths (nm) employed in each case were 331.7, 343.8, 347.5, 358.8, 370.0 in ethanol; 357, 360, 370, 380 in 3-methylpentane; 342.5, 362.5, 364, 382 in cyclohexane; and 346.5, 363, 367.8, 368.3, 370, 372.5, 384 in benzene. The spectral

bandpass of the excitation monochromator was ~ 1 nm in each case. In order to minimize reabsorption effects, the solutions for both quantum yield and lifetime measurements were prepared such that the optical density was generally about 0.02 at the 0–0 band maximum, but was never higher than 0.05 for our 1-cm path length. Because it was deemed necessary to determine the effect on the quantum yield measurements of the slit geometry at the emission face of the sample cell, the sample holder shown in Figure 1 was employed for a separate series of experiments. To arrive at the results given in Table I, a very similar arrangement with fixed apertures of 5 mm width and 10 mm height on both excitation and emission faces of the cell holder was used in place of the central portion of the apparatus in Figure 1. In the experiments using the pictured sample holder, DPA in benzene, cyclohexane, and ethanol were compared with quinine bisulfate for a range of slit widths from 5 to 0.1 mm. This series of measurements was performed with the same wavelengths for all three solvents. The fluorescence lifetime measurements were carried out on an Ortec 9200 single-photon counting system equipped with an Ortec 462 time calibrator. Excitation was provided by a free-running air lamp and isolated by a bandpass filter (300–400 nm). The emission, after passing through a Spex 1670 Minimate focal length 220 mm, f/4 analyzing monochromator, was monitored by either an RCA 8850 photomultiplier tube or an RCA C31034 cooled photomultiplier tube. Samples for both lifetime and quantum yield measurements were normally deoxygenated by bubbling nitrogen through the solution for 20 min before being stoppered; this procedure was held to be sufficient after comparison with several degassed solutions. Lamp decay curves were determined by using a mixture of fluorescence-free glycerin (Merck) and aluminum oxide in a 2-cm quartz cell as a scatterer. This method of acquiring the lamp function $I(t)$ was found to fit the criteria for apparent optical density and optical path which must be met in order that the convoluted function²⁴

$$F'(t) = \int_0^t I(t-t')e^{-t'/\tau} dt' \quad (2)$$

yields a good fit when compared with the measured function $F(t)$. The goodness of fit was determined by minimizing the weighted sum of squares of residuals for the measured and calculated decay functions.²⁵

Oscillator strengths were obtained by integrating absorption spectra measured with a Cary 17 spectrometer, using a Hewlett-Packard 9820A calculator equipped with a 9864A digitizer unit. The short wavelength limit of integration was chosen as 310 nm for spectra in all four solvents.

Results

Quantum Yields. For reasons discussed below, we have presented the quantum yield results both with and without the correction for refractive index (n_s^2/n_r^2 ; cf. eq 1). The quantum yield values for DPA in the four different solvents are listed in Table I. When the correction is applied (parameters labeled with superscript n), the quantum yield of DPA appears to remain constant in different solvents. Although Gusten reports a quantum yield value of unity in cyclohexane, his room temperature values in both benzene ($\phi_f = 0.96$) and ethanol ($\phi_f = 0.94$) are in excellent agreement with ours.^{13,26} The quantum yield of 0.93 in 95% ethanol from the work of Lentz et al.²⁹ also agree quite well with our value. In addition, our ethanol result is consistent

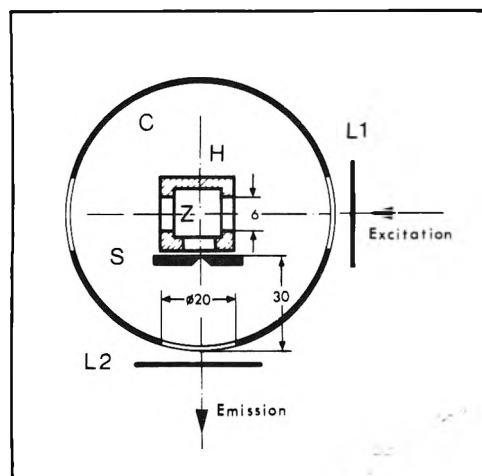


Figure 1. Cylindrical "can" C containing sample holder H with variable slit S on the emission face. Variable slit on excitation face (not shown here) was kept constant at 4 mm in these experiments. Sample cell (1 cm) is positioned at Z. Lenses L1 (focal length 76.1 mm) and L2 (focal length 63.4 mm) are each part of a two-lens collimating system between the excitation or emission monochromator slits and the sample holder.

TABLE I: Fluorescence Quantum Yields ϕ_f , Fluorescence Lifetimes τ_f , Oscillator Strengths f , and Radiative Rate Constants k_f^0 for 9,10-Diphenylanthracene in Solution at Room Temperature^a

	Ethanol	3-Methyl-pentane	Cyclo-hexane	Benzene
ϕ_f	0.95	0.93	0.86	0.82
τ_f , ns	8.19(7.95)	7.88(7.90)	7.58	7.34
f	0.175	0.178	0.176	0.175
k_f^0 , 10^8 s^{-1} ^b	1.16	1.18	1.13	1.12
$\phi_f^{(n)}$	0.95	0.95	0.95	0.96
$k_f^{0(n)}$, 10^8 s^{-1} ^b	1.16	1.21	1.25	1.30

^a Values in parentheses were determined at 77 K. Super-script n denotes application of the standard refractive index correction (eq 1). ^b $k_f^0 = \phi_f/\tau_f$.

with the triplet efficiency of 0.03 in ethanol published by Parker and Joyce³⁰ which they measured by delayed fluorescence. Aside from these quantum yields, the remaining values found in the literature tend to lie between two extremes, unity and ~ 0.8 . Several authors have reported fluorescence quantum yields of unity or greater for DPA in various solvents. Some of these higher quantum yields can be attributed to reabsorption effects. Bowen and Sahu used "concentrations necessary to give practically total light absorption";³¹ Berlman²³ reported using 0.32 g/l. (giving an optical density at the 0-0 band of ~ 12). Due to the lack of published information, the concentrations used by Eastman³² are unknown. Other researchers^{15,33,34} have observed lower quantum yields than ours, generally centering around 0.84. Given universal application of the refractive index correction, we have no explanation for this discrepancy.

If, however, the refractive index correction is neglected,

an interesting correlation appears (cf. Table I). The quantum yields determined in this manner parallel the behavior of the fluorescence lifetimes, yielding values for the radiative rate constant of fluorescence k_f^0 which are practically independent of solvent. Comparison of these quantum yields with those of Melhuish,¹⁵ Birks and Dyson,³³ and Medinger and Wilkinson³⁴ reveals a reasonable agreement among the values in benzene solution. The failure to correspond with the values given in ethanol is simply presented noting that some older values of the lifetime of DPA in ethanol are also too low.³⁵

Omission of the refractive index in the determination of quantum yields is justified only for an integrating sphere technique, although for some viewing geometries the correction factor may lie between 1 and n^2 .¹⁷ To ascertain the role played by differences between the index of refraction of the sample and of the reference in our measurements, the quantum yield determinations were repeated with the sample holder shown in Figure 1. In these experiments, the emission slit was varied from 5 to 0.1 mm as quinine bisulfate in aqueous 0.1 N H₂SO₄ and DPA in benzene were compared. As a result, a continuous dependence of the quantum yield of DPA upon slit width was found when the n^2 factor was universally applied, ranging from the 0.95 value for wide slits to 0.84 for 0.5-mm slits (cf. Table II). No further decrease was found for narrower slits. A similar effect was observed when DPA in cyclohexane was measured against quinine bisulfate, whereas no discernable dependence was found for DPA in ethanol.

Lifetimes. Our data presented in Table I and literature values of the fluorescence lifetime of DPA demonstrate a distinct solvent dependence which has been little noted to date. The data of Gusten and co-workers¹³ essentially agrees with our work, with the exception of benzene solution. In addition, we match the value in cyclohexane of Birch and Imhof¹⁴ but again we differ with their value for benzene. Our measured lifetime in benzene solution does agree quite well with the values of Ware and Baldwin³⁶ and of Birks and Dyson.³³ In contrast to this grouping of relatively consistent data, a few strongly divergent values are to be found. The long lifetime of Berlman²³ in cyclohexane and that of Amata et al.,³⁷ whom he quotes as support, can be explained on the basis of the high concentrations used and the resulting reabsorption effects.

Possible effects of water in the ethanol were investigated by adding distilled water dropwise to absolute ethanol solutions of DPA and measuring the lifetime after rebubbling with nitrogen. No significant difference was found for up to 10% water. Reabsorption effects resulting from high concentrations combined with high quantum yield are well known.¹⁵ To confirm and graphically demonstrate this effect, fluorescence lifetimes were determined for a series of concentrations in cyclohexane. These results are presented in Figure 2. This curve was not extended to the upper limit of total reabsorption found by Melhuish because of the difficulty encountered in dissolving the necessary quantities of DPA.

Oscillator Strengths. The oscillator strengths were derived by means of the relationship³⁸

$$f = 4.32 \times 10^{-9} \int \epsilon d\bar{\nu} \quad (3)$$

As these results are presented in Table I, they appear independent of solvent indicating a solvent independent radiative rate constant.

TABLE II: Variation in the Measured Quantum Yield of Fluorescence ϕ_f for 9,10-Diphenylanthracene in Benzene and Ethanol as Determined against Quinine Bisulfate in Aqueous 0.1 N H₂SO₄ as a Function of Emission Slit Width (cf. Figure 1) with Application of Refractive Index Correction (Eq 1)

Slit width, mm	ϕ_f (benzene)	ϕ_f (ethanol)
5	0.96	0.95
4	0.94	0.95
3	0.92	
2	0.90	
1	0.86	0.95
0.5	0.84	0.95
0.1	0.84	0.95

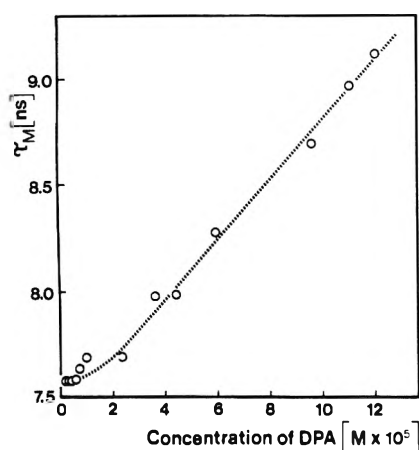


Figure 2. Measured lifetime τ_M , as determined by convolution (eq 2) with the lamp function, vs. concentration of DPA in cyclohexane.

Discussion

High concentrations and consequent reabsorption effects appear to account for at least some of the discrepancies in the literature, generally resulting in quantum yields which are too high and lifetimes which are too long. Of course, if the standard employed strongly reabsorbs, it is quite possible that quantum yields measured against it will be too low. Reabsorption and reemission can take place at concentrations much lower than 10^{-3} M, depending on the amount of overlap between absorption and emission. As has been noted above, Melhuish has previously treated this subject from the standpoint of the effect on quantum yields and has presented an integral expression for the intensity of fluorescence from a concentrated solution.¹⁵ Although portions of the expression are specific for his front-face viewing geometry, we have not attempted to rewrite these parts to fit our right-angle setup, since the description of the solid angle of observation will be individual to the instrument. However, the effect of reabsorption on the emission lifetime can be expressed independently of viewing geometry because the measurement is not based on absolute intensity. The observed decay curve for a single exponential in the absence of reabsorption may be expressed by the convolution integral²⁴

$$F(t) = \int_0^t I(t-t')e^{-t'/\tau} dt' \quad (4)$$

where $F(t)$ is the observed decay, $I(t)$ is the lamp function, and τ is the single-exponential decay time. When a portion

of this light is reabsorbed, the reemitted light will follow an exponential decay convoluted not with the lamp function, but with the first decay, thus

$$F'(t) = \int_0^t F(t-t')e^{-t'/\tau} dt \quad (5)$$

Subsequent reabsorption of this light will result in a function $F''(t)$ which is a convolution with $F'(t)$, and so forth. Each of these observed decay functions is additive, with the proper normalization factor for their relative intensities. The lamp intensity is the strongest, with a factor

$$L = \int_0^\infty \int_0^l I(\bar{\nu})(1 - e^{-2.3\epsilon(\bar{\nu})cz}) d\bar{\nu} dz \quad (6)$$

where $\epsilon(\bar{\nu})$ is the extinction coefficient as a function of wave number, c the concentration, l the path length in the z direction, and $I(\bar{\nu})$ is the frequency distribution of the excitation. Here we have neglected the cross sectional area of the exciting light, leaving only one dimension. This function is of course normalized such that $\int_0^\infty I(\bar{\nu}) d\bar{\nu} = 1$. The less intense reemission curves are multiplied by factors similar to Melhuish's K integrals¹⁵

$$A = \phi_f \int_0^\infty \int_V f(\bar{\nu})(1 - e^{-2.3\epsilon(\bar{\nu})c(r)}) dr d\bar{\nu} \quad (7)$$

where r indicates integration over all coordinates of the cell, and the fluorescence distribution function is normalized such that $\int_0^\infty f(\bar{\nu}) d\bar{\nu} = 1$. The observed decay function in the presence of reabsorption is consequently

$$F^*(t) = L F(t) + A F'(t) + A^2 F''(t) + \dots \quad (8)$$

This resultant functional form of the decay, when treated by normal deconvolution procedures or even a simple least-squares analysis, will yield a measured lifetime τ_M longer than the intrinsic fluorescence lifetime τ_f which would be found in the absence of reabsorption effects. Elimination of all reabsorption terms leaves only the simple convolution integral $F(t)$ times a constant, reducing τ_M to τ_f . Note that the viewing geometry of the detecting system does not enter this expression, since only the relative amounts of emission and reemission are important for the determination of the final decay function. The dimensions of the cell are the only geometrical factors necessary to define the amount of reabsorption. Given the difficulty of calculating the integrals involved in this formula and the expression of Melhuish, it is advised to keep the optical density of the 0-0 band below 0.05/cm for solutes which strongly self-absorb.

It appears that another possible source of error in quantum yield determinations lies in too broad an application of the standard n^2 correction term for the index of refraction (cf. eq 1). Hermans and Levinson derived this factor with the admonition that it was appropriate for systems of small slits.¹⁷ For example, these authors determined a relative error of 8% arising from a system of two slits between the sample and detector where the angle δ in the horizontal plane viewed by the detector is 0.1 radians, considered typical for their instrument. This approximation is of course reasonable only when $\sin \delta \sim \delta$. If one considers the "can" illustrated in Figure 1 as the limiting optics of the instrument, one finds δ to be beyond the range of this approximation, which probably indicates a large error in the refractive index correction. The results of varying the emission slit seem to confirm that errors can result from larger slit widths. The probability that these results are simply an ar-

tifact is reduced by the fact that, although a decrease is observed with narrower slit width for both benzene and cyclohexane, no measurable effect is observed for ethanol, which has an index of refraction very similar to that of the standard solution. This finding would seem to indicate that the dependence on slit width is a function of solvent. This dependence suggests that the normal correction for the difference in refractive index between the sample and the reference is best applied when the emission approximates a point source. As the slits are widened, the viewing geometry approaches a sphere, with a consequent decrease in the proper refractive index correction factor from n^2 to 1. The possibility that this effect can manifest itself at much smaller slit widths than is commonly thought (5 mm and smaller) may provide one explanation for the wide range of quantum yield values found in the literature. Since nearly all determinations are performed with guanine bisulfate in either aqueous 1.0 or 0.1 N H₂SO₄ or anthracene in ethanol as a standard, measurements made in solvents with refractive indices much different from 1.35 such as benzene and cyclohexane can be expected to show peculiarities of viewing geometry. It is therefore important that the individual system be tested to ascertain the true dependence upon index of refraction for its limiting optics.

Accepting the universal application of the n^2 form of the refractive index correction term, one is forced to explain the occurrence of solvent independence of the quantum yield together with solvent dependence of the fluorescence lifetime. As observed in Table I, this would indicate that the radiative rate constant k_f^0 would be a function of the solvent medium. If an actual dependence exists, it should also be reflected in the oscillator strengths. Immediately we find ourselves confronted with yet another question involving the index of refraction. Although throughout much of the literature³⁸ any factor involving the refractive index n in the oscillator strength calculation is neglected, a large number of possibilities for such a correction for the solvent medium exist in the literature. The more common ones range from the $1/n$ factor of Birks,³⁹ derived from the slowdown of light upon passage through condensed media, to the direct proportionality of Mataga and Kubota,⁴⁰ based on the formulations of Förster⁴¹ for the transition probabilities. However, Förster's expression for the oscillator strength does not involve refractive index. Berlman⁴² also presents a factor of n in his expression for f , but his constant is a factor of 3 larger than the accepted one. No explanation is given for this difference. Scheibe and co-workers⁴³ have extracted an interesting refractive index correction term from the work of Onsager⁴⁴ on electric dipole moments. They have applied their correction factor of $n\{(2n^2 + 1)/3n^2\}^2$ (which might be approximated as $\sim 0.7n$ for the solvents used here) to oscillator strengths on the basis that the electric transition dipole is acted upon in a manner similar to a static dipole. A correction factor which has been quoted by several authors is the Lorentz-Lorenz term derived by Chako⁴⁵ in the form $9/(n^2 + 2)^2$. This expression is often found in the literature as $9n/(n^2 + 2)^2$.^{46,47} However, Chako compared this factor and others by means of experimentally measured quantities and found that it alone could not account for solvent dependences, and that there was not enough variation to decide among the possibilities. Also, Bayliss and Hulme,⁴⁸ in their study of solvent shifts in the absorption spectra of benzene and its derivatives, found no effect of solvent upon the oscillator strength except for highly interactive solvents such as the chlorinat-

ed methanes. Though theoretical justifications for considering the index of refraction in the oscillator strength calculation can be advanced, the resulting correction factor depends on the model used. The possibility that more than one of these models may be valid, and that the resulting correction terms could cancel each other out, must be considered. Nevertheless, the experimental findings indicate that this correction is quite small. We have thus neglected any factor involving n in the f values shown in Table I. The solvent independence of the oscillator strengths would favor the corollary solvent independence of the radiative rate constants k_f^0 . This statement in turn supports the contention that the quantum yield of fluorescence should follow the lifetime in its behavior upon change of medium. Because of the greater number of experimental errors intrinsic to quantum yield measurements, and because the agreement in the literature is more widespread for the lifetimes, we tend to favor the latter quantities among our data. A constant k_f^0 in conjunction with a solvent dependent ϕ_f and τ_f requires that a nonradiative channel be enhanced in DPA by the solvent medium. It can be recognized from the red shift (~ 500 cm⁻¹) in the absorption spectrum of DPA in benzene relative to the other three solvents that there is slight alteration of the electronic wavefunctions of the ground state, the first excited state, or both. What role this change might play in stimulating a radiationless channel is not obvious. It is known that intersystem crossing is the only significant deactivation other than fluorescence in the singlet manifold of large aromatic hydrocarbons.³⁴ There does appear to be some solvent dependence of the triplet yield, as indicated by the value of 0.03 in ethanol of Parker and Joyce,³⁰ and the value of 0.12 in liquid paraffin found by Medinger and Wilkinson.³⁴ The shifts observed in the singlet absorption spectrum can result in a stronger interaction with an intermediate triplet state. In the work of Kearvell and Wilkinson on substituted anthracenes, although the k_f^0 values given were slightly solvent dependent (see above), the bulk of the solvent and temperature dependence lay in the intersystem crossing rate constant k_{ISC} .⁴⁹ Considering this fact, a small shift in electronic energy levels due to the solvent medium will certainly have a greater effect on the intersystem crossing process involving a narrow energy gap than on a radiative channel covering well over 20 000 cm⁻¹, particularly since the upper states are well separated from the lowest excited singlet. Thus we conclude that k_f^0 should be solvent independent, and so the quantum yield values should follow the behavior of the fluorescence lifetimes. Bearing this in mind, we are inclined to believe that the values of ϕ_f presented in Table I without the superscript n represent the true quantum yields of DPA in the various solvents.

The controversy^{11,12} about the photophysical properties of DPA appears to have arisen partly from the failure to recognize the solvent dependence, and partly from the use of high concentrations by certain authors. In addition, many researchers may be introducing errors into their data through their failure to recognize that the correction for differences in index of refraction between sample and reference may deviate from n^2 (cf. eq 1). In order to correctly apply this factor, the angle δ viewed by the detector (see above) must be kept small. It is obvious that with sufficiently small slit widths the sample will appear to the detector as a point source, allowing the n^2 term to be used in accordance with Snell's law. Whether complete neglect of this correction factor is permitted for systems of larger slit

short of a complete integrating sphere is not entirely clear and demands further study.

Acknowledgments. Support of this work by the Deutsche Forschungsgemeinschaft and the Verband der Chemischen Industrie is greatly appreciated. Many thanks are due to Mr. Friedrich Oberhage for performing some of the fluorescence lifetime measurements. We also thank Dr. Jochen Haink and Mr. Rodolfo Barreca for their assistance with the spectrofluorimeter.

References and Notes

- (1) E. H. Gilmore, G. E. Gibson, and D. S. McClure, *J. Chem. Phys.*, **20**, 829 (1952); **23**, 399 (1955).
- (2) G. Weber and F. W. J. Teale *Trans. Faraday Soc.*, **54**, 640 (1958).
- (3) J. N. Demas and G. A. Crosby, *J. Phys. Chem.*, **75**, 991 (1971).
- (4) B. Gelernt, A. Findeisen, A. Stein, and J. A. Poole, *J. Chem. Soc., Faraday Trans. 2*, **70**, 939 (1974).
- (5) W. R. Ware and B. A. Baldwin, *J. Chem. Phys.*, **43**, 1194 (1965).
- (6) E. C. Lim and J. Stanislaus, *J. Chem. Phys.*, **53**, 2096 (1970).
- (7) F. Hirayama and S. Lipsky, *J. Chem. Phys.*, **62**, 576 (1975).
- (8) R. Rusakowicz and A. C. Testa, *J. Phys. Chem.*, **72**, 793 (1968).
- (9) A. Greenberg, M. Furst, and H. Kallmann, International Symposium on Luminescence, K. Thiemig, München, 1966, p 71.
- (10) C. A. Heller, R. A. Henry, B. A. McLaughlin, and D. E. Bliss, *J. Chem. Eng. Data*, **19**, 214 (1974).
- (11) J. B. Birks, *Chem. Phys. Lett.*, **17**, 370 (1972).
- (12) I. B. Berlman, *Chem. Phys. Lett.*, **21**, 344 (1973).
- (13) G. Heinrich, S. Schoof, and H. Gusten, *J. Photochem.*, **3**, 315 (1974).
- (14) D. J. S. Birch and R. E. Imhof, *Chem. Phys. Lett.*, **32**, 56 (1975).
- (15) W. H. Melhuish, *J. Phys. Chem.*, **65**, 229 (1961).
- (16) Th. Förster, "Fluoreszenz Organischer Verbindungen", Vanderhoeck und Ruprecht, Göttingen, 1951, p 35f.
- (17) J. J. Hermans and S. Levinson, *J. Opt. Soc. Am.*, **41**, 460 (1951).
- (18) "Handbook of Chemistry and Physics", R. C. West, Ed., 53rd ed, Chemical Rubber Co., Cleveland, Ohio, 1972.
- (19) R. H. Müller and S. T. Zenchelsky, *Anal. Chem.*, **24**, 844 (1952).
- (20) C. K. Bradsher and E. S. Smith, *J. Am. Chem. Soc.*, **65**, 451 (1943).
- (21) H. J. Haink and J. R. Huber, to be published; J. V. Morris, U. Brühlmann, O. Serafimov, and J. R. Huber, *Ber. Bunsenges Phys. Chem.*, **78**, 1348 (1974).
- (22) H. J. Pownall and J. R. Huber, *J. Am. Chem. Soc.*, **93**, 6429 (1971).
- (23) I. B. Berlman, "Handbook of Fluorescence Spectra of Aromatic Molecules", 2nd ed, Academic Press, New York, N.Y., 1971.
- (24) A. E. W. Knight and B. K. Selinger, *Spectrochim. Acta, Part A*, **27**, 1223 (1971).
- (25) C. Lewis, W. R. Ware, L. J. Doemeny, and T. L. Nemzek, *Rev. Sci. Instrum.*, **44**, 107 (1973).
- (26) To avoid further misunderstanding, we reiterate our statement that the value of unity mentioned by Mantulin and Huber²⁷ was simply an estimate. Moreover, in the absence of oxygen, the ϕ_f of DPA shows no temperature dependence in either ethanol or EPA,²⁸ contrary to implications found in ref 13, although we have found a slight decrease of the τ_1 of DPA in ethanol in going to 77 K from room temperature.
- (27) W. W. Mantulin and J. R. Huber, *Photochem. Photobiol.*, **17**, 139 (1973).
- (28) J. R. Huber, M. A. Mahaney, and W. W. Mantulin, *J. Photochem.*, **2**, 67 (1973).
- (29) P. Lentz, H. Blume, and D. Schulte-Frohlinde, *Ber. Bunsenges. Phys. Chem.*, **74**, 484 (1970).
- (30) C. A. Parker and T. A. Joyce, *Chem. Commun.*, 744 (1967).
- (31) E. J. Bowen and J. Sahu, *J. Phys. Chem.*, **63**, 4 (1959).
- (32) J. W. Eastman, *Spectrochim. Acta, Part A*, **26**, 1545 (1970).
- (33) J. B. Birks and D. J. Dyson, *Proc. R. Soc. London, Ser. A*, **275**, 135 (1963).
- (34) T. Medinger and F. Wilkinson, *Trans. Faraday Soc.*, **61**, 620 (1965).
- (35) There exist many more fluorescence quantum yields for DPA in the literature (cf. ref 13), but we have considered here only those values for which the experimental conditions were given in sufficient detail for discussion.
- (36) W. R. Ware and B. A. Baldwin, *J. Chem. Phys.*, **40**, 1703 (1964).
- (37) C. D. Amata, M. Burton, W. P. Helman, P. K. Ludwig, and S. A. Rodemeyer, *J. Chem. Phys.*, **48**, 2374 (1968).
- (38) See, for example, R. S. Becker, "Theory and Interpretation of Fluorescence and Phosphorescence", Wiley-Interscience, New York, N.Y., 1969, p 29; S. P. McGlynn, T. Azumi, and M. Kinoshita, "Molecular Spectroscopy of the Triplet State", Prentice-Hall, Englewood Cliffs, N.J., 1969, p 17; H. H. Jaffé and M. Orchin, "Theory and Applications of Ultraviolet Spectroscopy", Wiley, New York, N.Y., 1962, p 115; and although different by a factor of 10^4 , C. A. Parker, "Photoluminescence of Solutions", Elsevier, Amsterdam, 1968, p 27.
- (39) J. B. Birks, "Photophysics of Aromatic Molecules", Wiley-Interscience, London, 1970, p 48ff.
- (40) N. Mataga and T. Kubota, "Molecular Interactions and Electronic Spectra", Marcel Dekker, New York, N.Y., 1970, p 114.
- (41) Reference 16, p 67f.
- (42) Reference 23, 1st ed, p 217. No dependence of f on n is given in the 2nd edition.
- (43) G. Scheibe, H. J. Friedrich, and G. Hohlneicher, *Angew. Chem.*, **73**, 383 (1961).
- (44) L. Onsager, *J. Am. Chem. Soc.*, **58**, 1486 (1936).
- (45) N. Q. Chako, *J. Chem. Phys.*, **2**, 644 (1934).
- (46) H. Suzuki, "Electronic Absorption Spectra and Geometry of Organic Molecules", Academic Press, New York, N.Y., 1967, p 100.
- (47) J. G. Calvert and J. N. Pitts, Jr., "Photochemistry", Wiley, New York, N.Y., 1966, p 172.
- (48) N. S. Bayliss and L. Hulme, *Austr. J. Chem.*, **6**, 257 (1953).
- (49) A. Kearvell and F. Wilkinson, *J. Chim. Phys.*, 125 (1970).

Inter- and Intramolecular Quenching of Indole Fluorescence by Carbonyl Compounds

Robert W. Ricci* and Joseph M. Nesta

Department of Chemistry, College of the Holy Cross, Worcester, Massachusetts 01610 (Received October 20, 1975)

Indole fluorescence was found to be quenched by a variety of carbonyl compounds. In the case of carboxylic acids the quenching rates were proportional to the K_a of the acid. The acid proton was not essential for quenching, however, as the ester derivatives were found to retain their quenching ability to a great degree. Quenching is interpreted as resulting through formation of an excited state charge-transfer complex in which the photoexcited indole acts as the donor. A simple molecular orbital scheme is presented which correlates these results with complimentary studies in which carbonyl fluorescence is quenched by aromatics and other π -electron systems. Intramolecular quenching by indole-3-carboxylic acids may take place through a complex stabilized by a σ interaction between photoexcited indole and the carbonyl carbon.

Introduction

The fluorescence yield of the indole ring system is sensitive to additives in solution as well as to groups attached to the ring itself.¹ The hydronium ion is an excellent quencher^{1a}

as are other potential proton-donating groups, particularly the $-\text{NH}_3^+$ moiety when attached to the ring as in the case of tryptophan.² In addition, studies have revealed the importance of the carboxyl group as a quenching center of indole fluorescence.³ Several mechanisms have been sug-

gested to explain the quenching process; they include transfer of an electron from the excited indole to the quencher and quenching by proton donation to the excited indole ring in the case of those quenchers which are potential proton donors.

The purpose of this paper is to report the finding of a correlation between the kinetics of indole fluorescence quenching by carbonyl compounds and their molecular structure. This leads us to believe that quenching occurs primarily through a charge-transfer mechanism though a σ complex may be important in the case of intramolecular quenching through attached carboxyl groups.

Experimental Section

The apparatus used to measure the fluorescence has been described previously.¹¹ All fluorescence yields were determined by the method of Parker and Rees⁴ using corrected fluorescence curves.⁵ Ultraviolet absorption curves were run on all quenchers to ensure that they were transparent at the wavelength of indole excitation. The indole samples were purified through sublimation. Deuterium oxide (99.8%) was purchased from Thompson-Packard Co. No attempt was made to remove dissolved oxygen from the aqueous solutions as its effect on the fluorescence lifetime of indole is known to be negligible under the conditions of these experiments.⁶ pH measurements were made on a Corning Model 10 pH meter. It was assumed that in D₂O the pH accurately measured the concentration of D₃O⁺. All indole samples were irradiated at 280 nm and the fluorescence was measured at 340 nm. Indole fluorescence quenching constants for hydronium ion varied by less than 5% when the indole sample was excited at wavelengths between 224 and 300 nm. The temperature of the indole samples was maintained at 23 °C unless otherwise stated. All quenching constants are reproducible to within 1% and the fluorescence yields within 5%.

Results and Discussion

The quenching of indole fluorescence by carbonyl compounds was analyzed using the Stern-Volmer (SV) equation in the form

$$(Q^0_f/Q_f - 1) = \sum [K_{sv}]_n [M]_n \quad (1)$$

where Q^0_f and Q_f represent the fluorescence yield of indole in the absence and in the presence of quencher, respectively. The n 's refer to the several quenching agents which may be in solution and the $[K_{sv}]_n$'s are their respective SV quenching constants. $[M]_n$ refers to the molar concentration of the quenchers. This approach is necessary when studying quenching by weak acids where appreciable quantities of hydronium ion and anion are present in equilibrium with the acid. In our case the SV equation takes on the particular form

$$(Q^0_f/Q_f - 1) = (K_{sv})_{H_3O^+} [H_3O^+] + (K_{sv})_{HA} [HA] + (K_{sv})_{A^-} [A^-] \quad (2)$$

The right-hand side of eq 2 contains three constants and three concentration terms. The latter can be determined from a knowledge of the stoichiometric concentration of the acid together with the measured pH and the pK_a of the acid. At a pH ≈ 7.0 the first two right-hand terms of eq 2 are negligible and $(K_{sv})_{A^-}$ can be determined from the slope of a $(Q^0_f/Q_f - 1)$ vs. $[A^-]$ plot. Further, the value of

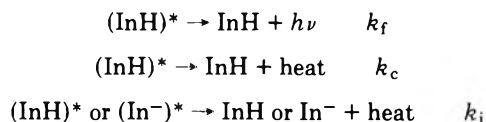
$(K_{sv})_{H_3O^+}$ can be determined independently by measuring the quenching effect of hydrochloric acid, a strong acid, in which case the second and third right-hand terms of eq 2 are negligible. Having determined the values of $(K_{sv})_{H_3O^+}$ and $(K_{sv})_{A^-}$ in this way, eq 2 can be used directly to obtain $(K_{sv})_{HA}$.

The SV constants are converted into kinetic, second-order, quenching rate constants (k_q) through division by τ , the fluorescence lifetime of indole in the absence of quencher. Quenching rate constants for several acids, anions, esters, amides, and acetone are listed in columns 2-5 of Table I. Some of the quenching data was obtained in a deuterium oxide solvent and is so indicated in column 1.

Using a technique described in ref 11 the quenching rate constants were found to increase with increasing temperature and conformed to the Arrhenius equation between 5 and 45 °C, the temperature range studied. The results can be seen in Figure 1 which is an Arrhenius plot for quenching by (a) H₃O⁺, (b) cyanoacetic, and (c) acetic acid. The numerical values in the graph represent the activation energies (E_a) in cal mol⁻¹.

Intramolecular fluorescence quenching of photoexcited indole has been reported,⁷ and we have included in our study three examples of intramolecular fluorescence quenching through attached carboxylic acid residues. The pH profile of the fluorescence yield of three indole-3-carboxylic acids which differ only in the length of the aliphatic side chains linking the carboxylic acid group to the indole ring are shown in Figure 2. The precipitous decrease in fluorescence yield between pH 6 and 4 parallels the titration curve of the carboxylic acids, suggesting that in this pH range the decreasing fluorescence yield reflect the appearance of a new nonradiative deactivation pathway associated with the protonated acid side chain.

A molecular interpretation of these results can be obtained from the following reaction scheme:



where (InH)* represents the photoexcited indole-3-carboxylic acid and (In⁻)* the corresponding anion. The rate constants have the following meaning: k_f , the rate constant for fluorescence; k_c , the rate constant for the nonradiative decay pathway due to the presence of the protonated side chain; and k_i , the rate constant for all other nonradiative decay paths from the excited singlet of indole. Between a pH of about 7 and 9 the fluorescence yield of Q_f is defined as $k_f/(k_f + k_i)$ while at pH 3 it will have the value $k_f/(k_f + k_i + k_c)$. With these two equations and the reasonable assumption that k_f is the same for all three acids and equal to $4.5 \times 10^7 \text{ s}^{-1}$ ¹¹ the data in Table II were assembled. For comparison, data on 3-methylindole are also included. The fluorescence yield ($Q_f = 0.34$) of this compound is independent of pH over the acid range studied and its value is represented in Figure 2 as the dotted line. Fluorescence yield for the acids were also obtained in D₂O and these data have been included in Table II. In the last column of Table II is the ratio of phosphorescence yield to fluorescence yield obtained at 77 K for the three acids.

Weber and Rosenheck⁸ have studied the quenching effect of carboxylic acids on the fluorescence of phenol and concluded that the process was occurring through the formation of a ground-state nonfluorescent complex. On the

TABLE I: Quenching of Indole Fluorescence^a

Quenching agent	$10^{-9} k_q, M^{-1} s^{-1}$				Bronsted catalysis plot		
	Acid	Anion	Ester	Amide	$\log k_q$	$\log K_a$	$\log K_e$
a. Acetic	0.40	<0.01	0.27	<0.01	8.60	-4.45	-1.34
Acetic (D ₂ O)	0.40						
b. Butyric	0.50	<0.01			8.70	-4.50	-1.24
c. Citric	1.7				9.23	-2.78	-0.64
Citric (D ₂ O)	1.7						
d. Chloroacetic	5.2	1.3			9.72	-2.54	0.12
Chloroacetic (D ₂ O)	7.8						
e. 2-Chloropropionic	5.8	1.4			9.76	-2.53	0.24
f. 3-Chloropropionic	2.4	1.2			9.38	-3.68	-0.45
g. Cyanoacetic	2.8	0.065	2.1 ^b		9.44	-2.15	-0.35
Cyanoacetic (D ₂ O)	2.3						
h. Dichloroacetic	8.1	6.5			9.91	-1.18	0.91
i. Formic	1.6	<0.01	0.84		9.20	-3.45	-0.61
Formic (D ₂ O)	1.8						
j. Glycolic	0.94	<0.01			8.97	-3.53	-0.94
Glycolic (D ₂ O)	0.82						
k. H ₃ O ⁺	10.0				10.0	1.27	
D ₃ O ⁺	7.5						
l. Propionic	0.49	<0.01			8.69	-4.57	-1.24
m. Sodium citrate	0.45				8.65	-4.44	-1.28
Trichloroacetic ^c		6.3					
Urea				0.01			
Acetone	10.0						

^a All measurements were taken at 23 °C and the solvent is water except where D₂O is indicated. The fluorescence lifetime of indole in the absence of quencher in H₂O is 4.9×10^{-9} s and in D₂O it is 6.5×10^{-9} s.¹¹ All pK_a values for the acids are from "Handbook of Chemistry and Physics", 51st ed, The Chemical Rubber Company, Cleveland, Ohio. All esters are the ethyl derivatives except in the case of methylformate. ^b Solvent is 50% H₂O-50% methanol. ^c Large K_a of this acid made it impossible to measure its k_q.

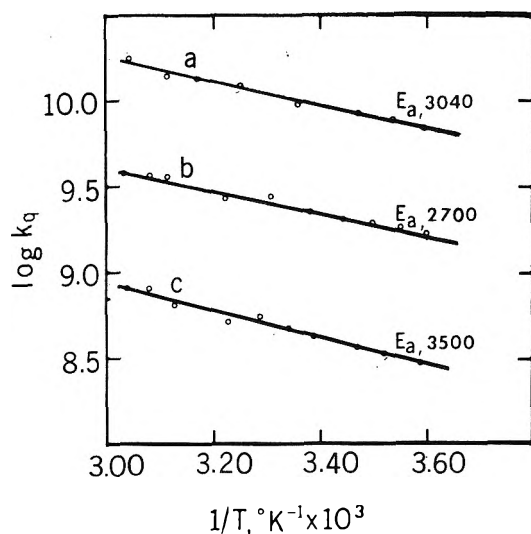


Figure 1. Arrhenius plot for the quenching of indole fluorescence: (a) hydronium ion, (b) cyanoacetic acid, (c) acetic acid. Values in graph refer to the activation energies in cal mol⁻¹.

other hand, we feel fluorescence quenching of indole by acids and other carbonyl containing compounds is primarily dynamic in nature and base this conclusion on the following facts. DeLauder and Wahl,⁹ utilizing fluorescent lifetime techniques, showed unequivocally that hydronium ion quenched indole ring fluorescence through a dynamic mechanism. Using the same technique, Steiner and Kirby found that the amino acids cysteine and lysine also quench the indole ring system dynamically.¹⁶ In Figure 1 we show

an Arrhenius plot of the quenching constant for hydronium ion together with acetic and cyanoacetic acids. The similarity in activation energy between hydronium ion, the known dynamic quencher, and the two carboxylic acids suggests a similar mechanism in the case of the acids. In fact, the range of activation energies encountered are characteristic of diffusion-controlled processes. Lastly, the uv absorption spectra of the indole quencher mixtures were, within experimental error, the sum of the indole and quencher uv absorption spectrum measured separately, indicating no appreciable ground-state interaction between the two species. Our findings, combined with the cited evidence, strongly support the hypothesis of a dynamic mechanism in the case of the quenchers under study.

Bronsted has pointed out that in the case of general-acid-catalyzed processes the reaction rate constant is often related to the ionization constant of the catalyzing acid in a linear fashion.^{10,11} In Figure 3 is shown the results of a plot of $\log k_q$ vs. $\log K_a$ for the quenching of indole fluorescence by weak carboxylic acids. The nonhalogenated acid points fall on a good straight line with the exception of formic acid and H₃O⁺. The negative deviation in the latter case is probably due to the fact that the quenching rate constant has reached a diffusion-controlled limiting value. As a group, the four chlorinated acids are better quenchers than their K_a's would have suggested, nor do they fall on a straight line when plotted but rather form the smooth curve in Figure 3 which appears to level off at a rate controlled by the diffusion of the species involved. The dotted line in Figure 3 represents a diffusion-controlled limiting value of $9.1 \times 10^9 M^{-1} s^{-1}$, a reasonable value for small uncharged molecules in H₂O at 23 °C.¹² A linear Bronsted re-

TABLE II: Intramolecular Quenching of Indole Fluorescence^a

Compound	$10^{-7} k_i, s^{-1}$			$10^{-7} k_c, s^{-1}$			Q_p/Q_f
	H ₂ O	D ₂ O	$k_{i(H_2O)}/k_{i(D_2O)}$	H ₂ O	D ₂ O	$k_{c(H_2O)}/k_{c(D_2O)}$	
Indole-3-acetic acid	8.4	4.7	1.8	12	11	1.09	0.31
Indole-3-propionic acid	7.7	4.3	1.8	47	41	1.15	0.29
Indole-3-butyric acid	7.0	3.7	1.9	9.0	9.1	0.99	0.29
3-Methylindole	8.7	4.3	2.0				

^a For experimental conditions see Table I. Data for 3-methylindole from ref 1i-j.

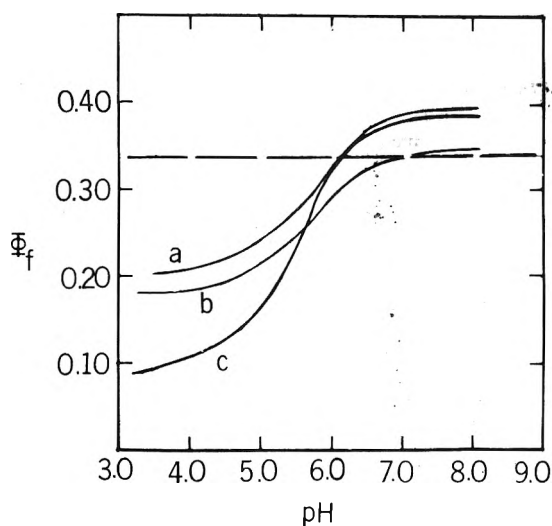


Figure 2. Fluorescence yield for (a) indole-3-butyric acid, (b) indole-3-acetic acid, (c) indole-3-propionic acid as a function of pH in an aqueous solution at 23 °C. The dotted line refers to the fluorescence yield of 3-methylindole under similar conditions.

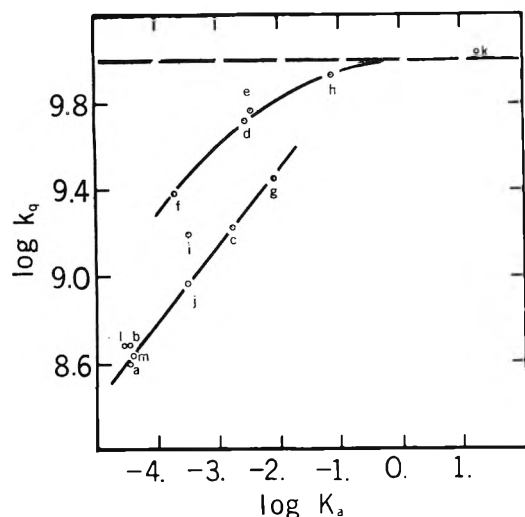


Figure 3. Fluorescence quenching of indole fluorescence by carboxylic acids. Letters refer to the acids in Table I.

relationship similar to that of the nonchlorinated acids holds for these acids (as we shall show below) but is somewhat obscured by virtue of the fact that the rate of quenching is now being controlled both by the rate of encounter of the acid and fluorophore as well as the actual quenching process which occurs once the encounter complex is formed. It is possible to distinguish mechanistically between these

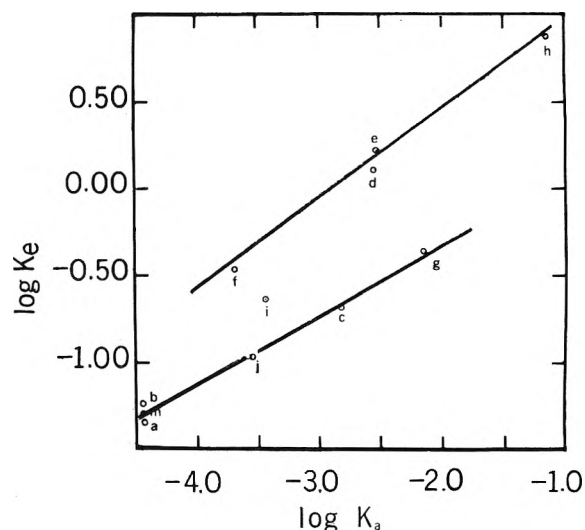
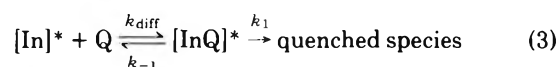


Figure 4. Fluorescence quenching of indole fluorescence by carboxylic acids. Data corrected for diffusion of reactants. Letters refer to the acids in Table I.

two controlling processes through the use of the following reaction



The encounter complex, $[InQ]^*$, is formed at a diffusion-controlled rate represented by k_{diff} from which the excited species can either be quenched by k_1 or leave the complex unquenched through k_{-1} . This reaction has been proposed in the past, particularly for encounter complexes stabilized by charge transfer.^{13,14}

It follows from this mechanism that

$$k_q = k_{diff} \frac{k_1}{k_{-1} + k_1} \quad (4)$$

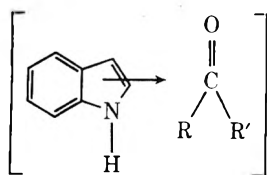
where k_q is the measured quenching constant. Rearranging again

$$\frac{k_q}{k_{diff} - k_q} = \frac{k_1}{k_{-1}} = K_e \quad (5)$$

This ratio represents a quasi-equilibrium constant K_e , which measures the effectiveness of the acid as a quenching agent. In Figure 4 is shown a plot of $\log K_e$ vs. $\log K_a$. The chlorinated acids now conform to the Bronsted relationship to a good degree. Conformity to the Bronsted relationship would normally imply that quenching is occurring via proton transfer. This idea is substantiated in the case of the nonchlorinated acids by the fact that their anions, lacking acid protons, are uniformly poor quenchers. On the other hand, Table I reveals that the esters of acetic, cyanoacetic,

and formic acid are themselves good quenchers despite their lack of an acidic proton. In addition, the anions of the chloroacids can also be seen to be good quenchers. These facts call into question the importance of the proton as a quenching species and obscures our interpretation of the Bronsted relationship as seen in Figure 4. What is required is a more general interpretation.

In several cases of quenching of photoexcited states, a charge-transfer type mechanism has been suggested based on studies of a linear-free-energy change character which reveal a strong correlation between quenching efficiency and related physical properties such as ionization potentials and reduction potentials. For example, in the quenching of acridine fluorescence by a series of amines a close correlation exists between the rate of quenching and the ionization potential of the amine thus providing indirect evidence in favor of a charge-transfer mechanism.¹⁵ Similarly, it has been shown that the quenching of ketone triplets by amines correlates closely with the ionization potential of the amine as well as the reduction potential of the ketone.¹⁶ Also, the quenching of fluorescing substituted benzenes by diolefins has been found to correlate well with the electron affinity of the aromatic component.¹³ Finally, it has been shown that quenching of the indole ring system by lanthanide ions paralleled the ease with which the ions were reduced at a mercury electrode.¹¹ In a similar way indole quenching by carbonyl compounds can also be interpreted as charge-transfer in nature. Within the encounter complex excited indole transfers a charge to the electrophilic carbonyl group, i.e.



which rapidly undergoes nonradiative decay to the ground state. Differences in quenching ability are due to the presence of the attached groups R and R' which modifies the electrophilicity of the carbonyl group. The trend is clearly seen in the case of the carboxylic acids (R = OH) where the relationship between structure and acidity is well understood.¹⁷ In general, electron-withdrawing substituents on the acid bring about increased acidity through an inductive effect, via the carbonyl group, which stabilizes the anion by fortifying delocalization of the electron pair. The substituents will modify the capability of the carbonyl group to enter into a charge-transfer interaction in the same way. Because of this common underlying effect the rate of charge transfer parallels the acidity of the acid as measured by its K_a and plots analogous to a classical Bronsted relationship are found. Similar reasoning can be advanced to explain the rate of quenching by carbonyl compounds in the CH_3COR family of compounds in which the quenching order is $\text{CH}_3\text{COCH}_2 > \text{CH}_3\text{COOH} \approx \text{CH}_3\text{COOEt} > \text{CH}_3\text{CONH}_2 \approx \text{CH}_3\text{COO}^-$. Each R group in the series is increasingly capable of electron release to the carbonyl carbon thus reducing its ability to accommodate charge transfer from photoexcited indole resulting in diminished quenching efficiency for that agent. In this light, it is not surprising that urea, NH_2CONH_2 , is a very poor quencher. The chlorinated acids also quench by charge transfer. In

addition, the chlorine atom(s) in the molecule are the center of a second nonradiative pathway.

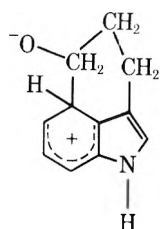
The presence of this new quenching pathway is indicated by the fact that the anions of these acids are excellent quenchers in themselves. In addition, the chloroacids have higher quenching constants than would have been predicted from the Bronsted relationship for the simple carboxylic acids. The highly electronegative chlorines would appear to be acting in a synergistic fashion. On one hand, they enhance the ability of the carbonyl group to quench indole fluorescence while, in addition, are themselves the center of a charge-transfer interaction. The linear relationship seen in Figure 4 for the chlorinated acids suggests that the ability of the chlorine atoms to act as a quenching center is directly related to their ability to enhance carbonyl quenching and therefore indirectly to the acidity of the molecule.

For the majority of acids studied the quenching was found to proceed a little more readily in H_2O than D_2O (Table I). The isotope effects were uniformly low, in the 1–1.4 range. These results are consistent with the uniformly low activation energies found for the quenching process¹⁸ and also support the theory that, in the case of the carboxylic acids, quenching is occurring primarily through a charge-transfer rather than a proton-transfer mechanism. The small isotope effect found for H_3O^+ may also suggest that quenching in this case is primarily by charge-transfer. We do not know why formic acid and chloroacetic acid should have a reversed isotope effect.

In Figure 1 and Table II are data on intramolecular quenching of indole fluorescence by carboxylic acids. This study provides an interesting case of first-order quenching which may be important to the understanding of protein and enzyme luminescence. In column I are listed the non-radiative decay constants, k_i . The near equivalence in value of k_i for the three acids and 3-methylindole suggests that it represents primarily a ring-centered decay pathway perturbed only slightly by the nature of the methylene substituent at the 3 position. The value of k_i in each case is halved in D_2O (see column 2). This isotope effect is due to the exchange of the hydrogen on the ring nitrogen with deuterium since it has been found that k_i for 1-methylindole is relatively insensitive to the presence of D_2O .^{11,19} The nonradiative decay constants representing the quenching effect of the RCOOH side chains are listed in column 3. As in the case of intermolecular quenching by acids, k_c is only slightly depressed by the presence of D_2O (see column 4). In contrast to k_i , the value of k_c varies by a factor of 5 among the three acids studied reaching a maximum value in the case of indole-3-propionic acid. It is difficult to attribute this variation to differences in $\text{p}K_a$ which would be expected to vary directly with increasing length of the alkyl side chain.

The order of reactivity may indicate the presence of a steric factor in this quenching process. A study of Dreiding molecular models for these compounds suggest that in addition to quenching by charge transfer, which is presumably of the type requiring a plane-to-plane configuration of carbonyl and indole ring, quenching may also be occurring via a σ complex. The carbonyl group of the side chain approaches the indole ring most closely at the 4 position. In the case of indole-3-propionic acid the carbon of the carbonyl group can be centered within a van der Waals radius of this position through the formation of a six-membered ring; but in the case of acetic and butyric acid side chains, less stable five- and seven-membered rings are required resulting in the lower quenching rate constants. The encoun-

ter complex would have the zwitterionic structure



In either mechanism quenching can only occur subsequent to rotational diffusion of the side chain to bring it into the proper orientation with respect to the indole ring. Intramolecular quenching, therefore, might be expected to be reduced under conditions which hinder rotational diffusion, and in this regard it has been shown that intramolecular quenching of indole fluorescence by σ -aminopropionic acid decreases in media of high viscosity and completely disappears in rigid solution.⁷

Cowgill^{1c} and Feitelson^{1h} have studied the fluorescent properties of several indole-3-carboxylic acid derivatives and both report that the fluorescent yield in water decreases in the order $RCH_2COO^- \approx RCH_2CONH_2 > RCH_2COOH \approx RCH_2COCH_3$, which is expected sequence if intramolecular quenching is dependent on the electrophilicity of the carbonyl group.

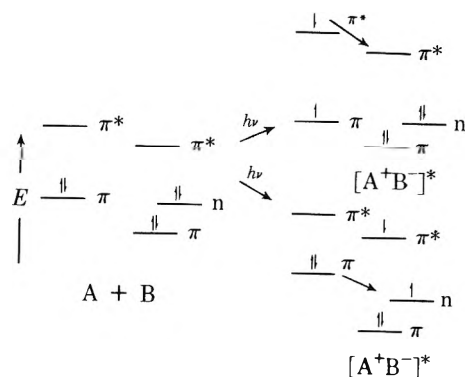
Finally, Tournon and El-Bayoumi²⁰ observed intramolecular quenching with phenyl alkyl carboxylic acids, a system similar to indole carboxylic acids. They found that the attached acid groups quenched by enhancing intersystem crossing rates since their presence led to an increase in the Q_p/Q_f ratio of the phenyl group. Indole-3-carboxylic acid quenching appears to be different on at least two counts. First it is viscosity dependent which points to a dynamic mechanism and secondly, the Q_p/Q_f ratio for all three acids are the same even though their quenching ability varies by a factor of 5. (See column 5, Table II.)

Summary

The evidence indicates that carbonyl compounds quench indole fluorescence through a mechanism involving an encounter complex stabilized by a charge-transfer interaction from the photoexcited indole to the carbonyl group. It should be noted that a purely electronic singlet-singlet energy transfer mechanism for this system can be ruled out on energetic grounds. The 0-0 band for the first excited singlet of indole is at 285 nm in water while the carbonyl compounds are well to the blue of this.

Fluorescence quenching of carbonyl compounds should not be limited to the indole fluorophore alone. We have found, for example, that ethyl cyanoacetate quenches *p*-xylene fluorescence and we are presently investigating the generality of this phenomenon.

Interestingly enough, it has been found that the fluorescence of ketones is quenched by dienes, electron-rich ethylenes, and some aromatics.^{21,22} In this case a quenching mechanism was proposed involving the formation of an excited-state complex partly stabilized by a charge-transfer interaction from the π system of the quencher to the photoexcited ketone. Their interpretation compliments our findings as may be seen in the following simple orbital scheme



where A, B, and $[A+B]^*$ represent the aromatic or diene, the carbonyl compound, and the charge-transfer complex, respectively. Thus, photoexcitation of either the diene (aromatic) or the carbonyl compound leads, in the encounter complex, to a charge transfer from the π system to the carbonyl compound. We have seen that an electron-rich group on the carbonyl diminished its ability to quench indole fluorescence and it is not surprising that similar groups attached to the diene enhance fluorescence quenching of the carbonyl group. For example, ethylene is a very poor quencher of carbonyl fluorescence, however, substitution of electron-releasing methyl groups increases its quenching ability. Substitution of the electron-rich moieties $-C=CR_2$ and $-OR$ as in the diene and alkoxyethylenes result in further quenching. Conversely, it is found that the addition of an electron-withdrawing chloro group diminishes the quenching ability of the diene.

Acknowledgment. We are grateful to the College of the Holy Cross Research and Publication Committee for financial support.

We wish also to acknowledge the helpful discussion with Dr. F. Vellaccio on the intramolecular quenching mechanism as well as to thank Professors J. Brown, A. VanHook, and G. Vidulich for their editorial comments.

References and Notes

- (1) (a) A. White, *Biochem. J.*, **71**, 217 (1959); (b) I. Weinryb and R. F. Steiner, *Biochemistry*, **7**, 2488 (1968); (c) R. W. Cowgill, *Arch. Biochem. Biophys.*, **100**, 36 (1963); (d) R. W. Cowgill, *Biochem. Biophys. Acta*, **75**, 272 (1963); (e) R. W. Cowgill, *ibid.*, **133**, 6 (1967); (f) M. S. Walker, T. W. Bednar, and R. Lumry, *J. Chem. Phys.*, **47**, 1020 (1967); (g) R. F. Steiner and E. P. Kirby, *J. Phys. Chem.*, **73**, 4130 (1969); (h) J. Feitelson, *Isr. J. Chem.*, **8**, 241 (1970); (i) R. W. Ricci and K. Kilichowski, *J. Phys. Chem.*, **78**, 1953 (1974); (j) R. W. Ricci, *Photochem. Photobiol.*, **12**, 67 (1970).
- (2) R. Gould and R. W. Ricci, paper presented at the 165th National Meeting of the American Chemical Society, Dallas, Tex., 1973.
- (3) R. W. Cowgill, *Biochem. Biophys. Acta*, **200**, 18 (1970).
- (4) C. A. Parker and W. T. Rees, *Analyst*, **85**, 587 (1960).
- (5) W. H. Melhuish, "Accuracy in Spectrophotometry and Luminescence Measurements", R. Mavodineanu, J. I. Shultz, and O. Memis, Eds., NBS Publication No. 378, p 137.
- (6) W. B. DeLauder and B. H. Wahl, *Biochem. Biophys. Acta*, **243**, 153 (1971).
- (7) G. Weber, "Light and Life", W. D. McElroy and B. Glass, Eds., Johns Hopkins Press, Baltimore, Md., 1961, p 82.
- (8) G. Weber and K. Rosenheck, *Biopolym. Symp.*, **No. 1**, 333 (1964).
- (9) W. B. DeLauder and P. Wahl, *Biochemistry*, **9**, 2750 (1970).
- (10) J. E. Leffler and E. Grunwald, "Rates and Equilibria of Organic Reactions", Wiley, New York, N.Y., 1963, p 235.
- (11) W. P. Jencks, "Catalysis in Chemistry and Enzymology", McGraw-Hill, New York, N.Y., 1969, p 170.
- (12) C. A. Parker, "Photoluminescence of Solutions", Elsevier, New York, N.Y., 1968, p 74.
- (13) R. G. Brown and D. Phillips, *J. Am. Chem. Soc.*, **96**, 4784 (1974).
- (14) A. Manikawa and R. J. Cretenoric, *J. Chem. Phys.*, **49**, 1214 (1968).

- (15) A. Weller, *Prog. React. Kinet.*, **1**, 187 (1961).
 (16) J. Guttenplan and S. Cohen, *Tetrahedron Lett.*, **22**, 2163 (1972).
 (17) R. P. Bell, "The Proton in Chemistry", Cornell University Press, Ithica, N.Y., 1973, Chapter 6.
 (18) K. B. Wiberg, *Chem. Rev.*, **55**, 718 (1955).
 (19) L. Stryer, *J. Am. Chem. Soc.*, **88**, 5708 (1966).
 (20) Tournon and M. El-Bayoumi, *J. Am. Chem. Soc.*, **93**, 639-646 (1971).
 (21) B. M. Monroe, C. Lee, and N. J. Turro, *Mol. Photochem.*, **6**, 271 (1974), and references cited therein.
 (22) N. E. Schore and N. J. Turro, *J. Am. Chem. Soc.*, **97**, 2482 (1975).

Electronic Spectra of the Anion Radicals of Heterocyclic Amine *N*-Oxides and Related Substances

Kiyoshi Ezumi, Tanekazu Kubota,* Hiroshi Miyazaki, and Masumi Yamakawa

Shionogi Research Laboratory, Shionogi and Company, Limited, Fukushima-ku, Osaka, 553 Japan (Received August 22, 1975)

Publication costs assisted by Shionogi Research Laboratory

Visible-to-near-ultraviolet absorption spectra of the anion radicals of some heterocyclic amine *N*-oxides, 4-nitro-substituted pyridine and quinoline *N*-oxides, and their related substances were recorded, the radicals being generated by electrolysis techniques. These spectra were interpreted by applying open shell SCFMO-CI calculations. From these the mutual correlation of the electronic spectra among the anion radicals of pyridine, quinoline, and acridine *N*-oxides has been established. The blue shift of visible spectra upon aza (N) substitution was observed with the naphthalene, anthracene, and acridine *N*-oxide anion radicals. The main reason for this phenomenon was clarified. Finally, the visible spectra of 4-nitropyridine *N*-oxide and 4-nitroquinoline *N*-oxide anion radicals were extensively discussed on the basis of SCFMO-CI calculations.

Introduction

So far the anion and the cation radicals of heterocyclic amine *N*-oxides have been mainly studied by recording the electron spin resonance (ESR) spectra,¹⁻⁷ the analyses of which gave us valuable information on the electronic structures of the amine *N*-oxide ion radicals. As for the generation of the amine *N*-oxide free radicals, we previously reported an electrochemical technique¹⁻⁴ that is very convenient. Besides the ESR investigation, this technique was also used for studying the infrared spectra of the anion radicals of 4-nitropyridine *N*-oxide (4NPO) and related nitro compounds.⁸ However, as far as we know, there have been only a few discussions on the electronic spectra of heterocyclic amine *N*-oxide free radicals.^{7,9} In this paper the visible-to-near-ultraviolet spectra of heterocyclic amine *N*-oxide anion radicals have been systematically discussed in relation to those of their neutral species.

Experimental Section

Spectral Measurement of Anion Radicals. For the visible-to-ultraviolet (uv) spectral measurement of free radicals we have employed two types of controlled-potential electrolysis cells. One is that which was already reported by us,⁸ and is the type involving circulation of the cathode solution (anion radical solution) through the optical quartz cell. The other is the flow type cell shown in the Figure 1. This type cell is more suitable for recording the spectra of less stable anion radicals.¹⁰ Radical concentration in the absorption cell depends on the flow rate and on the concentration of mother compounds. In general 0.025 cm³/s is the rate suitable for the optical measurement, and the concen-

tration of mother compounds is on the order of $\sim 10^{-3}$ and $\sim 10^{-4}$ M for longer and shorter wavelength regions of the absorption spectra, respectively. The cell length used is 0.1 cm unless otherwise noted. Unfortunately, however, the valid value of the molecular extinction coefficient (ϵ) was not determined. The anion radicals were generated by the controlled potential electrolysis method at room temperature, the set (reduction) potential being determined by recording the polarogram vs. saturated calomel electrode (SCE) using the same solution as for the radical generation, where tetra-*n*-propylammonium perchlorate (0.1 M) was added as a supporting electrolyte.^{1,2} The anion radicals produced were also certified by recording their ESR spectra as well as by checking their absorption spectra after introducing air into the radical solution; the absorption spectra due to the anion radicals studied usually were easily quenched by this technique. As another check of our electronic spectra of the anion radicals we compared our visible spectrum of the 4NPO anion radical with that obtained by γ -ray irradiation of a 2-methyltetrahydrofuran matrix of the sample at 77 K. This technique is also well known as a good method for ion radical formation.¹¹⁻¹³ It is clear from Figure 2 that the two spectra are quite similar to each other in spite of the different experimental conditions.

The instruments used for the measurement of uv and ESR spectra were a Hitachi EPS-3T uv spectrometer and a Varian V-4502-15 X-band spectrometer with a 100-kHz magnetic field modulation, respectively. A Yanagimoto polarograph Model P8-AP (three-electrode system), and a Yanagimoto VE-2 constant-potential electrolyzer were employed for obtaining dc and ac polarograms and for radical generation, respectively. See our previous papers for the

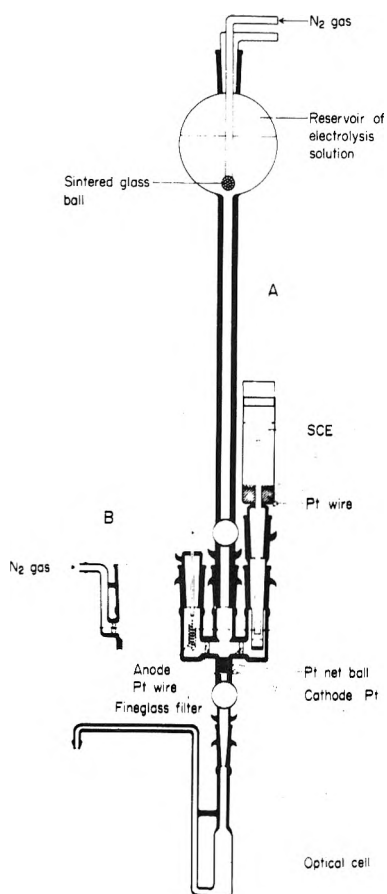


Figure 1. Controlled potential electrolysis cell for recording the electronic spectra of anion radicals. Part B is a side view of the corresponding part in the front view (A). Purified dry N_2 gas was bubbled from the upper side of part A and from part B in order to remove the dissolved oxygen gas.

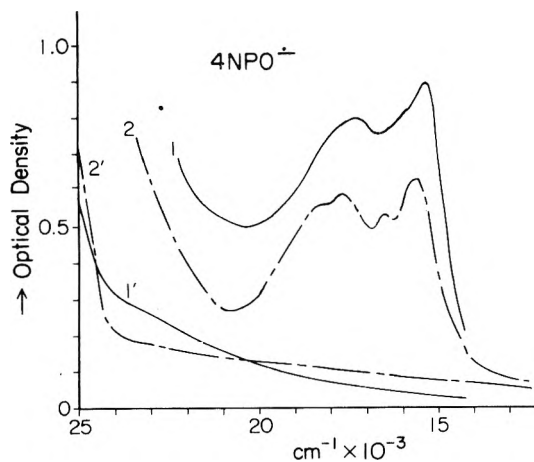


Figure 2. Comparison of the visible spectrum of the 4-nitropyridine *N*-oxide anion radical prepared by two different methods. Curves 1 and 1' are the spectra obtained by the present flow technique and for the solution exposed to air, respectively. Curves 2 and 2' are the spectra yielded after and before the γ -ray irradiation of 2-methyltetrahydrofuran matrix at 77 K.

details of the instrument operation and the radical generation technique.^{1,8,14} An example showing the spectral behavior with the lapse of electrolysis time is depicted in Figure 3 for 4-nitroquinoline *N*-oxide (4NQO), where a circu-

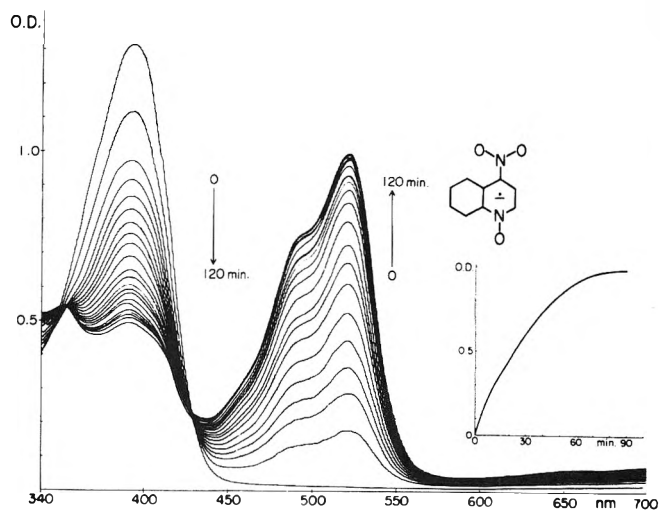


Figure 3. The spectral change of 4-nitroquinoline *N*-oxide (1.05×10^{-3} M) with electrolysis time. Circulation type cell (see ref 8) was used. The inserted small figure indicates the change in optical density at 518 nm upon electrolysis time.

lation type cell was used. That the radical formation reaches a maximum after about 90 min is seen in this figure. This spectrum due to the radical was quenched with air (see Figure 11).

Solvents and Samples. The solvent used for obtaining electronic spectra, polarograms, and ESR spectra was dimethylformamide (DMF). The purification of DMF and of tetra-*n*-propylammonium perchlorate for use as a supporting electrolyte has already been reported elsewhere.^{1,14} Of the heterocyclic amine *N*-oxides, the compounds for which reliable spectra of the anion radicals were recorded are acridine *N*-oxide (ANO), phenazine mono- and di-*N*-oxides (PMNO and PDNO), 1,5-naphthyridine di-*N*-oxide (NDNO), 4NPO, and 4NQO. These *N*-oxides, except for NDNO, were synthesized and purified according to the methods reported in our previous papers.^{1,14,15} For PDNO, silica gel column chromatography was applied, with special care of removing a small amount of PMNO, elutions being made with benzene, benzene-chloroform mixture, and finally chloroform alone. The pure di-*N*-oxide was obtained from the chloroform fraction (mp 185 °C after changing its color at ~160 °C). NDNO was synthesized by the oxidation of 1,5-naphthyridine with an excess amount of *m*-chloroperbenzoic acid in chloroform. The resulting NDNO was recrystallized several times from alcohol.¹⁶ It decomposes gradually with sublimation at a temperature greater than 260 °C.

In addition, samples of acridine (AC), phenazine (PH), quinoxaline (QU), 1,5-naphthylidene (NA), 4-nitropyridine (4NP), and 4-nitroquinoline (4NQ) were also used for obtaining the electronic spectra of their anion radicals, for comparison with the above *N*-oxides. For these amines, except 4NP and 4NQ, commercially available samples were purified using the usual methods: for PH, recrystallization from alcohol; for AC, sublimation after recrystallizing from aqueous alcohol; and for NA, repeated sublimation. QU was distilled carefully under reduced pressure. 4NP and 4NQ were deoxygenated from 4NPO and from 4NQO, respectively, according to the literature, and then purified.^{16,17} All the above samples were submitted to elemental analyses. Agreement between experimental and calculated values was good.

TABLE I: Calculated Transition Energies (eV), Oscillator Strengths, Main Configurations (%), Observed Values, and Tentative Assignment of the Anion Radicals Given

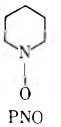
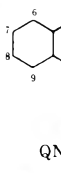


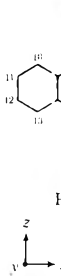
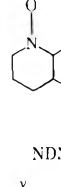
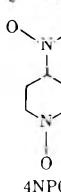
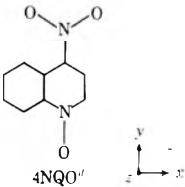
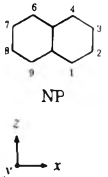
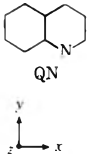
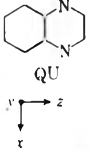
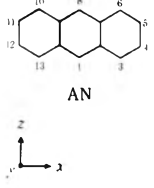
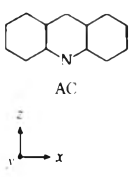
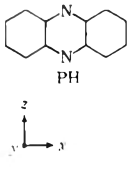
Compounds	ΔE_{calcd}	f_{calcd}	${}^2\Gamma^a$	Polarization ^b	Configuration, wt % ^c	ΔE_{obsd}
 PNO	0.00	0	2B_2		96.2 (G)	
	0.35	0.000	2A_2	x	93.4 (5/6)	
	2.46	0.020	2B_2	z	73.0 (5/7), 11.5 (3/6) ^β , 10 (4/5)	
	3.27	0.121	2B_2	z	76.7 (4/5), 13.5 (3/6) ^β	
	3.81	0.108	2A_2	x	79.0 (4/6) ^α , 18.8 (4/6) ^β	
 QNO	0.00	0	${}^2A''$		97.1 (G)	
	1.29	0.001	${}^2A''$		97.0 (7/8)	
	1.90	0.054	${}^2A''$		50.8 (7/9), 35.8 (6/7)	
	2.17	0.060	${}^2A''$		41.0 (7/9), 39.9 (6/7)	
	2.90	0.120	${}^2A''$		64.0 (7/10), 13.5 (4/8) ^β	
	3.53	0.027	${}^2A''$		46.5 (5/7), 17.8 (7/11), 13.1 (5/9) ^β	
	3.64	0.231	${}^2A''$		66.3 (6/8) ^α , 20.3 (6/8) ^β	
 ANO	0.00	0	2B_2		94.2 (G)	
	1.53	0.062	2B_2	z	82.4 (8/9)	1.63
	1.94	0.002	2A_2	x	95.6 (9/10)	} 2.02
	2.17	0.120	2A_2	x	89.7 (9/11)	
	2.98	0.001	2B_2	z	51.1 (9/13), 22.8 (7/9), 11.5 (9/12)	} 3.24 ~ 3.87
	3.15	0.126	2B_2	z	66.3 (9/12), 17.2 (7/9)	
	3.33	0.354	2B_2	z	40.6 (7/9), 39.4 (9/13)	
	3.63	0.066	2A_2	x	65.4 (8/10) ^α , 23.1 (8/10) ^β	
	3.80	0.205	2A_2	x	75.3 (8/11) ^α , 12.9 (8/11) ^β	
 PMNO	0.00	0	2B_2		96.2 (G)	
	1.55	0.094	2B_2	z	83.2 (8/9)	1.77 ~ 1.95
	2.17	0.000	2A_2	x	92.2 (9/10)	} 2.36
	2.41	0.109	2A_2	x	86.1 (9/11)	
	3.18	0.118	2B_2	z	54.3 (9/12), 30.6 (9/13)	} 3.94
	3.39	0.135	2B_2	z	38.3 (9/13), 36.6 (7/9), 15.4 (9/12)	
	3.43	0.121	2A_2	x	66.4 (8/10) ^α , 21.2 (8/10) ^β	
	3.61	0.069	2B_2	z	54.9 (7/9), 17.0 (9/13)	
3.85	0.251	2A_2	x	50.3 (8/11) ^α , 17.4 (5/9), 17.4 (8/11) ^β		
 PDNO	0.00	0	${}^2B_{2u}$		97.8 (G)	
	1.11	0.181	${}^2B_{3g}$	z	90.8 (9/10)	1.36 ~ 1.51
	2.22	0	2A_u		97.6 (10/11)	} 2.30
	2.41	0.000	${}^2B_{1g}$	x	43.8 (10/12), 41.0 (9/11) ^α , 14.9 (9/11) ^β	
	2.48	0.371	${}^2B_{1g}$	x	52.9 (10/12), 32.0 (9/11) ^α	} 3.12 ~ 3.67
	2.88	0	${}^2B_{2u}$		78.3 (8/10), 19.9 (10/13)	
	3.17	0	2A_u		81.0 (9/12) ^α , 17.3 (9/12) ^β	
	3.44	0	${}^2B_{2u}$		77.1 (10/13), 20.7 (8/10)	
	3.53	0.328	${}^2B_{3g}$	z	73.6 (10/14), 13.1 (5/11) ^β	
3.98	0.040	${}^2B_{3g}$	z	90.6 (7/10)		
 NDNO	0.00	0	2B_g		98.3 (G)	
	1.30	0	2B_g		96.4 (8/9)	1.26 ~ 1.43
	1.48	0.065	2A_u		45.9 (8/10), 44.0 (7/8)	1.82 ~ 2.00
	1.98	0.136	2A_u		45.3 (8/10), 36.3 (7/8)	} 2.25
	2.29	0	2B_g		75.3 (6/8), 15.8 (7/10) ^β	
	3.02	0.187	2A_u		73.1 (8/11), 16.0 (5/9) ^β	
	3.36	0.235	2A_u		68.4 (7/9) ^α , 20.2 (7/9) ^β	
4.08	0	2B_g		73.5 (6/9) ^α , 19.6 (6/9) ^β		
 4NPO	0.00	0	2B_2		91.6 (G)	
	1.74	0.055	2B_2	z	47.8 (7/9), 30.4 (6/7), 17.1 (6/9) ^β	} 1.91 ~ 2.16
	2.23	0.003	2A_1	x	88.3 (7/8)	
	3.00	0.308	2B_2	z	40.0 (7/9), 28.3 (6/7), 16.5 (6/9) ^α	} 3.01
	4.00	0.000	2B_2	z	67.5 (4/8) ^β , 27.7 (7/10)	

TABLE I (continued)

Compounds	ΔE_{calcd}	f_{calcd}	${}^2\Gamma^a$	Polarization ^b	Configuration, wt % ^c	ΔE_{obsd}
 4NQO ⁻	0.00	0	${}^2A''$		88.3 (G)	} 2.39
	1.35	0.026	${}^2A''$		47.5 (9/10), 37.6 (8/9)	
	2.47	0.217	${}^2A''$		35.9 (9/10), 33.5 (8/9)	
	2.73	0.008	${}^2A''$		91.1 (9/11)	
	3.45	0.019	${}^2A''$		33.1 (9/12), 22.4 (6/9), 15.4 (6/10) ^β	
	3.80	0.020	${}^2A''$		28.7 (9/12), 21.9 (8/11) ^α , 21.5 (6/9)	
4.02	0.040	${}^2A''$		41.0 (8/11) ^α , 19.8 (9/12), 10.2 (8/11) ^β		
 NP	0.00	0	${}^2B_{1g}$		98.4 (G)	} See ref 13, 20
	0.94	0	${}^2B_{3g}$		94.6 (6/7)	
	1.95	0.093	${}^2B_{2u}$	x	94.3 (6/8)	
	2.40	0.008	2A_u	z	62.4 (6/9), 29.7 (5/6)	
	3.35	0.145	2A_u	z	56.0 (5/6), 21.1 (6/9), 15.4 (4/7) ^β	
	3.68	0	${}^2B_{2g}$		44.5 (6/10), 32.0 (3/6), 21.9 (5/8) ^β	
4.32	0.239	${}^2B_{2u}$	x	56.3 (5/7) ^α , 26.6 (4/6), 14.9 (5/7) ^β		
 QN	0.00	0	${}^2A''$		98.2 (G)	} See ref 28
	1.10	0.000	${}^2A''$		95.1 (6/7)	
	2.05	0.095	${}^2A''$		93.4 (6/8)	
	2.49	0.009	${}^2A''$		61.6 (6/9), 29.1 (5/6)	
	3.42	0.127	${}^2A''$		53.7 (5/6), 18.1 (6/9), 14.4 (4/7) ^β	
3.80	0.014	${}^2A''$		40.4 (6/10), 31.0 (3/6), 19.4 (5/8) ^β		
 QU	0.00	0	2B_2		98.0 (G)	} 1.39 ~ 1.57 2.04 ~ 3.00
	1.29	0.000	2A_2	x	94.6 (6/7)	
	2.18	0.093	2B_2	z	92.7 (6/8)	
	2.57	0.006	2A_2	x	57.6 (6/9), 30.9 (5/6)	
	3.40	0.108	2A_2	x	49.8 (5/6), 17.8 (6/9), 14.2 (4/7) ^β	
3.97	0.027	2A_2	x	37.0 (6/10), 32.8 (3/6), 15.8 (5/8) ^β		
 AN	0.00	0	${}^2B_{2u}$		98.1 (G)	} See refs 13, 20
	1.73	0	2A_u		98.2 (8/9)	
	1.84	0.187	${}^2B_{1g}$	x	94.5 (8/10)	
	2.08	0.018	${}^2B_{3g}$	z	72.3 (7/8), 21.8 (8/11)	
	2.87	0	${}^2B_{2u}$		89.9 (8/12)	
	3.11	0.181	${}^2B_{3g}$	z	60.4 (8/11), 19.4 (7/8), 11.2 (6/9) ^β	
	3.71	0	2A_u		52.4 (5/8), 28.9 (7/10) ^β , 17.7 (8/13)	
	3.78	0.011	${}^2B_{3g}$	z	40.7 (4/8), 20.5 (7/12) ^β , 16.9 (5/10) ^β , 14.9 (8/14)	
	3.95	0.384	${}^2B_{1g}$	x	57.0 (7/9) ^α , 22.0 (6/8), 19.8 (7/9) ^β	
	4.54	0	2A_u		98.8 (7/10) ^α	
4.59	0.768	${}^2B_{1g}$	x	59.3 (6/8), 36.6 (7/9) ^β		
 AC	0.00	0	2B_2		98.0 (G)	} 1.54 ~ 1.72 1.94 ~ 2.43 3.10 ~
	1.95	0.016	2A_2	x	63.5 (8/9), 34.2 (8/10)	
	2.06	0.174	2A_2	x	62.6 (8/10), 32.4 (8/9)	
	2.21	0.019	2B_2	z	71.6 (7/8), 21.4 (8/11)	
	2.98	0.000	2B_2	z	86.7 (8/12)	
	3.20	0.161	2B_2	z	54.5 (8/11), 17.9 (7/8)	
	3.67	0.000	2A_2	x	58.2 (5/8), 17.4 (7/9) ^β , 11.9 (8/13)	
	3.92	0.032	2B_2	z	26.9 (4/8), 18.4 (7/12) ^β , 13.2 (8/14), 12.9 (3/8)	
	4.09	0.042	2A_2	x	48.2 (6/8), 24.4 (7/10) ^α , 17.6 (7/9) ^α	
	4.69	1.362	2A_2	x	37.0 (6/8), 25.0 (7/10) ^β , 14.4 (7/9) ^β , 14.1 (7/10) ^α	
 PH	0.00	0	${}^2B_{2u}$		97.9 (G)	} 2.05 ~ 2.41 4.23
	2.20	0	2A_u		98.0 (8/10)	
	2.28	0.025	${}^2B_{3g}$	z	74.6 (7/8), 17.8 (8/11)	
	2.28	0.178	${}^2B_{1g}$	x	93.7 (8/9)	
	3.12	0	${}^2B_{2u}$		85.7 (8/12)	
	3.36	0.170	${}^2B_{3g}$	z	64.0 (8/11), 15.8 (6/10) ^β , 15.1 (7/8)	
	3.59	0	2A_u		68.7 (5/8), 23.1 (7/9) ^β	
	4.06	0.050	${}^2B_{1g}$	x	74.5 (6/8), 22.7 (7/10) ^α	
	4.79	0.012	${}^2B_{3g}$	z	65.0 (3/8), 17.4 (5/9) ^β , 13.5 (8/14)	
	4.84	1.558	${}^2B_{1g}$	x	39.9 (7/10) ^α , 39.1 (7/10) ^β , 16.6 (6/8)	

^aThe species for $\Delta E_{\text{calcd}} = 0.00$ is for the ground state of the anion radicals. ^bThe polarization of each transition is given by ${}^2\Gamma_{\text{ground state}} \times {}^2\Gamma_{\text{excited state}}$. ^cFor example (5/6) means a one-electron transition from MO 5 to 6. In addition the right superscript α or β represents the spin configuration of three half-filled MO's; ψ_i, ψ_k, ψ_m . The α and β correspond to $1/\sqrt{2}(|\psi_i\psi_k\psi_m| + |\psi_k\psi_i\psi_m|)$ and $1/\sqrt{6}(|\psi_i\psi_k\psi_m| - |\psi_k\psi_i\psi_m| + 2|\psi_i\psi_m\psi_k|)$, respectively. ^dIn our MO calculation of these nitro-substituted anion radicals the $a_2\pi$:NO₂ orbital (or the orbital having this character) seems to be quite a bit unstabilized, so that the transition contributed largely from this orbital is omitted in a visible region. The deleted transitions are 1.63 eV ($x:f = 0.055$) and 1.47 eV ($f = 0.036$) for 4NPO⁻ and 4NQO⁻, respectively. These transitions seem to be irregular. See text in detailed discussions.

Molecular Orbital (MO) Calculation

In order to interpret the electronic structures and electronic spectra of the doublet state free radicals, a standard restricted Longuet-Higgins-Pople type open shell SCFMO-CI (hereafter abbreviated as LP-SCFMO-CI) calculation was programmed.¹⁸⁻²⁰ Here one-electron transitions alone were taken into consideration, since lower energy excited states are mainly considered here. The program was carefully checked and compared with the data of other workers on hydrocarbons^{19,20} etc., the results being very reasonable.²¹ According to the diagonal and the off-diagonal matrix elements given already in literature,^{19,20} electronic transitions are classified as follows. Spin orbital (SO) configurations are defined as the transitions from SO (half-filled MO of the ground state) to unoccupied MO's (type A), and also from lower filled MO's to SO (type B). For the transition to unoccupied MO's from filled MO's by jumping over SO, there occur two independent configurations (α and β types) because of the three half-filled MO's resulting from the transition. See ref 19 and 20, and footnote c of Table I for the detailed descriptions. All the calculations were made using a Facom 270-30 computer in our laboratory. The parameters, geometries, and the expression of the two-electron Coulomb repulsion integrals (Nishimoto-Mataga approximation) for the SCFMO calculation of the anion radicals of the N heterocycles and their *N*-oxides were the same as those used in our previous papers for computing the electronic states of the neutral molecules,^{14,15,22} except for the $\beta_{\text{N}^{\ominus}\text{O}}^{\text{core}}$ value of the *N*-oxide bond. After doing various trials, the value of $\beta_{\text{N}^{\ominus}\text{O}}^{\text{core}} = -1.90$ eV was adopted. This absolute value is a little smaller than that (-2.00 eV) of the neutral species. This is because our foregoing work verified that the $\text{N}^{\ominus}\text{O}$ valence bond in aromatic $\text{N} \rightarrow \text{O}$ and NO_2 groups of anion radicals turns out to be sacrificial compared with that in neutral molecules.⁸ The parameters for the NO_2 group will be discussed later in this text. The coordinates of all the molecules studied here are given in Table I.

Results and Discussion

Correlation of Energy Levels and Excitation Energies among the Anion Radicals of Pyridine N-Oxide, Quinoline N-Oxide, and Acridine N-Oxide. Although the electronic spectra of pyridine *N*-oxide (PNO) and quinoline *N*-oxide (QNO) anion radicals could not be observed, the correlation of energy levels and excitation energies among PNO, QNO, and ANO anion radicals (abbreviated as ANO⁻ etc.) was examined on the basis of the LP-SCFMO-CI calculation. This seems to be important as part of the theoretical background for assigning the spectrum of ANO⁻; for, since the above correlation was already established for the ¹L_a, ¹L_b, and T₁ ((the lowest triplet state) ← N (ground state)) transitions in PNO, QNO, and ANO,²² the comparison of the correlation between the spectra of the neutral *N*-oxides and their anion radicals is of great interest. All the calculations and observed results are listed in Table I. In Figures 4 and 5 are illustrated the LP-SCFMO's and the calculated transition energies in the lower excited state region. It is evident from Figure 4 that the SO energy is considerably stabilized with increasing ring size, resulting in the blue shift of the type 1 transition (see Figures 4 and 5),²³ which may appear in the longest wavelength region in the case of PNO⁻ and QNO⁻. On the other hand, the type 2 transition is considerably red shifted as the ring size increases, as

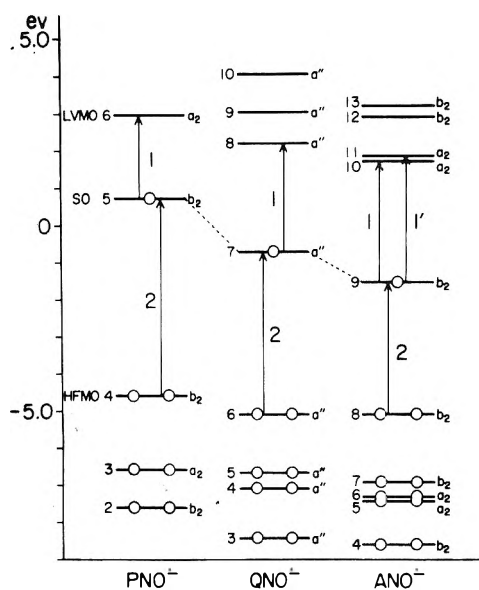


Figure 4. LP-SCFMO energies of the anion radicals of pyridine, quinoline, and acridine *N*-oxides. The notation of one-electron transitions connected largely with visible spectra are defined as types 1, 1', and 2. The abbreviation of HFMO (highest filled MO), SO (spin orbital), and LVMO (lowest vacant MO) is employed for the orbitals, for example, of MO 4, 5, and 6 of PNO⁻, respectively.

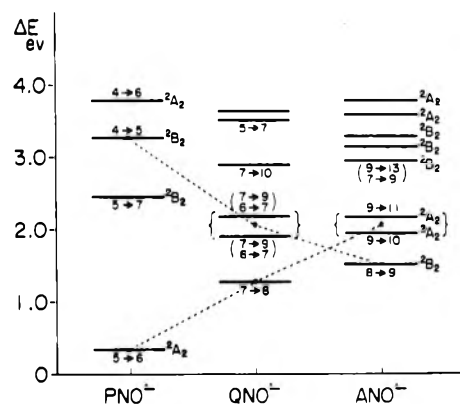


Figure 5. Correlation diagram of the electronic transitions having the same character among the anion radicals of pyridine *N*-oxide, quinoline *N*-oxide, and acridine *N*-oxide.

Figures 4 and 5 indicate. Here note that the MO sequence and the characteristics of each MO given in Figure 4 are almost the same as the calculated results for the corresponding neutral *N*-oxides,²² which have recently been born out by the analyses of the photoelectron spectra of various aromatic *N*-oxides.²⁴ Experimental³ and MO calculation results suggest that at the highest filled MO of the neutral *N*-oxides and their anion radicals, the orbital electron densities are greatly localized at the *N*-oxide group oxygen atom. As a result the type 2 transition in Figure 4 causes quite a large charge transfer from the oxygen atom of $\text{N} \rightarrow \text{O}$ bond to the ring residue. All of these characteristics (orbitals and their natures entering into the transition) are quite similar to the ¹L_a (CT) band of neutral *N*-oxides²⁵ except for the problem of band intensity, which is large in the neutral species. So, for the above *N*-oxide series the type 2 transition may be called a ²L_a (CT) band, and this band shows a red shift with increasing ring size, just as does the ¹L_a (CT) band.

Absorption Spectra of the Anion Radicals of ANO, PMNO, and PDNO. Experimental and calculated results are included in Table I, and the spectra are illustrated in Figure 6. First let us consider the spectrum of ANO⁻. As has been understood from the correlation curves and the energy level diagram (Figures 4 and 5), the visible spectrum appearing in a longer than ~450-nm wavelength region would consist of three electronic states, i.e., one ²B₂ ← ²B₂ and two ²A₂ ← ²B₂ species. Of these, the ²B₂ ← ²B₂ band is assigned to lie in the longest wavelength region and may have ²L_a nature. The strong band at ~600 nm is necessarily identified with one of the ²A₂ ← ²B₂ species, which have mainly the character of a type A transition from calculated energy and intensity, and from the correlation diagram (Figure 5). The other ²A₂ ← ²B₂ band with weak intensity may be overshadowed by the above two bands. The argument about the bands in the uv region will not be made here in detail, since there are too many calculated excited states compared with observed ones. Tentative assignment, however, is given in Table I. As Figure 6 shows, the spectrum of PMNO⁻ in the visible region is similar to that of ANO⁻ except that the longest wavelength ²B₂ ← ²B₂ band of ANO⁻ is divided into two bands for the case of PMNO⁻, which may be either the vibrational structure of the ²B₂ ← ²B₂ band or the two electronic states composed of the ²B₂ ← ²B₂ band and an intensified ²A₂ ← ²B₂ band. Particularly note that the visible spectrum of PMNO⁻ is blue shifted in comparison with that of ANO⁻. By introducing the nitrogen atom at the 8 position of ANO⁻, stabilization of SO and the highest filled MO occurs, and the transition energies labeled as 1, 1', and 2 in Figure 4 result in a more or less higher energy.²⁶ This may be one of main reasons for the blue shift phenomenon. The aforementioned circumstances are very similar to the blue shift phenomenon in the absorption spectra in the longest wavelength region of anthracene and naphthalene anion radicals with the following sequence of structure changes: anthracene → AC → PH, and naphthalene → quinoline → QU (vide infra). Alternatively, the visible spectrum of PDNO⁻ appears in a longer wavelength region than ANO⁻ or PMNO⁻, as Figure 6 indicates. This seems to be quite reasonable. Based on the consideration of a composite system, the two *N*-oxide group oxygen atoms of PDNO are written as $1/\sqrt{2}(0_1 \pm 0_2)$, which can interact with the MO's of the parent molecule PH. As a result the present calculations show that the highest filled MO and the penultimate occupied MO of PDNO⁻ derive from these orbitals, where the contribution from $1/\sqrt{2}(0_1 - 0_2)$ is large for the former and the plus combination mainly contributes to the latter.²⁷ In other words, the highest filled MO of PMNO⁻, localized largely on the *N*-oxide group oxygen atom, splits into two MO's contributed mainly from $1/\sqrt{2}(0_1 \pm 0_2)$, so that the energy difference between the highest filled MO and the SO becomes smaller for PDNO⁻ than for PMNO⁻. This may lead to the red shift of the longer wavelength band of PMNO⁻. Note that the longest wavelength absorption band, corresponding to the first excited state of all the anion radicals of ANO, PMNO, and PDNO, is *Z* axis polarized and has the character of intramolecular charge transfer from the oxygen atom of *N*-oxide group to the ring residue (vide supra).

Shift of Visible Absorption Spectra of Anthracene and Naphthalene Anion Radicals by Introducing *N* Hetero Atoms. Referring to the discussions given in the preceding sections, let us now consider the problem given in the title.

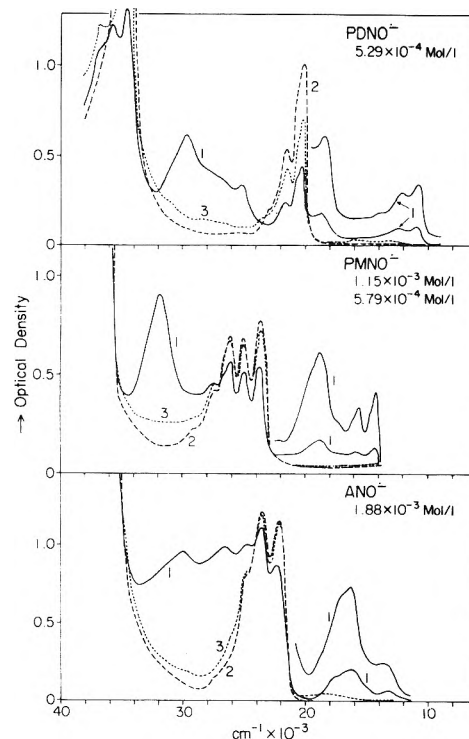


Figure 6. Electronic spectra of the anion radicals (curve 1) of phenazine di-*N*-oxide, phenazine mono-*N*-oxide, and acridine *N*-oxide, and of the solutions obtained by quenching the radicals with air (curve 3). Curve 2 is for the neutral molecules. That the neutral substances were not completely converted to the anion radicals is clear by comparing curves 1 and 2. The concentrations given in the figure are for the neutral species.

Spectra and their assignments for the anion radicals of anthracene and naphthalene were already reported.^{19,20} Our present calculation has also supported those. In Figures 7 and 8 are shown the blue shifts of the visible spectra as well as the changes in the orbital energies of anthracene and naphthalene anion radicals, as AN⁻ becomes AC⁻, and PH⁻ and as NP⁻ becomes quinoline⁻ and QU⁻. Spectra other than those recorded here were cited from the literature.^{13,28} Roughly speaking, the first three bands of all the spectra in Figures 7 and 8 are quite largely due to the electron transition from SO to upper vacant MO's. Keeping in mind these theoretical results, and also considering the fact that in the successive structure change the *N* atom replacement causes especially the stabilization of the filled MO and SO energies,²⁹ the blue shift phenomenon of the visible bands of anthracene and naphthalene anion radicals is reasonably expected even if only the orbital energies are considered. In connection with this section we would like to discuss the spectrum of NDNO⁻, since its electronic transitions are somewhat similar to those of the aforementioned anion radicals. The spectrum is illustrated in Figure 9. The first excited state of NDNO⁻ may be primarily due to a one-electron transition from the SO to the lowest vacant MO (see Table I). This result is quite different from the case of PDNO⁻, although the highest two filled MO's come from the combination of two *N*-oxide group oxygen atoms written as $1/\sqrt{2}(0_1 \pm 0_2)$, just like those of PDNO⁻. This may be due to the difference of the ring size of conjugated system, so that the calculated results for NDNO⁻ are rather similar to those of the anion radicals of QNO and quinoxaline mono- and di-*N*-oxides, as deduced from the correlation diagram of Figure 5.

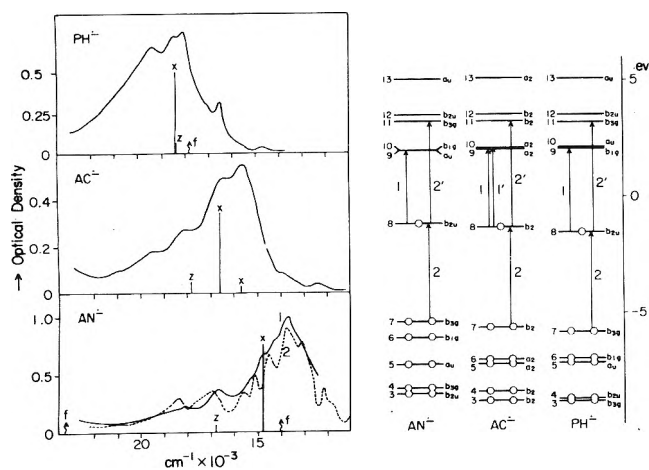


Figure 7. Electronic spectra, LP-SCFMO energies, and one-electron transitions contributing largely to visible spectra of the anion radicals of anthracene (AN), acridine (AC), and phenazine (PH). Curves 1 and 2 of the spectra of AN⁻ were taken from ref 28b and 13, respectively. The calculated transition energies and intensities are given in the spectra as stick diagrams. The transitions of the types such as 2 and 2', or 1 and 1' are in strong CI.

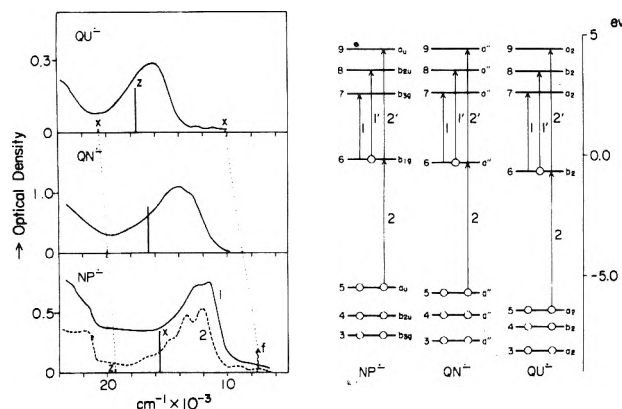


Figure 8. Electronic spectra, LP-SCFMO energies, and one-electron transitions contributing largely to visible spectra of the anion radicals of naphthalene (NP), quinoline (QN), and quinoxaline (QU). Curves 1 and 2 of the spectra of NP⁻ are those recorded by us and taken from ref 13, respectively. The calculated transition energies and intensities are given in the spectra as stick diagram (see Table I for adopted coordinates). The transition types of 2 and 2' are in strong CI.

Absorption Spectra of the Anion Radicals of 4NPO, 4NQO, and Related Compounds. In Figures 10 and 11 are depicted the spectra of 4NPO⁻ and 4NQO⁻, along with those of 4NP⁻ and 4NQ⁻ for comparison. The spectral patterns of 4NP⁻ and 4NQ⁻ in our recorded region are very analogous to those of the anion radicals of nitrobenzene and α -nitronaphthalene, respectively. The experimental and theoretical interpretation of the spectra of many nitro-substituted aromatic hydrocarbon anion radicals has been extensively studied by Shida and Iwata.¹² That the visible spectra of 4NPO⁻ and 4NQO⁻ occur at much longer wavelengths than for the corresponding 4NP⁻ and 4NQ⁻ is noted. The LP-SCFMO-CI calculations were performed for interpreting the spectra shown in Figures 10 and 11. The parameters of NO₂ group are the same as those of the neutral species used in our previous paper¹⁵ except for $\beta_{\text{NO}(\text{NO}_2)}^{\text{core}}$ which is -2.20 eV compared with -3.00 eV for the neutral species. This takes into account the fact that the N—O stretching vibrations, $\nu_{\text{NO}_2}^{\text{NO}}$ (syn and anti forms),

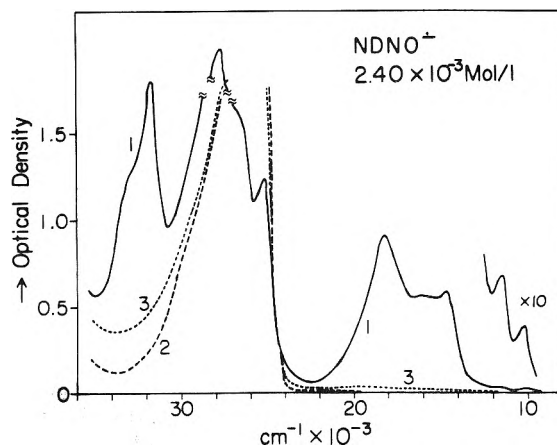


Figure 9. The electronic spectra of 1,5-naphthyridine di-*N*-oxide anion radical (curve 1), and the solution exposed to air (curve 3). Curve 2 and the concentration given in the figure are both for the neutral species.

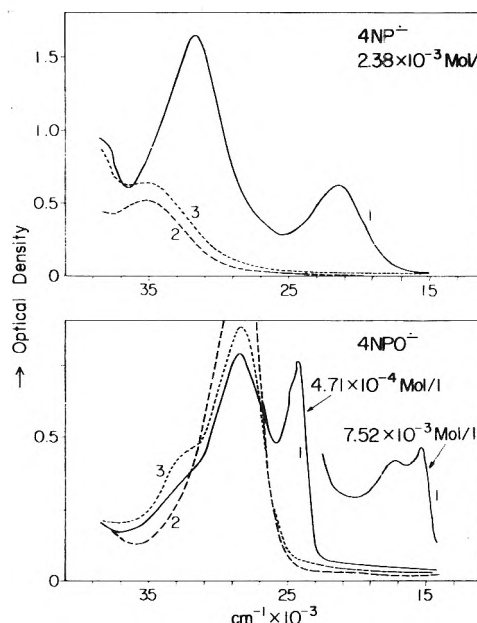


Figure 10. The electronic spectra of the anion radicals of 4-nitropyridine and its *N*-oxide (4NPO). Curves 1, 2, and 3 are for the radical species, the neutral species, and the solution obtained after quenching the radicals with air, respectively. Curve 1 of 4NPO⁻ consists of the radical species and a small amount of the neutral species. The concentrations given in the figure are for the neutral substances.

are shifted quite strongly to lower frequency by the formation of 4NPO and nitrobenzene anion radicals.⁸ The value of $\beta_{\text{NO}(\text{NO}_2)}^{\text{core}} = -2.20$ eV reproduces the 465-nm band (${}^2B_2 \leftarrow {}^2B_2$) of the nitrobenzene anion radical and the 412-nm band (${}^2B_2 \leftarrow {}^2B_2$) of 4NPO⁻ recorded by the present flow technique. Recently the photoelectron (PE) spectra of various basic heterocyclic amine *N*-oxides and their derivatives including 4NPO were recorded and interpreted,²⁴ the results of our calculation being compared with those. The order of calculated filled π MO's of the PNO neutral species is in good agreement with that obtained from the PE spectra²⁴ according to Koopmans' theorem, except that the lone pair orbital energy of *N*-oxide group oxygen atom appears as the second vertical ionization energy. This calculated order is also kept in the case of the PNO anion radical (see Figure 4). However, in the case of the 4NPO anion

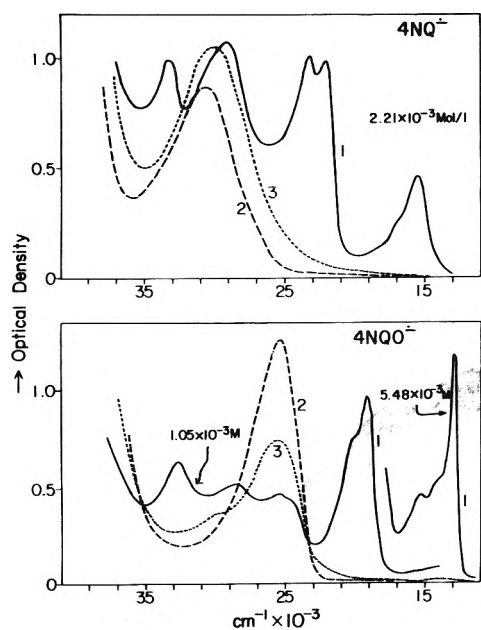


Figure 11. The electronic spectra of the anion radicals of 4-nitroquinoline and its *N*-oxide. Curves 1, 2, and 3 are for the anion radical, starting solution (neutral substances), and the solution exposed to air, respectively. Note that curve 1 consists of the radical species and a small amount of the neutral species. Concentrations shown in the figure are for neutral substances.

radical our LP-SCFM-CI calculation (π electron approximation) shows that the highest filled MO is a $b_{2\pi}$ orbital localized largely on the *N*-oxide group oxygen atom ($b_{2\pi}$: $N \rightarrow O$), but the second and third highest filled MO's are $a_{2\pi}$, localized respectively largely on the NO_2 group oxygen atoms ($a_{2\pi}$: NO_2) and on carbon atoms not present on the molecular C_2 axis ($a_{2\pi}$: ring). Considering the fact that both the PE spectra and our calculation for neutral 4NPO lead to the same order for the first three highest filled MO's, namely, as $b_{2\pi}$: $N \rightarrow O$, lone pair electrons on the $N \rightarrow O$ group oxygen atom, and $a_{2\pi}$: ring; and also taking into account the fact that the sequence of the filled MO's and their characters may not alter greatly between neutral and anion radical species of nitro-substituted aromatics,³⁰ the MO's of 4NPO \cdot^- in the present calculation are good, excepting only the point that the $a_{2\pi}$: NO_2 MO seems to be quite a bit unstabilized. This remains the situation for 4NQO \cdot^- in spite of several modifications of valence state ionization potentials, electron affinities, and β_{NO}^{SOM} in the NO_2 group. From the aforementioned points, and since there is no irregularity on the order of vacant MO's compared with that found in references,^{12,15} it may safely be said that the excited states calculated here, where one-electron transitions from SO to vacant MO's, and from the highest filled MO to SO are the main configurations, could be used for assigning the visible spectra of 4NPO \cdot^- and 4NQO \cdot^- . Such calculated results and the plausible assignment are included in Table I. It is noticed that the calculated excited states for 4NPO \cdot^- listed in Table I agree with those by Gamba et al.⁷ That the NO_2 group in 4NQO is twisted from the ring molecular plane is certain,¹⁵ but the nature of calculated excited states is not greatly affected by a twist angle of $\sim 50^\circ$. Data shown in Table I are for the planar structure. Note that the observed bands of ~ 649 nm (${}^2B_2 \leftarrow {}^2B_2$) and ~ 412 nm (${}^2B_2 \leftarrow {}^2B_2$) of 4NPO \cdot^- arise mainly from the CI of the one-electron transitions from SO (b_2) and the highest filled MO (b_2) to the lowest b_2 vacant

MO and SO, respectively. The ~ 760 - and ~ 518 -nm bands of 4NQO \cdot^- have the same character as those of the ~ 649 - and ~ 412 -nm bands of 4NPO \cdot^- , respectively. That is, the above two bands of 4NQO \cdot^- mainly come from the CI between the one-electron transitions of the lowest vacant MO \leftarrow SO and SO \leftarrow highest filled MO. On the other hand, the absorption band at 461 nm (${}^2B_2 \leftarrow {}^2B_2$) of 4NPO \cdot^- may originate from the electron transition from SO to the lowest vacant b_2 type MO, and the weak band having the transition ${}^2A_2 \leftarrow {}^2B_2$ would be hidden under the 461-nm band. Alternatively it may be said that the 316-nm band of 4NPO \cdot^- corresponds to the 327-nm band of the nitrobenzene anion radical. These interpretations are due to the present calculation results, which are similar to those reported by Shida and Iwata.¹² The observed bands at ~ 646 and 430–453 nm for the 4NQ anion radical may have character similar to the 746- and 400–450-nm bands of 1-nitronaphthalene.¹²

Acknowledgment. The authors are grateful to Professor T. Shida of Kyoto University for carrying out the γ -ray irradiation experiment on 4NPO. The authors wish to express their sincere thanks to Professor emeritus Eiji Ochiai of the University of Tokyo, deceased on Nov. 4, 1974 at 76 years of age, for his continuing interest and encouragement from the beginning of our first work on physicochemical studies of aromatic amine oxides, and pray that he rests in peace.

References and Notes

- (1) T. Kubota, K. Nishikida, H. Miyazaki, K. Iwatani, and Y. Oishi, *J. Am. Chem. Soc.*, **90**, 5080 (1968).
- (2) T. Kubota, Y. Oishi, K. Nishikida, and H. Miyazaki, *Bull. Chem. Soc. Jpn.*, **43**, 1622 (1970).
- (3) K. Nishikida, T. Kubota, H. Miyazaki, and S. Sakata, *J. Magn. Reson.*, **7**, 260 (1972).
- (4) Y. Kawamura, K. Nishikida, and T. Kubota, *Bull. Chem. Soc. Jpn.*, **46**, 737 (1973), and other papers given in ref 1-4.
- (5) E. G. Janzen and J. W. Happ, *J. Phys. Chem.*, **73**, 2335 (1969).
- (6) L. Lunazzi, A. Mangini, G. Placucci, and F. Taddei, *J. Chem. Soc. B*, 440 (1970).
- (7) A. Gamba, V. Malatesta, G. Morosi, C. Oliva, and M. Simonetta, *J. Phys. Chem.*, **77**, 2744 (1973).
- (8) K. Ezumi, H. Miyazaki, and T. Kubota, *J. Phys. Chem.*, **74**, 2397 (1970).
- (9) M. Itoh, T. Okamoto, and S. Nagakura, *Bull. Chem. Soc. Jpn.*, **36**, 1665 (1963). Note that the electronic spectra of aromatic amine *N*-oxide anion radicals have not yet been reported as figures.
- (10) R. E. Sioda and W. Kemula, *J. Electroanal. Chem.*, **31**, 113 (1971).
- (11) T. Shida, *Kagaku No Ryoiki*, **21**, 991 (1967) (review in Japanese).
- (12) T. Shida and S. Iwata, *J. Phys. Chem.*, **75**, 2591 (1971).
- (13) T. Shida and S. Iwata, *J. Am. Chem. Soc.*, **95**, 3473 (1973), and other references therein. Both the electrolysis and the γ -ray irradiation methods also gave the same spectra for the nitrobenzene anion radical.¹²
- (14) H. Miyazaki, T. Kubota, and M. Yamakawa, *Bull. Chem. Soc. Jpn.*, **45**, 780 (1972).
- (15) M. Yamakawa, T. Kubota, K. Ezumi, and Y. Mizuno, *Spectrochim. Acta, Part A*, **30**, 2103 (1974).
- (16) (a) E. Ochiai, "Aromatic Amine Oxides", Elsevier, Amsterdam, New York, N. Y., 1967; (b) A. R. Katritzky and J. M. Lagowski, "Chemistry of the Heterocyclic *N*-Oxides", Academic Press, London, 1971.
- (17) M. Hamana and H. Yoshimura, *J. Pharm. Soc. Jpn.*, **72**, 1051 (1952); M. Hamana, Y. Hoshida, and K. Kaneda, *ibid.*, **76**, 1337 (1956).
- (18) H. C. Longuet-Higgins and J. A. Pople, *Proc. Phys. Soc., London, Sec. A*, **68**, 591 (1955).
- (19) A. Ishitani and S. Nagakura, *Theor. Chim. Acta (Berlin)*, **4**, 236 (1966).
- (20) (a) R. Zahradnik and P. Carsky, *J. Phys. Chem.*, **74**, 1235, 1240, 1249 (1970); (b) S. Hünig, D. Scheutzow, P. Carsky, and R. Zahradnik, *ibid.*, **75**, 335 (1971). (c) R. Zahradnik and P. Carsky, *Theor. Chim. Acta (Berlin)*, **27**, 121 (1972); (d) H. M. Chang and H. H. Jaffe, *Chem. Phys. Lett.*, **23**, 146 (1973).
- (21) The authors wish to thank Mrs. Y. Yamamoto (née Mizuno) in our laboratory for her great cooperation throughout the program check and Dr. S. Iwata of the Institute of Physical and Chemical Research, Japan, for giving us his results.
- (22) (a) M. Yamakawa, T. Kubota, and H. Akazawa, *Theor. Chim. Acta (Berlin)*, **15**, 244 (1969); (b) T. Kubota, M. Yamakawa, and Y. Mizuno, *Bull. Chem. Soc. Jpn.*, **45**, 3282 (1972), and other papers therein.
- (23) This kind of result was also reported for the case of hydrocarbons or heteroconjugated substances.^{13,20}
- (24) (a) J. P. Maier and J.-F. Muller, *Tetrahedron Lett.*, **35**, 2987 (1974); J.

- Chem. Soc., Faraday Trans. 2*, 1991 (1974); (b) J. P. Maier, J.-F. Muller, and T. Kubota, *Helv. Chim. Acta*, **58**, 1634 (1975); (c) J. P. Maier, J.-F. Muller, T. Kubota, and M. Yamakawa, *ibid.*, **58**, 1641 (1975).
- (25) That the type 2 transition (see Figure 4) for QNO⁻ is divided into the 2.17- and 1.90-eV bands (see Table I) and mixes greatly with the 7 → 9 transition (type A) should be noted.
- (26) It is noted that the orbital energy change of MO 10 and 11 (see Figure 4) of ANO⁻ by introducing the N atom at the 8 position (see Table I) is quite small, since the symmetry of these orbitals is a₂, having the nodal plane through the C₂ axis, so that the atomic orbital coefficient at the atoms along the C₂ axis is zero. We can find the same relation as the above in anthracene and naphthalene, too. The atomic orbital coefficients at the 1 and 8 positions of the anthracene anion radical and at the 1, 4, 6, and 9 positions of the naphthalene anion radical are zero for the lowest vacant MO and the next higher MO of the former, and almost are zero for the lowest vacant MO of the latter. The orbital energies of these MO's are therefore insensitive to the replacement of the carbon atoms by nitrogen.
- (27) In the case of pyrazine di-N-oxide this fact was confirmed by analysis of photoelectron spectra.²⁴
- (28) (a) J. Chaudhuri, S. Kume, J. J-Grodzinski, and M. Szwarc, *J. Am. Chem. Soc.*, **90**, 6421 (1968); (b) K. Suga and S. Aoyagui, *Bull. Chem. Soc. Jpn.*, **45**, 1375 (1972).
- (29) Here the change, upon N atom replacement, in the lowest three vacant MO energies, which are intimately correlated with the visible bands, was very small. See ref 26 for explanation.
- (30) For nitrobenzene neutral species our calculated π MO sequence from the highest occupied MO to deeper MO's is: a₂ π : ring, b₂ π , and a₂ π : NO₂, this order being in good agreement with that reported by Kobayashi and Nagakura³¹ using the technique of PE spectroscopy. Alternatively Shida and Iwata¹² gave the corresponding π MO sequence for the nitrobenzene anion radical as: b₂ π (SO), b₂ π , a₂ π : ring, and a₂ π : NO₂. Note that a₂ π : NO₂ MO is deep in energy for both the cases. Since Shida and Iwata's interpretation of the anion radicals of nitrosubstituted aromatics seems to be reasonable, it may be assumed that the a₂ π : NO₂ MO level is deep in these anion radicals, though the MO energies attributable to substituents are quite sensitive to the electron densities upon them.³¹ From this viewpoint the visible spectra of the anion radicals of 4NP⁻ and 4NQ⁻ given in Figures 10 and 11 may be reasonably explained on the basis of the assignment of nitrosubstituted benzene and naphthalene anion radicals.¹²
- (31) T. Kobayashi and S. Nagakura, *Bull. Chem. Soc. Jpn.*, **47**, 2563 (1974).

2,3,7,8-Tetramethoxythianthrene. A Novel Ground State Triplet Dication, the Neutral Photogenerated Triplet, and the Radical Cation

Ira B. Goldberg,* Harry R. Crowe,

Science Center, Rockwell International, Thousand Oaks, California 91360

George S. Wilson, and Richard S. Glass

Chemistry Department, University of Arizona, Tucson, Arizona 85721 (Received October 9, 1975)

Publication costs assisted by Rockwell International

The dication of 2,3,7,8-tetramethoxythianthrene was studied in solid nitromethane at 77 K by computer-controlled electron spin resonance. The $\Delta m = 2$ transition was observed, yielding a value of $D^* = 0.106 \text{ cm}^{-1}$. For comparison the values of D^* for thianthrene and 2,3,7,8-tetramethoxythianthrene photogenerated triplets determined were 0.135 and 0.121 cm^{-1} , respectively. Lifetimes of these triplet states were also determined. Frozen solutions of the tetramethoxythianthrene dication exhibited a very broad $\Delta m = 1$ signal that could not be resolved into components D and E of the dipolar tensor. The free energy separation between the triplet and singlet states is between 90 and 190 cm^{-1} . The ESR spectrum of the cation was re-determined. The hyperfine splittings at 23 °C in nitromethane were $a_S = 7.30 \pm 0.05 \text{ G}$, $a_H(\text{OCH}_3) = 0.28 \pm 0.02 \text{ G}$, and $a_H(1,4,6,9) = 0.87 \pm 0.04 \text{ G}$, and the g factor is 2.00732 ± 0.00006 .

Introduction

A recent publication reported the preparation and isolation of the diperchlorate salt of the 2,3,7,8-tetramethoxythianthrene (TMTh²⁺) dication.¹ The NMR spectrum of solutions of TMTh²⁺ consisted of two broad singlets. The singlets due to both the methoxy group protons as well as the aromatic protons were shifted farther downfield from Me₄Si than expected. In addition, this spectrum was found to be broad and also concentration dependent, suggesting some paramagnetic character to the solution, although these solutions exhibited no ESR spectrum. Furthermore, the optical absorption maximum of TMTh⁺ occurred at 765 nm while that of TMTh²⁺ occurred at 710 nm. In comparison, the absorption maxima of Th⁺ and Th²⁺ occurred at 543 nm^{2,3} and 311 nm,⁴ respectively.

These results suggested that the ground state of TMTh²⁺ may be a triplet, or that the triplet state is ther-

mally accessible. A structure of the form TMTh²⁺ would not be expected to have a low-lying triplet state. Typically, aromatic species which exhibit this property have D_{3h} or greater symmetry, or the unpaired electrons may be localized on either of two sites such as in biradicals, where the electron-electron interactions are weak.

We report here preliminary ESR studies on the diperchlorate salt of TMTh²⁺ in nitromethane. During these studies we found that very little information on the photogenerated triplet states of thianthrene is available in the literature. As a result, we also report here preliminary ESR studies on ³Th and ³TMTh since these data were necessary for comparison with ESR data on ³TMTh²⁺. The ESR spectrum of TMTh⁺ in nitromethane was reinvestigated. A previous publication reports ³³S hyperfine splittings (hfs) of the ESR spectrum, but no interpretation of the proton hfs is given.⁵

Experimental Section

TMTh was prepared by the method of Fries et al.⁶ The salt $\text{TMTh}^{2+}(\text{ClO}_4^-)_2$ was prepared by oxidation with perchloric acid.¹ Th was obtained from Aldrich Chemical Co. and purified by sublimation prior to use. Nitromethane (Matheson, spectral grade) was purified by drying and storage over calcium hydride, followed by vacuum distillation into aluminum chloride then to the ESR sample tube immediately before use. Spectral grade toluene and absolute ethanol were used as received for photolysis experiments.

The ESR spectrometer was a modified Varian V-4502 X-band spectrometer interfaced with a laboratory computer (Digital Equipment PDP-8m). The apparatus and programs used in this work are described elsewhere.⁷ Continuous photolysis was carried out using a 200-W mercury lamp. In several cases, the ESR spectrum was averaged by sweeping the field at about 30 G/s 128 times, collecting data at increments of between 0.3 and 6 G. Flash photolysis experiments which were used to determine lifetimes were carried out using a flash lamp constructed by Photochemical Research Associates, London, Ontario, Canada. The method of stepping the field to desired locations and averaging between 32 and 128 flashes was used.⁷ The modulation frequency used was 100 kHz, with a 3-ms filter. Lifetimes were determined from the decay curves. Spectra at different times were reconstructed from the time-dependent data.

ESR spectra of the radical ion were recorded as described elsewhere.⁸ A perylene radical anion reference⁹ was used for field calibration and for the g factor determination.¹⁰

The temperature dependence of the Q factor was corrected in quantitative studies of the temperature dependence of the $\Delta m = 2$ transition of TMTh^{2+} by using a sample of DPPH dissolved in nitromethane. The ESR signal was double integrated and multiplied by temperature. A 5% decrease of this value was observed between 115 and 220 K. At 230 K, the double integral decreased considerably due to the loss of the high dielectric liquid.

Results and Discussion

Photogenerated Triplet States. ESR spectra recorded in the region $\Delta m = 2$ for ${}^3\text{Th}$, ${}^3\text{TMTh}$, and ${}^3\text{TMTh}^{2+}$ are shown in Figure 1. In all cases only the $\Delta m = 2$ transition could be utilized. In the cases of ${}^3\text{Th}$ and ${}^3\text{TMTh}$, the $\Delta m = 1$ transition of the randomly oriented material is too weak to detect even after averaging up to 64 repetitive field scans from 1500 to 5500 G. In the case of ${}^3\text{TMTh}^{2+}$, the $\Delta m = 1$ transition region gave a broad line with a peak-to-peak width of about 3000 G, showing no structure. Values of D^*

$$D^* = (D^2 + 3E^2)^{1/2} \quad (1)$$

where D and E are the principal components of the traceless electron-electron dipolar interaction tensor,¹¹ were calculated from the magnetic field at the derivative maximum (H_m) of the $\Delta m = 2$ transition using

$$D^* = [3/4(h\nu)^2 - 3(g\beta H_m)^2]^{1/2} \quad (2)$$

The g factors were assumed to be those of the respective radical cations:¹⁵ 2.0081 for ${}^3\text{Th}$ and 2.0073 for ${}^3\text{TMTh}$ and ${}^3\text{TMTh}^{2+}$. Values of D^* are given in Table I.

Lifetimes measured for the metastable triplets are also given in Table I. The lifetime of ${}^3\text{Th}$ is in reasonable agreement with the value of 58 ms in ethanol-ether-isopentane

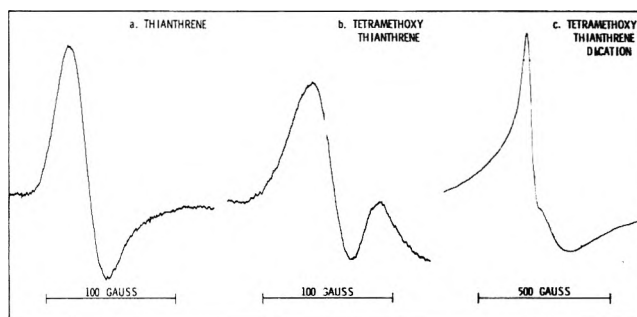


Figure 1. ESR spectra of the $\Delta m = 2$ transition of triplet states of thianthrene derivatives at -196°C : (a) thianthrene in toluene, $\nu = 9.275$ GHz; (b) tetramethoxythianthrene in toluene, $\nu = 9.275$ GHz; (c) tetramethoxythianthrene dication in nitromethane, $\nu = 9.278$ GHz.

TABLE I: Parameters of Triplet States of Thianthrene and Tetramethoxythianthrene

	Solvent	D^* , cm^{-1}	$\tau_{1/2}$, ^c ms
${}^3\text{Th}$	Ethanol	0.135 ^a	45
${}^3\text{Th}$	Toluene	0.132 ^a	40
${}^3\text{TMTh}$	Ethanol	0.121 ^b	
${}^3\text{TMTh}$	Toluene	0.117 ^b	34
${}^3\text{TMTh}^{2+}$	Nitromethane	0.106 ^b	

^a Assume $g = 2.0081$. ^b Assume $g = 2.0073$. ^c Temperature is -196°C .

at -196°C , measured by phosphorescence techniques.¹² Local heating due to the intense flash may be responsible for slightly smaller lifetimes observed here. The fact that ${}^3\text{TMTh}$ has a shorter lifetime than ${}^3\text{Th}$ is consistent with its more complex structure. Lifetimes of triplet states are also generally inversely dependent upon the spin-orbit coupling of atoms conjugated with the heterocyclic structure.

The value of D^* for ${}^3\text{Th}$ is slightly larger than that of ${}^3\text{TMTh}$. This suggests similar structures of both triplet states, but with larger delocalization of the unpaired electrons in ${}^3\text{TMTh}$. The stabilizing effect of the OCH_3 groups would be expected to have this effect. The value of D^* of ${}^3\text{Th}$ (0.135 cm^{-1}) is much larger than that of triplet anthracene (${}^3\text{An}$) ($D^* = 0.0770$,¹³ $D = 0.0724$, $E = 0.0081 \text{ cm}^{-1}$ ¹⁴).

The values of D and E are determined from the expectation values of interelectron distances shown in

$$|D| = \frac{3}{4} g^2 \beta^2 \left\langle \frac{r^2 - 3z^2}{r^5} \right\rangle \quad (3)$$

and

$$|E| = \frac{3}{4} g^2 \beta^2 \left\langle \frac{x^2 - y^2}{r^5} \right\rangle \quad (4)$$

The coordinate system of the molecule is determined by the diagonalized dipolar interaction tensor. For ${}^3\text{An}$, x is the long axis and y is the short axis of the molecule, and z is perpendicular to the plane of the molecule.¹⁵ For discussion, the same axis system for ${}^3\text{Th}$ may be assumed, although ${}^3\text{An}$ is planar while ${}^3\text{Th}$ may be nonplanar as in its ground state which is bent by about 128° .¹⁶ Assuming similar electron distribution in ${}^3\text{Th}$ and ${}^3\text{An}$, then in ${}^3\text{An}$, $r^2 - 3z^2$ and $x^2 - y^2$ are expected to be larger than in ${}^3\text{Th}$, but also r^5 should be much larger resulting in smaller values of D and E than in ${}^3\text{Th}$. Also, in ${}^3\text{Th}$, the electron density

would be expected to be centered around the sulfur atoms which would also result in a larger value of D^* . The delocalizing ability of the OCH_3 can similarly account for the fact that D^* of ^3Th is larger than that of $^3\text{TMTh}$. In a series of measurements, values of D^* were found to decrease in the following order: dibenzothiophene > dibenzofuran > fluorene > carbazole; however, the entire range of values is from 0.113 to 0.103 cm^{-1} .¹⁷ In the above series, the heteroatom does not contribute significantly, whereas here, the heteroatom plays a significant role in the determination of the zero field splittings.

Tetramethoxythianthrene Dication. The spectrum of $^3\text{TMTh}^{2+}$ in the $\Delta m = 2$ region is shown in Figure 1c. The value of D^* is 0.106 cm^{-1} , somewhat smaller than that of $^3\text{TMTh}$. Several species may be postulated which exhibit this spectrum: ground state triplet of TMTh^{2+} , the dimer of the form $(\text{TMTh}^+)_2$, or an entirely different ground state triplet.

Solutions of TMTh^{2+} which exhibit no ESR spectrum at the $g = 2$ region at 25 °C exhibit a strong spectrum in the $\Delta m = 2$ region of the triplet state spectrum at -196 °C. If excess TMTh is added to the warm solution a spectrum attributed to TMTh^+ is observed. Freezing the solution again results in a strong absorption at the $g = 2$ region as well as a weaker absorption at $\Delta m = 2$. It will be shown elsewhere that there is significant disproportionation of TMTh^+ into the neutral molecule and dication. These results rule out the possibility of the dimer of TMTh^+ as well as an impurity due to reaction of TMTh^{2+} with the solvent as being responsible for the $\Delta m = 2$ spectrum. Furthermore, dimers of similar sized molecules which are in ground triplet states generally exhibit considerably smaller values of D^* . For example, the value of D^* of the dimer of the phenothiazine cation is 0.021 cm^{-1} .¹⁸ The thianthrene cation was also found to dimerize,² but the aggregate exhibited no ESR spectrum. This was confirmed by our own measurements at -196 °C.

The magnitude and reproducibility of the $\Delta m = 2$ spectrum indicates that this spectrum is due to the $^3\text{TMTh}^{2+}$. By comparison dianions and dications, which exhibit ground state triplets, generally have D_{3h} or greater symmetry, such as $\text{C}_6\text{Cl}_6^{2+}$ ¹⁹ and hexamethoxytriphenylene²⁺.²⁰ Simple Hückel molecular orbital (HMO) calculations (see below) do not predict the degeneracy required to obtain a triplet state dication.

The molar susceptibility of a system containing a ground state triplet and a thermally accessible singlet is given by²¹

$$\chi_m = \frac{S(S+1)}{3kT} g^2 \beta^2 N \frac{1}{[1 + \exp(-\Delta G/RT)]} \quad (5)$$

A plot of the ESR signal multiplied by the temperature and corrected for the temperature dependence of the Q factor of the cavity is plotted against the temperature in Figure 2. If ΔG is treated as a constant then two curves fit this data, $\Delta G = 0.54 \pm 0.10$ kcal and $\Delta G = 0.026 \pm 0.08$ kcal. Since these values are based on observations of the $\Delta m = 2$ transitions where the complete triplet state wavefunction must be known in order to compute the transition probability, we have no method of determining the concentration in order to determine the experimental error. This may be due in part to a smaller value for the entropy than the expected $R \ln 3$, due to solvation or structural differences between the singlet and triplet dications. Consequently, we must assign a value of 0.40 ± 0.20 kcal to the free energy difference. This small value of ΔG indicates that the near

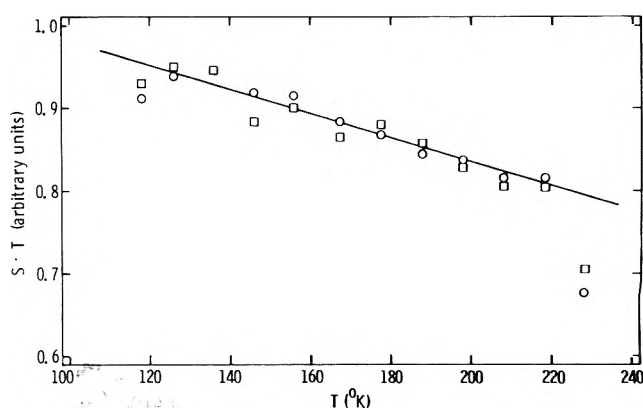


Figure 2. Temperature dependence of the $\Delta m = 2$ ESR signal of the tetramethoxythianthrene dication in nitromethane: O, double integration of the line shape; □, peak-to-peak amplitude.

degeneracy required for the formation of the triplet state is accidental and results from unique properties resulting from the substituent groups.

The magnitude of D^* for $^3\text{TMTh}^{2+}$ is smaller than that of $^3\text{TMTh}$. In the dication, due to greater repulsive forces, the unpaired electrons are probably more separated. Simple resonance structures also suggest that the $^3\text{TMTh}^{2+}$ will be more planar resulting in smaller values for D and E as described above.

The absence of a well-resolved spectrum of $\Delta m = 1$ transitions and the relatively large line width of the $\Delta m = 2$ transition suggest that the dication may be undergoing some intramolecular processes. This bears further investigation at temperatures below -196 °C.

Radical Cation. The ESR parameters derived from the TMTh^+ cation radical are given in Table II, and the ESR spectrum and simulation are shown in Figure 3. A recent publication⁵ reported a similar spectrum but gave no analysis of the proton hyperfine lines. The ^{33}S hfs was re-measured and found to be 7.30 ± 0.05 G over the temperature range -25 to +35 °C, significantly smaller than the value 7.91 G previously reported.⁵ The g factor of TMTh^+ was determined to be 2.00732 ± 0.00006 . Similar measurements on Th^+ were also carried out. A solution of $\text{Th}^+\text{ClO}_4^-$ salt in CH_3NO_2 yielded the following parameters at 20 °C: the proton hfs were 1.29 and 0.14 G each for four equivalent protons; the ^{33}S hfs was 8.97 ± 0.04 G; the g factor was 2.00830 ± 0.00006 , in good agreement with published values.^{3,5,27}

The large difference between g factors of TMTh^+ and Th^+ can be explained by the different spin distributions in radical ions. The largest contribution to the g factors arise from the sulfur atoms which exhibit the largest spin-orbit coupling constant ζ ($\zeta_{\text{S}} = 382$ cm^{-1} , $\zeta_{\text{O}} = 151$ cm^{-1} , and $\zeta_{\text{C}} = 28$ cm^{-1}), and also have the largest contribution to the spin density. In this case, the shift of the g factor from the free electron value is approximately given by²⁶

$$g - g_e \sim \frac{2}{3} \frac{\zeta_{\text{S}} \rho_{\text{S}} \pi}{\Delta E_{(n-\pi^*)}} \quad (6)$$

The ratio of $(g - g_e)$ for Th^+ to that for TMTh^+ is 1.20 ± 0.02 , in excellent agreement with the ratio of the sulfur hyperfine splittings of 1.23. This assumes that $E_{(n-\pi^*)}$ is nearly the same for both cations.

HMO calculations were carried out to support the analysis of TMTh^+ . The resonance and Coulomb integral pa-

TABLE II: ESR Parameters and Molecular Orbital Calculations for 2,3,7,8-Tetramethoxythianthrene Cation Radicals

Position	Atom	Experimental hfs ^a	Molecular orbital calculations ^b			
			$k_{CO} = 1.22$	$h_O = 1.51$	$k_{CO} = 1.00$	$h_O = 2.50$
			ρ^π	a	ρ^π	a
1,4,6,9	C	0.87 ± 0.04 (H)	-0.027	0.74 (H)	-0.024	0.61 (H)
2,3,7,8	C		0.087		0.078	
11,12,13,14	C		0.082		0.094	
OCH ₃	O	0.28 ± 0.02 (H)	0.057	1.11 (H)	0.013	0.25 (H)
5,10	S	7.30 ± 0.05 (S)	0.103	3.44 (S)	0.177	7.16 (S)
ΔE				$0.22\beta_0$		$0.40\beta_0$
g		2.00732 ± 0.00006				

^a TMTh⁺ClO₄⁻ at 23 °C in nitromethane. ^b $Q_{CH^H} = -26$, $Q_{OCH_3^H} = 19.7$ (ref 23), $Q_S^S = 40.3$. Other parameters are discussed in the text.

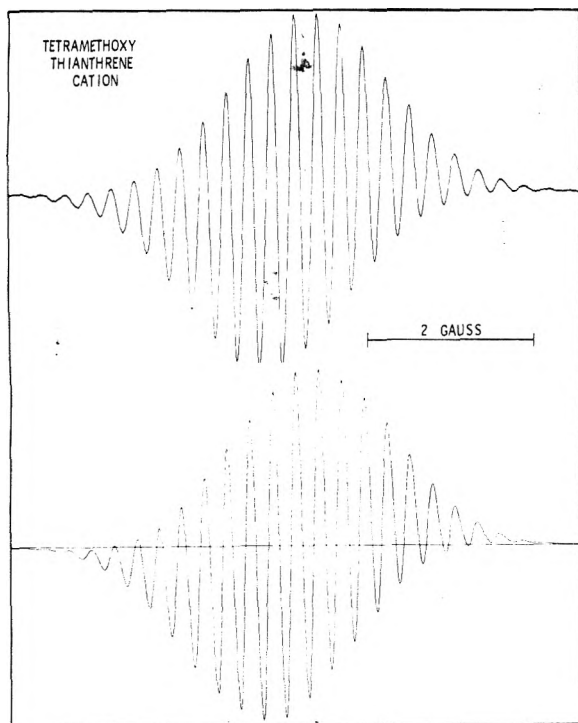


Figure 3. ESR spectrum of the 2,3,7,8-tetramethoxythianthrene cation at 23 °C, and spectrum simulation.

Parameters were $k_{OC} = 0.65\beta^0$ and $h_S = \alpha^0 + 1.20\beta^0$,⁵ where β^0 is the Coulomb integral for a C-C π bond. The C-OCH₃ fragment was treated using the heteroatom model. Values of k_{OC} were varied between 0.6 and $1.2\beta^0$ while h_{OCH_3} was varied between $\alpha^0 + 1.3\beta^0$ and $\alpha^0 + 3.0\beta^0$ as was done for the dimethoxy derivatives of anthracene, naphthalene, and benzene.²² The heteroatom model gives nearly identical results to the hyperconjugative model if the parameters listed in ref 22 are used. The value of λ for the McLachlan perturbation calculation was 1.20.²³ In order to calculate the hyperfine splittings, the following equations were used: $a_S = Q_S^S \rho_S^\pi$ where $Q_S^S = 40.3$,^{5,28} $a_H(CH) = Q_{CH^H} \rho_C^\pi$ where $Q_{CH^H} = -26$, and $a_H(OCH_3) = Q_{OCH_3^H} \rho_O^\pi$ where $Q_{OCH_3^H} = 19.7$.²⁴

Calculated hyperfine splittings and spin densities are given in Table II. The results are tabulated for the parameters $h_O = \alpha^0 + 1.51\beta^0$ and $k_{CO} = 1.22\beta^0$ which are the optimum parameters for the dimethoxybenzene cation, and the values $h_O = \alpha^0 + 2.50\beta^0$ and $k_{CO} = 1.00\beta^0$ which give the

best agreement with the experimental results. Sullivan et al.²² suggested that, as the degree of conjugation in the aromatic system increases, the value of k_{CO} should decrease while that of h_O should increase because of reduced conjugation of the OCH₃ groups with the aromatic system. This behavior is confirmed here.

It is also of interest to compare the energy separation between the two highest energy bonding orbitals so that these could be related to the triplet TMTh²⁺. Depending on the parameters used in the calculation the energy difference between the two highest bonding orbitals is between 0.2 and $0.4\beta^0$, or about 0.5 to 1 eV. This separation is larger than one would expect from HMO values for accidental degeneracy. It is possible that there are some conformational changes between the cation and dication.

An anomaly of the ESR spectrum of TMTh⁺ is the large line width (0.16 G peak-to-peak). In comparison the line width of Th⁺ is about 0.07 G. The large line width may in fact be due to a large variety of relaxation processes, one of which may be relaxation due to Jahn-Teller effects such as in the benzene or triphenylene radical ions.

Conclusions

The $\Delta m = 2$ transitions of the photogenerated triplet states of Th and TMTh were investigated and their lifetimes were determined.

The dication TMTh²⁺ was found to be in a ground triplet state. The value of D^* determined from the $\Delta m = 2$ transition is similar to that of ³TMTh. This result is unexpected considering the symmetry and high degree of conjugation within the molecule.

The hyperfine splittings and g factor of the spectrum of TMTh⁺ were measured. The optimum HMO parameters were determined. Based on these values, the energy level separation between the two highest energy bonding orbitals is predicted to be too large for the dication to be in a ground triplet state. This may reflect conformational changes between TMTh⁺ and TMTh²⁺. More sophisticated calculations are now in progress.

Acknowledgments. This work was supported by the Office of Naval Research and by the National Institutes of Health. Helpful discussions with Dr. Paul Sullivan (Ohio University) are appreciated.

References and Notes

- (1) R. S. Glass, W. J. Britt, W. N. Miller, and G. S. Wilson, *J. Am. Chem. Soc.*, **95**, 2375 (1973).
- (2) M. deSorgo, B. Wasserman, and M. Szwarc, *J. Phys. Chem.*, **76**, 3468

- (1972).
- (3) H. J. Shine, C. F. Dais, and R. J. Small, *J. Org. Chem.*, **29**, 21 (1964).
- (4) H. J. Shine and D. R. Thompson, *Tetrahedron Lett.*, 1591 (1966).
- (5) P. D. Sullivan, *J. Am. Chem. Soc.*, **90**, 3618 (1968).
- (6) K. Fries, H. Koch, and H. Stuckenbrock, *Justus Liebigs Ann. Chem.*, **478**, 162 (1929).
- (7) I. B. Goldberg, R. S. Carpenter, II, and H. R. Crowe, *J. Magn. Reson.*, **18**, 84 (1975).
- (8) I. B. Goldberg, H. R. Crowe, and R. W. Franck, *J. Phys. Chem.*, **79**, 1740 (1975).
- (9) J. R. Bolton, *J. Phys. Chem.*, **72**, 3702 (1967).
- (10) R. D. Allendoerfer, *J. Chem. Phys.*, **55**, 3615 (1971); B. G. Segal, M. Kaplan, and G. K. Fraenkel, *ibid.*, **43**, 4191 (1965).
- (11) J. E. Wertz and J. R. Bolton, "Electron Spin Resonance", McGraw-Hill, New York, N.Y., 1972, Chapter 10.
- (12) H. V. Drushel and A. L. Sommers, *Anal. Chem.*, **38**, 10 (1966).
- (13) B. J. Smaller, *J. Chem. Phys.*, **37**, 1578 (1962).
- (14) E. Wasserman, L. C. Snyder, and W. A. Yager, *J. Chem. Phys.*, **37**, 1148 (1962).
- (15) J-Ph. Grivet, *Chem. Phys. Lett.*, **4**, 104 (1969).
- (16) I. Rowe and B. Post, *Acta Crystallogr.*, **11**, 372 (1958); H. Lynton and E. G. Cox, *J. Chem. Soc.*, 4886 (1956).
- (17) S. Siegel and H. S. Judeikis, *J. Phys. Chem.*, **70**, 2201 (1966).
- (18) Y. Tsujino, *Tetrahedron Lett.*, 2545 (1968).
- (19) E. Wasserman, R. S. Hutton, V. J. Kuck, and E. A. Chandross, *J. Am. Chem. Soc.*, **96**, 1965 (1974).
- (20) K. Bechgaard and V. D. Parker, *J. Am. Chem. Soc.*, **94**, 4749 (1972).
- (21) W. D. Horrocks, Jr., *J. Am. Chem. Soc.*, **87**, 3779 (1965).
- (22) P. D. Sullivan, *J. Phys. Chem.*, **74**, 2563 (1970).
- (23) A. D. McLachlan, *Mol. Phys.*, **3**, 233 (1960).
- (24) W. F. Forbes and P. D. Sullivan, *Can. J. Chem.*, **48**, 1501 (1968).
- (25) P. D. Sullivan and J. R. Bolton, *J. Magn. Reson.*, **1**, 357 (1969).
- (26) A. J. Stone, *Mol. Phys.*, **6**, 509 (1963).
- (27) J. E. Wertz and J. L. Vivo, *J. Chem. Phys.*, **23**, 2193 (1955).
- (28) To preserve the pairing theorem, in the McLachlan calculation, cation radicals and anion radicals of aromatic hydrocarbons are both considered to have all bonding orbitals occupied.²³ This treatment is extended to the thianthrene derivatives here. In ref 5 and 25 the unpaired electron is considered to be in an "empty" orbital. Thus spin densities calculated here are about 10% smaller than those of Sullivan^{5,25} and Q_S^5 would therefore be 10% larger. This magnitude of discrepancy is only found when energy level separations are small.

A Unified Theory for Molecular Charge Transfer

Ying-Nan Chiu

Center for Molecular Dynamics and Energy Transfer, Department of Chemistry, The Catholic University of America, Washington, D.C. 20064 (Received July 7, 1975; Revised Manuscript Received January 21, 1976)

Publication costs assisted by a Gulf Oil Foundation Grant to the Department of Chemistry, The Catholic University of America

A unified molecular charge transfer (CT) theory is developed which embraces all ranges of molecular interactions. In the limit of strong electronic effect (uv and visible region), it reduces to Mulliken's theory of CT molecular complexes; in the limit of dominating vibrational effect (ir and far-ir region), it reduces to Hush's theory of intervalence charge transfer. This unifying theory introduces internal molecular vibration into Mulliken's electronic CT theory and electronic resonance interaction into Hush's simple model. It shows the relationship between the two existing theories and introduces Franck-Condon factors into the intensity formula of both. Generalized energy (eq 2c) and intensity (eq 5c) formulas are derived to cover all ranges of electronic resonance interaction and vibrational structural changes. It is shown that in the case of weak electronic coupling, a double well potential results (eq 8) which is the basis of Hush's double harmonic oscillator model. Modified formulas for optical transition frequencies (eq 9) and for the Franck-Condon thermal barrier (eq 10) are derived to include electronic effects in intervalence electron transfer. Self-consistent ways for the construction of vibrational wave functions and derivation of intervalence transition intensity under different weak coupling conditions are shown (eq 11-13). These generalized formulas containing different interaction parameters, when applied to experimental data, will help identify the size and nature of such interactions.

Electron transfer theory has been developed along two separated lines. One line traces back to the charge transfer theory of Mulliken.^{1,2} It deals mainly with electronic effects and is related to transitions in the uv or visible region (e.g., the 2900-Å absorption of the benzene-iodine complex¹). It is also related to the formation of molecular complexes.² Another line traces back to the intervalence transfer theory of Hush.³ It deals mainly with vibrational effects and is related to transitions in the ir or far-infrared region (e.g., the 19 000-Å absorption of the ferrocene complex⁴). It is also related to electron-transfer reactions.⁵

Mulliken's theory makes no explicit mention of molecular structural change upon charge transfer, nor does it treat vibrational structure in the transition. The only nuclear parameter used, the intermolecular distance R , is completely

divorced from the internal molecular vibrational coordinates. Hush's theory, in its use of two displaced harmonic oscillators, neglects electronic effect and does not lend itself to the inclusion of two Franck-Condon overlap factors (one for the donor and one for the acceptor).

Even though there are some modern improvements in the above theories,^{6,7} it remains highly desirable to have a theory which relates the two theories and covers the whole (electronic and vibrational) range and which gives more general formulas for intensity and energies that, when compared with experiment, will shed light on the nature and size of the molecular interactions involved. This is especially important in view of current experimental interests.⁸

We shall attempt to give semiquantitatively such a unified theory, useful in all ranges, and will show that in the

limit it reproduces the essential features of Mulliken's as well as Hush's theory. We shall also introduce Franck-Condon factors not previously included. Our formalism is parallel to the exciton theory for energy transfer between dimers treated by Förster⁹ and others.¹⁰

Our theory starts by considering both electronic and vibrational energies. In the limit of large electronic effect it is shown to reduce to Mulliken's theory for charge transfer between (electronically dissimilar) molecules. In the limit of vanishing electronic effect it is shown to reduce to Hush's theory for intervalence transfer between (electronically "similar") molecule and its own ion. In the intermediate range, it accounts for both electronic and vibrational effects hitherto not considered. Mulliken's and Hush's results are, of course, not new. However, a unifying view and a self-consistent derivation of both from the same starting point and for all ranges of interaction is new.

Given a "donor" (D) and an "acceptor" (A) molecule, we start with the "neutral" (DA) and charge-transferred (D^+A^-) wave functions and their corresponding electronic and vibrational energies as follows:

$$\begin{aligned} \psi_1 &= \phi_D \phi_A; W_{DA} = W_D + W_A + V_{DA} \\ &+ \frac{1}{2} \frac{\partial^2 V_{DA}}{\partial R^2} R^2 + \frac{k_D}{2} (Q_D - Q_D^0)^2 + \frac{k_A}{2} (Q_A - Q_A^0)^2 \quad (1a) \\ \psi_2 &= \phi_{D^+} \phi_{A^-}; W_{D^+A^-} = W_{D^+} + W_{A^-} + V_{D^+A^-} \\ &+ \frac{1}{2} \frac{\partial^2 V_{D^+A^-}}{\partial R^2} R^2 + \frac{k_{D^+}}{2} (Q_D - Q_D^0)^2 \\ &+ \frac{k_{A^-}}{2} (Q_A - Q_A^0)^2 \quad (1b) \end{aligned}$$

where R is a symbol for pertinent intermolecular distance, other symbols such as the force constant, k , and the nuclear coordinate, Q , in the harmonic oscillator approximation are self-explanatory. Specifically, Q_D^0 is the equilibrium nuclear configurational coordinate of the free donor D before the charge is given away. Q_D is the instantaneous nuclear coordinate of the donor. Since Q_D describes the nuclear positions, it is, of course, the same variable whether the donor is charged (D^+) or neutral (D). k_D is the force constant for free D and $(k_D/2)(Q_D - Q_D^0)^2$ is the harmonic oscillator energy for displacement from the equilibrium nuclear coordinates of D. Other symbols in k and Q have parallel meaning. The energy² G_0 due to the formation of the hypothetical neutral DA is contained in the interaction V_{DA} and the latter's coordinate dependence, e.g. $\frac{1}{2}(\partial^2 V_{DA}/\partial R^2)R^2$ at the equilibrium separation of D and A. Introduction of interaction mixing results in a 2×2 secular determinant with standard solutions and energies:

$$\Psi_+ = \Psi_N = \cos \alpha \phi_D \phi_A + \sin \alpha \phi_{D^+} \phi_{A^-} \quad (2a)$$

$$\Psi_- = \Psi_V = \sin \alpha \phi_D \phi_A - \cos \alpha \phi_{D^+} \phi_{A^-} \quad (2b)$$

$$W_{\pm} = \frac{1}{2}(W_{DA} + W_{D^+A^-}) \mp \frac{1}{2}[(W_{D^+A^-} - W_{DA})^2 + 4|u|^2]^{1/2} \quad (2c)$$

where $u = H_{12} - ES_{12}$ is the resonance integral in Hückel approximation and α is defined through

$$\tan 2\alpha = \frac{2u}{W_{DA} - W_{D^+A^-}} \quad (3)$$

Inasmuch as the resonance integral u in the numerator is dependent on molecular separation R , the state function Ψ_{\pm} is dependent on R as well as on the vibrational coordinates Q which occur in the denominator. It will be shown

later (eq 6b) that the wave function will depend on the out-of-phase combination of the nuclear coordinates of the donor and acceptor.

For charge transfer between dissimilar molecules, the electronic energy difference predominates over vibrational energy difference and gives a large denominator in (3) compared with the numerator, thus giving a small α . As a result we obtain, after identifying $W_D - W_{D^+}$ ($= -I_A$) as the negative of the ionization potential and $W_A - W_{A^-}$ ($= E_A$) as the electron affinity

$$\tan 2\alpha \approx 2\alpha; \cos \alpha \approx 1$$

$$\begin{aligned} \sin \alpha \approx \alpha \approx & \frac{u}{(W_D + W_A + V_{DA}) - (W_{D^+} + W_{A^-} + V_{D^+A^-})} \\ \approx & \frac{u}{-I_D + E_A + V_{DA} - V_{D^+A^-}} \quad (4a) \end{aligned}$$

and

$$\Psi_+ = \Psi_N \approx \phi_D \phi_A + \alpha \phi_{D^+} \phi_{A^-} \quad (4b)$$

$$\Psi_- = \Psi_V \approx \alpha \phi_D \phi_A - \phi_{D^+} \phi_{A^-} \quad (4c)$$

which, except for normalization, is in essential agreement with Mulliken's wave functions for the ground and charge-transferred states.^{1,2} The corresponding charge-transfer energy also approximates the acknowledged form $W_- - W_+ \equiv W_{D^+A^-} - W_{DA} \approx I_D - E_A + V_{D^+A^-} - V_{DA}$. When the electronic energy difference is of the same order as the vibrational energy spacing, the complete formulas (2c), (1a), (1b) may then be used. Taking into account the vertical Franck-Condon transition from equilibrium configuration of the donor (D) and acceptor (A) (to D^+ and A^- , respectively), one may set $Q_D = Q_D^0$ and $Q_A = Q_A^0$.

If the donor and acceptor electronic states interact strongly to form a complex, then their vibration is governed by one resultant *molecular* potential curve. The linear combination of electronic states in eq 4b,c will be multiplied¹¹ by one vibrational wave function χ^{\pm} . Since the equilibrium position of the lower (Ψ_+) and upper states (Ψ_-) do not coincide, vertical transition from the ground vibrational level necessarily ends in the excited vibrational level of the upper state. The wave functions and charge transfer transition moment up to the first order in α are

$$\Psi_+^N = (\phi_D \phi_A + \alpha \phi_{D^+} \phi_{A^-}) \chi_{00}^+ \quad (5a)$$

$$\Psi_-^V = (\alpha \phi_D \phi_A - \phi_{D^+} \phi_{A^-}) \chi_{\mu\nu}^- \quad (5b)$$

$$D = \alpha(r_D - r_A) \int \chi_{00}^+ \chi_{\mu\nu}^- d\mathbf{Q} - \int \phi_{D^+} \phi_{A^-} r \phi_D \phi_A d\zeta \int \chi_{00}^+ \chi_{\mu\nu}^- d\mathbf{Q} \quad (5c)$$

which is also in essential agreement with Mulliken's results except for our introduction of Franck-Condon factors. It should be noted that because of the relatively small coefficient α (eq 4a, compared with vibrational trapping see below) for electronic mixing of the "neutral" and charge-transferred wave functions, the first term in the transition moment containing α may be less significant than the second term, which contains the "overlap" moment $r_{DA} = \int \phi_{D^+} \phi_{A^-} r \phi_D \phi_A d\zeta$. The relative contribution of these two theoretical terms in intensity, when checked by experimental total intensity, should yield information on the nature of the intermolecular interaction.

In the other extreme, when the electronic energy difference is zero (as in the case of symmetric intervalence transfer between the same species treated by Hush), only the vibrational energy difference will remain in $W_{D^+A^-} - W_{DA}$ in the energy expression (2c). As a result, the relative size of

the vibrational energy and the resonance integral (u) becomes important. Symbolically, instead of $D + A \rightarrow D^+ + A^-$ we now have $M_1 + M_2^+ \rightarrow M_1^+ + M_2$ where M_1 and M_2 refer to similar molecules. If we assume the force constant (k) to be the same for the molecule (M) and its ion (M^+) but the equilibrium distances to be different ($Q^+ > Q^0$), then the energy and parameter α in eq 2 and 3 are defined as

$$W_{\pm} = W_M + W_{M^+} + V_{MM^+} + (k/4) [(Q^+ - Q^0)^2 + (Q_1 + Q_2 - Q^+ - Q^0)^2 + (Q_1 - Q_2)^2] \\ = \frac{1}{2} [k^2(Q_1 - Q_2)^2(Q^0 - Q^+)^2 + 4|u|^2]^{1/2} \quad (6a)$$

$$\tan 2\alpha = \frac{2u}{k(Q_1 - Q_2)(Q^+ - Q^0)} \quad (6b)$$

Therefore the coefficients $\cos \alpha$ and $\sin \alpha$ in the wave function will contain the out-of-phase combination $(Q_1 - Q_2)$ of nuclear coordinates. Regardless of the size of (u), the upper potential W_- always has one minimum at $Q_1 = Q_2 = \frac{1}{2}(Q^+ + Q^0)$.

$$W_{-}^{\min}(\text{strong and weak coupling}) = W_M + W_{M^+} + V_{MM^+} + (k/4)(Q^+ - Q^0)^2 + |u| \quad (7a)$$

For $|u| \geq \frac{1}{2}k(Q^+ - Q^0)^2$, the lower potential W_+ also has one minimum at $Q_1 = Q_2 = \frac{1}{2}(Q^+ + Q^0)$

$$W_{+}^{\min}(\text{strong coupling}) = W_M + W_{M^+} + V_{MM^+} + (k/4)(Q^+ - Q^0)^2 - |u| \quad (7b)$$

This is the strong (electronic resonance) coupling case. For the weak coupling case, $|u| \leq \frac{1}{2}k(Q^+ - Q^0)^2$, the lower potential W_+ has one maximum at $Q_1 = Q_2 = \frac{1}{2}(Q^+ + Q^0)$

$$W_{+}^{\max}(\text{weak coupling}) = W_M + W_{M^+} + V_{MM^+} + (k/4)(Q^+ - Q^0)^2 - |u| \quad (7c)$$

but has two minima at

$$Q_1 = \frac{1}{2}(Q^+ + Q^0) \pm \frac{1}{2} \{ (Q^0 - Q^+)^2 - 4|u|^2/[k^2(Q^0 - Q^+)^2] \}^{1/2} \quad (8a)$$

$$Q_2 = \frac{1}{2}(Q^+ + Q^0) \mp \frac{1}{2} \{ (Q^0 - Q^+)^2 - 4|u|^2/[k^2(Q^0 - Q^+)^2] \}^{1/2} \quad (8b)$$

with the same energy which is

$$W_{+}^{\min}(\text{weak coupling}) = W_M + W_{M^+} + V_{MM^+} - |u|^2/[k(Q^0 - Q^+)^2] \quad (8c)$$

When plotted⁹ against $(Q_1 - Q_2)/(Q^+ - Q^0)$, the lower double-minimum potential curve plus the upper one minimum potential curve then correspond to the avoided crossing of two displaced harmonic oscillator potential curves of Hush. Therefore, the variable x in Hush's theory should rightly be interpreted as $(Q_1 - Q_2)/(Q^+ - Q^0)$.

In the limit of zero resonance interaction $u = 0$, $\tan 2\alpha = 0$, and $\alpha = 0$, $\Psi_+ = \phi_{M_1}\phi_{M_2^+}$, $\Psi_- = -\phi_{M_1^+}\phi_{M_2}$ the energies in eq 6 reduce to

$$W_{\pm} = W_M + W_{M^+} + V_{MM^+} + (k/2)(Q_{1,2} - Q^0)^2 + (k/2)(Q_{2,1} - Q^+)^2$$

which are the energies of two noninteracting harmonic oscillator systems. The two minima in eq 8 also reduce to $(Q_1, Q_2) = (Q^0, Q^+)$ and $(Q_1, Q_2) = (Q^+, Q^0)$ which are at the left and the right of the coordinate origin of $(Q_1 - Q_2)/(Q^+ - Q^0)$, respectively. Without resonance interaction then the electron may be (valence) trapped say at left with $(Q_1, Q_2) = (Q^0, Q^+)$. Then vertical transition from Ψ_+ to Ψ_-

using eq 6a with u set to zero yields $W_+ - W_- = \Delta E_{\text{op}} \simeq k(Q^0 - Q^+)^2$ which is in agreement with Hush's theory. It is, therefore, only in this limiting sense that Hush's theory is valid. When u is not zero and vertical upward transition from equilibrium configuration $(Q_1, Q_2) = (Q^0, Q^+)$ is still assumed, the corrected transition energy should be

$$\Delta E_{\text{op}} = [k^2(Q^0 - Q^+)^4 + 4|u|^2]^{1/2} \quad (9a)$$

which is an improvement over Hush's theory. For unsymmetrical intervalence transfer, the electronic energy difference should be included to give

$$\Delta E_{\text{op}} = [(W_{D^+A^-} - W_{DA})^2 + 4|u|^2]^{1/2} \quad (9b)$$

In the weak coupling case when $|u|$ is not negligible but still less than $(k/2)(Q^+ - Q^0)^2$, the difference in the maximum and minimum of the lower curve then gives the vibrational potential barrier (the Franck-Condon barrier)

$$W_{+}^{\max}(\text{weak coupling}) - W_{+}^{\min}(\text{weak coupling}) \\ = \Delta E_{\text{Th}} = \frac{k}{4}(Q^+ - Q^0)^2 - |u| + \frac{|u|^2}{k(Q^0 - Q^+)^2} \quad (10)$$

This should be the thermal barrier for electron transfer reaction, corrected for electronic resonance interaction. It is also an improvement over Hush's formula for ΔE_{Th} . The latter can be obtained by setting $u = 0$ in eq 10. This has been used to compute the rate of thermally activated electron transfer

$$k_{\text{Th}} \simeq \frac{kT}{h} \exp[-\Delta E_{\text{Th}}/kT]$$

In the other extreme limit when $|u|$ is large, compared with $\frac{1}{2}k(Q^+ - Q^0)^2$, $\tan 2\alpha \rightarrow \infty$, both the upper (W_-) and lower curves (W_+) have one minimum and there is no potential barrier and the electronic wave functions are completely mixed as expected with equal amounts on both molecules; namely, $\Psi_{\pm} = (1/\sqrt{2})(\phi_{M_1}\phi_{M_2^+} \pm \phi_{M_1^+}\phi_{M_2})$. This is also true at $Q_1 = Q_2$ which also gives $\tan 2\alpha = \alpha$ and $\alpha = \pi/4$. This is the point at the top of the Franck-Condon barrier ($W_{+}^{\max}(\text{weak coupling})$) and the vibrational amplitudes of the molecule M and its ion M^+ have just surmounted the thermal barrier at a transition state for electron transfer. This leads to a cooperative effect between electron transfer and vibration, and to high conductivity.¹²

Now we turn to the difference of the present intervalence transfer intensity from Mulliken's charge transfer intensity. For strong electronic coupling $|u| \geq (k/2)(Q^+ - Q^0)^2$, the transition moment for intervalence transfer is the same as eq 5. The only difference will be a larger α due to a smaller denominator of vibrational difference in eq 4a. However, for weak electronic coupling $|u| \leq (k/2)(Q^+ - Q^0)^2$ the lower curve W_+ had double minima and a potential barrier which splits the vibrational levels of the lower electronic state into a closely spaced doublet, one symmetric (S) and one antisymmetric (A). For the symmetrical intervalence transfer complex and for low vibrational states, the vibronic wave function may be approximated by

$$\Psi_{+}^{\text{N}} \begin{pmatrix} \text{S} \\ \text{A} \end{pmatrix} = (\phi_{M_1}\phi_{M_2^+} + \alpha\phi_{M_1^+}\phi_{M_2}) \frac{1}{\sqrt{2}} [\chi_0^{\text{M}}(Q_1)\chi_0^{\text{M}^+}(Q_2) \\ \pm \chi_0^{\text{M}^+}(Q_1)\chi_0^{\text{M}}(Q_2)] \quad (11a)$$

$$\Psi_{+}^{\text{N}^*} \begin{pmatrix} \text{S} \\ \text{A} \end{pmatrix} = (\phi_{M_1}\phi_{M_2^+} + \alpha\phi_{M_1^+}\phi_{M_2}) \frac{1}{\sqrt{2}} [\chi_{\nu}^{\text{M}}(Q_1)\chi_{\nu}^{\text{M}^+}(Q_2) \\ \pm \chi_{\nu}^{\text{M}^+}(Q_1)\chi_{\nu}^{\text{M}}(Q_2)] \quad (11b)$$

As a result, the spectral transition from the lower ground vibrational state will show a doublet with unequal intensity. As in the case of ammonia inversion doubling, when the barrier gets lower or when vibrational level gets higher the spacing of the doublet gets larger and larger. Such double-well potential leads to valence trapping (see below) in a mixed-valence compound (e.g., the ruthenium(II,III)-pyrazine complex⁴). Such trapping, aside from giving rise to a special "charge-transfer" absorption band (e.g., the 6.5 kK in the ruthenium(II,III) complex which is not present in the (II,II) or (III,III) complexes), may also be studied by magnetic resonance and Mössbauer spectroscopy¹³ (e.g., for the biferrocene-Fe(II)-Fe(III) compound) which detect the difference between the two valence states. In such studies, the rate of electron transfer is a limiting factor and is of great interest.¹⁴

In the extreme case of intervalence transfer in a valence-trapped complex (or compound), the mere fact that the electron is valence trapped by vibrational potential barrier implies a very weak coupling case $|u| \ll \frac{1}{2}k(Q^+ - Q^0)^2$. Under this circumstance, there may be very little mixing of electronic states and the potential and vibrational wave function of each molecular moiety remains essentially intact. When the resonance interaction is smaller than the vibrational spacing of the individual molecules, instead of linear combination of electronic wave function as in eq 2, one should use the vibronic wave functions as zeroth order function and combine them, viz.

$$\Psi_+^N = \frac{1}{\sqrt{2}} [\phi_{M_1} \phi_{M_2} + \chi_0^M(Q_1) \chi_0^{M^+}(Q_2) + \phi_{M_1} + \phi_{M_2} \chi_0^{M^+}(Q_1) \chi_0^M(Q_2)] \quad (12a)$$

$$\Psi_-^V = \frac{1}{\sqrt{2}} [\phi_{M_1} \phi_{M_2} + \chi_\mu^M(Q_1) \chi_\nu^{M^+}(Q_2) - \phi_{M_1} + \phi_{M_2} \chi_\nu^{M^+}(Q_1) \chi_\mu^M(Q_2)] \quad (12b)$$

where the mixing coefficients are equal because of degeneracy of the two zeroth-order wave functions. Only such a combination will give the correct vibronic dissociation limit.¹⁵ The transition moment will be, due to the orthogonality of the unperturbed vibrational wave functions, exclusively the overlap moment, viz.

$$D = - \int \phi_{M_1} + \phi_{M_2} r \phi_{M_1} \phi_{M_2} + d \int R_{v0} R_{0\mu} \quad (13)$$

with

$$R_{v0} = \int \chi_\nu^{M^+}(Q_1) \chi_0^M(Q_1) dQ_1$$

This transition moment with a product of two Franck-Condon overlaps of the individual molecular moiety is consistent with the expectation for small electronic overlap $\alpha \sim 0$. It is a limiting case for Mulliken's intensity formula (see eq 5c). Thus, theoretical calculation of intensity and energy when checked against experimental data will yield rich information on the magnitude and nature of charge transfer interaction in various molecular systems. Application of this theory to the specific case of biferrocene involving electron transfer between doubly degenerate orbitals and including electronic overlap is now being pursued in this laboratory.¹⁶

The above treatment gives a self-consistent account for improved formulas of energy, intensity, and wave functions from a generalized consideration which in the limit agrees with the special case of Mulliken and Hush. The treatment is based on the Born-Oppenheimer (BO) separation of electronic and nuclear coordinates. In the case of strong

electronic coupling, the splitting due to intermolecular (electronic) interaction is large compared with nuclear vibrational level spacing. In this case the BO approximation is obviously valid. When the splitting due to weak electronic coupling is small, it may be comparable or smaller than the vibrational spacing of the complex. As a result, the nuclear motion may no longer be considered adiabatic. However, in such weak electronic coupling, avoided crossing of the two essentially independent left (e.g., for charge at left) and right (for charge at right) potential curves gives rise to a (symmetrical) double well potential for the lower curve. For low vibrational states that are localized and stay near the bottom of the well, the simple BO approximation may still apply. This is because it is far from the top of the barrier where the avoided crossing takes place and where the electronic degeneracy occurs. At this crossing point, the electronic energy does not depend sufficiently smoothly on nuclear coordinate for the zeroth-order BO approximation to apply.

However, it was contended by a number of authors¹⁷⁻¹⁹ that even such a breakdown in excited dimer is perhaps overestimated. These authors showed that if vibronic equations are written starting with coupled wave functions, the total wave function may reduce to a single product both in the weak and strong coupling limit; namely, a linear combination of electronic factors (such as our eq 2) multiplied by two nuclear factors $\xi(Q^+) \chi(Q^-)$ dependent on the in-phase ($Q^+ = Q_1 + Q_2$) and out-of-phase ($Q^- = Q_1 - Q_2$) combination of nuclear coordinates. These nuclear factors ξ and χ obey coupled equations.^{20,21} Making use of these coupled equations, Lefebvre et al.^{17,18} compared their BO result favorably with the exact numerical calculation of Merrifield.²²

We have here used only the product of monomer vibrational wave functions (dependent on Q_1 and Q_2 , respectively) because of the physical insight they give to the intensity problem. Such a product can be obtained from a coordinate transformation of the coupled nuclear wave functions that are dependent on $Q_1 \pm Q_2$. It will be noted that many of these theoretical works on excimers^{17-19,22} all used the assumption that the force constant is the same for ground and excited states of the monomer, only the equilibrium nuclear distances may be different. The same assumption is also used in the polaron study²³ of an excess electron moving among an aggregate of molecules in a lattice. We have used this assumption for the monomer (M) and its ion (M^+). This amounts to the assumption that the transferred electron interacts with vibration only linearly in the vibrational coordinate.

Acknowledgment. Work supported in part by a Shell Company Grant, and in part by a Gulf Oil Foundation grant given to the Department of Chemistry, The Catholic University of America. The author is indebted to the inspiration provided by a joint seminar with Dr. F. A. Journak in June 1973 in which rudiments of the idea in this paper were mentioned and discussed.

References and Notes

- (1) R. S. Mulliken, *J. Am. Chem. Soc.*, **74**, 811 (1952).
- (2) R. S. Mulliken and W. B. Person, "Molecular Complexes", Wiley, New York, N.Y., 1969; J. N. Murrell, "Theory of Electronic Spectra of Organic Molecules", Wiley, New York, N.Y., 1963.
- (3) N. S. Hush, *Prog. Inorg. Chem.*, **8**, 391 (1967).
- (4) D. O. Cowan, C. Le Vanda, J. Park, and F. Kaufman, *Acc. Chem. Res.*, **6**, 1 (1973).
- (5) H. Taube, "Electron Transfer Reactions of Complex Ions in Solution",

- Academic Press, New York, N.Y., 1970.
- (6) B. Mayoh and P. Day, *J. Am. Chem. Soc.*, **94**, 2885 (1972).
- (7) Y.-N. Chiu and Y. K. Pan, *Chem. Phys. Lett.*, **32**, 67 (1975).
- (8) G. Emschwiler and C. K. Jørgensen, *Chem. Phys. Lett.*, **5**, 561 (1970); H. So and M. T. Pope, *Inorg. Chem.*, **11**, 1441 (1972); J. Ferraris, D. O. Cowan, V. Walatka, Jr., and J. H. Perlstein, *J. Am. Chem. Soc.*, **95**, 948 (1973); M. D. Glick, J. M. Kuszaj, and J. F. Endicott, *J. Am. Chem. Soc.*, **95**, 5097 (1973); S. S. Isied and H. Taube, *J. Am. Chem. Soc.*, **95**, 8198 (1973); J. C. Chen and E. S. Gould, *J. Am. Chem. Soc.*, **95**, 5539 (1973); J. K. Hurst and R. H. Lane, *J. Am. Chem. Soc.*, **95**, 1703 (1973); C. R. Bock, T. J. Meyer, and D. G. Whitten, *J. Am. Chem. Soc.*, **96**, 4170 (1974).
- (9) Th. Förster, Bulletin No. 18, Division of Biology and Medicine, U.S. Atomic Energy Commission, report from Institute of Molecular Biophysics, Florida State University, Tallahassee, Fla., 1965; M. Berrondo and M. Garcia Sucre, *Phys. Rev. A*, **2**, 1181 (1970).
- (10) D. P. Craig and S. H. Walmsley, "Excitons in Molecular Crystals", W. A. Benjamin, New York, N.Y., 1968; R. M. Hochstrasser, *Annu. Rev. Phys. Chem.*, **17**, 457 (1966); G. W. Robinson, *ibid.*, **21**, 429 (1970).
- (11) D. S. McClure, *Can. J. Chem.*, **36**, 59 (1958).
- (12) F. E. Wang and Y.-N. Chiu, *Chem. Phys.*, **12**, 225 (1976).
- (13) D. O. Cowan, R. L. Collins, and F. Kaufman, *J. Chem. Phys.*, **75**, 2025 (1971).
- (14) N. R. Kestner, J. Logan, and J. Jortner, *J. Phys. Chem.*, **78**, 2148 (1974).
- (15) Y.-N. Chiu, *J. Chem. Phys.*, in press.
- (16) J. R. Letelier and Y.-N. Chiu, to be submitted for publication.
- (17) R. Lefebvre and M. Garcia Sucre, *Int. J. Quantum Chem.*, **15**, 339 (1967).
- (18) M. Garcia Sucre, F. Geny, and R. Lefebvre, *J. Chem. Phys.*, **49**, 458 (1968).
- (19) A. Bierman, *J. Chem. Phys.*, **45**, 647 (1966).
- (20) A. Witkowski and W. Moffitt, *J. Chem. Phys.*, **33**, 872 (1960).
- (21) R. L. Fulton and M. Gouterman, *J. Chem. Phys.*, **35**, 1059 (1961).
- (22) R. E. Merrifield, *Radiat. Res.*, **20**, 154 (1963).
- (23) W. Siebrand, *J. Chem. Phys.*, **40**, 2223, 2231 (1964).

Theoretical Derivation of Partition Coefficient from Solubility Parameters

Shalom Srebnik* and Sasson Cohen

Department of Chemistry, McMaster University, Hamilton, Ontario, Canada and Department of Pharmacology, Sackler School of Medicine, Tel Aviv University, Israel (Received June 10, 1975; Revised Manuscript Received February 5, 1976)

Using the free energy expansion series of Scatchard and Prentiss, we have derived an expression for the partition coefficient in terms of solubility parameters of solute and solvents, their molar volumes, and the *partial* molal volumes of the solute in these solvents. This treatment assumes: (1) total separation of phases; (2) absence of complexes; (3) no contribution from three-center interaction; (4) low concentration of solute; and (5) geometric mean assumption for unlike interactions.

Introduction

In the course of an investigation of the partitioning of structurally nonspecific agents between two biophases that differ in composition, the need arose for a theoretically derived expression relating the concentration partition coefficient, K , to the solubility parameters of the agent and the phases involved. Such a relationship was deduced by Davis¹ from the Hildebrand-Scatchard equations² for the excess free energy of a regular solution:

$$\ln K = \frac{V_i}{RT} [(\delta_a - \delta_i)^2 - (\delta_o - \delta_i)^2] + \ln \frac{V_a}{V_o} \quad (1)$$

where V_i is the molar volume of solute i , δ_i its solubility parameter, and V_a , δ_a and V_o , δ_o those of the aqueous and organic phases, respectively. Equation 1 is based on the assumption that both organic and aqueous solutions of i abide by the criteria for a regular solution³ and that the *partial* molal volume of i is not different from its molar volume, V_i . Also, the value of δ_a is still unsettled, ranging from 15.5 to 24.^{4,5} Indeed, Davis himself cautioned against too much reliance on K values derived theoretically by assuming regular solution theory.

We contend that eq 1 could be refined to an extent that

would allow a more accurate prediction of K , provided: (a) the *partial* molal volume of i in the corresponding phase be considered rather than its molar volume. This is necessitated from the fact that certain solutes incur a considerable expansion in molar volume in their regular solution, e.g., a 70% increment in the case of iodine in C_7F_{16} .⁶ (b) Partitioning be considered between two phases, both of which are organic but held immiscible by an imaginary boundary. The experimental value of K that corresponds to such a hypothetical situation could be readily obtained by relating the oil/water partition coefficient of i for phase 1 to that for phase 2. This procedure obviates the need to use δ_a . A basic assumption in this procedure is the total separation of the phases. (c) Derivation beyond regular solution theory, by including S^E , the partial excess entropy, in the derivation.

Derivation

When a species i is distributed between two phases 1 and 2 at equilibrium, then its chemical potential in one phase is equal to that in the other:

$$\partial F_1 / \partial N_i = \partial F_2 / \partial N_i \quad (2)$$

F_1 and F_2 are the Gibbs free energies of the two totally separated phases, 1 and 2. For a nonionic solution, this energy can be represented by an expansion series of Scatchard and Prentiss:^{7,8,16}

* Address correspondence to this author at McMaster University.

$$\frac{F}{RT} = \sum_i N_i B_i + \sum_i N_i \ln C_i + \frac{1}{V} \sum_{ij} N_i N_j \beta_{ij} + \frac{1}{V^2} \sum_{ijk} N_i N_j N_k \gamma_{ijk} + \dots \quad (3)$$

where, V is the total volume of the mixture, N_i the number of moles of component i , C_i the concentration of component i , B_i a constant for component i (related to its free energy per mole in the gas phase), β_{ij} a constant related to the interaction between molecules i and j (independent of concentration), and γ_{ijk} a constant associated with three-center interactions (excluded in this treatment).

For phase 1 which consists only of solvent 1 and solute i , we obtain

$$\frac{1}{RT} \frac{\partial F_1}{\partial N_i} = B_i + 1 + (2\beta_{1i} - \bar{V}_{i1})C_1 - \bar{V}_{i1}(C_1^2\beta_{11} + 2\beta_{1i}C_1C_1 + \beta_{ii}C_i^2) + 2\beta_{ii}C_i + \ln C_i \quad (4)$$

where

$$\bar{V}_{i1} = \partial V / \partial N_i$$

is defined as the *partial* molal volume of solute i in phase 1.

By applying eq 4 to phase 2, assuming $C_i \ll C_1$ or C_2 and substituting for $\partial F_1 / \partial N_i$ and $\partial F_2 / \partial N_i$ in eq 2, we obtain

$$\ln \frac{C_{i2}}{C_{i1}} = (2\beta_{1i} - \bar{V}_{i1})C_1 - (2\beta_{2i} - \bar{V}_{i2})C_2 - \bar{V}_{i1}C_1^2\beta_{11} + \bar{V}_{i2}C_2^2\beta_{22} \quad (5)$$

Since C_{i1} and C_{i2} are the equilibrium concentrations of i in phases 1 and 2, then

$$C_{i2}/C_{i1} = K \quad (6)$$

where K is the partition coefficient. It can be shown that [Appendix A]

$$\beta_{11} = -\frac{(\Delta H_1^v - RT)V_1}{RT} = -\frac{\delta_1^2 V_1^2}{RT} \quad (7)$$

where ΔH_1^v is the heat of vaporization of pure solvent 1 and V_1 is its molar volume. The solubility parameter, δ_1 , is numerically equal to $[(\Delta H_1^v - RT)/V_1]^{1/2}$.³

By substituting for β_{ij} its commonly used geometric mean approximation:^{3,7,8}

$$\beta_{ij} = -(\beta_{ii}\beta_{jj})^{1/2}$$

and for C_1 of the pure solvent $1/V_1$, then eq 5 may be rewritten as:

$$\ln K = -\frac{2\delta_1\delta_i}{RT} V_i + \frac{\delta_1^2}{RT} \bar{V}_{i1} - \frac{\bar{V}_{i1}}{V_1} - \left(-\frac{2\delta_2\delta_i}{RT} V_i + \frac{\delta_2^2}{RT} \bar{V}_{i2} - \frac{\bar{V}_{i2}}{V_2} \right) \quad (8)$$

For comparison with Davis' equation, another form of eq 8 is useful.

$$\ln K = \frac{V_i}{RT} [(\delta_1 - \delta_i)^2 - (\delta_2 - \delta_i)^2] + (\bar{V}_{i1} - V_i) \left(\frac{\delta_1^2}{RT} - \frac{1}{V_1} \right) - (\bar{V}_{i2} - V_i) \left(\frac{\delta_2^2}{RT} - \frac{1}{V_2} \right) - V_i \left(\frac{1}{V_1} - \frac{1}{V_2} \right) \quad (9)$$

In case we do not have the required values for the partial molal volumes, we suggest the use of the fairly good approximation³

$$\frac{\bar{V}_{i1} - V_i}{V_i} = \frac{(\delta_1 - \delta_i)^2}{(\partial E_1 / \partial V_1)} \quad (10)$$

where $(\partial E_1 / \partial V_1)$ is the internal pressure for pure solvent 1.

Thus, we obtain an alternative but more approximate form of eq 9.

$$\ln K = \frac{V_i}{RT} \left[(\delta_1 - \delta_i)^2 \left(1 + \frac{\delta_1^2}{(\partial E_1 / \partial V_1)} - \frac{RT}{(\partial E_1 / \partial V_1)V_1} \right) - (\delta_2 - \delta_i)^2 \left(1 + \frac{\delta_2^2}{(\partial E_2 / \partial V_2)} - \frac{RT}{(\partial E_2 / \partial V_2)V_2} \right) \right] - V_i \left(\frac{1}{V_1} - \frac{1}{V_2} \right) \quad (11)$$

By assuming $\bar{V}_{i1} = \bar{V}_{i2} = V_i$ and neglecting $(V_i/V_2) - (V_i/V_1)$, then eq 9 reduces to the form given by Davis, eq 1. As will be shown, this is not always justifiable.

This derivation is different than that of Davis by not assuming the regular solution model. By "regular solution" model we refer to the original definition given by Hildebrand. A regular solution is defined only by its partial excess entropy S^E , being zero,³ whereas the solubility parameter and the geometric mean assumption (which are sometimes mistakenly identified with regular solution theory) are general concepts that happen to hold well in regular solutions, but can be used in other models as well. Our model retains the use of the solubility parameter and geometric mean assumption, but stretches beyond regular solution theory by including S^E in the derivation.

Discussion

The application of eq 9 or 3 requires knowledge of solubility parameters and of *partial* molal volumes. Usually, values of δ for most organic solvents appear to be well documented,⁹ with the reservation that values for hydrocarbons derived from ΔH^v are less reliable than those obtained by a dilatometric procedure. This subject, referred to as the anomalous behavior of hydrocarbon solution, has been reviewed by Scott¹⁰ and recently by Hildebrand.³ A more serious limitation is the extreme paucity of data on partial molal volumes, the main source being the published results of Hildebrand and coworkers.³ Among these, only two systems lend themselves to accurate inspection. These are the solutions of iodine and bromine in CCl_4 and CS_2 and for which the experimental partition coefficients have also been given in the literature.¹¹

The results (Table I) show very good agreement between the theoretically and experimentally derived values, probably within the experimental error of the data. Regular solution theory is less satisfactory in this comparison but still gives an estimate within 0.1 of the experimental data. This points out the role of the volume change even in systems which are considered to be typical of regular solutions.

The application of eq 8 to other systems would be possible only by obtaining values or estimates for the related partition coefficients. An approximate method is to use the solubilities of the solute in the two phases, which for iodine are known for all the solvents where the partial molal volume is known. We limit ourselves to noncomplexing systems, so that the only restriction for this method is the failure of the assumption of dilute solutions. Observation in different systems¹² leads to an estimated error in this method of ± 0.05 on the average for $\log K$ (up to 0.1 for I_2 in $\text{C}_3\text{H}_8\text{O}_3\text{-CCl}_4$).

In Table II we compare the values of $\log K^s$, the log of

TABLE I: Values of Log K Obtained by Use of Eq 1 and 8

Solute ^a i	Phase ^a		Log K, exptl ^b			Log K $\frac{\text{phase 2}}{\text{phase 1}}$ calcd	
			Phase 1	Phase 2	Phase 2	Eq 1	Eq 8
	1	2	H ₂ O	H ₂ O	phase 1		
I ₂	CCl ₄	CS ₂	1.93	2.77	0.84	0.78	0.86
Br ₂	CCl ₄	CS ₂	1.35	1.89	0.54	0.44	0.54

^a δ values (ref 3) used are: I₂, 14.1; Br₂, 11.5; CS₂, 10.0; CCl₄, 8.6 (cal/cm³)^{1/2}. V_{298° values (ref 3 and 15) used are: I₂ (liquid), 58.5; Br₂, 51.5; CS₂, 60.7; CCl₄, 97.1 cm³. V_i values (ref 3 and 15) used are: I₂-CCl₄, 66.7; I₂-CS₂, 62.8, Br₂-CCl₄, 56.4; Br₂-CS₂, 52.6 cm³.
^b Values obtained from compilation by Leo, Hansch, and Elkins (ref 11).

TABLE II

Phase 1	Phase 2					
	CS ₂	CCl ₄	CHCl ₃	C ₇ F ₁₆	SiCl ₄	c-C ₆ H ₁₂
CS ₂						
CCl ₄	0.857					
	0.794					
	0.779					
CHCl ₃	0.531	-0.326				
	0.498	-0.296				
	0.433	-0.347				
C ₇ F ₁₆	3.139	2.282	2.608			
	3.059	2.265	2.561			
	2.770	1.890	2.236			
SiCl ₄	1.342	0.485	0.811	-1.797		
	1.322	0.528	0.824	-1.737		
	1.370	0.591	0.937	-1.300		
c-C ₆ H ₁₂	1.114	0.257	0.583	-2.025	-0.228	
	1.034	0.240	0.536	-2.026	-0.289	
	1.027	0.248	0.594	-1.642	-0.343	

^a The values of log K of I₂ between different phases are given according to three methods: (1) calculated by eq 8 (the upper value); (2) calculated from solubilities of I₂ (intermediate value); and, (3) calculated by eq 1 (the lower value). All the required data were taken from Tables 8.3, 8.4, 9.1, and Appendix 4 of ref 14. V_i of I₂ was taken as 58.5 according to ref 3.

the partition coefficient obtained from solubilities, with those evaluated by eq 1 and 8. The same results are compared graphically in Figure 1. We can conclude that the results obtained from our equation agree with the experiment values of log K^s with a maximum deviation of ± 0.08 , a range of values not much greater than the estimated error for log K^s.

Relatively large discrepancies are found when CS₂ forms one of the phases. This is due to the high solubility of iodine in CS₂ (more than in the other solvents). Comparison of the log K^s value for iodine partitioned between CS₂ and CCl₄ (Table II) with the corresponding value of log K^{exptl} (Table I) shows that the theory correlates better with the data derived in a dilute solution.

Regular solution theory gives good estimate for the value of log K^s in all solvents but C₇F₁₆, where it is quite bad. Scott¹⁰ and Hildebrand³ have suggested that the anomalous behavior of fluorocarbons may be due to a failure of the mean value assumption resulting from the action of special dispersion forces in such systems. However, agreement is obtained with the present theory which does employ the mean value assumption. Thus, the failure of the regular solution theory in this case is more likely due to its neglect of the large increase in the partial molal volume of the solute in the fluorocarbon solvent.

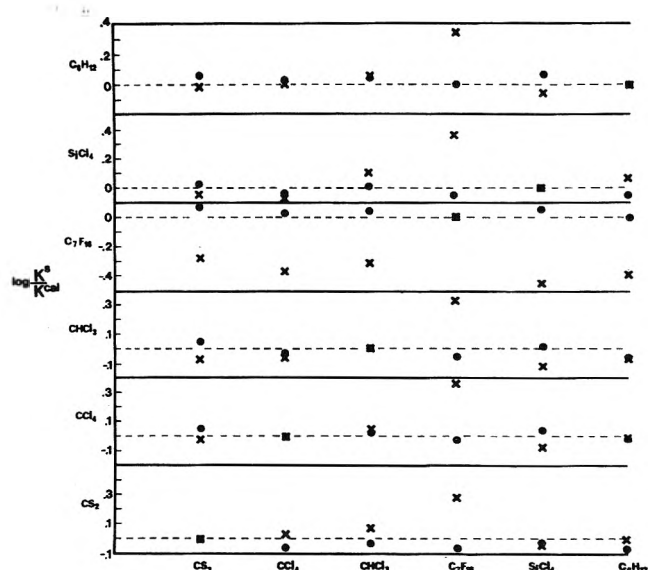


Figure 1. Values of log K^s - log K^{cal} are given according to two methods: (●) denotes calculation by eq 8; (x) denotes calculation by eq 1. (■) Denotes a reference point placed on the zero lines (dashed) by definition. The vertical solvent is phase 2 and the numerical values are shown in Table II.

This theory was applied¹³ to build a model to account for the differing behavior of the anesthetic and convulsant drugs in terms of their differing distributions between the phases within a membrane.

Acknowledgment. One of the authors (S.S.) wishes to thank the National Research Council of Canada for financial support of this research.

Appendix A

Comparison of the two-center interaction terms in the free energy expansion series with the "cohesive energy", $-E$, of Scatchard-Hildebrand gives

$$\beta_{11} = \frac{EV_1}{RT} = -\frac{(-E/V_1)V_1^2}{RT} = -\frac{\delta_1^2 V_1^2}{RT} \quad (\text{A1})$$

Essentially, $-E$ is the molar energy of vaporization to the gas at zero pressure. However, the chemical potential of Hildebrand, and hence the partition coefficient of Davis, have been derived from the heat of mixing, while the present derivation deals with the *total* free energy. The following is, therefore, an independent derivation of β_{11} .

The free energies of the liquid phase, F^s , and the gas phase, F^g , are given by

$$\frac{F^s}{RT} = N^s B + N^s \ln C^s + \frac{1}{V^s} \beta_{11} N^s{}^2 \quad (\text{A2})$$

$$F^g/RT = N^g B + N^g \ln C^g \quad (\text{A3})$$

where s denotes the standard, i.e., the liquid state and g the gas state.

At equilibrium, we write

$$\partial F^g/\partial N^g = \partial F^s/\partial N^s \quad (\text{A4})$$

Using the following relations, $C^s = N^s/V^s = 1/V_1$; $\partial C^s/\partial N^s = 0$; $C^g = N^g/V^g$; at constant volume $\partial C^g/\partial N^g = 1/V^g$; $P V^g = N^g R T$; and combining eq A2, A3, and A4, we obtain

$$\ln P = \ln \frac{RT}{V_1} + \frac{\beta_{11}}{V_1} - 1 \quad (\text{A5})$$

but

$$\Delta H^v = -R \frac{\partial \ln P}{\partial (1/T)} \quad (\text{A6})$$

hence

$$\Delta H^v = RT - \frac{R}{V_1} \frac{\partial \beta_{11}}{\partial (1/T)} \quad (\text{A7})$$

Therefore

$$\beta_{11} = - \frac{\Delta H^v - RT}{RT} V_1 + D \quad (\text{A8})$$

where D is a constant independent of temperature.

Using the definition of δ given above

$$\beta_{11} = - \frac{\delta_1^2 V_1^2}{RT} + D \quad (\text{A9})$$

The significance of D would require arguments as those given by Guggenheim, as quoted by Hildebrand and Scott,¹⁴ but the actual effect would be to shift all δ values upward.

This alternative derivation of δ from the total free energy can explain the fact that the chemical potential $\bar{\mu} - \bar{\mu}^{\text{ideal}}$ correlates better with \bar{F}^E than with \bar{H}^E in regular solution theory, a point which has been emphasized by Scott.¹⁰

References and Notes

- (1) S. S. Davis, *Experientia*, **26**, 671 (1970).
- (2) J. H. Hildebrand and R. L. Scott, "Solubility of Nonelectrolytes", 3rd ed, Reinhold, New York, N.Y., 1950.
- (3) J. H. Hildebrand, J. M. Prausnitz, and R. L. Scott, "Regular and Related Solutions", Van Nostrand-Reinhold, New York, N.Y., 1970.
- (4) A. Koskas and J. Durand, *Chim. Ind.*, **98**, 1386 (1967).
- (5) T. Wakabayashi, S. Oki, T. Omori, and N. Suzuki, *J. Inorg. Nucl. Chem.*, **25**, 1351 (1963).
- (6) D. N. Glew and J. H. Hildebrand, *J. Phys. Chem.*, **60**, 616 (1956).
- (7) G. Scatchard and S. S. Prentiss, *J. Am. Chem. Soc.*, **56**, 1486 (1934).
- (8) J. E. Leffler and E. Grunwald, "Rates and Equilibria of Organic Reactions", Wiley, New York, N.Y., 1963.
- (9) H. Burrell in "Polymer Handbook", J. Brandrup and E. H. Immergut, Ed., Interscience, New York, N.Y., 1966.
- (10) R. L. Scott, *J. Phys. Chem.*, **62**, 136 (1958); I. M. Croll and R. L. Scott, *ibid.*, **62**, 954 (1958).
- (11) A. Leo, C. Hansch, and D. Elkins, *Chem. Rev.*, **71**, 525 (1971).
- (12) H. Stephen and T. Stephen, "Solubilities of Inorganic and Organic Compounds", Vol. 2, Part I, Macmillan, New York, N.Y., 1964, pp 34-52.
- (13) S. Cohen, A. Goldschmid, G. Shtacher, S. Srebrenik, and S. Gitter, *Mol. Pharmacol.*, **11**, 379 (1975).
- (14) J. H. Hildebrand and R. L. Scott, "Regular Solutions", Prentice-Hall, Englewood Cliffs, N.J., 1962, p 167.
- (15) R. Fujishiro, K. Shinoda, and J. H. Hildebrand, *J. Phys. Chem.*, **65**, 2268 (1961).
- (16) Leffler and Grunwald⁸ suggested to rewrite the expansion series of Scatchard and Prentiss in terms of molar concentrations rather than molar fractions. They point out that in this way we get for dilute solutions the known relation $\bar{F}_i = \bar{F}_i^0 + RT \ln C_i$. Using this kind of expansion we have to analyze the coefficient β_{ij} which we do in Appendix A.

The Influence of Solute Size on the Thermodynamic Parameter of Transfer of a Nonpolar Hydrophobic Solute from Gas to Water or from Light to Heavy Water

M. Lucas*

Commissariat à l'Energie Atomique, Service de Chimie-Physique, Centre d'Etudes Nucléaires de Saclay, 91190 Gif sur Yvette, France

and R. Bury

Laboratoire d'Electrochimie, Université de Paris VI, 75230 Paris, France (Received November 13, 1975)

Publication costs assisted by Commissariat à l'Energie Atomique

Using the modified versions of the scaled particle theory amended by Stillinger, we have considered the influence of nonpolar solute size on its thermodynamic parameters of transfer from gas to water or from light to heavy water. In the first case it is found that the process is dominated by an entropy contribution at small solute size and an enthalpy contribution at larger size. In the second process the increase in solute size also results in a change in the sign of the free energy and enthalpy of transfer, which is supported by our experimental data on bulky solutes, such as adamantanemethanol or sodium adamantanecarboxylate.

I. Introduction

In a previous paper,¹ we have considered the influence of solvent size on transfer of nonpolar hydrophobic solutes from one solvent to another or to the gaseous state. It has been

observed that the difference in solvent size is important to determine the free energy of transfer of the solute.

That the solute size may well be important in the solution processes into water appears from experimental studies of various solutes. Whereas Philip and Jolicoeur² have shown

that the scaled particle theory (SPT), as suggested previously,³ gives the possibility of predicting various thermodynamic properties of transfer of solutes with linear alkyl chains from H₂O to D₂O, Jolicœur and Lacroix⁴ have shown that replacing linear chains by branched one in ketones, thus increasing the bulkiness of the solute, changes the sign of ΔG of transfer from H₂O to D₂O; the ΔH also becomes much more positive. They have ascribed these changes to the possibility that a large solute may break H bonds in water instead of fitting into the water cages as this possibility is generally ascribed to linear alkyl chains.⁴ Very recently it has been found by Wilson and Wen⁵ that the bulky bicyclic quaternary ammonium halides (azoniaspirohalides) had a distinctly more positive heat of transfer from H₂O to D₂O than the tetra-*n*-alkylammonium halides with comparable molar volume.

The SPT in its original version⁶ does not incorporate explicitly¹ tetrahedral water coordination, but its Stillinger's amended version⁷ does and therefore is more suitable to considering changes in solute thermodynamic properties when the hard sphere solute diameter is increased from zero to infinity.

In the first part of the Discussion we shall consider the thermodynamic properties of transfer of a nonpolar hard-sphere solute from the gaseous state to water and in the second part the transfer of the solute from H₂O to D₂O.

II. Discussion

(a) *Transfer of a Nonpolar Hard-Sphere Hydrophobic Solute from the Gaseous State to Water at Infinite Dilution.* A hard-sphere solute is characterized by its hard-sphere diameter a_2 . The process of solution is defined by $\Delta G = RT \ln K$, where K , the Henry constant, is equal to p/x , p being the partial pressure of the solute in the gaseous state and x its mole fraction in solution. (In the following calculations p is in atmospheres.) The ΔG , ΔH , and $T\Delta S$ have been computed by the same procedure as in ref 1 from data in ref 7.

The ΔG , ΔH , and $T\Delta S$ have been computed at 4 °C. The influence of dispersion has been neglected, as it is more difficult to assess in Stillinger's than in Pierotti's analyses.

In Figure 1 we have plotted the reduced quantities $\Delta G/a_2^2$, $T\Delta S/a_2^2$, and $\Delta H/a_2^2$ computed from modified SPT (labeled STL from Stillinger) and original SPT against the solute hard-sphere diameter a_2 in angstroms as the abscissa.

These plots show some interesting features: if it is assumed that Stillinger's analysis improves upon Pierotti's, then the original SPT is excellent for $a_2 < 1.4$ Å and acceptable as an approximation for $a_2 < 4$ Å, in the sense that the G_{SPT} differs only from G_{STL} by less than 10%, and $T\Delta S$ by 25%. At higher values for a_2 , the SPT gives different, and presumably much less accurate, results. (A possible exception is for the ΔG values which seem relatively insensitive to the fact that tetrahedral coordination of water has been or not built into the model. This supports the conclusions of ref 1 on the relative insensitivity of ΔG to structural features, opposed to the large influence of solvent structure on ΔH and $T\Delta S$. This implies also that there is a large compensation between enthalpy and entropy.) At higher values for a_2 , the process of solution as viewed from the Stillinger model is dominated by the enthalpy rather than the entropy contribution.

From purely extrathermodynamic, intuitive grounds, these findings suggest that the possibility exists that the influence of the solute on water structure may be the opposite when the solute is small where it may not disrupt the water structure, or when it is large where the high positive enthalpy and small

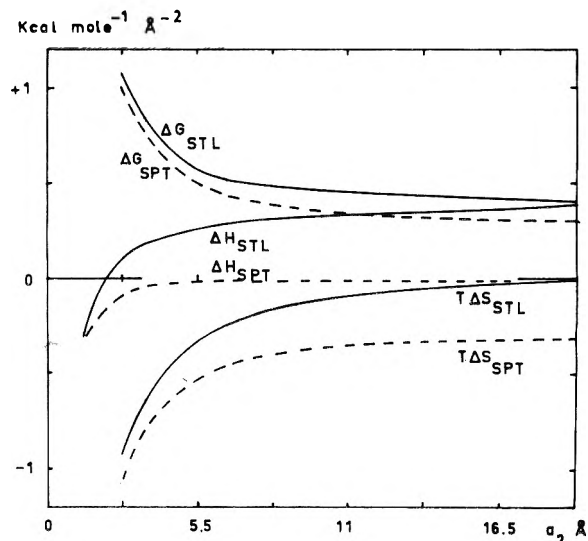


Figure 1. Plots of the reduced quantities $\Delta G/a_2^2$, $\Delta H/a_2^2$, and $T\Delta S/a_2^2$ against solute hard-sphere diameter a_2 as the abscissa: full lines, Stillinger's model; dotted line, original SPT. Temperature 4 °C.

negative entropy seem more consistent with a process of breaking H bonds.

The initial success of calculations using the SPT^{2,6} can be explained because it dealt mainly with small solutes,² or large solutes⁶ with linear alkyl chains which can fit in the water structure,⁸ and therefore could perhaps be considered as cumulating the effect of methylene and methyl groups, the size of which does not exceed 3.2 Å, so that it is in the range where the SPT still does work.

(b) *Thermodynamic Properties of Transfer from H₂O or D₂O for Nonpolar Hard-Sphere Solutes.* They can be computed by applying the preceding procedure to D₂O and subtracting the related quantities obtained with H₂O as a solvent. However as the radial distribution function for D₂O is not known except at 4 °C,⁹ we have to make some assumptions about the value of the function $G(\lambda)$ which is used⁷ in the calculation of ΔG . First we assume that D₂O has more structure than H₂O so that it behaves as H₂O colder by a few degrees. That assumption, usual in that type of studies, is now questioned.¹⁰ However, Narten states⁹ that "the distribution of O - - H(D) - O angles about a mean value is sharper in D₂O than in H₂O" at 4 °C. This may be interpreted as showing that D₂O is really more structured than H₂O,⁵ so that D₂O has the same $G(\lambda)$ as H₂O at a lower temperature. We have now to decide to what extent D₂O is "colder" than H₂O. A first estimate can be made considering the fact that D₂O melts 4 °C higher than H₂O. Another different estimate can be made, since the isothermal expansion coefficient, which is probably an index of the structure in the liquid, is equal to zero, 7 °C higher for D₂O than for H₂O. Therefore we have carried out the calculation of the G of transfer in two cases, assuming first that D₂O at 25 °C has the same $G(\lambda)$ as H₂O at 19 °C, or the same as H₂O at 22 °C in the second case. Then from data in ref 7, it is possible to compute $G(\lambda)$ for D₂O in the two cases. In the calculations the same value a for the diameter of H₂O and D₂O has been taken.

Now if we want to compute ΔH and $T\Delta S$ as well, it is necessary to make some assumptions about the variation of $G(\lambda)$ with the temperature for D₂O. As D₂O's boiling point is 1.5 °C higher than that of H₂O, from melting and boiling point we may assume that the structure of D₂O changes in a temperature range of 97.5 °C to the same extent as that of H₂O in a

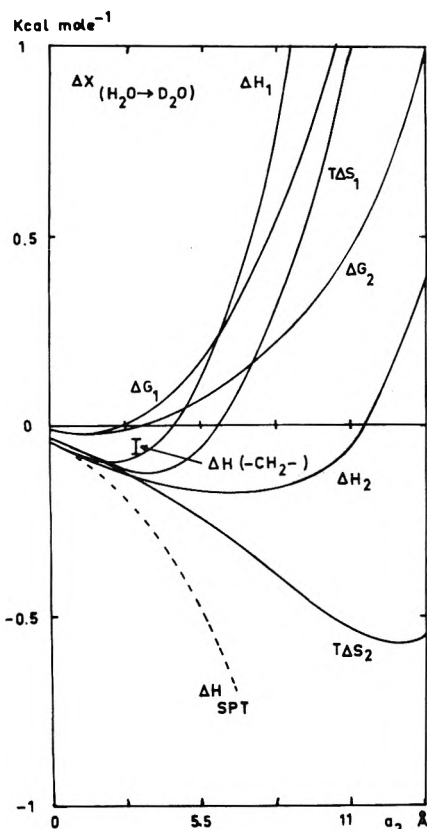


Figure 2. Plots of the ΔG , ΔH , and $T\Delta S$ of transfer of a nonpolar hard-sphere solute from H_2O to D_2O against solute hard sphere diameter a_2 as the abscissa: full lines, Stillinger's model with assumptions 1 (curves labeled 1) or assumptions 2 (curves labeled 2); dotted line, original SPT. Temperature 25 °C.

range of 100 °C, or from the temperature at which the two liquids have their expansion coefficient equal to zero and their boiling points, the structure of D_2O changes in a temperature range of 90 °C as that of H_2O in a range of 96 °C. In the first case $dG(\lambda)/dT$ is assumed to decrease 1.025 time faster for D_2O than for H_2O , and 1.06 time faster in the second case. In fact in the calculations we have used the slightly smaller values of 1.02 and 1.05. Then the calculations have been carried out with the following assumptions. In the first case $G(\lambda)$ for D_2O at 25 °C is the same as for H_2O at 19 °C and $dG(\lambda)/dT$ for D_2O is 1.05 time that for H_2O . In the second case $G(\lambda)$ for D_2O at 25 °C is the same as for H_2O at 22 °C and $dG(\lambda)/dT$ for D_2O is 1.02 time that for H_2O . In Figure 2 we have plotted the ΔG , ΔH , and $T\Delta S$ of transfer for a nonpolar solute from H_2O to D_2O , against solute hard-sphere diameter a_2 (in angstroms) as the abscissa. Curves 1 refer to parameters computed with the first assumption. Curves 2 refer to the second assumption. Dotted curves are calculated from the original SPT.

It is apparent that for solutes with a moderate size ($<4.8 \text{ \AA}$) the sign of ΔH and $T\Delta S$ is the same in the three cases considered (original SPT, first, and second assumptions). In contrast the ΔG_{tr} , always negative when computed from the original SPT, is positive for $a_2 > \sim 3.0 \text{ \AA}$. This is consistent with the trend observed by Jolicœur⁴ for branched aliphatic ketones. Data for hydrocarbons are very scarce and not consistent: ΔG_{tr} for butane is either slightly negative¹¹ (-17 cal mol^{-1}) or positive¹² ($+8 \text{ cal mol}^{-1}$) at 25 °C; ΔG_{tr} for cyclohexane at 25 °C is slightly positive.¹³ The more accurate ΔG_{tr} measured for a series of sodium *n*-alkyl carboxylate¹⁴ shows an increase of ca. 2 cal mol^{-1} by addition of a methylene group

TABLE I: Molal Heat of Solution (kcal mol^{-1}) of Various Solutes from the Solid State to Dilute Solution in Water^{a,b,d}

	D_2O	H_2O	$\Delta H_{tr}(\text{H}_2\text{O}-\text{D}_2\text{O})$
Methanol			$(-0.18)^c$
<i>tert</i> -Butyl alcohol	-4.45	-4.00	-0.45
1-Adamantanol	+0.45	$(-0.70)^e$	$(-0.51)^c$
Sodium acetate	-3.49	-3.54	+1.15
			$(+0.07)^c$
Sodium trimethylacetate	-6.68	-6.33	-0.35
Sodium adamantylcarboxylate	-3.30	-4.40	+1.10

^a For the sodium salts, the transfer is measured from a 0.02 *m* NaOH solution in H_2O to a 0.02 *m* NaOH solution in D_2O in order to prevent hydrolysis. The added salt final molality is about $3 \times 10^{-3} \text{ M}$. A correction for the Debye-Hückel limiting law should be applied to the heat solutions ($-0.9c^{1/2}$ in kcal mol^{-1}), but in the transfer this correction nearly cancels, due to similar dielectric constant of H_2O and D_2O . ^b Reproducibility better than $\pm 0.05 \text{ kcal mol}^{-1}$. ^c Literature values (ref 15). ^d Improved adiabatic calorimeter as in J. Jordan, *J. Chem. Educ.*, 40, A5 (1963). ^e D. J. T. Hill, Ph.D. Thesis, University of Queensland, Queensland, Australia, 1965. For the alcohols no correction has been done for the OH isotopic exchange.

neglecting the first terms in the series. On the other hand, there are many calorimetric data available for the ΔH of transfer of various classes of solutes with linear alkyl chains.¹⁵ The ΔH_{tr} corresponding to the addition of a methylene group is between -30 and -60 cal mol^{-1} depending upon the class investigated: if the size of such a group is about 3.4 \AA , this is smaller than the -80 cal mol^{-1} predicted in the present calculations (with ΔH_1), but this last value is nevertheless a marked improvement upon the $-220 \text{ cal mol}^{-1}$ predicted by the original SPT. When more bulky solutes as 6-azoniaspiroalkane bromide are considered,⁵ the ΔH_{tr} is found to be $0.24 \text{ kcal mol}^{-1}$ more positive than for the corresponding tetra-*n*-alkylammonium bromide with the same molar volume, in agreement with the trend exhibited by curve 1 for ΔH_{tr} in Figure 2.

In order to examine which approximate choice for the parameters is the best for the ΔH_{tr} , we have measured the heat of solution of some solutes of increasing bulkiness: sodium acetate, sodium trimethylacetate, sodium adamantylcarboxylate, *tert*-butyl alcohol, and 1-adamantanol in order to examine the influence of the solute bulkiness.

Due to the poor solubility of the corresponding hydrocarbons more soluble compounds as alcohols or acid sodium salts have to be used.

The enthalpy of solution and enthalpy of transfer, with some experimental details, are given in Table I.

It is apparent from the data in this table that there is an increase in the ΔH_{tr} when the *tert*-butyl group is replaced by the more compact adamantyl group. This increase is very important, about $1.60 \text{ kcal mol}^{-1}$ in the alcohol series and $+1.45 \text{ kcal mol}^{-1}$ in the sodium carboxylate series. These values are very similar in view of the experimental error ($+0.05$) and the fact that eight different experimental heats of transfer are involved in this type of comparison.

The increase in the enthalpy of transfer for the methyl and adamantyl group is $+1.3$ in the alcohol series and $+1.05$ in the sodium acid salt series. When the size of the alkyl group is

increased from methyl (ca. 3.4 Å in diameter) to adamantyl (ca. 7 Å), the increase in the enthalpy of transfer is about +1 kcal mol⁻¹. This shows that the approximate choice for the parameters which gives the curve labeled ΔH_1 is much better than that which gives the curve labeled ΔH_2 . More experimental data are needed to further determine the parameters that give the best fit. In any case the experimental findings appear to give some support to the theory used in this paper.

Finally one may comment on the physical interpretation of the calculated thermodynamic quantities of transfer. It has been observed previously¹ that when one solute is transferred from one solvent to another with a sufficiently different molecular diameter, the ΔG_{tr} is mainly a function of the different solvent size (for a given solute hard-sphere diameter), and is relatively independent on the structural features that can be built into the model. On the contrary when two solvents are considered, with the same hard-sphere diameter and very similar molar volumes, as D₂O and H₂O, the difference in the structure of the two solvents is likely to play an important role in determining the sign of the ΔG_{tr} . Here the interpretation for the $\Delta G_{tr} > 0$ for solutes with large size is possibly that proposed by Jolicoeur,⁴ that is that the large solute which cannot fit into the solvent cages is more difficult to insert in the more structured D₂O than in H₂O.

The interpretation of the sign of the ΔH_{tr} is much more difficult since it is related to the relative decrease in structure with increasing temperature of H₂O and D₂O through their $G(\lambda)$. In the present calculation, the sign of ΔH_{tr} changes with solute size because we have assumed that $G(\lambda)$ decreases sufficiently faster for D₂O than for H₂O when the temperature is increased.

References and Notes

- (1) M. Lucas, *J. Phys. Chem.*, **80**, 359 (1976).
- (2) P. R. Philip and C. Jolicoeur, *J. Solution Chem.*, **4**, 105 (1975).
- (3) M. M. Marciacq-Rousselot and M. Lucas, *J. Phys. Chem.*, **77**, 1056 (1973).
- (4) C. Jolicoeur and G. Lacroix, *Can. J. Chem.*, **51**, 3051 (1973).
- (5) D. P. Wilson and W. Y. Wen, *J. Phys. Chem.*, **79**, 1527 (1975).
- (6) R. A. Pierotti, *J. Phys. Chem.*, **69**, 281 (1965).
- (7) F. H. Stillinger, *J. Solution Chem.*, **2**, 141 (1973).
- (8) A. H. Narten and S. Lindenbaum, *J. Chem. Phys.*, **51**, 1108 (1969).
- (9) A. H. Narten and H. A. Levy, "Water: a Comprehensive Treatise", Vol. 1, F. Franks, Ed., Plenum Press, New York, N.Y., 1972, Chapter 8.
- (10) H. S. Frank, ref 14, Chapter 14.
- (11) G. C. Kresheck, H. Schneider, and H. A. Shceraga, *J. Phys. Chem.*, **69**, 3132 (1965).
- (12) A. Ben Naim, J. Wilf, and M. Yaacobi, *J. Phys. Chem.*, **77**, 95 (1973).
- (13) A. N. Guseva and E. J. Parnov, *Sov. Radiochem.*, **5**, 507 (1963).
- (14) H. Snell and J. Greyson, *J. Phys. Chem.*, **74**, 2148 (1970).
- (15) G. Jancso and W. A. Van Hook, *Chem. Rev.*, **74**, 689 (1974).

Viscosities and Conductivities of the Liquid Salt Triethyl-*n*-hexylammonium Triethyl-*n*-hexylboride and Its Benzene Solutions¹

Warren T. Ford* and Donald J. Hart

Department of Chemistry, University of Illinois, Urbana, Illinois 61801 (Received October 30, 1975)

Publication costs assisted by the University of Illinois

The viscosity of neat liquid triethyl-*n*-hexylammonium triethyl-*n*-hexylboride (N₂₂₂₆B₂₂₂₆) decreases nonexponentially with 1/*T* by a factor of 15 in the range 20–80 °C while its equivalent conductance increases similarly by a factor of 13. Dilution of liquid N₂₂₂₆B₂₂₂₆ with an equal volume of benzene increases the specific conductance at 25 °C by a factor of 10.5.

Introduction

Triethyl-*n*-hexylammonium triethyl-*n*-hexylboride (N₂₂₂₆B₂₂₂₆) is a liquid salt at room temperature.² It resembles a charged alkane: the cation and anion are nearly equal in size, and both are isoelectronic with 3,3-diethylnonane. N₂₂₂₆B₂₂₂₆ is miscible in all proportions with most organic solvents, but immiscible with hexane, which it resembles structurally, and immiscible with water, nature's ubiquitous solvent for ions.

We now have studied transport properties of N₂₂₂₆B₂₂₂₆ with two aims. First, we wanted to determine whether N₂₂₂₆B₂₂₂₆ could be a suitable conductor for electrochemical applications. Second, we wanted to compare tempera-

ture effects on its transport properties, which depend on translational diffusion, to the temperature effects on its carbon-13 spin-lattice relaxation times, which depend on rotational diffusion.

The compatibility of N₂₂₂₆B₂₂₂₆ with a wide variety of organic materials makes it intriguing for possible electrochemical uses, either as a supporting electrolyte in high concentration in nonaqueous solvents or as both solvent and supporting electrolyte in neat liquid form. Preliminary conductivity and cyclic voltammetry experiments indicated that neat N₂₂₂₆B₂₂₂₆ may be suitable for cathodic electrochemistry.³

Earlier information on viscosities and conductivities of molten salts at low temperature is limited to tetra-*n*-butylammonium picrate at 91 °C⁴ and tetra-*n*-amylammonium thiocyanate at 52–110 °C⁵. The specific resistance of tetra-

* Address correspondence to this author at Rohm and Haas Co., Research Laboratories, Spring House, Pa. 19477.

TABLE I: Viscosity and Conductance of Neat N₂₂₂₆B₂₂₂₆

<i>T</i> , °C	η , cP	<i>T</i> , °C	Λ , equiv ⁻¹ ohm ⁻¹ cm ²	<i>d</i> , g cm ⁻³
0.00 ^a	1544			0.8445
10.00	702			0.8405
20.00	346	20.02	0.1509	0.8368
		25.00	0.204	0.8350
30.00	188.5	30.05	0.272	0.8330
		35.01	0.365	0.8312
40.00	112.3	40.08	0.447	0.8294
		45.06	0.582	0.8273
50.00	71.1	50.05	0.703	0.8252
		54.99	0.875	0.8231
60.00	47.0	60.10	1.046	0.8213
		65.08	1.260	0.8194
70.00	32.4	70.16	1.477	0.8174
		74.63	1.717	0.8156
80.00 ^a	23.0	79.73	1.997	0.8137

^a ±0.1 °C.TABLE II: Walden Products and Activation Energies for Viscosity and Conductance of Neat N₂₂₂₆B₂₂₂₆

<i>T</i> , °C	$\Lambda\eta^a$	$E^A,^b$ kcal mol ⁻¹	$E^\eta,^b$ kcal mol ⁻¹	E^η/E^A
20.00	52.3			
30.00	51.1	9.86	10.41	1.056
40.00	50.1	9.25	9.71	1.050
50.00	49.9	8.79	9.02	1.026
60.00	49.0	8.15	8.72	1.070
70.00	47.7	7.72	8.39	1.087
80.00	46.4			

^a Λ values interpolated from Table I. ^b Calculated from data at ca. +10 and -10 °C from indicated temperature.TABLE III: Viscosity and Conductance of N₂₂₂₆B₂₂₂₆-Benzene at 25.00 °C

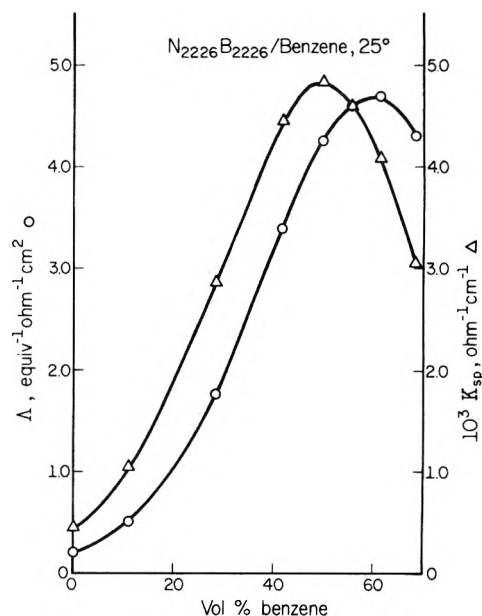
N ₂₂₂₆ B ₂₂₂₆ concn, M	η , cP	Λ , equiv ⁻¹ ohm ⁻¹ cm ²	$\Lambda\eta$
2.26	254 ^a	0.204	51.7
2.01	87.2	0.522	45.5
1.617	23.0	1.769	40.7
1.315	9.01	3.39	30.5
1.132	6.00	4.26	25.6
1.004	3.96	4.59	18.2
0.873	3.15	4.69	14.8
0.712	2.33	4.30	10.02

^a Interpolated from 20 and 30 °C values in Table I.

n-hexylammonium benzoate hemihydrate at 25 °C also has been reported.⁶ Viscosities and pVT properties of some tetraalkylammonium tetraalkylborides⁷ and viscosities and conductances of some tetraalkylammonium tetrafluoroborates⁸ have been explored at >100 °C. Walden and co-workers examined viscosities and conductances of molten tetraalkylammonium picrates at >100 °C 50 years ago.⁹

Results

Viscosities and equivalent conductances of neat liquid N₂₂₂₆B₂₂₂₆ are given in Table I. From 0 to 80 °C its viscosity decreases by a factor of 67 and from 20 to 80 °C its conductance increases by a factor of 13. The Walden product decreases somewhat with increased temperature (Table II). Arrhenius plots of the viscosity and conductance data are not linear; the apparent activation energies decrease with increased temperature (Table II).

Figure 1. Specific conductance and equivalent conductance of N₂₂₂₆B₂₂₂₆-benzene solutions at 25 °C.

The viscosity and conductance data on N₂₂₂₆B₂₂₂₆-benzene solutions in Table III extend from the molten salt to near the solubility limit of benzene in N₂₂₂₆B₂₂₂₆. (An attempt to prepare a 71.4 vol % benzene solution gave a two phase mixture.) In this range the viscosity decreases by a factor of 109 and the specific conductance and equivalent conductance reach maxima at about 50 and 61 vol % benzene, respectively, as shown in Figure 1. These maxima are 10.5 times greater than the K_{sp} and 23 times greater than the Λ of the neat liquid salt.

Discussion

Qualitatively the nonexponential dependences of conductance and viscosity of N₂₂₂₆B₂₂₂₆ on $1/T$ resemble earlier reports of tetraalkylammonium picrates^{9,10} and tetrafluoroborates⁸ at >100 °C and tetra-*n*-pentylammonium thiocyanate (N₅₅₅SCN) at 52–110 °C.^{5b} The values of E^η and E^A for N₂₂₂₆B₂₂₂₆ at 20–80 °C are larger than reported for other molten salts, but would not be larger if they were extrapolated to the higher temperatures required to melt the other salts. The small decrease in $\Lambda\eta$ of N₂₂₂₆B₂₂₂₆ with increasing temperature also resembles the behavior of other molten tetraalkylammonium salts.^{5b,9,10} The ratio E^η/E^A is greater than unity in a wide variety of molten salts and has been explained in terms of a difference in transport mechanisms. Viscous flow requires movement of both ions at the same rate in the same direction, but cation and anion must move in opposite directions in electrical conductance and may have unequal transport numbers. When the ions are nearly equal in size, they often are assumed to have equal transport numbers. This assumption is based on limiting equivalent conductances in water of many electrolytes. As their transport numbers approach equality, E^η/E^A should approach unity, as it does in N₂₂₂₆B₂₂₂₆. (Actually typical N–C and B–C bond lengths in quaternary ions, 1.52 and 1.65 Å, respectively,^{11,12} imply that the B₂₂₂₆ anion is slightly larger than the N₂₂₂₆ cation.) An alternative explanation for values of E^η/E^A close to unity is that the alkyl chains of the N₂₂₂₆ and B₂₂₂₆ ions are entwined, and consequently conductance requires cooperative motion of anion and cation just as viscous flow does.¹⁰

The activation energies E^η and E^λ are substantially larger than the activation energies for effective rotational correlation times calculated from carbon-13 NMR spin lattice relaxation times of individual carbon atoms in $N_{2226}B_{2226}$.¹³ The NMR correlation times depend on both overall reorientation (Brownian motion) and internal rotation about single bonds. At the carbon atoms where the overall reorientation contribution is the greatest, those bound directly to nitrogen or boron, $E_a = 6.4\text{--}7.0$ kcal/mol from data at 10–120 °C. Apparently the frictional forces which impede rotational diffusion are less dependent on temperature than those which impede translational diffusion.

Molten salts have been described as unassociated because Λ_η of the melt is approximately equal to Λ_η^0 extrapolated to infinite dilution.^{4,5,9} As benzene is added to $N_{2226}B_{2226}$ at 25 °C or *p*-xylene is added to $N_{5555}SCN$ at 52 or 90 °C,⁵ Λ_η decreases, presumably due to ion association in the nonpolar solvent. The fraction of dissociated ions in concentrated solutions has been defined as $F_i = (\Lambda_\eta)/(\Lambda_\eta)_0$, the ratio of the Walden product of the solution to that of the neat liquid salt.⁵ However, Λ_η of $N_{5555}SCN$ increases when small amounts of nitrobenzene are added,¹⁴ which contradicts the complete dissociation hypothesis of Kenausis, Evers, and Kraus⁵ for liquid salts. We have rationalized relative rates of some ion-molecule reactions in $N_{2226}B_{2226}$ on the basis of cooperative anion-cation motion.¹⁵ Addition of a low dielectric constant solvent such as benzene or *p*-xylene may enhance the cooperativity, while a higher dielectric constant solvent such as nitrobenzene may reduce the cooperative motion by separating the ions whose alkyl chains are entwined in the melt.

The specific conductance of a 50/50 (v/v) $N_{2226}B_{2226}$ -benzene solution is >10 times higher than that of any other benzene solution at 25 °C listed in the massive compilation of Janz and Tomkins.¹⁶ Dilution with more polar organic solvents would probably give even higher specific conductances. Such solutions may be highly useful media for cathodic organic electrochemistry.³

Experimental Section

$N_{2226}B_{2226}$ was prepared as described before and analyzed to contain $<4 \times 10^{-5}$ M Li, $<1.4 \times 10^{-4}$ M Br, and $<10^{-3}$ M water.² It is not stable to air indefinitely, and the batch used for all experiments in this paper was pale yellow due to a trace of unknown decomposition product which is detectable by uv-visible but not by ir or PMR spectral methods. Compared to preliminary measurements¹⁷ with colorless samples of $N_{2226}B_{2226}$, the conductance of the material used in this work is 12% lower at 25 °C and its viscosity is 9–11% lower at 20–40 °C. These observations imply that the decomposition products are less viscous nonelectrolytes. To prevent decomposition during viscosity and conductance experiments the $N_{2226}B_{2226}$ was kept in a nitrogen atmosphere. After higher temperature experiments measurements were made again at low temperature to check for decomposition. No change of more than 1% was observed in the resistance or efflux time. Densities of $N_{2226}B_{2226}$ were measured at four temperatures from 22 to 65 °C in a 2-ml pycnometer. The densities in Table I were extrapolated or interpolated from the measurements and are estimated to be accurate to ± 0.0005 g cm⁻³. Benzene (Burdick and Jackson, distilled in glass) was used without

further purification. Volumes of $N_{2226}B_{2226}$ -benzene were determined to be equal to the sum of the volumes of the pure components within 0.3%, so densities of mixtures were taken as linear combinations of densities of the components. $N_{2226}B_{2226}$ -benzene mixtures were prepared by weight.

Conductivities were measured in a home-made cell with platinum black plates about 1 cm apart and a volume of 4 ml in a mineral oil bath. The cell constant of 0.686 ± 0.001 cm⁻¹ was determined with aqueous potassium chloride solutions. Temperature was measured with calibrated thermometers and controlled to ± 0.01 °C. Resistances of 150–2000 ohm were measured at 1 and 3 kHz with a conductivity bridge from Industrial Instruments, Inc., Cedar Grove, N.J. Observed resistances at 3 kHz were up to 0.4% lower than at 1 kHz when $R_{\text{obsd}} \approx 150$ ohm, but the values differed by <0.1% at $R_{\text{obsd}} > 400$ ohm. No impedance measurements to correct for polarization were attempted. The 3-kHz values were used to calculate Λ .

Viscosities were measured in six different Cannon and Ostwald capillary viscometers which were calibrated with water, benzene, glycerol, and castor oil with efflux times comparable to those used in the $N_{2226}B_{2226}$ experiments. Temperature was measured with calibrated thermometers and controlled to ± 0.02 °C except where noted in Table I. Two viscometers were used for each determination of neat $N_{2226}B_{2226}$ except at 0 and 10 °C. The results differed by <1.0% except at 20 °C where they differed by 2.0%. Average values are reported in Table III. A single Cannon viscometer was used for each $N_{2226}B_{2226}$ -benzene mixture.

Acknowledgments. We thank S. G. Smith for use of the conductivity bridge and several helpful discussions and T. Hanratty for use of the viscometers.

References and Notes

- (1) This research was supported by National Science Foundation Grant No. GP 38493.
- (2) W. T. Ford, R. J. Hauri, and D. J. Hart, *J. Org. Chem.*, **38**, 3916–3918 (1973).
- (3) W. T. Ford, *Anal. Chem.*, **47**, 1125–1126 (1975).
- (4) (a) R. P. Seward, *J. Am. Chem. Soc.*, **73**, 515–517 (1951); (b) R. P. Seward, *J. Phys. Chem.*, **62**, 758–759 (1958).
- (5) (a) L. C. Kenausis, E. C. Evers, and C. A. Kraus, *Proc. Natl. Acad. Soc. U.S.A.*, **48**, 121–128 (1962); (b) L. C. Kenausis, E. C. Evers, and C. A. Kraus, *ibid.*, **49**, 141–146 (1963).
- (6) C. G. Swain, A. Ohno, D. K. Roe, R. Brown, and T. Maugh, II, *J. Am. Chem. Soc.*, **89**, 2648–2649 (1967).
- (7) (a) G. Morrison and J. E. Lind, Jr., *J. Chem. Phys.*, **49**, 5310–5316 (1968); (b) T. Grindley and J. E. Lind, Jr., *ibid.*, **56**, 3602–3607 (1972). (c) For a review see J. E. Lind, Jr., in "Advances in Molten Salt Chemistry", Vol. 2, J. Braunstein, G. Mamantov, and G. P. Smith, Ed., Plenum Press, New York, N.Y., 1973, pp 1–26.
- (8) J. E. Lind, Jr., H. A. A. Abdel-Rehim, and S. W. Rudich, *J. Phys. Chem.*, **70**, 3610–3619 (1966).
- (9) P. Walden, H. Ulich, and E. J. Birr, *Z. Phys. Chem.*, **131**, 1–21 (1927).
- (10) G. J. Janz, R. D. Reeves, and A. T. Ward, *Nature (London)*, **204**, 1188–1189 (1964).
- (11) (a) J. D. Forrester, A. Zalkin, and D. H. Templeton, *Inorg. Chem.*, **3**, 1500–1515 (1964); (b) D. St. Clair, A. Zalkin, and D. H. Templeton, *ibid.*, **11**, 377–381 (1972).
- (12) K. Hoffmann and E. Weiss, *J. Organomet. Chem.*, **67**, 221–228 (1974).
- (13) W. T. Ford, *J. Am. Chem. Soc.*, in press.
- (14) F. R. Longo, P. H. Daum, R. Chapman, and W. G. Thomas, *J. Phys. Chem.*, **71**, 2755–2756 (1967).
- (15) W. T. Ford, R. J. Hauri, and S. G. Smith, *J. Am. Chem. Soc.*, **96**, 4316–4318 (1974).
- (16) G. J. Janz and R. P. T. Tomkins, "Nonaqueous Electrolytes Handbook", Vol. 1, Academic Press, New York, N.Y., 1972.
- (17) Conductance: ref. 3. Viscosity: 20.0 °C, 379 cP; 30.0 °C, 213 cP; 40.0 °C, 126 cP.

Effect of Association Complexes on the Glass Transition in Organic Halide Mixtures

Arnold V. Lesikar

Department of Physics, St. Cloud State University, St. Cloud, Minnesota 56301 (Received September 25, 1975)

Publication costs assisted by St. Cloud State University

The glass transition temperatures of binary mixtures of chloroform, dichloromethane, and trichloroethylene with several Lewis bases have been measured as a function of composition. The glass transition temperatures of the mixtures are shown to be increased by complex formation between the chloride and the base, and the glass transition temperature is shown to increase with base strength. The chloroform mixtures show the greatest effect of complex formation. A cusp is found in the composition dependence of the glass transition temperature T_g of mixtures of chloroform with triethylamine. The cusp is found at the equimolar composition. It is taken as evidence for the complete association of chloroform with triethylamine into a 1:1 complex at T_g . The trichloroethylene mixtures show greater effects of complex formation than do the dichloromethane mixtures, although evidence from the literature seems to indicate that dichloromethane is the stronger acid.

Introduction

Association between the components of a mixture has been shown to increase the viscosity¹ and thereby the glass transition temperature.² Recent work by Angell and co-workers³ has demonstrated the effect on the glass transition of the formation of a stoichiometric ionic complex in electrolyte solutions. To date, however, no studies of the glass transition illustrating the effect of the formation of stoichiometric molecular complexes in nonelectrolyte solutions have been published. Solutions of the chlorinated hydrocarbons are well suited to such a study. The protons of such hydrocarbons have been shown to be activated to hydrogen bond formation by the attached chlorine atoms.^{4,5} Formation of hydrogen-bonded association complexes between chloroform (CFM) and various organic bases has been demonstrated by calorimetry and various spectroscopic techniques.⁶ Since trichloroethylene (TCE) and dichloromethane (DCM) have also been shown to be capable of serving as electron acceptors in the formation of a hydrogen bond, such complex formation can be expected to occur with these materials as well. In order to examine the effect of this complex formation on the glass transition, the glass transition temperature T_g was measured as a function of composition for binary mixtures of CFM, TCE, and DCM with various electron donors.

Experimental Section

The bases chosen for study were triethylamine (TEA); the ethers, tetrahydrofuran (THF), diethyl ether (DEE), and isopropyl ether (IPE); the carbonyls, acetone, methyl ethyl ketone (MEK), methyl isobutyl ketone (MIK), and benzaldehyde (BZA); the ester, ethyl acetate (EtAC); and the aromatic π donor, toluene. The sources of the materials are listed in Table I. All materials were of reagent grade with the exception of the TEA which was practical grade. All materials were used as received with the exception of acetone and TEA. Because the acetone was common laboratory stock dispensed from a 5-gal drum, it was dried before use by stirring with Drierite, from which it was removed by simple distillation. The TEA was stirred for 2 h or more with KOH pellets from which it was removed by simple distillation. It was then fractionally distilled at a 20

to 1 reflux ratio in a 50 plate Penn State column. The central 80% was taken for measurement. The TEA used in the extrapolations to determine T_g values of the pure organic chlorides was purified by a simpler procedure. Samples of TEA were subjected to simple distillation off of KOH pellets. They were then refluxed with metallic potassium to remove water and again subjected to simple distillation. These samples showed T_g values agreeing to within 1 °C with those of TEA purified by fractional distillation. Because of the tendency of the BZA to oxidize upon exposure to the atmosphere, fresh unopened bottles were frequently exchanged with bottles of the material in use. The water content of all the reagent material was listed by the manufacturer as under 0.2% with the exception of the Baker CFM and the Mallinckrodt BZA for which no water content was given.

Mixtures were prepared gravimetrically. The T_g values were determined by means of differential thermal analysis (DTA) using apparatus previously described.⁷ In the present work the strip chart recorders previously used to record the sample temperature T and the temperature difference ΔT of the sample from the DTA reference material have been replaced by a single X-Y recorder recording ΔT on the vertical axis against T on the horizontal axis. A suitable choice of scale was made to allow recording a 40 deg range of temperature around the glass transition. The T_g values were taken to represent the onset of the transition determined using the procedure of Thompson.⁸ They were found to be reproducible in the present work to within 0.3 °C, and the absolute accuracy is estimated to be 1.5 °C. Absorption of water from the atmosphere during the course of a run was estimated to be less than 0.2% of the sample material by weight by making the tests previously described.⁷

DTA measurements were carried out at a heating rate of 12 deg/min. Samples were contained in 1-mm diameter melting point capillaries. In most of the measurements samples were vitrified by immersion of the sample capillary in liquid nitrogen. It was then inserted into the DTA block, which was maintained under liquid nitrogen. Quenching the sample often leads to a small exothermic peak following the transition.⁹ Because this peak sometimes became confused with the glass transition, making it difficult to deter-

TABLE I: Sources and T_g Values of Solvents

Compound	Manufacturer	T_g , °C
Chloroform (CFM)	Baker, Mallinckrodt	-167.3
Dichloromethane (DCM)	Baker, Mallinckrodt	-170.1
Trichloroethylene (TCE)	Baker, Mallinckrodt	-166.9
Triethylamine (TEA)	Matheson, Eastman	-170.0
Diethyl ether (DEE)	Mallinckrodt	-180.6
Isopropyl ether (IPE)	Mallinckrodt	-171.8
Tetrahydrofuran (THF)	Baker	-193 ± 3
Acetone	Matheson	-173 ± 2.5
Methyl ethyl ketone (MEK)	Mallinckrodt	-161.8
Methyl isobutyl ketone (MIK)	Mallinckrodt	-153.3
Ethyl acetate (EtAC)	Eastman	-155.5
Benzaldehyde (BZA)	Mallinckrodt	-124.1
Toluene	Baker	-155.9

mine T_g , certain samples were rapidly cooled to a point somewhat above T_g but well below their melting point by inserting them into the block at the intermediate temperature. The samples were then slowly cooled through the glass transition by pouring liquid nitrogen directly onto the DTA block. Samples vitrified in this fashion demonstrated a very clean glass transition free of subsidiary peaks. Test measurements on material vitrified by both methods produced T_g values agreeing to better than 1 °C.

Samples were checked for crystallinity by visual inspection. Samples of material to be run by DTA were quenched to liquid nitrogen temperature and then removed from the nitrogen bath. Crystalline areas in the sample were clearly visible as the glass softened. In almost all cases the appearance of crystals under visual inspection was associated with a drastic decrease in the prominence of the glass transition in the DTA record.

The T_g values of the pure solvents are listed in Table I. The uncertainty in each value should be taken to be 1.5 °C unless otherwise indicated. This error represents mainly the overall uncertainty in the temperature measurement. The relative error among the different T_g values is much better than 1 °C. Of the materials listed, toluene, BZA, EtAC, DEE, TEA, and MIK can be vitrified as pure materials, and the values listed for these materials were determined as the means of many direct measurements. THF appears to the eye to vitrify when quenched to the temperature of liquid nitrogen. However, the T_g value is so close to liquid nitrogen temperature that the signature of the transition is lost in the starting transient of the DTA measurement, and the T_g value had to be determined by extrapolation. Similarly, IPE can apparently be vitrified in a capillary tube by quenching in liquid nitrogen. However, the presence of a thermocouple in the sample tube seems to nucleate crystallization so that no direct measurement of the T_g values of this material could be made. The T_g of this material and the remaining solvents were determined by extrapolation. The T_g value for MEK is the mean of extrapolations in six binary mixtures of MEK with CFM, TCE, DCM, reagent methanol, reagent 1-propanol, and reagent 1-butanol. In each mixture the glass transition could be traced to within 90 mol % of the pure MEK. The T_g of IPE is the mean of extrapolations in TCE and DCM mixtures from better than 90 mol % IPE. The THF and acetone T_g values are the result of linear extrapolations in CFM and TCE binary mixtures from 85 mol % or better to

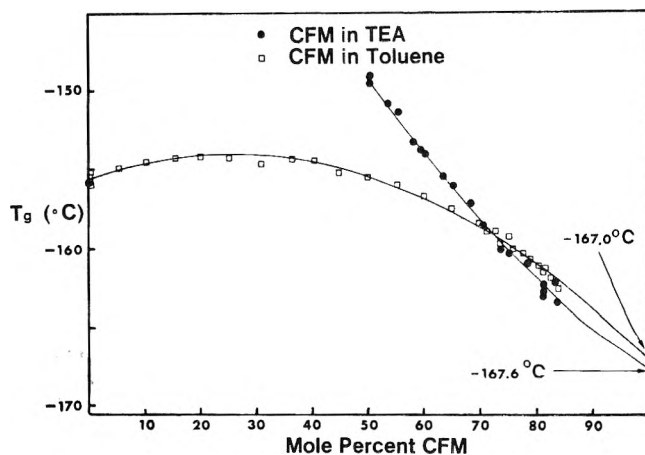


Figure 1. T_g as a function of composition for CFM mixtures: determination of the CFM T_g .

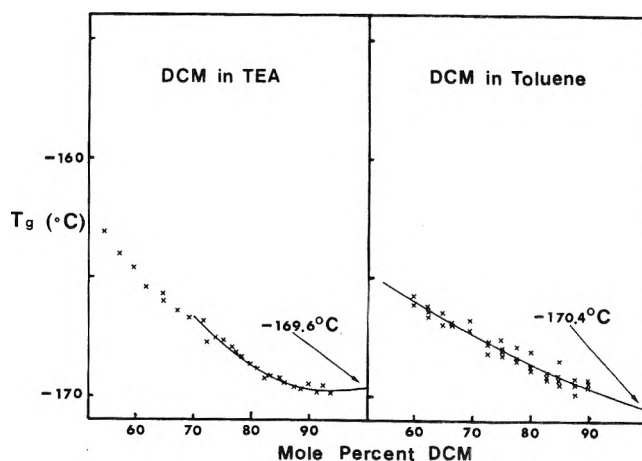


Figure 2. T_g as a function of composition for DCM mixtures: determination of the DCM T_g .

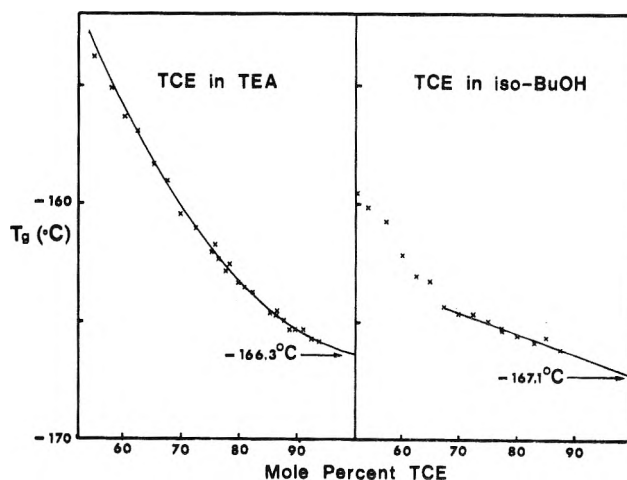


Figure 3. T_g as a function of composition for TCE mixtures: determination of the TCE T_g .

pure acetone or from 75 mol % or better to pure THF.

The T_g extrapolations for the organic chlorides were made with particular care. The T_g value reported for TCE is the mean of extrapolations in binary mixtures with three different reagent alcohols and with TEA. Examples of these extrapolations are shown in Figure 1. The DCM value

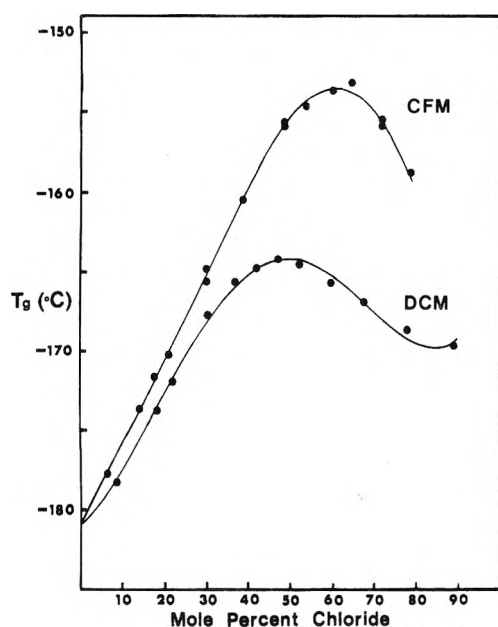


Figure 4. Mixtures of DEE with organic chlorides: T_g as a function of composition.

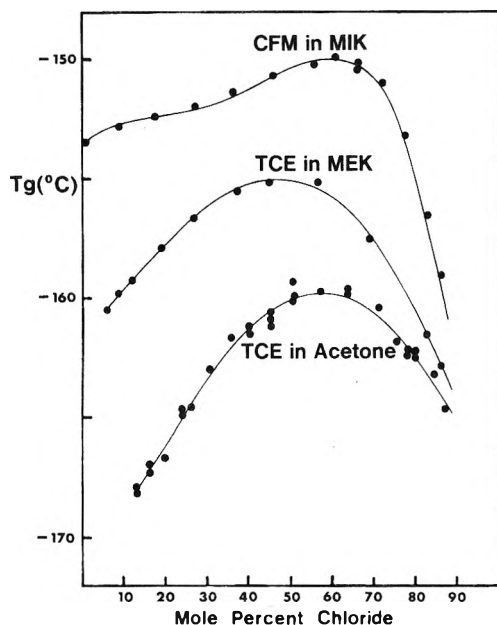


Figure 5. Mixtures of carbonyls with the organic chlorides: T_g as a function of composition.

is the mean of extrapolations in binary mixtures with toluene, TEA, EtAC, and BZA (Figure 2). The CFM value is the mean of extrapolations in binary mixtures with toluene and with TEA (Figure 3).

Results

All possible combinations of chloride proton donors with the bases listed above were studied. Glass formation over wide central ranges of composition was observed even in those mixtures where neither pure component is by itself a glass former. Only in DCM-acetone mixtures and CFM-IPE mixtures was crystallization observed to intervene in the central region of composition. In the former, crystallization was observed over a range of about 20% centered on the equimolar composition, while in the latter mixtures,

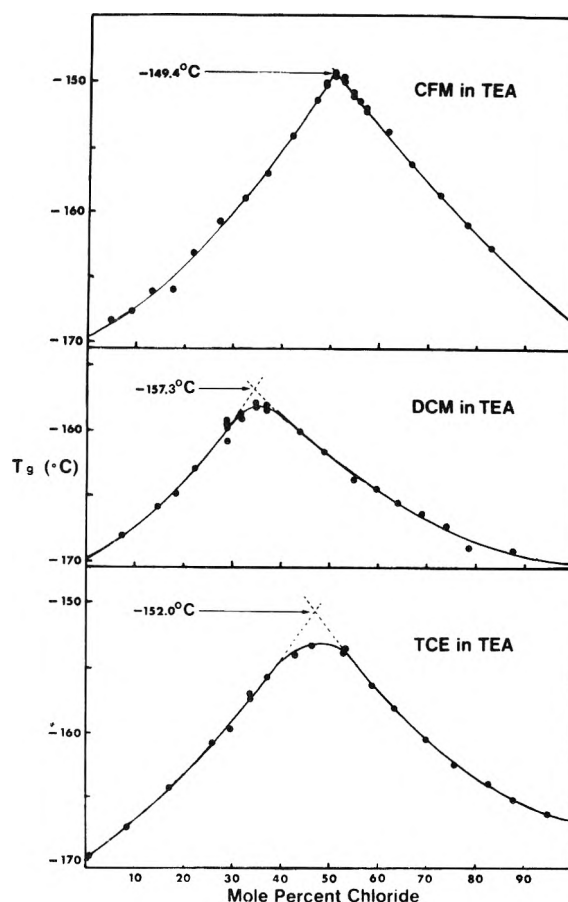


Figure 6. Mixtures of TEA with the organic chlorides: T_g as a function of composition. Arrows indicate the estimated T_g for each chloride-TEA complex.

crystallization was observed to occur only at the equimolar composition.

Figures 4-6 show representative examples of the composition dependence of T_g in the mixtures studied. In all cases but one the T_g value of the mixture lies above the value predicted by a linear composition dependence. In most mixtures this results in a well defined maximum in the T_g curve. The TEA mixtures are of particular interest. A very sharp maximum is found at 50 mol % in mixtures between this material and CFM. The maximum takes the form of a cusp in so far as the accuracy of the measurements allow it to be determined. A similar maximum is found in the DCM-TEA mixtures near 33 mol % DCM. In this case these data indicate definite rounding at the peak. The TCE-TEA mixtures display a very rounded maximum, near the 50 mol % point.

An excess glass temperature T_e may be defined as the difference between the observed T_g and that predicted assuming a linear variation of T_g with molar composition. Regularities in the data appear when this T_e is plotted against composition as in Figures 7-9. In all mixtures except that between toluene and DCM the T_e value shows a maximum. TEA and BZA mixtures have not been included in these figures. TEA attains maximum T_e values of 19, 15, and 12 °C in the CFM, TCE, and DCM mixtures, respectively. BZA shows a maximum comparable in shape to that of the other carbonyls and attains a maximum T_e of 11, 3.5, and 2 °C in the CFM, TCE, and DCM mixtures, respectively. In mixtures with each proton donor the T_e value is approximately the same for each class of base. The T_e

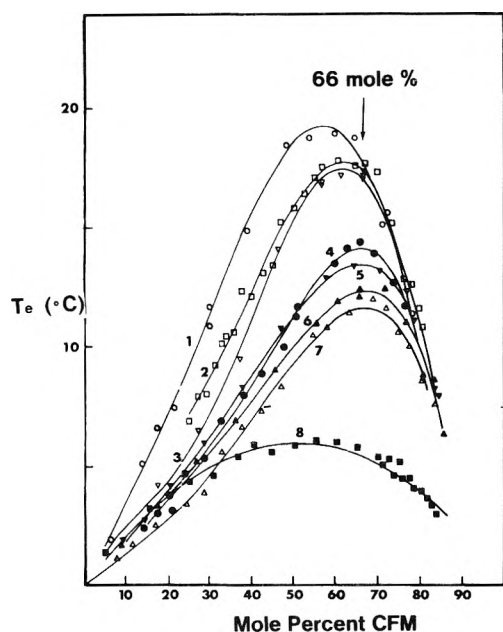


Figure 7. Excess glass temperature as a function of composition: CFM mixtures. The numeral on each curve indicates the second component of the mixture as follows: 1, DEE; 2, THF; 3, IPE; 4, acetone; 5, MEK; 6, MIK; 7, E:Ac; and 8, toluene.

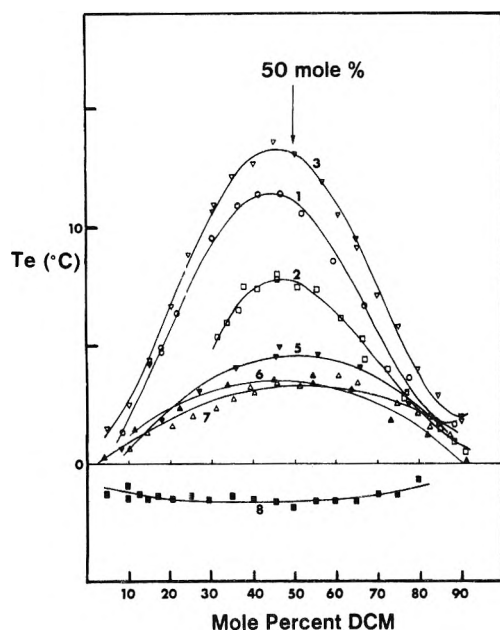


Figure 8. Excess glass temperature as a function of composition: DCM mixtures. The numeral on each curve indicates the second component of the mixture as in Figure 7.

value is greatest in size when the base is TEA or an ether. The carbonyls, including BZA and EtAC, show a generally smaller T_e value. The T_e maximum is smallest in size for toluene, and toluene in fact exhibits a T_e minimum rather than a maximum in the DCM mixtures. In the DCM mixtures (with the exception of the TEA-DCM mixture) and in the TCE mixtures the position of the T_e maximum is very nearly at the equimolar composition, while among the CFM mixtures the T_e maximum lies at almost exactly 66 mol % CFM in mixtures with the carbonyls and in the range 55–60 mol % CFM in mixtures with ethers.

Besides using the listed bases we have studied mixtures

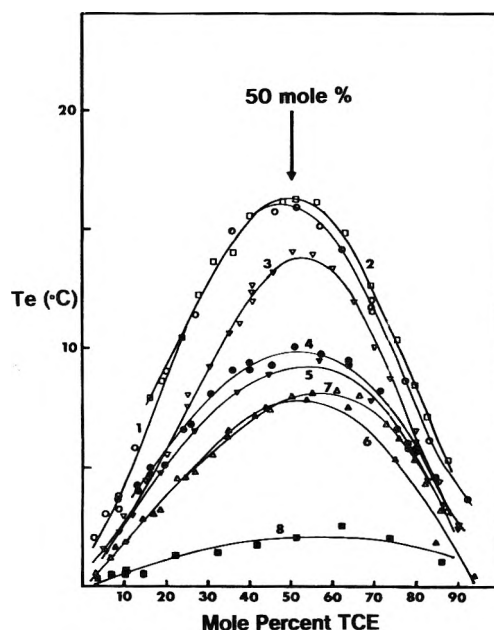


Figure 9. Excess glass temperature as a function of composition: TCE mixtures. The numeral on each curve indicates the second component of the mixture as in Figure 7.

of the organic chlorides with pyridine and cyclohexanone. We found again a broad central range of glass formation in each of these mixtures. We have not included these data in present study because we have not been able to make a reliable determination of the glass point of the pure base. We have also investigated mixtures of CFM with dimethyl sulfoxide and with *p*-dioxane. In these mixtures we observed glass formation only in a 40% molar range of composition centered on the 60 mol % CFM point.

Discussion

We believe that the maxima observed in the excess glass temperature in these mixtures are due to the formation of hydrogen-bonded association complexes between the chloride and the base. The T_e value at the maximum correlates with published values^{10–15} of the excess enthalpy of mixing at the equimolar composition. In Figure 10 this correlation is shown for the CFM mixtures; the T_e value at the maximum is found to increase more or less linearly with excess enthalpy. In these systems the major contribution to the enthalpy of mixing is believed to be the energy released upon formation of the hydrogen bond of the complex.^{16–19} The correlation therefore indicates that the T_e value increases in size with the stability of the complex. The T_e value is also found to correlate with infrared measures of base strength. The shift $\Delta\nu_s$ in the phenol O–H stretching frequency upon formation of a hydrogen bond to a particular base has been shown to correlate with base strength.²⁰ Accordingly we have plotted in Figure 11 the observed maximum T_e value for mixtures with a particular base against the base strength as measured by the $\Delta\nu_s$ for the hydrogen bond formed by that base with phenol in CCl_4 at 20 °C as tabulated by Murthy and Rao.²¹ Again we find that T_e increases with base strength and a least-squares fit of a straight line to the data points leads to a correlation coefficient greater than 0.9.

Trends in tabulated²² T_g values indicate that a positive T_e is to be expected as a result of the formation of molecular complexes. The T_g values of homologous liquids in gen-

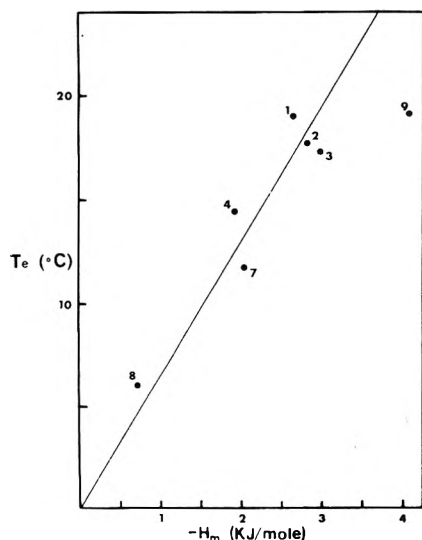


Figure 10. Peak excess glass temperature in relation to the equimolar excess enthalpy of mixing: CFM mixtures. The numeral at each point indicates the second component of the mixture as in Figure 7 (9, TEA).

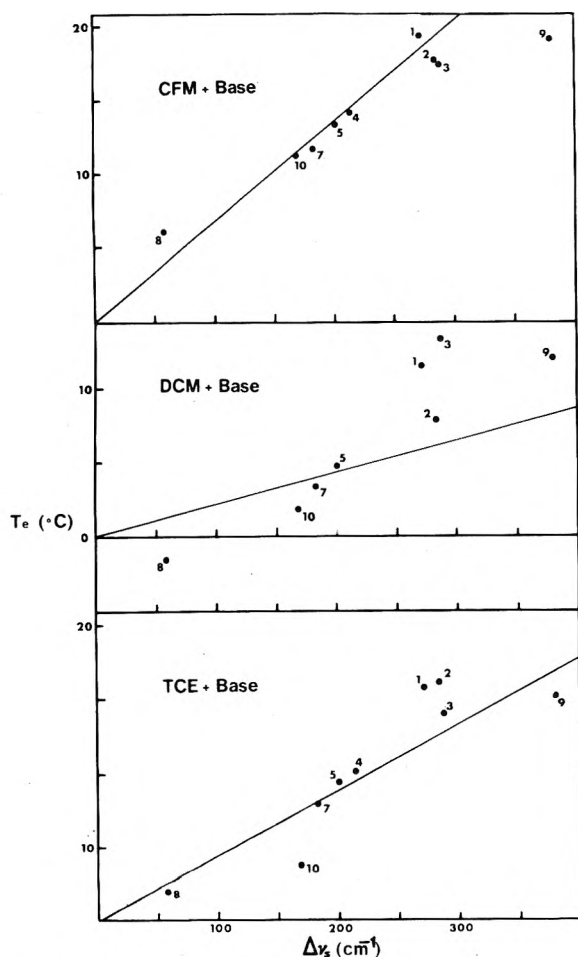


Figure 11. Peak excess glass temperature in relation to the phenol $\Delta\nu_s$ for the base. The numeral at each point indicates the base as in Figure 10 (10, BZA).

eral increase with molecular size. Since the free energy release upon formation of a complex can be shown to be large in comparison with the thermal energy at the glass point, most of the molecules in solution capable of participating

in complex formation can be expected to do so. Such complexes once formed can be expected to live a long time in comparison with the mean time between molecular collisions. The creation of larger molecular units will then have the effect of increasing T_g .

The cusp found in the T_g curve for the CFM-TEA mixtures strongly suggests that we are observing virtually complete association between CFM and TEA. That the association is in the form of a 1:1 complex is indicated by the occurrence of the cusp at the 50 mol % composition. The cusp appears because the character of the mixture changes sharply at the 50 mol % point. If association is complete the species in solution change from TEA plus complex to CFM plus complex at the 50 mol % point. The conclusion that association is virtually complete in these mixtures is supported by the NMR measurements of Wiley and Miller.²³ These authors report the enthalpy ΔH of formation of the CFM-TEA hydrogen bond to be -17.0 kJ/mol and the entropy change to be -63.6 J/mol deg at room temperature. If these values are assumed to be temperature independent, the free energy change upon bonding at the cusp temperature must be -9.1 kJ/mol implying an association constant K of 6900 (mole fraction)⁻¹ at this temperature. This K value implies that complex formation is almost 99% complete at the cusp temperature. Accordingly we believe that we are observing complete CFM-TEA association and that the cusp temperature of -149 °C represents the T_g value of the complex.

The rounding of the peak in the DCM-TEA mixtures suggests that association in these mixtures is not complete. The position of the maximum indicates the formation of a 2:1 complex representing the bonding of TEA molecule to each of the two DCM protons. The intersection points of quadratic curves fit to the two sides of the maximum lead to an estimate -157 °C as the T_g value of this complex as shown in Figure 6.

The T_g maximum in the TEA-TCE mixtures occurs at a point near 50 mol % TCE, which indicates formation of a 1:1 complex. The pronounced rounding of the maximum in these mixtures suggests that complex formation is far from completion. This conclusion is consistent with the weakness of TCE as a proton donor.^{4,5}

The fact that the carbonyls and ethers show a T_e maximum in the CFM mixtures near 60 mol % CFM suggests that the formation of a 2:1 CFM:base bicomplex is the predominant mode of association in these mixtures. The formation of such a bicomplex between CFM and acetone, in which two CFM molecules are most likely directly bonded to each acetone oxygen, has been reported by several authors.^{12,24-27} Since an ether is in general a stronger base than a carbonyl,²⁰ bicomplex formation of this type can be expected in ether mixtures as well.

Among the DCM mixtures with an oxygen carrying base, the T_e maximum occurs at the 50 mol % composition. DCM is known to be a rather strong proton donor, although weaker than CFM.²⁸ Since each oxygen atom has two proton acceptor sites, and each DCM molecule can donate two protons to a bond, chainwise association with DCM and base serving as alternate links in the chain should be possible. The bond entropy and enthalpy for the DCM-acetone bond given by Pang and Ng²⁹ imply association very nearly as extensive as in the CFM mixtures at the glass temperature. Therefore the presumed association chains should grow very long as the equimolar composition is approached. The Gibbs-DiMarzio theory of the glass transition in long

chain polymers³⁰ should describe the effect of this chain growth qualitatively.³¹ This theory predicts a steep initial rise in T_g leading to large increases in T_g as chains form from the monomer. Because the T_e values in the DCM mixtures are smaller than in the CFM mixtures where this sort of chain formation cannot occur, we doubt that chain formation occurs in the DCM mixtures. We believe that the position of the T_e peak near the equimolar composition indicates the formation of a 1:1 complex with a single DCM molecule bound to a single base. Bond angles should prevent the formation of a second hydrogen bond between the two molecules. The hydrogen atom in a bond seldom deviates far from the line connecting the two atoms bound together,³² and bond angles at the hydrogen are seldom smaller than 150° . For the two DCM protons to occupy both acceptor sites on the oxygen atom would require a C-H-O bond angle of about 71° in each bond. Further evidence that one DCM proton is free in the 1:1 complex is the fact that the T_e peak occurs at compositions slightly poorer in the DCM than 50 mol % among the ether mixtures. This indicates a small amount of bicomplex formation with a single DCM molecule binding two ether molecules. The presence of the bicomplex shows that one DCM proton is free in the 1:1 complex to bind a second molecule.

The effect of complex formation on the glass transition is most easily understood in terms of its effect on the entropy of the mixture. There is increasing evidence^{33,34} that the occurrence of the glass transition is due to the decrease of configurational entropy associated with structural rearrangements in the liquid. Complex formation in the mixtures investigated in the present work produces negative excess entropies of mixing whose composition dependence runs generally parallel to that of the excess enthalpy of mixing. Much of the entropy loss upon formation of a complex must be configurational as the molecules associating lose the ability to move independently of each other. A further loss in configurational entropy must arise from the increase in the so-called "physical interactions"³⁵ produced by association. The materials that we are concerned with here are highly polar with electric dipole moments of the order of 1 to 2 D.³⁶ The combination of these moments can be expected to lead to a complex having a large dipole moment, which will be further increased by the dipole moment enhancement known to occur upon formation of a hydrogen bond.³⁷⁻³⁹ The increased cohesion produced by these larger dipole moments will lead to a loss of both translational and rotational freedom among the molecules of the mixture producing a loss of entropy.

The temperature at which the glass transition is observed will depend upon the rate of decrease of the remaining configurational entropy with temperature, that is, upon the liquid-glass specific heat difference ΔC_p . If association does not produce a large decrease in ΔC_p , complex formation must increase T_g . Conversely, the observed increase in T_g implies that ΔC_p must vary little with composition. This point is accessible to test, for the size of ΔC_p determines the magnitude of the DTA signature of the glass transition. Although we can make no quantitative measurements of the size of ΔC_p with our present apparatus, we observe no dramatic variation in the size of the DTA signal with composition. Further measurements to confirm the constancy ΔC_p would nevertheless be important to make.

Our results indicate that T_e correlates with the binding energy of the association complex formed in the mixture. The size of T_e implies the following order in proton donat-

ing power; CFM > TCE > DCM. We have previously found the same order in mixtures of these chlorides with the normal alcohols.⁷ The position of TCE in this series seems to be anomalous. Trew and Watkins⁴⁰ report excess enthalpies of mixing in TCE-acetone mixtures that are about one-half as great as the values given by Findlay and Kavanagh⁴¹ for DCM-acetone mixtures. The weakness of TCE as a proton donor is further shown by the lack of maximum boiling azeotropes with this material. The tabulation of Lecat⁴² lists only a single such azeotrope, that between TCE and ethylal, which boils within 1.5°C of TCE, while the bases which give maximum boiling mixtures with DCM span a range of about 15°C about the DCM boiling point. These data indicate that TCE is in fact a much weaker proton donor than DCM, although it shows larger T_e values. This anomaly is very difficult to explain in terms of molecular interactions. Consideration of the configurational entropy, however, suggests that the large T_e values of TCE may be due to an unusually large ΔC_p values in its mixtures. As our present data give only a very qualitative estimate of ΔC_p , it would be interesting to obtain additional calorimetric data to test this suggestion. We are grateful to the referee who suggested this possible resolution of the anomaly.

Conclusion

We have demonstrated that the formation of hydrogen bonded complexes between organic chlorides and various bases produces an increase in the glass transition temperature of the solution. For a particular chloride the T_g value increases with the strength of the bond, but the size of the increase for different chlorides and the same base is related in no obvious fashion to the bonding power of the chloride.

Acknowledgment. The author wishes to acknowledge with gratitude the support of the Physics and Chemistry Departments of St. Cloud State University. He is also grateful for the help of his student Mr. Dawson Deuermeyer with the calculations. He also wishes to thank the St. Cloud State University and the School of Liberal Arts and Sciences for aid with the publication costs.

References and Notes

- (1) A. Bondi, "Physical Properties of Molecular Crystals, Liquids, and Glasses", Wiley, New York, N.Y., 1968, p 365.
- (2) J. Sutter and C. A. Angell, *J. Phys. Chem.*, **75**, 1826 (1971).
- (3) A. J. Easteal, E. J. Sare, C. T. Moynihan, and C. A. Angell, *J. Solution Chem.*, **3**, 807 (1974).
- (4) C. S. Marvel, F. C. Dietz, and M. J. Copley, *J. Am. Chem. Soc.*, **62**, 2273 (1940).
- (5) C. S. Marvel, J. J. Copley, and E. Ginsberg, *J. Am. Chem. Soc.*, **62**, 3109 (1940).
- (6) G. C. Pimentel and A. L. McClellan, "The Hydrogen Bond", W. H. Freeman, San Francisco, Calif., 1960.
- (7) A. V. Lesikar, *J. Chem. Phys.*, **63**, 2297 (1975).
- (8) E. V. Thompson, *J. Polym. Sci., Part A*, **4**, 199 (1966).
- (9) W. Wrasidlo, *Adv. Polym. Sci.*, **13**, 3 (1974).
- (10) L. G. Hepler and D. V. Fenby, *J. Chem. Thermodyn.*, **5**, 471 (1973).
- (11) L. A. Beath and A. G. Williamson, *J. Chem. Thermodyn.*, **1**, 51 (1969).
- (12) K. W. Morcom and D. N. Travers, *Trans. Faraday Soc.*, **61**, 230 (1965).
- (13) S. Murakami, M. Koyama, and R. Fujishiro, *Bull. Chem. Soc. Jpn.*, **41**, 1540 (1968).
- (14) H. Hirobe, *J. Fac. Sci., Imp. Univ. Tokyo, Sect. 4*, **1**, 155 (1926).
- (15) L. Abello, *J. Chim. Phys.*, **70**, 1355 (1973).
- (16) J. A. Barker and F. A. Smith, *J. Chem. Phys.*, **22**, 375 (1954).
- (17) A. N. Campbell and E. M. Kartzmark, *Can. J. Chem.*, **38**, 652 (1960).
- (18) M. L. McGlashan and R. P. Rastogi, *Trans. Faraday Soc.*, **54**, 496 (1958).
- (19) T. J. V. Findlay, J. S. Keniry, A. D. Kidman, and V. A. Pickles, *Trans. Faraday Soc.*, **63**, 846 (1967).
- (20) G. C. Pimentel and A. L. McClellan, *Annu. Rev. Phys. Chem.*, **22**, 369 (1971).

- (21) A. S. N. Murthy and C. N. R. Rao, *Appl. Spectrosc. Rev.*, **2**, 69 (1968).
 (22) A. Bondi, ref 1, p 376.
 (23) G. R. Wiley and S. I. Miller, *J. Am. Chem. Soc.*, **94**, 3287 (1972).
 (24) E. R. Kearns, *J. Phys. Chem.*, **65**, 314 (1961).
 (25) K. B. Whetsel and R. E. Kagarise, *Spectrochim. Acta*, **18**, 329 (1962).
 (26) T. Matsui, L. G. Hepler, and D. V. Fenby, *J. Phys. Chem.*, **77**, 2397 (1973).
 (27) G. S. Denisov, *Opt. Spectrosc.*, **11**, 232 (1961).
 (28) R. H. Ewell and L. M. Welch, *J. Am. Chem. Soc.*, **63**, 2475 (1941).
 (29) T. S. Pang and S. Ng, *Spectrochim. Acta, Part A*, **29**, 207 (1973).
 (30) J. H. Gibbs and E. A. DiMarzio, *J. Chem. Phys.*, **28**, 373 (1958).
 (31) A. J. Easteal and C. A. Angell, *J. Phys. Chem.*, **74**, 3987 (1970).
 (32) G. C. Pimentel and A. L. McClellan, ref 6, p 265.
 (33) M. Goldstein, *J. Chem. Phys.*, **39**, 3369 (1963).
 (34) M. Goldstein, *J. Phys. Chem.*, **77**, 667 (1973).
 (35) J. H. Hildebrand and R. L. Scott, "The Solubility of Nonelectrolytes", 3d ed, Dover Publications, New York, N.Y., 1964, Chapters IV and XI.
 (36) A. L. McClellan, "Tables of Experimental Dipole Moments", W. H. Freeman, San Francisco, Calif., 1963.
 (37) H. Ratajczak, *J. Phys. Chem.*, **76**, 3000 (1972).
 (38) H. Ratajczak, *J. Chem. Phys.*, **58**, 911 (1973).
 (39) J. R. Hulett, J. A. Pegg, and L. E. Sutton, *J. Chem. Soc.*, 3901 (1955).
 (40) V. C. G. Trew and G. M. C. Watkins, *Trans. Faraday Soc.*, **29**, 660 (1933).
 (41) T. J. V. Findlay and P. J. Kavanagh, *J. Chem. Thermodyn.*, **6**, 367 (1974).
 (42) M. Lecat, "Tables Azeotropiques, Vol. I, Azeotropes binaires orthobares", 2nd ed, Uccle, Brussels, 1949.

Reactions of Cation Radicals of EE Systems. IV. The Kinetics and Mechanism of the Homogeneous and the Electrocatalyzed Reaction of the Cation Radical of 9,10-Diphenylanthracene with Hydrogen Sulfide¹

John F. Evans and Henry N. Blount*

Brown Chemical Laboratory, The University of Delaware, Newark, Delaware 19711 (Received October 17, 1975)

Potential step spectroelectrochemical studies of the reaction of H₂S with electrogenerated DPA^{•+} at Pt-OTE's on which PtS has been anodically formed prior to the pulsed experiment shows unusually fast consumption of cation radical during the initial stages of the pulse. Similar experiments using electrodes on which PtS has not been formed as well as those on which PtS has been formed and then cathodically discharged do not give rise to this behavior. On the basis of these experiments, it is concluded that H₂S is adsorbed onto PtS where it reacts with electrogenerated DPA^{•+} and further, that the adsorption process is kinetically slow. Open circuit relaxation spectroelectrochemical experiments of varying pulse duration show that the consumption of DPA^{•+} is initially a zero-order process involving H₂S adsorbed onto the PtS surface and, as this adsorbed material is depleted, the consumption of DPA^{•+} becomes a second-order process. In concert with the potential step experiments, these pulse time studies show the parallel nature of the heterogeneous and homogeneous reaction pathways. The zero-order rate constant for the heterogeneous process was evaluated from pulse relaxation experiments (by extrapolation to zero pulse duration) to be $1.51(\pm 0.05) \times 10^{-2} \text{ M s}^{-1}$. The bimolecular rate constant for the homogeneous process was evaluated from potential step and pulsed relaxation spectroelectrochemical measurements and stopped-flow kinetic spectrophotometry to be $6.6(\pm 1.2) \text{ M}^{-1} \text{ s}^{-1}$.

Introduction

Reactions of the cation radical derived from 9,10-diphenylanthracene (DPA), a representative EE system,² have been addressed in several recent studies in these³⁻⁶ and other⁷⁻¹² laboratories. These investigations have shown that reactions of this cation radical (DPA^{•+}) with various nucleophiles afford both addition and electron transfer products. In the course of examining the reactivity of various such "hard" and "soft" nucleophiles²² with DPA^{•+}, the reaction of this cation radical with hydrogen sulfide was investigated.

It has recently been found that the oxidation of H₂S at platinum electrodes in acetonitrile solutions gives rise to the formation of platinum sulfide surfaces on these electrodes.²³ In view of this, the mechanistic role of these anodically modified surfaces in reactions of electrogenerated DPA^{•+} with H₂S was examined. In order to clearly delineate the extent of participation of the platinum sulfide sur-

face in the reaction of DPA^{•+} with H₂S, parallel experiments utilizing stopped-flow kinetic techniques were conducted. This paper reports the results of these studies which afford the first spectroelectrochemical²⁴ observation of an electrocatalyzed reaction.

Experimental Section

The sources of and purification procedures for acetonitrile, DPA, tetraethylammonium perchlorate (TEAP), and hydrogen sulfide have already been reported.²³ The test electrodes used in this work were vapor deposited platinum optically transparent electrodes (OTE) prepared after the manner of von Benken and Kuwana²⁵ and platinum sulfide OTE's prepared by anodic oxidation of platinum OTE's as previously reported.²³ These electrodes were incorporated into an electrochemical cell of a type which has been previously described.²⁶ The potentiostat used in this work was similar in design to that reported by Pilla.²⁷ The spectroelectrochemical apparatus has also been described.²⁶

Stopped-flow experiments employed a Durrum Model D-110B stopped-flow kinetic spectrophotometer. In these experiments, DPA^+ was electrogenerated in an electrochemical cell external to the stopped-flow apparatus by the controlled potential ($E = +1.40$ V) electrolysis of acetonitrile solutions of 0.10 M TEAP and the requisite concentration of DPA. These partially electrolyzed solutions were transferred via a closed system to one of the drive syringes of the stopped-flow spectrophotometer. The remaining drive syringe was filled with an acetonitrile solution containing 0.10 M TEAP and the desired concentration of hydrogen sulfide.²⁸ Solutions of this latter reagent were prepared and assayed in the manner previously reported.²⁹

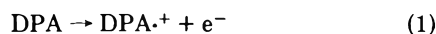
A dedicated NOVA 1200 computer system (Data General Corp.) was used to control both spectroelectrochemical and stopped-flow kinetic reactors, as well as to acquire and reduce the data therefrom. The wavelength employed for all kinetic spectrophotometry was the λ_{max} of DPA^+ , 653.0 nm.³⁰ All kinetic experiments were conducted at $25.0(\pm 0.2)$ °C. All electrode potentials are reported relative to the aqueous saturated calomel electrode.

The stoichiometry of the reaction of DPA^+ with H_2S was determined by measuring the amount of DPA produced relative to the amount of DPA^+ consumed. These measurements were effected by monitoring the absorbance of DPA at 392.5 nm and indicated that $97(\pm 3)\%$ of the DPA^+ consumed was reduced to DPA by the action of H_2S .³¹ Following macroscale reaction of electrogenerated DPA^+ with either gaseous H_2S or H_2S -saturated acetonitrile, the solvent was removed under vacuum and the residue extracted first with cold benzene and then with water to remove DPA and TEAP, respectively. The remaining residue was determined by mass spectral measurements to be oligomeric elemental sulfur containing up to eight atoms.

Results

The stoichiometry observed in this study reaffirms the electron transfer character of this reaction as originally reported by Sioda.²⁰ That such an electron transfer process occurs following the selective oxidation of DPA in the presence of H_2S is a manifestation of the relative magnitudes of the thermodynamically reversible electrode potentials (E°) of the two couples vis-a-vis the relative magnitudes of the observed discharge potentials of these redox couples. The potential at which H_2S undergoes oxidation is shifted anodically upon oxidative modification of the electrode surface (PtS formation)²³ whereas that of DPA is not as is shown in Figure 1. Cathodic discharge of this modified surface results in the return of the initial voltammetric response observed at pristine platinum.²³

Single Potential Step Spectroelectrochemistry. Utilizing this technique, the kinetics of the reaction of DPA^+ with H_2S were monitored by the in situ measurement of the time-dependent absorbance of the cation radical as the potential of the optically transparent electrode was stepped from a value (+0.60 V) at which the oxidation of DPA (eq 1) does not occur to a value (+1.40 V) at which this process



proceeds at a diffusion-controlled rate.³² At pristine platinum surfaces (free of PtS) the reaction between DPA^+ and H_2S was observed to be first order in each reactant over a wide range of concentrations as shown in Figure 2.

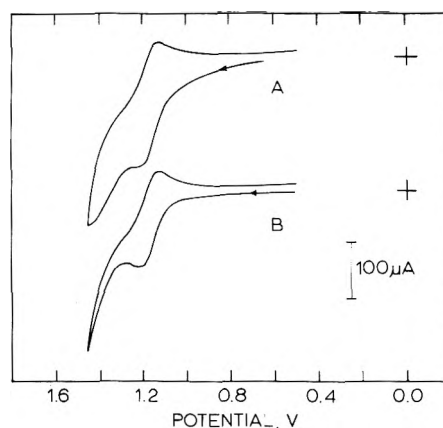


Figure 1. Anodic voltammetric behavior of acetonitrile solution containing 1.0 mM DPA, 0.50 mM H_2S , and 0.10 M TEAP at (A) pristine platinum and (B) platinum sulfide electrodes. Sweep rate = 0.10 V/s, electrode area = 0.36 cm^2 .

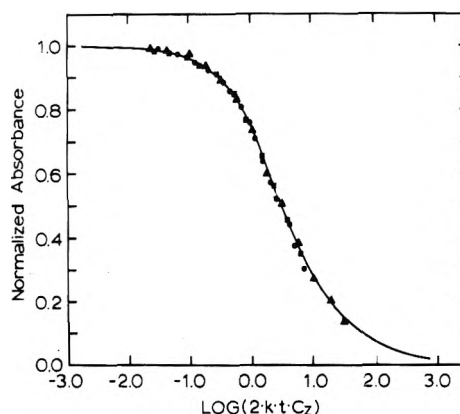


Figure 2. Dynamic single potential step spectroelectrochemical response for the DPA- H_2S system at pristine platinum electrodes. Solid line represents theoretical response predicted for totally regenerative system.³² Symbols mark experimental data: ■, $[\text{H}_2\text{S}]/[\text{DPA}] = 28.0$ ($[\text{DPA}] = 1.05 \text{ mM}$); ●, $[\text{H}_2\text{S}]/[\text{DPA}] = 62.1$ ($[\text{DPA}] = 1.13 \text{ mM}$); ▲, $[\text{H}_2\text{S}]/[\text{DPA}] = 93.7$ ($[\text{DPA}] = 1.13 \text{ mM}$). TEAP present at 0.20 M in all cases. Bimolecular rate constant, k , is that given in eq 8. C_2 is the molar concentration of H_2S .

It has been shown³² that for totally regenerative systems such as that represented by eq 1 and 2, the absorbance of the product of the electrode reaction (DPA^+) achieves a steady-state value at sufficiently long times of measurement, namely

$$\lim_{t \rightarrow \infty} A_{\text{DPA}^+}(\lambda, t) = A_{\text{DPA}^+}(\lambda)_{\text{ss}} =$$

$$\frac{\epsilon_{\text{DPA}^+}(\lambda) D_{\text{DPA}}^{1/2} C_{\text{DPA}}^0}{(k C_{\text{H}_2\text{S}}^0)^{1/2}} \quad (3)$$

which is valid if the bulk concentration of H_2S , $C_{\text{H}_2\text{S}}^0$, exceeds that of DPA, C_{DPA}^0 , by an amount sufficient to ensure pseudo-first-order reaction conditions. Time independent absorbances predicted by eq 3 were manifest in this present study at both pristine platinum and platinum sulfide surfaces. Representative behavior is shown in Figure 3.

When single potential step spectroelectrochemical experiments were carried out on anodically formed PtS surfaces, transient absorbance-time behavior was observed which was extremely dissimilar to that seen when pristine platinum surfaces were used. Immediately upon application of the potential step perturbation to the platinum sulfide sur-

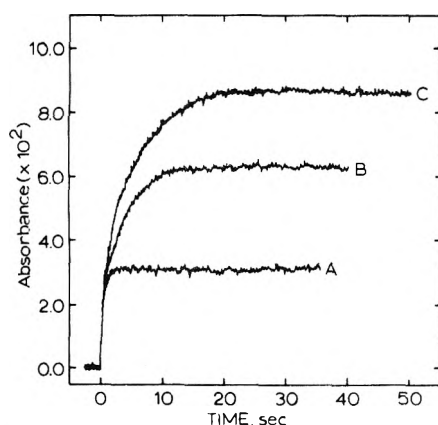


Figure 3. Steady-state single potential step spectroelectrochemical response observed for DPA-H₂S systems: (curve A) [DPA] = 1.13 mM, [H₂S] = 106. mM, pristine platinum electrode; (curve B) [DPA] = 1.05 mM, [H₂S] = 29.5 mM, platinum sulfide electrode; (curve C) [DPA] = 1.05 mM, [H₂S] = 15.5 mM, platinum sulfide electrode. TEAP present at 0.20 M in all cases.

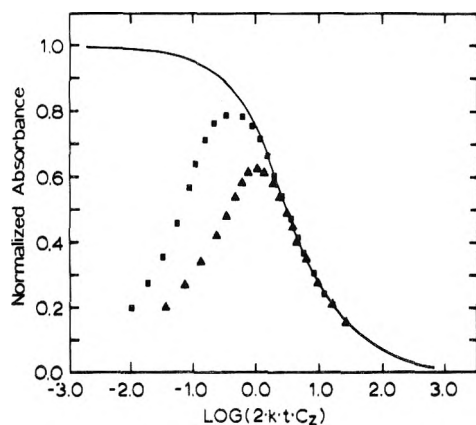


Figure 4. Dynamic single potential step spectroelectrochemical response for the DPA-H₂S system at platinum sulfide electrodes showing initial rapid consumption of DPA⁺. Solid line represents theoretical response predicted for totally regenerative system.³² Symbols mark experimental data: ■, [H₂S]/[DPA] = 28.0 ([DPA] = 1.05 mM); ▲, [H₂S]/[DPA] = 93.7 ([DPA] = 1.13 mM). TEAP present at 0.20 M in all cases. Bimolecular rate constant, *k*, is that given in eq 8. C₂ is the molar concentration of H₂S.

face, the absorbance of DPA⁺ was abnormally low but grew with time to coalesce with the dynamic response observed at pristine platinum. This behavior, shown in Figure 4, indicates a rapid consumption of DPA⁺ immediately following potential step perturbation due to a local excess of reducing agent (H₂S) in intimate proximity to the electrode. The coincidence of the longer time behavior reflects a surface-dependent phenomenon which decreases in significance with time and is not recurrent during the potential step. If, however, the solution is stirred or sufficient time allowed between potential step experiments to permit reequilibration of the PtS surface, then reproducible short-time, rapid consumption of DPA⁺ upon application of the potential step is again observed. The necessity of the anodically modified surface to the short-time behavior was demonstrated by reductively discharging the PtS at -0.70 V and then repeating the potential step oxidation DPA. The time-dependent normalized absorbance noted in such cases was identical with that observed at nonmodified platinum (Figure 2).

TABLE I: Kinetic Data for the Reaction of the DPA Cation Radical with Hydrogen Sulfide Determined by Single Potential Step Spectroelectrochemistry

Electrode surface	Method of evaluation	10 ³ [DPA], M	10 ³ [H ₂ S], M	<i>k</i> , ^d M ⁻¹ s ⁻¹
Pt	SPS ^a	1.05	29.5	5.27(±0.78)
Pt	SPS	1.13	70.2	7.62(±0.81)
Pt	SPS	1.13	106	6.85(±0.68)
PtS	SPS ^b	1.05	29.5	6.35(±0.24)
PtS	SPS	1.13	70.2	6.92(±0.77)
PtS	SPS	1.13	106	6.84(±0.86)
Pt	SPS/SS ^c	1.05	15.5	4.42(±0.38)
Pt	SPS/SS	1.05	29.5	4.58(±0.35)
Pt	SPS/SS	1.13	70.2	6.35(±0.38)
Pt	SPS/SS	1.13	106	6.36(±0.31)
PtS	SPS/SS	1.05	15.5	4.11(±0.69)
PtS	SPS/SS	1.05	29.5	4.56(±0.67)
PtS	SPS/SS	1.13	70.2	6.56(±0.62)
PtS	SPS/SS	1.13	106	6.21(±0.39)

^a Single potential step (SPS) dynamic response. ^b Single potential step dynamic response following decay of surface reaction (see Figure 4). ^c Single potential step steady state response according to eq 3. ^d Bimolecular rate constant (eq 8).

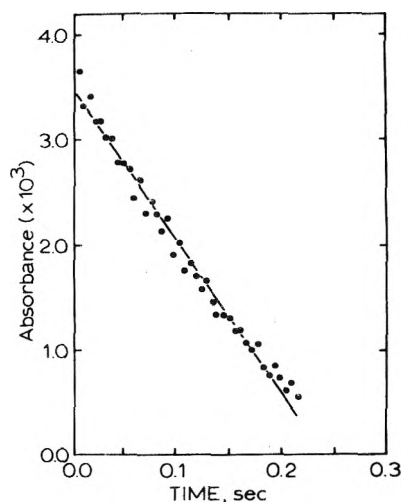


Figure 5. Open circuit relaxation spectroelectrochemical behavior of DPA-H₂S system following pulse of short duration at platinum sulfide electrode: $\tau = 0.100$ s, [DPA] = 1.05 mM, [H₂S] = 29.5 mM, [TEAP] = 0.20 M, coefficient of correlation = -0.9726.

Kinetic parameters obtained from single potential step measurements at pristine platinum, steady-state measurements at both pristine platinum and platinum sulfide, and single potential step measurements at platinum sulfide surfaces following the decay of the surface phenomenon are summarized in Table I. In all cases, the rate of reaction was seen to be independent of DPA concentration.

Open Circuit Relaxation Spectroelectrochemistry. The utility of this technique of examining the reactions of electrogenerated species has already been demonstrated.^{12,33-35} This experimental method utilizes a potential step perturbation of controlled duration followed by disconnection of the working electrode thereby allowing the system to relax without electrolysis.³³ In the present study this technique afforded a unique way of probing the nature of the surface-associated reaction occurring at the onset of the potential step oxidation of DPA at platinum sulfide surfaces. Choice of short pulse times permits examination of the surface reaction under relaxation conditions while the relaxation be-

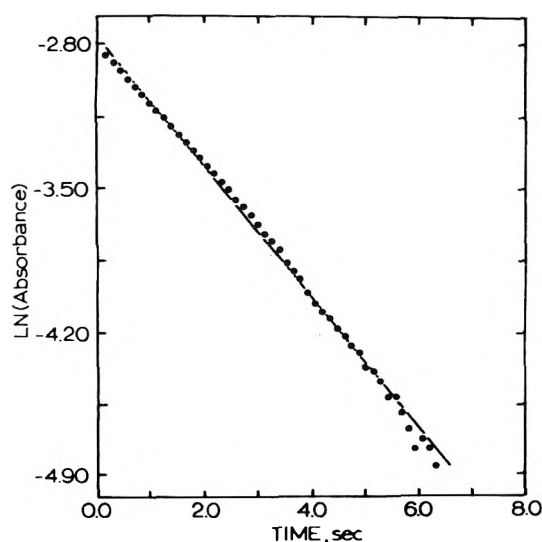


Figure 6. Open circuit relaxation spectroelectrochemical behavior of DPA-H₂S system following pulse of long duration at platinum sulfide electrode: $\tau = 10.0$ s, [DPA] = 1.05 mM, [H₂S] = 29.5 mM, [TEAP] = 0.20 M, coefficient of correlation = -0.9868.

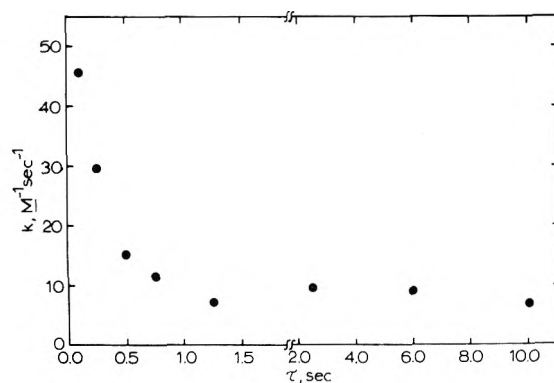


Figure 7. Dependence of the observed bimolecular rate constant for the reaction of DPA^{•+} with H₂S (eq 8) on pulse duration for open circuit relaxation spectroelectrochemistry at platinum sulfide electrodes: [DPA] = 1.05 mM, [H₂S] = 29.5 mM, [TEAP] = 0.20 M.

havior following pulses of longer duration chiefly reflects the "bulk" reaction. Under open circuit relaxation conditions following short duration pulses at platinum sulfide surfaces, the decay of the absorbance of DPA^{•+} was essentially linear with time indicating a predominantly zero order consumption of DPA^{•+} as shown in Figure 5. When pulses of considerably longer duration were employed, a first-order consumption of DPA^{•+} was in evidence during open circuit relaxation. Representative data are shown in Figure 6. As the pulse time, τ , was varied from 0.100 to 10.0 s, the apparent first-order rate constant for the consumption of DPA^{•+} decreased with increasing pulse duration, reaching an invariant value at $\tau > 1$ s as shown in Figure 7. The attendant uncertainty in the fit of the data to first-order behavior also decreased with increased pulse duration, corresponding to increased predominance of the first-order process.³⁶ Kinetic parameters derived from open circuit relaxation behavior following long duration pulses ($\tau > 2$ s) at platinum sulfide electrodes are shown in Table II.

Stopped-Flow Kinetic Spectrophotometry. In order to determine the degree to which the open circuit relaxation kinetic behavior following pulses of long duration at plati-

TABLE II: Kinetic Data for the Reaction of the DPA Cation Radical with Hydrogen Sulfide Determined by Open Circuit Relaxation at Platinum Sulfide Electrodes^a

$10^3[\text{DPA}], \text{M}$	$10^3[\text{H}_2\text{S}], \text{M}$	$k, \text{M}^{-1} \text{s}^{-1}$
1.05	29.5	8.56(±0.56)
1.13	70.2	5.99(±0.19)
1.13	106	6.67(±0.52)

^a $\tau > 2$ s. ^b Bimolecular rate constant (eq 8).

TABLE III: Kinetic Data for the Reaction of the DPA Cation Radical with Hydrogen Sulfide Determined by Stopped-Flow Kinetic Spectrophotometry

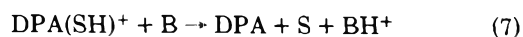
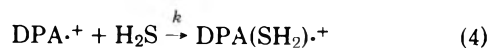
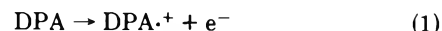
$10^4[\text{DPA}], \text{M}$	$10^3[\text{H}_2\text{S}], \text{M}$	$k, \text{M}^{-1} \text{s}^{-1}$
4.96	140	5.62(±0.70)
4.96	82.5	7.38(±0.33)
4.96	69.6	8.55(±0.25)
1.40	88.0	6.42(±0.25)
0.50	69.6	7.71(±0.46)
0.50	27.3	5.60(±0.99)

^a $[\text{DPA}^{\bullet+}]_0 \approx 5 \times 10^{-5}$ M in all experiments. ^b Bimolecular rate constant (eq 8).

num sulfide surfaces and single potential step experiments at pristine platinum electrodes reflect the reaction of DPA^{•+} with H₂S wherein the electrode per se is not a direct participant, the homogeneous reaction of DPA^{•+} with H₂S was examined via stopped-flow kinetic spectrophotometry. Over a tenfold range of DPA^{•+}/H₂S concentration ratios, the reaction was observed to be the first order in both cation radical and hydrogen sulfide, and independent of DPA. The results of these experiments are shown in Table III.

Discussion

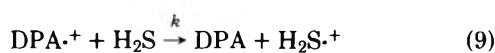
The Bulk Reaction. The coincidence with theory³² of both the transient and the steady-state absorbance behavior of DPA^{•+}, electrogenerated in the presence of H₂S, is indicative of a totally regenerative process in which the initial encounter of DPA^{•+} with reducing agent is rate determining. Since the conversion of H₂S to elemental sulfur requires the release of two electrons per molecule of H₂S oxidized, participation in the reaction sequence by a second DPA^{•+} is implied.³⁷ Incorporation of this implication into a mechanism consistent with the observed kinetics and reaction products suggests the following reaction sequence



where eq 4 is rate determining and B represents a general base³⁸ present in the acetonitrile solution.^{39,40} Solution of the kinetic equations describing the processes embodied in eq 4-7 affords the rate law,

$$d[\text{DPA}^{\bullet+}]/dt = -2k[\text{DPA}^{\bullet+}][\text{H}_2\text{S}] \quad (8)$$

Alternatively, bond formation may not occur in the rate-determining step (eq 4) and a mechanism of the following form may be tenable:



where eq 9 represents the rate-determining step. The overall reaction stoichiometry is maintained in this scheme, and with the stipulation that $\text{HS} \cdot \text{BH}^+$ is more reactive than H_2S toward $\text{DPA}^{\cdot+}$, this reaction sequence also gives rise to the rate law expressed in eq 8.

The applicability of either of these mechanistic pathways and the attendant rate law is demonstrated by the results derived from the three kinetic techniques shown in Tables I, II, and III. That single potential step spectroelectrochemical measurements at pristine platinum electrodes as well as long time open circuit relaxation and potential step measurements at platinum sulfide electrodes reflect the "bulk" process is shown by the agreement of the kinetic parameters arising from these electrochemical techniques (Tables I and II) with those determined via a purely homogeneous method (stopped flow; Table III). For 143 observations utilizing the three kinetic methodologies, the composite second-order rate constant (eq 8) was evaluated to be $6.6(\pm 1.2) \text{ M}^{-1} \text{ s}^{-1}$.

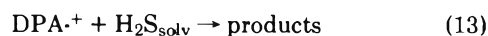
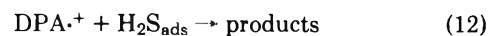
The Surface Reaction. In considering the anomalously fast consumption of $\text{DPA}^{\cdot+}$ generated at the modified surface, it is necessary to characterize the nature of this ancillary reaction. There is a high local excess of nucleophile at the electrode surface which reacts with the $\text{DPA}^{\cdot+}$ produced in the initial stages of the pulse perturbation. Clearly this is not simply H_2S adsorbed onto platinum since the anomalous kinetic effect is observed only after anodic modification of the electrode. The possibility of the PtS per se being the highly active reducing agent must also be considered. If this were the case, the PtS would be expended in reaction with $\text{DPA}^{\cdot+}$ which would reduce the PtS, thereby eliminating this heterogeneous reaction pathway. That this is not the case is shown both (a) by the presence of the cathodic wave for the reduction of the PtS surface (-0.70 V) following a potential step experiment yielding data of the type shown in Figure 4, and (b) by the reversible nature of the catalytic phenomenon. That is, when the solution is either stirred or allowed to stand for some time following the potential step experiment (ca. 60–100 s) to restore the initial conditions of the system (i.e., homogeneous distribution of the precursor; $C^{\text{DPA}}(x,0) = C^0_{\text{DPA}}$), a subsequent potential step spectroelectrochemical experiment again gives rise to this fast initial consumption of $\text{DPA}^{\cdot+}$. The continual repeatability of this sequence is indicative of adsorption of H_2S onto the PtS surface and reaction therefrom, rather than reaction of the PtS layer.

Hydrogen sulfide is well known to be strongly adsorbed on platinum surfaces.^{41–43} Yet on pristine platinum, it is not as reactive toward $\text{DPA}^{\cdot+}$ as it is on the PtS surface. Even though the PtS is not consumed in the reaction of the adsorbed H_2S with electrogenerated $\text{DPA}^{\cdot+}$, it nonetheless participates in the reaction as a specifically active surface for the process in question. This kinetic demeanor may well be an effect of a preferred molecular orientation of H_2S in the adsorbed state on PtS that renders it more reactive than the corresponding orientation in the adsorbed state on platinum.

In this work the bulk concentration of H_2S exceeded that of DPA by as much as 100-fold. It seems reasonable, then,

to ask why H_2S , present in this much greater concentration, is not reabsorbed from solution as the originally adsorbed material reacts. The most probable answer to this is that the adsorption of H_2S onto PtS is a kinetically slow process. Such slow adsorption processes are known^{44,45} and this phenomenon is substantiated in this case by the time required between potential step experiments to reestablish the conditions for initial fast reaction.

We are now addressing two reaction pathways which can be represented as



where $\text{H}_2\text{S}_{\text{ads}}$ and $\text{H}_2\text{S}_{\text{solv}}$ represent the adsorbed and solvated H_2S molecules, respectively. The surface reaction (eq 12) is of decreasing importance to the overall consumption of $\text{DPA}^{\cdot+}$ as the adsorbed H_2S is reacted. If one assumes a limiting *sequential* model for these two pathways, namely, that the adsorbed H_2S reacts *before* the solvated H_2S as is suggested by the behavior shown in Figure 4, then the time required to generate sufficient $\text{DPA}^{\cdot+}$ to strip the surface of adsorbed H_2S and consequently, the time at which the reaction pathway described by eq 12 becomes inoperative, can be calculated from elementary considerations. Taking the distance between centers of adsorbed H_2S molecules⁴¹ to be 4.5 \AA , one calculates the surface excess, $\Gamma_{\text{H}_2\text{S}}$, for monolayer coverage to be $8.2 \times 10^{-10} \text{ mol/cm}^2$. From the working electrode area of 0.36 cm^2 , one further calculates that for $\theta = 1.0$, $3.0 \times 10^{-10} \text{ mol}$ of H_2S is in the adsorbed state. On the basis of the stoichiometry given in eq 2, twice this amount of $\text{DPA}^{\cdot+}$, or $6.0 \times 10^{-10} \text{ mol}$ of the cation radical must be generated for complete reaction with the adsorbed hydrogen sulfide. In a 1.0 mM solution of DPA, the time required for generation of the requisite amount of cation radical is calculated from an integrated form of the Cottrell equation and a knowledge of the diffusion coefficient of DPA in this medium¹¹ to be ca. 175 ms.

In order to evaluate the extent to which this limiting model of "adsorbed H_2S reacting first" holds, open circuit relaxation spectroelectrochemical experiments were carried out on composite DPA– H_2S systems. At pulse times, τ , short compared to the calculated time, t_{calcd} , necessary for the production of the amount of $\text{DPA}^{\cdot+}$ required for complete reaction of the adsorbed H_2S , the observed relaxation kinetics should primarily reflect the heterogeneous reaction. However, when $\tau \gg t_{\text{calcd}}$, the observed relaxation kinetics should mirror the homogeneous process.

While the first-order rate constant for the homogeneous reaction of $\text{DPA}^{\cdot+}$ achieves a constant value when the bulk reaction prevails (Figure 7), the corresponding zero-order treatment of the observed kinetic data should *not* give rise to invariant values of the zero-order rate constant (k_0) at short pulse duration. Rather the zero-order rate constant embodies the activity of the adsorbed hydrogen sulfide and this parameter changes with surface coverage. Assuming dominance of the heterogeneous reaction, the adsorbed layer is being removed with a t dependence in reaction with $\text{DPA}^{\cdot+}$ which, in turn, is being generated with a $t^{1/2}$ dependence. This means that the observed zero-order rate constant should be approximately linear in $\tau^{1/2}$, and extrapolation to $\tau = 0$ affords a measure of k_0 at $\theta = 1.0$. This $\tau^{1/2}$ dependence and attendant extrapolation are shown in Figure 8 and afford a k_0 value at $\tau = 0$ of $1.51(\pm 0.05) \times 10^{-2} \text{ M s}^{-1}$.

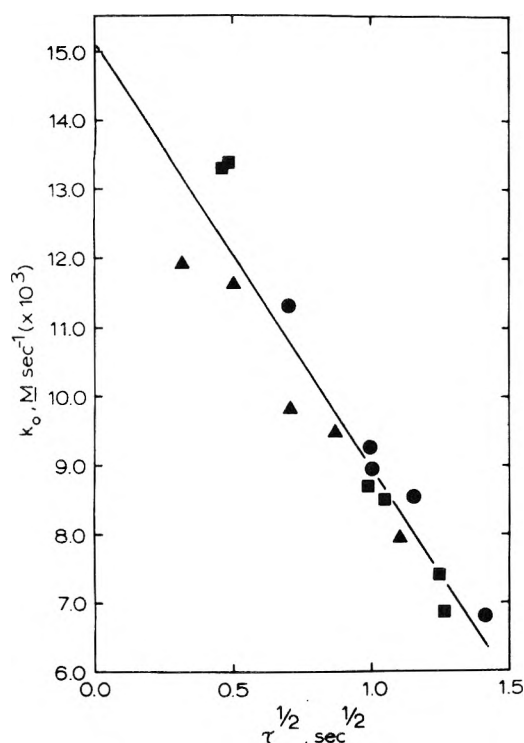


Figure 8. Pulse duration dependence of zero-order rate constant derived from open circuit relaxation spectroelectrochemical experiments for the reaction of $\text{DPA}^{\cdot+}$ with adsorbed H_2S at platinum sulfide electrodes: \blacksquare , $[\text{H}_2\text{S}]/[\text{DPA}] = 28.0$ ($[\text{DPA}] = 1.05$ mM); \bullet , $[\text{H}_2\text{S}]/[\text{DPA}] = 62.1$ ($[\text{DPA}] = 1.13$ mM); \blacktriangle , $[\text{H}_2\text{S}]/[\text{DPA}] = 93.7$ ($[\text{DPA}] = 1.13$ mM). TEAP present at 0.20 M in all cases.

From Figure 7, the pulse time corresponding to realization of a clean first-order decay of cation radical (second order overall) for relaxation experiments is approximately 1 s. Correspondingly, the time at which the expected second-order kinetic behavior (first order in radical ion) manifests itself during potential step experiments can be seen from Figure 4 to be approximately 2 s. The prolonged period required for the surface process to become an insignificant contributor to the observed kinetic behavior of this system provides clear indication of the *parallel* nature of the heterogeneous and homogeneous processes, rather than a *stepwise* "adsorbed first, solvated next" reaction sequence. The parallel nature of these processes is further supported by the data ensuing from the short pulse duration, open circuit relaxation experiments. Close examination of Figure 5 reveals some curvature present in this zero-order plot, and this is taken as indication of a higher order contribution to the observed kinetics even for cases of short pulse duration.

Upon cursory examination, it would seem that the short time behavior reflected in Figure 4 could be simulated in a straightforward fashion.³⁴ Such is not the case because of the necessity of knowing the adsorption isotherm for H_2S on PtS which dictates the functional dependence of k_0 on θ . Assuming a linear isotherm, a $[1 - (t/t_{\text{calcd}})^{1/2}]$ consumption of $\text{H}_2\text{S}_{\text{ads}}$, and parallel nature of the homogeneous and heterogeneous processes, an approximate fit to the behavior shown in Figure 4 has been achieved. Although kinetic parameters in agreement with those shown in Table I for the homogeneous portion of the process can be extracted, the interrelation of the zero-order and second-order rate constants in such a simulation is open to question.

Conclusions

From these studies, it is concluded that hydrogen sulfide is adsorbed onto platinum sulfide and that this adsorbed material is more reactive than hydrogen sulfide adsorbed onto platinum toward the electrogenerated cation radical of DPA. Moreover, this adsorption of H_2S onto PtS is a kinetically slow process.

It is further concluded that the reaction of $\text{DPA}^{\cdot+}$, electrogenerated at a platinum sulfide surface onto which hydrogen sulfide is adsorbed, proceeds via parallel heterogeneous (adsorbed H_2S) and homogeneous (solvated H_2S) pathways.

References and Notes

- (1) Presented at the 149th Meeting of the Electrochemical Society, Washington, D.C., May 1976.
- (2) "EE" systems are those species capable of undergoing two mono-electronic oxidation (or reduction) processes, i.e.

$$\text{A} \rightarrow \text{A}^{\cdot+} + \text{e}^- \quad (E_1)$$

$$\text{A}^{\cdot+} \rightarrow \text{A}^{2+} + \text{e}^- \quad (E_2)$$
 where $E_2 > E_1$.
- (3) (a) H. N. Blount, *J. Electroanal. Chem.*, **42**, 271 (1973); (b) D. T. Shang and H. N. Blount, *ibid.*, **54**, 305 (1974).
- (4) J. F. Evans and H. N. Blount, presented at the 168th National Meeting of the American Chemical Society, Atlantic City, N.J., 1974, Abstracts of Papers, ANAL-7.
- (5) J. F. Evans and H. N. Blount, presented at the 169th National Meeting of the American Chemical Society, Philadelphia, Pa. 1975, Abstracts of Papers, ANAL-106.
- (6) J. F. Evans and H. N. Blount, *J. Org. Chem.*, **41**, 516 (1976).
- (7) G. Manning, V. D. Parker, and R. N. Adams, *J. Am. Chem. Soc.*, **91**, 4584 (1969).
- (8) V. D. Parker and L. Ebersson, *Tetrahedron Lett.*, 2839 (1969).
- (9) V. D. Parker and L. Ebersson, *Acta Chem. Scand.*, **24**, 3542 (1970).
- (10) P. T. Kissinger and C. N. Reilley, *Anal. Chem.*, **42**, 12 (1970).
- (11) G. C. Grant and T. Kuwana, *J. Electroanal. Chem.*, **24**, 11 (1970).
- (12) H. N. Blount and T. Kuwana, *J. Electroanal. Chem.*, **27**, 464 (1970).
- (13) R. Dietz and B. E. Larcombe, *J. Chem. Soc. B*, 1369 (1970).
- (14) L. Marcoux, *J. Am. Chem. Soc.*, **93**, 537 (1971).
- (15) V. D. Parker, *J. Electroanal. Chem.*, **36**, App. 8 (1972).
- (16) O. Hammerich and V. D. Parker, *J. Electroanal. Chem.*, **38**, App. 9 (1972).
- (17) C. J. Ludman, E. M. McCarron, and R. F. O'Malley, *J. Electrochem. Soc.*, **119**, 874 (1972).
- (18) R. P. Van Duyne and C. N. Reilley, *Anal. Chem.*, **44**, 158 (1972).
- (19) U. Svanholm and V. D. Parker, *Acta Chem. Scand.*, **27**, 1454 (1973).
- (20) R. E. Sioda, *J. Phys. Chem.*, **72**, 2322 (1968).
- (21) L. Papauchado, R. N. Adams, and S. W. Feldberg, *J. Electroanal. Chem.*, **21**, 408 (1969).
- (22) R. G. Pearson, Ed., "Hard and Soft Acids and Bases," Dowden, Hutchinson, and Ross, Inc., Stroudsburg, Pa., 1973.
- (23) J. F. Evans, H. N. Blount, and C. R. Ginnard, *J. Electroanal. Chem.*, **59**, 169 (1975).
- (24) For a comprehensive discussion of spectroelectrochemistry, see T. Kuwana and N. Winograd in "Electroanalytical Chemistry", Vol. 7, A. J. Bard, Ed., Marcel Dekker, New York, N.Y., 1974.
- (25) W. von Benken and T. Kuwana, *Anal. Chem.*, **42**, 1114 (1970).
- (26) J. W. Strojek and T. Kuwana, *J. Electroanal. Chem.*, **16**, 471 (1968).
- (27) A. A. Pilla, *J. Electrochem. Soc.*, **118**, 702 (1971).
- (28) Supporting electrolyte must also be present in this reactant solution to prevent thermal effects and changes in refractive index upon mixing.
- (29) J. F. Evans and H. N. Blount, *Anal. Lett.*, **7**, 445 (1974).
- (30) At this wavelength, the value of $\epsilon_{\text{DPA}^{\cdot+}} D_{\text{DPA}}^{1/2}$ employed for spectroelectrochemical measurements was $30.8 \text{ M}^{-1} \text{ s}^{-1/2}$ which is in agreement with previously reported values (ref 11).
- (31) The DPA absorbance at 392.5 nm is free from interferences by all other species present. See ref 20 for details.
- (32) N. Winograd, H. N. Blount, and T. Kuwana, *J. Phys. Chem.*, **73**, 3456 (1969).
- (33) H. N. Blount, N. Winograd, and T. Kuwana, *J. Phys. Chem.*, **74**, 3231 (1970).
- (34) T. Kuwana, *Ber. Bunsenges. Phys. Chem.*, **77**, 858 (1973).
- (35) R. F. Broman, W. R. Heineman, and T. Kuwana, *Discuss. Faraday Soc.*, **56**, 16 (1973).
- (36) At pulse times greater than 1 s, the coefficient of correlation, R , for first-order kinetic fits was greater than 0.985 in all cases.
- (37) That the cation radical rather than the electrode functions as the ultimate electron receptor is further supported by the regenerative stoichiometry observed under purely homogeneous conditions.
- (38) B is most likely water. In the most carefully purified acetonitrile, water is present in at least millimolar concentration. Although water is re-

ported to be a fiftyfold stronger base than hydrogen sulfide in acetonitrile [I. M. Kolthoff, *Anal. Chem.*, **46**, 1992 (1974)], at the higher concentrations of hydrogen sulfide used in this work, H₂S may compete favorably with H₂O as the deprotonating agent, B. The identity of the base involved, however, is inconsequential to the proposed mechanism and the attendant kinetic assumptions.

- (39) Without question, the processes reflected in eq 5 and 6 involve some measure of reversibility. This does not, however, compromise the ensuing kinetic treatment so long as these processes are fast relative to the rate-determining step.
- (40) The order in which the carbon-sulfur bond cleavage and deprotonation

steps occur in eq 7 is not clear. The process reflected in this equation may indeed be far more complex than depicted here, e.g., the formation of various polysulfides may well complicate this step. The only necessary stipulation for this process is the rapidity of the kinetics of regeneration of DPA relative to the rate-determining consumption of DPA⁺, eq 4.

- (41) H. P. Bonzel and R. Ku, *J. Chem. Phys.*, **58**, 4617 (1973).
- (42) J. M. Saleh, *Trans. Faraday Soc.*, **67**, 1830 (1971).
- (43) J. Bénard, *Catal. Rev.*, **3**, 93 (1969).
- (44) T. Loučka, *J. Electroanal. Chem.*, **36**, 369 (1972).
- (45) J. D. E. McIntyre, private communication.

Emission Spectra and Chemical Reactions of Fluorinated Benzene Derivatives in a High-Frequency Discharge

R. Gilbert and A. Théorêt*

Physical and Organic Chemistry Group, Materials Science Department, Hydro-Québec Institute of Research (IREQ), Varennes, Québec, Canada (Received November 11, 1975)

Publication costs assisted by Hydro-Québec Institute of Research

The emission spectra of fluorinated benzene derivatives excited by radiofrequency discharges were measured and compared with those obtained using other modes of excitation. In the spectra of C₆H₅F and *o*-, *m*-, and *p*-C₆H₄F₂, the emissions were assigned to the fluorescence spectra of these molecules. Molecular emission spectra were never detected for C₆HF₅ and C₆F₆ although emission bands due mainly to CF₂ radicals were observed. The reaction products were analyzed by infrared spectroscopy, gel permeation chromatography, gas chromatography, and mass spectrometry, and the results show that they are formed mainly of medium and high molecular weight compounds. The degree of polymerization is higher as the monomer passes from C₆H₅F to C₆F₆ and, also, as the power applied to the discharge is increased. On the basis of the product analysis and electrical emission study, a general reaction mechanism was proposed involving interactions between excited molecules and fragmentation species. Finally an interesting relationship was found to exist between both the emission features and the degree of polymerization of these molecules in electrical discharges and fluorescence and triplet yield measurements reported by other authors.

Introduction

Many papers have already been published on the photochemistry of fluorinated benzene derivatives in the gas phase.¹⁻⁸ The quantum yield and lifetime of the first singlet (S₁) and triplet states (T₁) of these compounds have been measured as functions of the exciting wavelength and the pressure. Analysis of the energy relaxation processes emphasizes the following interesting point: the value of the quantum deficit $1 - (\phi_{S_1} + \phi_{T_1})$, where ϕ_{S_1} and ϕ_{T_1} represent the luminescence quantum yield of the first singlet and triplet states, respectively, tends to increase with both the energy of the photons and the number of fluorine atoms on the benzene ring (Table I).

The value of the quantum deficit gives an indication of the importance of photochemical processes over other modes of energy relaxation; in other words, photochemical reactions tend to become more important at higher vibronic levels of the first electronic excited state and with higher degrees of fluorine substitution on the benzene ring. Thus it appears from these earlier studies that a large fraction of these compounds in their excited states use photochemical processes to release their excess energy by dissociation, isomerization, or polymerization.

Monofluorobenzene (C₆H₅F) has also been studied by controlled electron impact in the gas phase. Ogawa et al.,⁹ in experiments carried out with an electron energy of 60 and 300 eV, have observed the fluorescence of C₆H₅F as well as the emission of species resulting from molecular fragmentation. Shukla et al.¹⁰ and Singh and Singh,¹¹ for their part, have investigated the high-resolution emission spectra of mono- and difluorobenzenes as excited by uncondensed transformer discharges and have made an exhaustive interpretation of the fine structure.

Although most of the authors referred to above make occasional mention of the formation of isomers and polymers, very few investigations have been carried out to identify the specific reaction products resulting from the interaction of fluorinated benzene derivatives with particles of high energy. The purpose of the study presented in this paper, therefore, was to obtain such additional information. The paper deals particularly with the reactions of C₆H₅F, the isomers of difluorobenzene (*o*-, *m*-, and *p*-C₆H₄F₂), pentafluorobenzene (C₆HF₅), and hexafluorobenzene (C₆F₆) in a capacitively coupled radiofrequency (rf) plasma discharge.¹²

First, the emission spectra of these compounds excited by electrical discharges are compared with those obtained with

TABLE I: Variation of the Quantum Yield of the First Singlet and Triplet States as a Function of the Exciting Wavelength and the Number of Fluorine Atoms on the Benzene Ring

MOLECULES	EXCITING WAVELENGTH (nm)	SINGLET AND TRIPLET QUANTUM YIELDS		QUANTUM DEFICIT $1-(\phi_{S_1} + \phi_{T_1})$	REFERENCES
		$\phi_{S_1} + \phi_{T_1}$			
C ₆ H ₅ F	267.0	0.82		0.18	2
	264.4 (0-0)				
	259.0	0.93		0.07	
	255.0	0.75		0.25	
1,2-C ₆ H ₄ F ₂	270.0	0.97		0.03	3
	266.0	0.75		0.25	
	262.2 (0-0)				
	258.0	0.52		0.48	
1,3-C ₆ H ₄ F ₂	274.0	1.05		0.00	4
	263.7 (0-0)				
	262.0	0.73		0.27	
	258.0	0.79		0.21	
1,4-C ₆ H ₄ F ₂	276.0	0.7		0.3	3
	274.0	0.5		0.5	
	271.3 (0-0)				
	266.0	0.5		0.5	
1,2,4,5-C ₆ H ₂ F ₄	273.1 (0-0)				5
	267.0	0.53		0.46	
	252.0	0.29		0.71	
C ₆ HF ₅	265.0	0.115		0.99	6
C ₆ F ₆	280.0	0.069		0.93	6
	270.0	0.029		0.98	
	265.0	0.035		0.97	

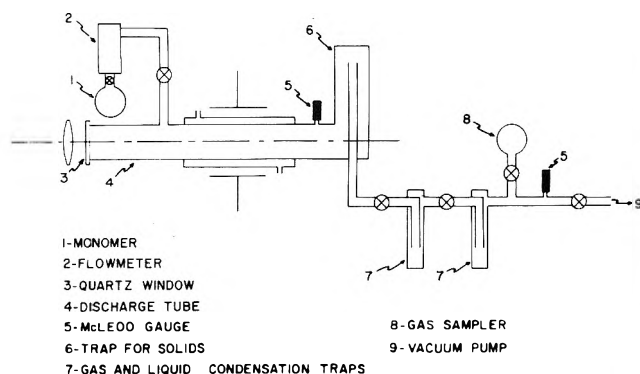


Figure 1. Schematic diagram of radiofrequency discharge apparatus.

other modes of excitation then the results of the analysis of the product reactions are discussed and compared with photochemical measurements.

Experimental Section

A schematic diagram of the rf discharge apparatus used for the present study is shown in Figure 1. Vapors of the fluorine-substituted benzene compounds were let into a quartz tube 30 cm long, and 2.5 cm o.d., at regulated pressure and flow rate, through two precision needle valves and one flowmeter. The plasma was maintained in the tube by means of rf-fed copper-sleeve electrodes connected to the outputs of the rf generator through an impedance-matching unit. The 250-W Tracerlab rf generator operates at a frequency of 13.56 MHz. The plasma emission spectra were observed through a quartz window and recorded from 700 to 200 nm by means of a Cary 17H spectrophotometer equipped with an EMI 9783 B photomultiplier. This photomultiplier offers the advantage of giving an almost linear response between 350 and 200 nm, which is the spectral region of particular interest in this study. All feed-troughs and connection joints have O-ring connectors or swagelock fittings. The system is evacuated and degassed prior to each experiment by applying an electrical discharge for several minutes at a pressure of 10^{-2} Torr. Table II gives the various discharges obtained with different pressures,

TABLE II: Experimental Conditions of Radiofrequency Discharge Through Fluorinated Benzene Derivatives and the Resulting Distribution of Reaction Products

MONOMER	C ₆ H ₆		C ₆ H ₅ F		1,2-C ₆ H ₄ F ₂		1,3-C ₆ H ₄ F ₂		1,4-C ₆ H ₄ F ₂		C ₆ HF ₅		C ₆ F ₆	
	POWER INPUT (watts)	RESIDENCE TIME (ms)	W/P (watts/torr)	FEED RATE (mole/min x 10 ⁴)	ENERGY INPUT/MOLE OF MONOMER SUPPLY (kcal/mole)	FEED RATE (mole/min x 10 ⁴)	ENERGY INPUT/MOLE OF MONOMER SUPPLY (kcal/mole)	FEED RATE (mole/min x 10 ⁴)	ENERGY INPUT/MOLE OF MONOMER SUPPLY (kcal/mole)	FEED RATE (mole/min x 10 ⁴)	ENERGY INPUT/MOLE OF MONOMER SUPPLY (kcal/mole)	FEED RATE (mole/min x 10 ⁴)	ENERGY INPUT/MOLE OF MONOMER SUPPLY (kcal/mole)	FEED RATE (mole/min x 10 ⁴)
DISTRIBUTION OF REACTION PRODUCTS	SOLID FRACTION A (wt %)	55.0	20	1.078	1.7435	6.44	1941	2414	2.789	420	2946	300	94	
	SOLID FRACTION B (wt %)	4.4	20	1.081	1.7435	6.44	1941	2414	2.789	420	2946	300	94	
	LIQUID FRACTION C (wt %)	25.1	20	20	1.081	1.7435	6.44	1941	2.789	420	2946	300	94	
	GAS FRACTION D (mole %)	3.6	20	20	1.081	1.7435	6.44	1941	2.789	420	2946	300	94	
	SOLID FRACTION A (wt %)	55.0	20	1.081	1.7435	6.44	1941	2414	2.789	420	2946	300	94	
	SOLID FRACTION B (wt %)	4.4	20	20	1.081	1.7435	6.44	1941	2.789	420	2946	300	94	
	LIQUID FRACTION C (wt %)	25.1	20	20	1.081	1.7435	6.44	1941	2.789	420	2946	300	94	
	GAS FRACTION D (mole %)	3.6	20	20	1.081	1.7435	6.44	1941	2.789	420	2946	300	94	
	SOLID FRACTION A (wt %)	55.0	20	20	1.081	1.7435	6.44	1941	2.789	420	2946	300	94	
	SOLID FRACTION B (wt %)	4.4	20	20	1.081	1.7435	6.44	1941	2.789	420	2946	300	94	
	LIQUID FRACTION C (wt %)	25.1	20	20	1.081	1.7435	6.44	1941	2.789	420	2946	300	94	
	GAS FRACTION D (mole %)	3.6	20	20	1.081	1.7435	6.44	1941	2.789	420	2946	300	94	

† Hydrofluoric acid was detected in these experiments.

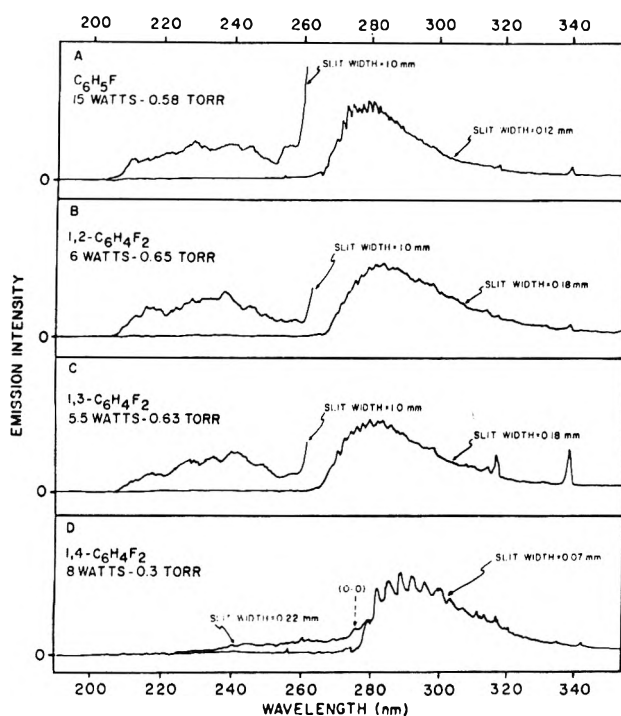


Figure 2. Emission of monofluorobenzene (A), *o*-difluorobenzene (B), *m*-difluorobenzene (C), and *p*-difluorobenzene (D) excited by rf discharge.

power levels, and flow rates. The ratio W/P of power level (W) over pressure (P) is a measure of the energy of the electrons in the plasma;¹³ high values of W/P correspond to plasma with an electron energy distribution displaced toward higher energy.

The fluorine-substituted benzene compounds were purchased from Pierce Chemical Co. All products were distilled prior to use. Solid products formed during the electrical discharge were removed from the tube with tetrahydrofuran (THF) solvent: products insoluble in THF (fraction B) were removed and weighed on micropore filters while the remaining solution (fraction A) was analyzed by gel permeation chromatography (GPC) with a set of low-porosity styragel columns, as described in an earlier publication.¹⁴ Besides gas and liquids collected in the cold traps, the low molecular weight solid products soluble in THF were analyzed by gas chromatography and mass spectrometry using a Hewlett Packard GC/MS Model 5981 A. Finally, the infrared spectra of the solid products were recorded with a Perkin-Elmer Model 180 spectrophotometer.

Results and Discussion

A. Emission Spectra. The emission spectra of fluorinated benzene derivatives excited by electrical discharges according to the experimental conditions tabulated in Table II are shown in Figures 2 and 3. Under mild electrical discharge conditions (application of approximately 10 W), C_6H_5F and the $C_6H_4F_2$ compounds are found to have an emission corresponding to the fluorescence spectra of these molecules. However, when the power applied to the discharge is increased, it is observed that the emission bands of the species resulting from the fragmentation of the molecules increase at the expense of molecular emission. On the other hand, even under the mildest discharge conditions needed to sustain the plasma, molecular emission spectra were never detected for C_6HF_5 and C_6F_6 while emission bands due mainly to CF_2 radicals were ob-

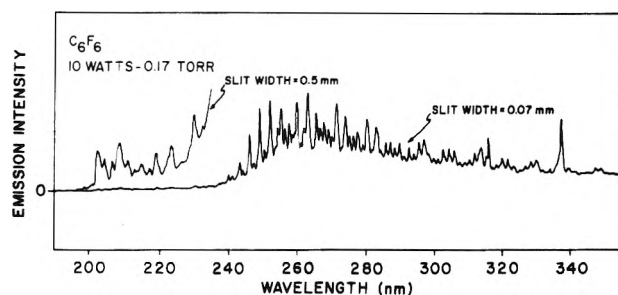


Figure 3. Emission spectrum of hexafluorobenzene excited by rf discharge.

served. For this reason, it was decided to discuss the emission spectra of the two groups of molecules separately.

Group I (C_6H_5F and *o*-, *m*-, and *p*- $C_6H_4F_2$). For this group of molecules, the emission spectra in the 350–265-nm region present a fine structure superposed on a high-intensity continuous background. The fine structure is made up of approximately 22, 12, 15, and 17 bands for C_6H_5F and *o*-, *m*-, and *p*- $C_6H_4F_2$, respectively. The emission spectra of these molecules are equivalent to the well-known forbidden transition $\pi \leftarrow \pi^*$ (${}^1A_{1g} \leftarrow {}^1B_{2u}$) of benzene which occurs weakly because of a vibronic coupling between the ${}^1A_{1g}$ and ${}^1B_{2u}$ states. Since these compounds are of lower symmetry than benzene, D_{2h} (${}^1A_{1g} \leftarrow {}^1B_{3u}$) for *p*- $C_6H_4F_2$ and C_{2v} (${}^1A_1 \leftarrow {}^1B_1$) for the other molecules, the electronic transition $\pi \leftarrow \pi^*$ is now allowed. In theory, these molecules should have a higher emission efficiency than benzene.

Recently, two independent research teams^{10,11} reported the results of their investigations on the high-resolution emission spectra of these molecules obtained by uncondensed transformer discharge excitation through the constant vapor flow of these compounds. The observed spectra were interpreted in terms of several fundamental vibrations in the ground and excited states. The frequencies observed in the ground state were found to correlate well with values measured in Raman and infrared spectra by other authors. According to Stockburger's interpretation¹⁵ of the emission spectrum of benzene, the continuous background can be assigned to a vibrational rearrangement among the vibronic levels in the first excited state ${}^1B_{3u}$ or 1B_1 .

In the case of the emission spectrum of C_6H_5F excited by a controlled electron impact with an energy of 60 and 300 eV, Ogawa et al.⁹ have observed, besides the $\pi \leftarrow \pi^*$ molecular transition, bands which were assigned to the emission of CH radicals ($A^2\Delta - X^2\pi$ and $B^2\Sigma^- - X^2\pi$) and hydrogen atoms (Balmer series). These bands appear in the spectral region between 450 and 350 nm and, under the experimental conditions used by the latter authors, their intensity is comparable to that of the ${}^1A_1 \leftarrow {}^1B_1$ transition.

Despite the difference in resolution of the spectra, the agreement between these results and those reported by the authors of this paper is generally very good. On the other hand, on the high-frequency side of the origin band (0–0 transition), emission bands were recorded which probably correspond to "resonance fluorescence".¹⁶ The low-pressure experimental conditions used are indeed favorable to the induction of such transitions. However, the intensity of the emitting light in this range of spectra is very weak and demanded an opening of the slit of the monochromator with the result that the resolution of the spectrophotometer was reduced to a value of approximately 2 nm. The spectra for mono- and difluorobenzene isomers between 255 and 210 nm show poorly resolved band

structures superposed on a continuous background. The possibility that these bands are due to the emission of nitrogen molecules still present as a trace in the discharge tube cannot be completely discarded.

It is also interesting to note the relationship between the general shape of the $\pi \leftarrow \pi^*$ emission band and the wavelength of the exciting light radiation. Examples of this effect for wavelengths between 260 and 250 nm have been reported by Nakamura¹⁷ for C_6H_5F and by Brewer¹⁸ for 1,3-difluorobenzene. On the basis of these results, the shape of the bands recorded by the present authors for the same molecules suggests that the electronic excitation of the molecules during electrical discharges is caused mainly by electrons with an energy equivalent to that of short wavelength radiation, i.e., ~ 250 nm or 4.95 eV, a feature which may prove useful for qualitative evaluations of the mean energy value of electrons in electrical discharges. At such short wavelengths, molecules populated in their high vibronic levels are more likely to subsequently undergo chemical relaxation processes.

Group II (C_6HF_5 and C_6F_6). Since electrical discharge emission spectra for C_6HF_5 and C_6F_6 give almost identical results, only the spectrum for the latter molecule has been reproduced in Figure 3. In the 350–235-nm part of the emission spectrum, over 60 bands were observed, all of which could be assigned to the fine structure of the CF_2 radical ${}^1A_1 \leftarrow {}^1B_1$ transition. The emission spectrum of the CF_2 species has already been measured by excitation through the vapor of tetrafluoromethane with an electrical discharge¹⁹ but, to the authors' knowledge, this is the first time the radical has been observed by fragmentation of aromatic molecules.

Furthermore, between 235 and 200 nm some 15 bands of very weak intensity were measured, some of which were assigned to the emission of $CF(X^2\pi \leftarrow A^2\Sigma^+ \text{ and } X^2\pi \leftarrow B)$ and $CF^+(X^1\Sigma^+ \leftarrow A^1\pi)$ radicals while others were believed to be associated with the emission of such impurities as CO and SiF_4 produced by the deactivation of fluorine-excited atoms on the reactor walls. However, the low resolution power of the spectrophotometer used, combined with the very short lifetime of CF and CF^+ radicals in comparison with the lifetime of CF_2 radicals,²⁰ hampers the interpretation of the very weak bands.

The $\pi \leftarrow \pi^*$ molecular emission spectra for these molecules excited with light radiation have been measured by different authors.^{21–23} The values for the fluorescence quantum yields were found to be very low compared with the same values for the mono- and disubstituted benzene derivatives. In the experiments carried out for this study, it was impossible, even under the mildest discharge conditions needed to sustain the plasma, to record the same molecular transition. Thus it seems that the mode of excitation used excites the molecules into higher electronic levels where the energy relaxation process takes place through molecular dissociation to yield CF_2 radicals for instance. The high intensity of the CF_2 emission bands probably obscures the $\pi \leftarrow \pi^*$ molecular emission.

B. Characterization of the Products. In this study, the experiment carried out with low and average values of W/P led to the formation of solid, liquid, and gaseous products whose distribution as a percentage is given in Table II. Under the present experimental conditions, an almost complete transformation of the compounds into either soluble solids (fraction A) or insoluble solids (fraction B) is observed in THF solvent. The remaining liquid and gaseous products, fractions C and D, respectively, constitute a relatively small proportion of the collected products and were therefore not subjected to extensive analysis. Besides, it has been observed that an increase in the W/P ratio of the discharge generally has the ef-

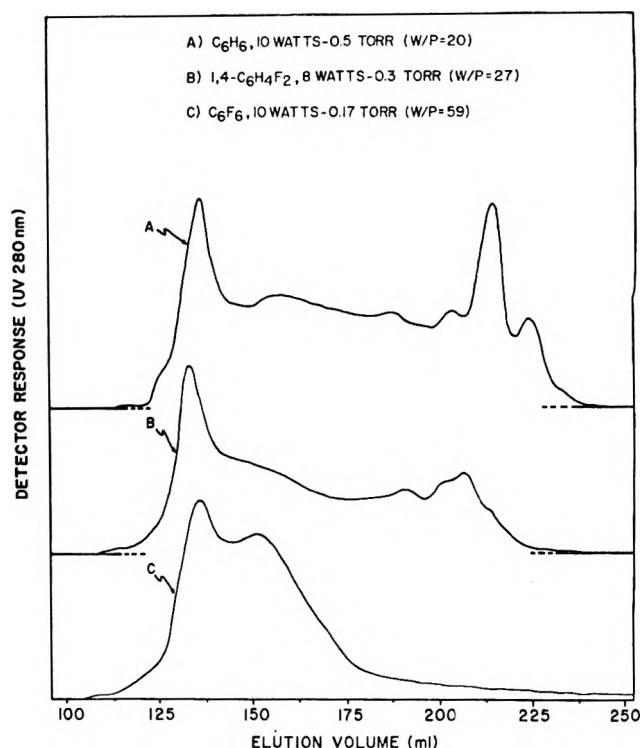


Figure 4. GPC chromatograms of soluble solids (fraction A) resulting from rf discharge through benzene (A), *p*-difluorobenzene (B), and hexafluorobenzene (C).

fect of increasing the insolubility of the solid products. For comparison, some experimental data obtained for benzene under similar experimental conditions have also been included in Table II.

Gas Analysis. The gas chromatographic analysis of the decomposition products of C_6F_6 identified C_2F_6 , C_2F_4 , C_3F_8 , C_3F_6 , and C_4F_{10} as the major reaction products. For the other partially fluorinated benzene derivatives, similar gas products with different ratios of H/F were obtained but no specific identification was undertaken.

The gas sampling procedure used did not permit the analysis of hydrogen, fluorine, and hydrofluoric acid. However, according to studies of the behavior of aromatic perfluorinated compounds irradiated with γ radiations in the liquid state,²⁴ a concentration of fluorine does not seem to build up in these liquids as opposed to hydrogenated liquid homologues where it has been found that hydrogen tends to accumulate in the reactive medium. The fluorine atoms formed are eliminated by additive reactions on the double bonds of molecules to produce saturated cyclic compounds, for example. As a matter of fact, the gaseous products resulting from the decomposition of C_6F_6 show an increase of the saturated carbon/unsaturated carbon ratio with increasing W/P values as a consequence of the earlier mentioned reactions in the gas phase. Thus, for high values of W/P , the production of fluorine atoms is increased because of a higher concentration of electrons in the discharge with sufficient energy to break C–F links (~ 145 kcal or 6.28 eV/mol for C_6F_6 ²⁴).

Analysis of Solid Products. The gel-permeation chromatography analysis (Figure 4) of the solid products (fraction A) resulting from rf discharges through the vapors of benzene indicates the presence of two sets of broad bands of approximately equal intensity corresponding to medium and high molecular weight compounds at long and short elution times, respectively. "Medium molecular weight" is used here to mean

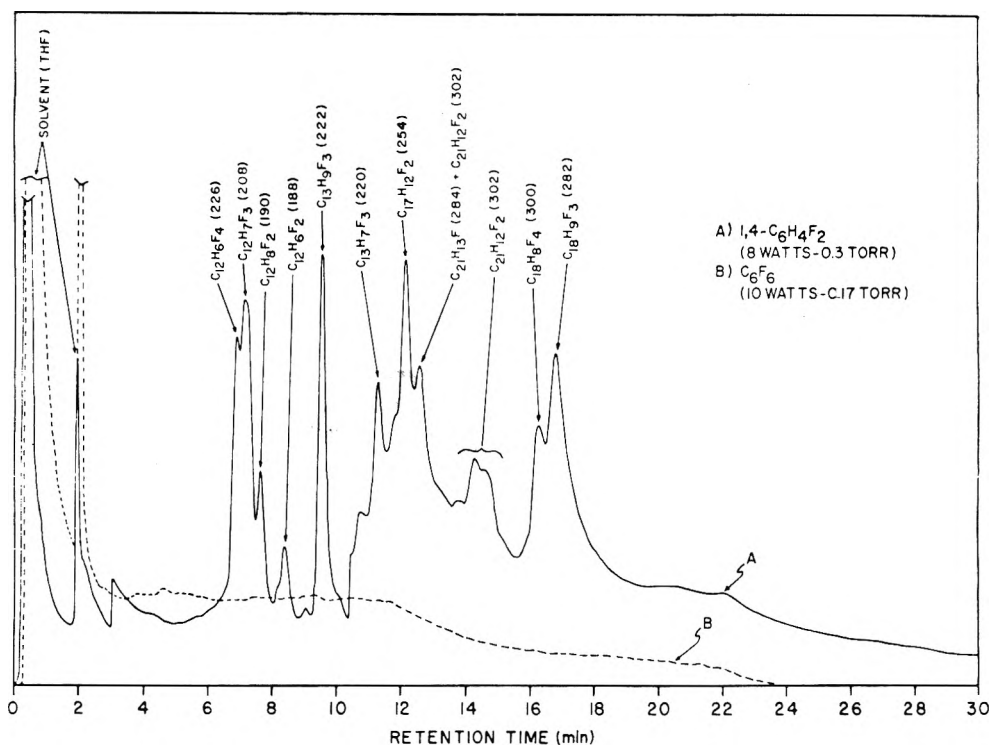


Figure 5. Gas chromatograms of low molecular weight products (fraction A) resulting from rf discharges through *p*-difluorobenzene (A) and hexafluorobenzene (B).

compounds formed of either a few condensed aromatic rings or short aliphatic chains. This pattern of the GPC chromatogram for benzene products is similar to that obtained by Duval and Théorêt¹⁴ from benzene with approximately the same experimental discharge conditions. The same two bands are observed for fluorinated benzene derivatives but the band corresponding to higher molecular weight products increases steadily in intensity with the number of fluorine atoms on the benzene ring at the expense of the other band. This behavior is well illustrated in the case of C_6F_6 where the long elution time band almost completely vanishes.

Furthermore, a gas chromatography-mass spectrometry (GC/MS) analysis was undertaken of the low molecular weight products. The results are illustrated in Figure 5 for 1,4- $C_6H_4F_2$ whose chromatogram is characteristic of all fluorinated benzene derivatives except C_6F_6 . As shown in the figure, the chromatogram for C_6F_6 gives an ill-defined baseline. On the other hand, according to the GPC analysis, the proportion of high molecular weight compounds which, for the purposes of this study, are termed polymers, increases when the ratio W/P applied to the discharge increases; at the same time, as mentioned before, the insolubility of the products, probably due to a higher degree of branched polymers and carbonized residues, increases in THF. An elemental analysis of the insoluble products tends to confirm the latter assumption, as can be seen by the weak but significant increase in the C/F and C/H ratios as compared to those of the monomers.

Finally, infrared spectra of the soluble reaction products obtained from the reactions of fluorinated benzene derivatives have been reproduced in Figure 6. For the products resulting from monomers with a low degree of fluorine substitution, the bands at 3020, 1600, and 1500 cm^{-1} are evidence of the strong aromatic character of these compounds while the strong bands at 750 and 690 cm^{-1} are characteristic of substituted aromatic rings. The presence of aliphatic chains is confirmed by the bands at 2920, 1450, and 1370 cm^{-1} . For the products obtained

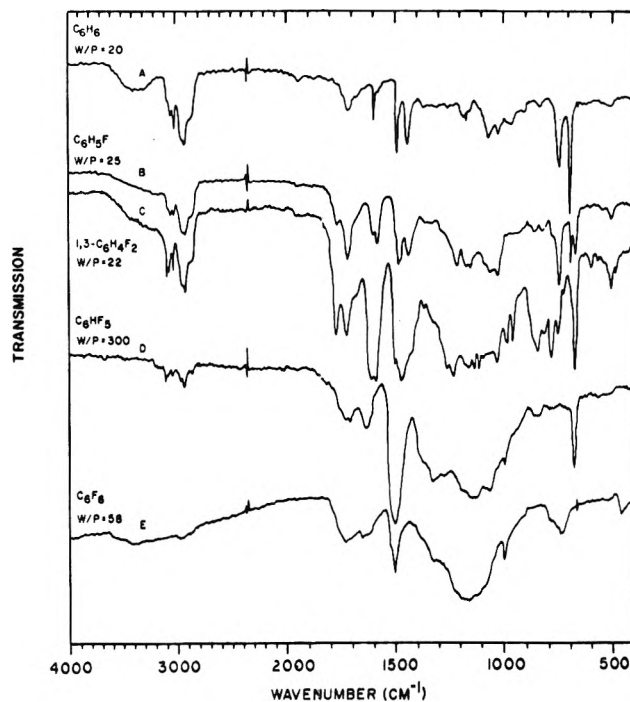


Figure 6. Infrared spectra of soluble solids (fraction A) resulting from rf discharges through benzene (A), monofluorobenzene (B), *m*-difluorobenzene (C), pentafluorobenzene (D), and hexafluorobenzene (E).

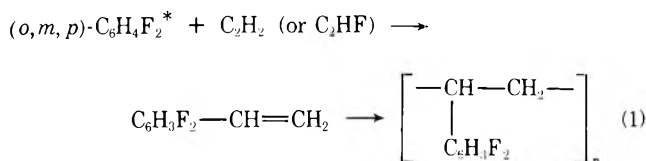
from C_6HF_5 and C_6F_6 , spectra d and e on Figure 6, the bands at 1500 and 995 cm^{-1} are assigned to perfluorinated aromatic rings. The other broad band located between 1000 and 1400 cm^{-1} is characteristic of CF and CF_2 stretching vibrations and, as expected, becomes more intense with the degree of fluorine atom substitution on the monomers.

In the region between 1600 and 1800 cm^{-1} , the infrared

spectra show some bands which may be assigned to double bond stretching vibrations although they could quite possibly result from carbonyl groups obtained by the oxidation of radicals trapped in the polymers.

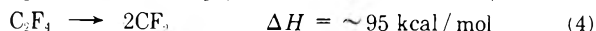
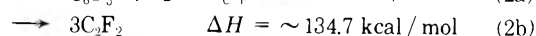
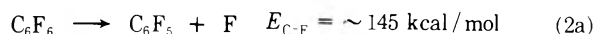
Reaction Mechanisms. From this product analysis and electrical discharge emission study, a simple, general reaction mechanism can now be proposed to explain the main feature of the results.

Group I (C_6H_5F and *o*-, *m*-, and *p*- $C_6H_4F_2$). For this group of monomers, the emission spectra result almost exclusively from a molecular emission equivalent to the well-known $\pi \leftarrow \pi^*$ band system of the benzene molecule. Emission bands due to molecular fragment species are of very weak intensity. A polymerization mechanism, similar to the one proposed for benzene,²⁵ can be applied to explain the formation of polymers for this group of monomers. According to this mechanism, polymerization takes place through the reaction of acetylene or acetylene derivatives formed during the discharge with electronically excited monomers to yield what can be termed a plasma version of a polystyrene polymer. Such a mechanism seems a reasonable explanation of the polymerization of this first group of monomers:

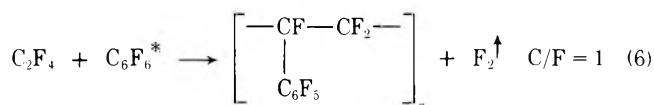
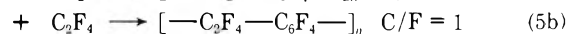
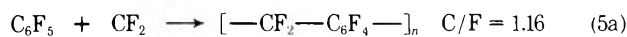


The theoretical ratio C/H (1.33) and C/F (4.00) for this polymer structure is in fair agreement with the values obtained from the elemental analysis which are 1.35 and 3.56, respectively, for *p*- $C_6H_4F_2$ polymers. Furthermore, the infrared spectra for these polymers suggest a structure similar to that of polystyrene.

Group II (C_6HF_5 and C_6F_6). The discharge emission spectra for this group of monomers are characterized by the strong emission of CF_2 radicals. The following reactions could explain the formation of this radical in rf discharges.



According to Baddour and Bronfin,²⁶ the difluoroacetylene molecule is very unstable at temperatures below 2000 K and reacts immediately with fluorine atoms to yield tetrafluoroethylene. Incidentally, this compound constitutes one of the major gaseous reaction products obtained in this work and accordingly supports the mechanism advanced to explain the formation of CF_2 radicals. As a matter of fact, it is well known that the decomposition of C_2F_4 either by pyrolysis²⁷ or in electrical discharges²⁶ is a major source of CF_2 radicals. There are thus many possible intermediate steps for the polymerization of these two monomers, the most probable being the following:



The polymer structure from eq 5a has a C/F ratio which shows the best agreement with the elemental analysis results obtained with C_6F_6 polymers.

Conclusion

In conclusion, even if the present study touches only lightly on the subject, the authors believe that this work shows the existence of a relationship between the value of quantum deficit $1 - (\phi_{S_1} + \phi_{T_1})$ and both the emission features and the degree of polymerization of these monomers in electrical discharges. The increase in the value of the quantum deficit with the degree of fluorine atom substitution on the benzene rings is reflected in the results by the disappearance of molecular emission and the enhancement of the emission of CF_2 radicals on the one hand and, on the other, by a greater yield of polymers in going from monofluorobenzene to perfluorobenzene.

Acknowledgment. The authors acknowledge Dr. M. Duval and Dr. J. Castonguay for their valuable help in the interpretation of the GPC and GC/MS chromatograms. Finally the authors are indebted to Y. Giguère for his assistance in carrying out this work.

References and Notes

- (1) A. S. Abramson, K. G. Spears, and S. A. Rice, *J. Chem. Phys.*, **56**, 2291 (1972).
- (2) M. E. MacBeath, G. P. Semeluk, and I. Unger, *J. Phys. Chem.*, **73**, 995 (1969).
- (3) J. L. Durham, G. P. Semeluk, and I. Unger, *Can. J. Chem.*, **46**, 3177 (1968).
- (4) F. W. Ayer, F. Grein, G. P. Semeluk, and I. Unger, *Ber. Bunsenges. Phys. Chem.*, **72**, 282 (1968).
- (5) B. H. Scholz and I. Unger, *Can. J. Chem.*, **48**, 2324 (1970).
- (6) D. Phillips, *Photochemistry*, **2**, 154 (1971).
- (7) M. E. MacBeath, *Diss. Abstr. Int. B*, **32**, 6874 (1972).
- (8) I. Haller, *J. Am. Chem. Soc.*, **88**, 2070 (1966).
- (9) T. Ogawa, M. Tsuji, M. Toyoda, and N. Ishibashi, *Bull. Chem. Soc. Jpn.*, **46**, 1063 (1973).
- (10) J. V. Shukla, K. N. Upadhyaya, and D. K. Rai, *Indian J. Pure Appl. Phys.*, **9**, 815 (1971).
- (11) S. N. Singh and I. S. Singh, *Indian J. Phys.*, **42**, 42 (1968).
- (12) The authors have not included the molecules $C_6H_3F_3$ and $C_6H_2F_4$ because of their nonavailability commercially and difficulties involved in preparing them at the laboratory.
- (13) P. L. Spedding, *Chem. Eng. (London)*, **No. 225**, CE 17 (1969).
- (14) M. Duval and A. Théorêt, *J. Appl. Polym. Sci.*, **17**, 527 (1973).
- (15) H. F. Kemper and M. Stockburger, *J. Chem. Phys.*, **53**, 268 (1970).
- (16) The term "resonance fluorescence" has already been used by Kemper and Stockburger (see ref 15). It is defined as any radiation originating from the initially excited vibronic levels.
- (17) K. Nakamura, *J. Chem. Phys.*, **53**, 998 (1970).
- (18) T. L. Brewer, *J. Phys. Chem.*, **75**, 1233 (1971).
- (19) P. Venkateswarlu, *Phys. Rev.*, **77**, 676 (1950).
- (20) R. K. Laird, E. B. Andrews, and R. F. Barrow, *Trans. Faraday Soc.*, **46**, 803 (1950).
- (21) S. L. Lem, G. P. Semeluk, and I. Unger, *Can. J. Chem.*, **49**, 1567 (1971).
- (22) Kh. Al-Ani and D. Phillips, *J. Phys. Chem.*, **74**, 4046 (1970).
- (23) D. Phillips, *J. Chem. Phys.*, **46**, 4679 (1967).
- (24) R. A. Falk, *Sperry Eng. Rev.*, **18**, 24 (1963).
- (25) M. Duval and A. Théorêt, *J. Electrochem. Soc.*, **122**, 581 (1975).
- (26) R. F. Baddour and B. R. Bronfin, *Ind. Eng. Chem., Process Des. Dev.*, **4**, 162 (1965).
- (27) B. Atkinson and V. A. Atkinson, *J. Chem. Soc.*, 2086 (1957).

Dynamic Nuclear Magnetic Resonance in the Gas Phase. The Torsional Barrier in *N,N*-Dimethylthioformamide

Torbjörn Drakenberg

Division of Physical Chemistry 2, The Lund Institute of Technology, Chemical Center, S-220 07 Lund 7, Sweden
(Received November 4, 1975)

The torsional barrier in gaseous *N,N*-dimethylthioformamide has been obtained from a total bandshape analysis of the proton NMR spectrum. The height of the same barrier for nonpolar solutions has also been estimated. It was found that the barrier was increased considerably by solute-solvent or solute-solute interaction, especially in the neat liquid. The gas phase barrier was found to be ca. 22.5 kcal/mol (ΔG^\ddagger), whereas the barrier in the neat liquid is greater than 25 kcal/mol.

Introduction

The dynamic NMR methods, especially the total bandshape analysis technique, have been very useful tools for the study of interconversion barriers with activation energies (ΔG^\ddagger) ranging from ca. 5 to ca. 25 kcal/mol.^{1,2} In almost every study neat liquids or solutions have been used, and only in very few cases has the gas phase been studied.³⁻⁶ The lack of data for the gas phase is easily understood as being due to the very low sensitivity of the NMR method, and furthermore the relaxation time in the gas phase is often short as a result of efficient spin-rotation relaxation. At least the problem with the low sensitivity can nowadays be partly overcome with the use of the pulsed Fourier transform technique, which was recently used in the study of the inversion barrier in gaseous aziridine.⁶

The lack of reliable gas phase data for most kinds of interconversion processes feasible for dynamic NMR studies is rather unfortunate, since most theoretical calculations, used for comparison with experimental data, refer to isolated molecules, which is best realized in the gas phase.

This work is a continuation of the attempts to obtain reasonably reliable data on various kinds of interconversion barriers, in the gas phase, and deals with the torsional barrier in *N,N*-dimethylthioformamide (DMTF), which has previously been studied as the neat liquid or in concentrated solutions.⁷ Attempts have also been made to study *N,N*-dimethylformamide, but up to now only a single line has been observed for all the methyl protons, probably due to chemical shift equivalence.

To test if data from nonpolar solvents could be used to estimate the true gas phase barrier, DMTF has also been studied in *m*-dichlorobenzene and decalin solutions.

Results and Discussion

In Figure 1 a few spectra of DMTF in the gas phase are reproduced. As can be seen, it is possible to obtain a reasonable signal-to-noise ratio even at temperatures far below the boiling point of the compound studied. It may be clearly seen from these spectra that the coalescence is not due to a temperature dependence in the chemical shift difference, but is caused by an exchange between the two methyl groups. From the spectra it was not possible to directly obtain the spin coupling between the methyl protons and the formyl proton. It was, however, possible from the high temperature spectrum, to show that the mean cou-

pling constant is less than or equal to 0.6 Hz, in good agreement with the coupling constants observed for DMTF in *m*-dichlorobenzene (*m*DCB) or decalin solutions. The coupling to the high-field methyl signal was found to be 0.5 Hz, and that to the low-field methyl signal 0.7 Hz.

For both solvents used, the DMTF methyl proton chemical shift difference is concentration dependent, as can be seen from Table I. The negative sign for the neat liquid indicates that the order of the chemical shifts has been inverted, as judged from the relative magnitudes of the coupling constants. The pronounced concentration dependence of the chemical shift difference for the *m*DCB solution is expected, due to the so-called ASIS effect.⁸ The concentration dependence of the chemical shift difference for the decalin solutions is most easily explained if it is assumed that the thioamide homoassociation causes an upfield shift of the signal due to the methyl protons *cis* to sulfur. This problem is, however, not the main interest of this paper and will not be discussed further.

From the observed chemical shift differences (see Table I), it is obvious that the assignment of the gas phase signals must be the same as for the dilute decalin solution, and in the total bandshape analysis performed to determine the activation energy of the hindered rotation, coupling constants of 0.5 and 0.7 Hz were used for the high- and low-field signals, respectively. The resulting free energy of activation is given in Table I, together with data for the liquid state. From this table it is obvious that the torsional barrier in DMTF is considerably higher in the liquid state than in the gas phase. This is in agreement with the data for *N,N*-dimethylnitrosamine.³ Harris and Spragg reported for this compound a difference in ΔG^\ddagger of ca. 2 kcal/mol between the gas phase and the neat liquid, with the gas phase lower. Similar results have been reported for the aldehyde rotation in benzaldehydes obtained from ir data.⁹

It was of interest to determine whether a dilute solution in an inert, nonpolar solvent could be used to estimate "gas phase" data in the case of DMTF as shown to be the case for some aziridines.⁴ Thus, the barrier to internal rotation in DMTF dissolved in decalin and *m*DCB was obtained from bandshape analysis, resulting in the data given in Table I. *m*DCB is not a nonpolar solvent, and in these solutions, even at the lowest concentration used, the barrier is considerably higher than in the gas phase. For decalin, on the other hand, it was difficult to obtain usable spectra at very low concentrations of DMTF due to the closeness of

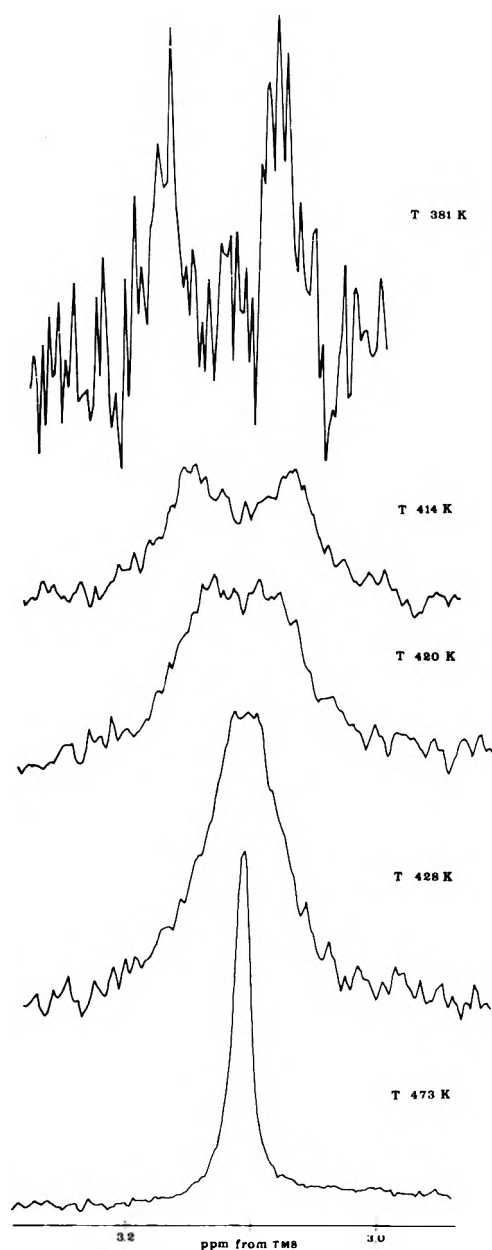


Figure 1. Proton NMR spectra of the methyl proton signal from *N,N*-dimethylthioformamide at a few temperatures in the gas phase.

the solvent NMR signals. However, for the lowest concentration, much higher than for the *m*DCB solution, the barrier is only ca. 1 kcal/mol higher than for the gas phase. From the variation of the chemical shift difference with concentration, it is plausible that there is an interaction between the DMTF molecules, responsible for the difference in both the chemical shift difference and the barrier between the solution and the gas phase. It thus seems possible to estimate gas phase barriers for thioamides (and probably amides) from data on dilute solutions in nonpolar solvents. Care must however be taken to ensure that a suf-

TABLE I: Chemical Shift Difference between the Methyl Proton NMR Signals and the Barrier to Internal Rotation in *N,N*-Dimethylthioformamide

Sample composition	$\Delta\nu$, ppm	(<i>T</i> , K)	ΔG^\ddagger , kcal/mol	(<i>T</i> , K)
DMTF gas + TMS gas	0.09	(381)	22.5	(420)
DMTF liquid	-0.12	(303)	25.5	(473)
1 M in <i>m</i> DCB	0.07	(303)	24.8	(443)
0.1 M in <i>m</i> DCB	0.14	(303)	24.6	(443)
0.01 M in <i>m</i> DCB	0.15	(303)	24.2	(443)
0.1 M in decalin	0.05	(303)	23.5	(431)
0.01 M in decalin	0.08	(303)		

ficiently low concentration has been used and that the solvent really is nonpolar.

The work on dynamic NMR studies in the gas phase will continue with studies on other types of interconversion barriers.

Experimental Section

The solvents, *m*-dichlorobenzene and decalin, were commercial products used without purification, and the *N,N*-dimethylthioformamide was a generous gift from J. Sandström, University of Lund. The gas phase samples were prepared in glass ampoules that fitted perfectly in 12-mm NMR tubes. The ampoules were filled on a vacuum line with DMTF and TMS and were sealed off under vacuum at dry-ice temperature. At temperatures above 150 °C the sample were completely gaseous.

The NMR spectra were recorded on a Varian XL-100 spectrometer operating in the Fourier transform mode and using external proton lock. The temperature was measured with a thermocouple as described previously.⁶ Typical settings for the parameters used for the FT spectra were: spectral width 2000 Hz, acquisition time 2 s, number of transients 2000, and pulse width 80 μ s (45° flip angle).

Acknowledgments. Professor J. Sandström is heartily thanked for the gift of the *N,N*-dimethylthioformamide compound, and Dr. R. E. Carter for valuable linguistic criticism. The cost of the XL-100 spectrometer was partly defrayed by a grant from the Knut and Alice Wallenberg Foundation. This work was made possible by financial support from the Swedish Natural Science Research Council.

References and Notes

- G. Binsch in "Topics in Stereochemistry", Vol. 3, E. L. Eliel and N. L. Allinger, Ed., Interscience, New York, N.Y., 1968.
- I. O. Sutherland in "Annual Reports on NMR Spectroscopy", Vol. 4, E. F. Mooney, Ed., Academic Press, London, 1971.
- R. K. Harris and R. A. Spragg, *Chem. Commun.*, 362 (1967).
- T. Drakenberg and J. M. Lehn, *J. Chem. Soc., Perkin Trans. 2*, 532 (1972).
- R. E. Carter and T. Drakenberg, *J. Chem. Soc., Chem. Commun.*, 582 (1972).
- R. E. Carter and T. Drakenberg, *J. Am. Chem. Soc.*, **97**, 6990 (1975).
- A. Loewenstein, A. Melera, P. Rigny, and W. Walter, *J. Phys. Chem.*, **68**, 1597 (1964).
- P. Laszlo in "Progress in Nuclear Magnetic Resonance Spectroscopy", Vol. 3, J. W. Emsley, J. Feeney, and L. H. Sutcliffe, Ed., Pergamon Press, London, 1967.
- W. G. Fatela, R. K. Harris, F. A. Miller, and R. E. Witkowski, *Spectrochim. Acta*, **21**, 231 (1965).

Kinetics of the Thermal Decomposition of Tetrakis(dimethylamino)ethylene in the Vapor Phase

Chas. E. Waring* and Raymond A. Berard

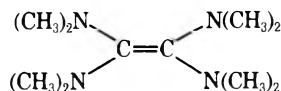
Department of Chemistry, University of Connecticut, Storrs, Connecticut 06268 (Received October 20, 1975)

Publication costs assisted by the University of Connecticut

The thermal decomposition of the chemiluminescent compound tetrakis(dimethylamino)ethylene (TMAE) has been investigated in a static system between 283 and 323 °C over initial pressures from 6.0 to 45 mmHg. The order of the reaction was first, as was the order for the formation of methane and dimethylamine, the major decomposition products. The Arrhenius parameters for the TMAE decomposition are given as $k_i = 9.0(\pm 1.0) \times 10^{11} e^{-39\,900(\pm 2000)/RT} \text{ s}^{-1}$ while those for CH_4 and DMA are $k_{\text{CH}_4} = 4.3(\pm 0.03) \times 10^{11} e^{-39\,300(\pm 300)/RT} \text{ s}^{-1}$ and $k_{\text{DMA}} = 2.5(\pm 0.01) \times 10^{10} e^{-36\,500(\pm 200)/RT} \text{ s}^{-1}$, respectively. The effect of certain foreign gases indicated that the decomposition was free radical in nature. A mechanism is suggested which accounts for the predominant gaseous products and calculations from experimental data are offered in support of the proposed mechanism.

Introduction

Tetrakis(dimethylamino)ethylene (TMAE) was first reported by Pruett et al.¹ and its structure is given as



This molecule has many interesting characteristics. When exposed to air at ambient temperatures, it chemiluminesces strongly in the visible region. Winberg, Downing, and Coffman² report that the fluorescence and chemiluminescence spectra of TMAE are essentially equivalent and without fine-line structure, with the maxima at 5150 Å. Since the known oxidation products³ do not fluoresce under these conditions, they conclude that an electronically activated TMAE molecule is the emitting species. From the overall chemiluminescence quantum yield, there appears to be only about three photons emitted for 10 000 molecules of TMAE oxidized. It is further reported² that the presence of protonic material is essential for chemiluminescence.

Fletcher and Heller^{4,5} studied the kinetics of the oxidation of TMAE in decane using octanol as a catalyst. They found the rate of disappearance of TMAE to be first order and the chemiluminescence to be second. They conclude that the oxidation mechanism is not free radical in nature. Urry and Sheets,⁶ on the other hand, investigated the autoxidation of TMAE in various solvents and give evidence for a free-radical mechanism. Paris,⁷ however, proposes an oxidation process which depends upon carbene formation and subsequent recombination of two carbenes to form an electronically excited TMAE. The TMAE* then decays to the ground state with the emission of light.

It is clear from the literature that the mechanism of the oxidation of TMAE in solution is a complicated process. Because of this, various investigators have been unable to agree on the initial step, the products, or the mechanism of light emission. The purpose of this investigation is to examine first the high-temperature pyrolysis of TMAE vapor for unusual thermal reactions and to see if there is any correlation between these reaction products with those reported for the oxidation of TMAE at ambient temperatures. A subsequent paper will

report on the kinetics of the gas phase oxidation of this unusual molecule.

Experimental Section

A. Apparatus. The thermal decomposition of TMAE was studied in a static manometric system. The reaction chamber was a 200-ml round-bottom Pyrex flask. This was centered in the furnace well and surrounded with asbestos. The furnace temperature was maintained to within ± 0.5 °C by a Leeds and Northrup Electromax control unit. Temperatures were measured with a chromel–alumel thermocouple in conjunction with an automatic recording potentiometer.

The system was evacuated by the usual techniques and no run was made unless the pressure (as measured with an NRC ion gauge) was 10^{-5} mmHg or less. Due to the low vapor pressure of TMAE, samples were introduced into the reaction chamber from a large expansion flask. All external lines and the expansion flask were maintained at 120 °C by asbestos heating tape. The pressure change in the reaction chamber was followed by means of a Consolidated Electroynamics Corp. absolute pressure transducer. Gaseous reaction products were withdrawn by an automatically controlled Toepler pump and transferred to a sample bulb.

B. Materials. The TMAE employed was obtained through the courtesy of the Naval Weapons Center, China Lake, Calif. It was placed in an I²R drybag which had previously been purged with nitrogen and dried for 12 h with P_2O_5 . The TMAE was then stirred with alumina to remove any polar products of oxidation, siphoned into an evacuated flask, removed from the drybag, and attached to the vacuum line through a Teflon connector.

Nitric oxide was obtained from the Matheson Co. and purified by methods previously described.⁸

Propylene was also furnished by the Matheson Co. It was vacuum distilled until a 99% purity was obtained.

The argon employed was from the Air Reduction Co. and the oxygen supplied by the Allstate Gas Co. Because of the high stated purity of these gases, they were used directly.

C. Analyses. Analyses of the gaseous reaction products were made on a Perkin-Elmer Model 154A gas chromatograph. The absolute identification of the components was checked on three different columns.

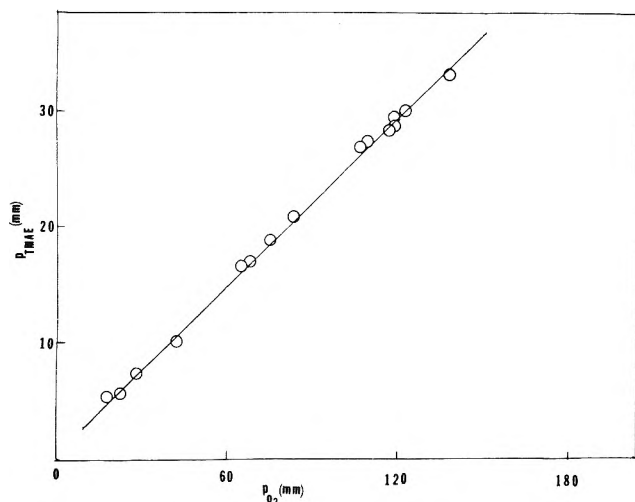


Figure 1. Calibration of the pressure of TMAE in the reaction vessel per mm of oxygen consumed in the special collector (slope = 0.242).

In order to determine the rates of disappearance of TMAE it was necessary to devise an analytical technique for measuring the amount of unreacted TMAE remaining. This was accomplished by adding an excess of oxygen to known amounts of TMAE and measuring the decrease in oxygen pressure which corresponded to the amount of TMAE consumed. Figure 1 shows the calibration curve in which the amount (mmHg) of TMAE in the reaction vessel is plotted against the corresponding amount (mmHg) of oxygen consumed. The slope of the line, which gives the ratio of the pressure of TMAE to the oxygen consumed, was 0.242. Thus, for each mmHg of TMAE present, 4.1 mmHg of O₂ are consumed.

Further, in order to determine if the products had any effect on the oxygen take-up, a sample of TMAE was pyrolyzed for 5 h, or until decomposition was complete. Upon addition of oxygen, no significant change in pressure was observed. It was concluded, therefore, that the products did not affect the TMAE analysis.

Results

1. *Nature of the Decomposition.* The thermal decomposition of TMAE vapor was found to be homogeneous over the temperature range 283–323 °C and over an initial pressure range of 6.0–45.0 mmHg. The ratio of the final to the initial pressure at five different temperatures was approximately 3.

2. *Order of Reaction.* For the decomposition of TMAE, the changes in pressure with time for ten different initial pressures were determined at five different temperatures. These data were programmed on an IBM 1620 computer to solve for k_i , the initial rate constant, and n , the order of reaction, in the equation

$$\log (dp/dt)_0 = \log k_i + n \log p_i \quad (1)$$

The values of n varied from 0.9 to 1.1 over the five temperatures and the average value was 1.02, indicating that the order of the decomposition is unquestionably first.

Using the calibration curve in Figure 1, the order of reaction, based upon the measured rate of disappearance of TMAE, was also determined. As before, the initial rate of disappearance was evaluated at each initial pressure and the data programmed to obtain k_i and n by eq 1. These data are presented in Table I. A plot of $\log (dp/dt)_0$ vs. p_i was also linear, giving a slope, $n = 1.0$.

TABLE I: Variation of the Initial Rate of Disappearance of TMAE with Initial Pressures at 310 °C

p_i , mm	8.7	15.4	19.3	27.3	32.0
$(dp/dt)_0 \times 10^3$	8.4	14.9	17.0	24.0	32.0
$k_i \times 10^4 \text{ s}^{-1}$	9.61	9.67	8.82	8.80	10.0 ($A_v = 9.38$)

TABLE II: Variation of Initial Rate Constants of TMAE, CH₄, and DMA with Temperature

t , °C	283	294	304	310	313	323
$k_{\text{TMAE}} \times 10^4$	1.89	3.38	5.15	9.56	11.9	20.9
$k_{\text{CH}_4} \times 10^4$			4.97		8.42	14.8
$k_{\text{DMA}} \times 10^4$			3.75		6.26	10.3

TABLE III: Mole Percent of Gaseous Products at 10 min from the Decomposition of 28 mm of TMAE at 323 °C

Product	CH ₄	(CH ₃) ₂ -NH	(CH ₃) ₃ -N	CH ₃ N-H ₂	C ₂ H ₆	(CH ₃) ₂ N-CH ₂ -N
Mol %	63	35	<1	<1	<1	<1

Since methane and dimethylamine (DMA) were the only predominant products from the decomposition of TMAE, their initial rates of formation were also determined at various initial pressures of TMAE. Again, by use of eq 1, n and k_i were evaluated for each compound at three different temperatures. The order of reaction, n , was found to be 1.1 for CH₄ and 0.9 for DMA.

3. *Activation Energies.* The activation energies and frequency factors for the thermal decomposition of TMAE, and for the formation of CH₄ and DMA, were determined by the method of least squares from the data in Table II.

The Arrhenius parameters for the decomposition of TMAE are given by

$$k_i = 9.0(\pm 1.0) \times 10^{11} e^{-39\,900(\pm 2000)/RT} \text{ s}^{-1} \quad (2)$$

The analogous expressions obtained for the formation of CH₄ and DMA are

$$k_{\text{CH}_4} = 4.3(\pm 0.03) \times 10^{11} e^{-39\,300(\pm 300)/RT} \text{ s}^{-1} \quad (3)$$

and

$$k_{\text{DMA}} = 2.5(\pm 0.01) \times 10^{10} e^{-36\,500(\pm 200)/RT} \text{ s}^{-1} \quad (4)$$

4. *Products of Reaction.* The thermal decomposition of TMAE produced only two major gaseous reaction products: methane and dimethylamine. Table III presents all the gaseous products that were formed. The identity of bis(dimethylamino)methane is somewhat uncertain since a known sample of the material could not be obtained. However, a mass spectrum of a chromatographic separation agrees well with the mass spectrum Urry⁹ obtained for this compound.

Two condensable products were also obtained. One was a volatile, clear liquid and the other a dark brown, nonvolatile, viscous liquid. The infrared spectra of the two liquids show they are not very different. A further indication that they may be the same is the fact that, on standing, the clear liquid becomes dark brown and viscous, apparently due to polymerization. Attempts to identify this material further were unsuccessful. The spectra indicate the presence of C–H, C=C without associated olefin C–H stretching, and C≡N. The

TABLE IV: Partial Pressures (mm) of CH₄ and DMA from the Decomposition of 28 mm of TMAE at Various Temperatures

Time, min	304 °C		313 °C		323 °C	
	p _{CH₄} , mm	p _{DMA} , mm	p _{CH₄} , mm	p _{DMA} , mm	p _{CH₄} , mm	p _{DMA} , mm
1	0.8	0.5	1.4	0.7	2.6	1.8
2	1.6	1.1	2.7	1.4	4.7	3.2
4	2.8	1.9	5.0	2.6	8.6	5.3
6	4.1	2.6	6.7	3.6	11.2	6.8
8	5.2	3.0	8.1	4.3	13.2	7.9
10	6.1	3.4	9.4	4.9	15.2	8.8
12	7.0	3.8	10.6	5.5	16.7	9.7
15	7.8	4.2	12.1	6.4	18.6	11.2

Av CH₄/DMA = 1.6

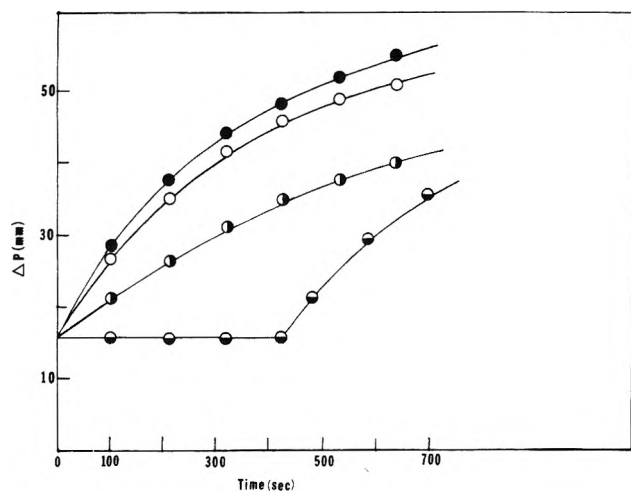


Figure 2. Variation of pressure with time for the decomposition of 28 mm of TMAE in the presence of various foreign gases at 317 °C: (O) 0 mm foreign gas; (●) 30 mm of propylene; (●) 100 mm of argon; (◐) 0.3 mm of nitric oxide.

presence of a conjugated system, C=C-N, is possible but difficult to determine with any certainty.

The change in the partial pressures of the major products of reaction with time at several different temperatures are given in Table IV.

5. *Effect of Foreign Gases. A. Propylene.* The addition of propylene significantly decreases the initial rate of decomposition of TMAE. Relatively large amounts of propylene are required to produce maximum inhibition. For example, 80 mm of this inhibitor are required to reduce 28 mm of TMAE to a limiting rate of one-quarter of that of the uninhibited reaction. Figure 2 compares the effect of propylene with the uninhibited decomposition of TMAE.

B. *Argon.* It was suspected that the inhibition by propylene might be due to a mass action effect rather than to an actual chain termination process. To resolve this, the rate of pressure increase for the decomposition of TMAE was determined in the presence of various partial pressures of argon. In Figure 2, it can be seen that 100 mm of argon in the presence of 28 mm of TMAE produces only a slight increase in the rate of decomposition. This result clearly indicates that the propylene inhibition is not a mass action phenomenon. It does suggest, however, that the effect of argon may be to reduce chain termination at the walls.

C. *Nitric Oxide.* The effect of NO on the pyrolysis of TMAE was unusual. With the addition of 1.0 mm or less of NO to 28.0

TABLE V: Comparison of the Rates of Formation of CH₄ from the Inhibited and Uninhibited Decompositions of 28 mm of TMAE at 313 °C (p_{NO} = 2.0 mm)

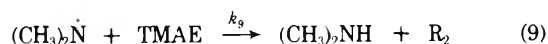
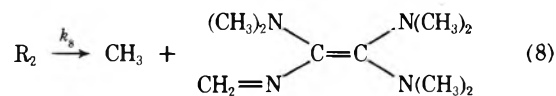
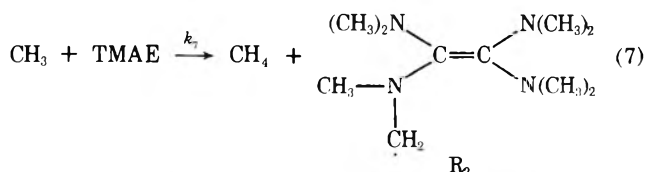
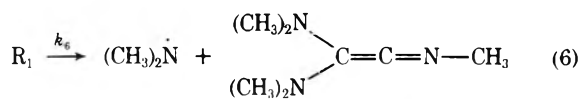
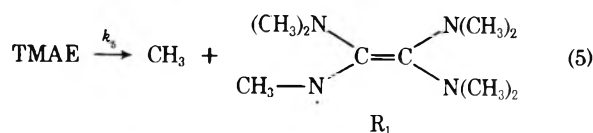
Time, s	100	200	300	400	500	600	700	800
CH ₄ (un), mm	2.3	4.3	5.8	7.0	8.2	9.4	10.1	11.2
CH ₄ (in), mm	0.13	0.24	0.34	0.43	0.50	0.56	0.61	0.65

mm of TMAE, there was an induction period of approximately 400 s. During this time, very little TMAE reacted. Throughout the induction period, the only gaseous decomposition products were methane, nitrogen, and small amounts of carbon monoxide. This is in sharp contrast to the products obtained from the uninhibited reaction. Table V gives the comparison between the rates of formation of CH₄ in the NO inhibited and uninhibited reactions. It is of interest to mention that rate of formation of CH₄ throughout the induction periods was always roughly inversely proportional to the rate of disappearance of NO.

A number of runs were made pyrolyzing a fixed partial pressure of TMAE in the presence of different initial pressures of NO. Under these conditions, the length of the induction period was a linear function of the partial pressure of NO. At the end of the induction period, mass spectrographic analyses showed no nitric oxide to be present. At this point, the rate of pressure increase is slightly greater than that in the absence of NO, as seen in Figure 2. In this latter pressure increase region, the proportion of the major gaseous products are the same as in the uninhibited reaction, namely, 63% CH₄ and 37% DMA.

Discussion

The inhibiting effects of propylene and nitric oxide indicate that the decomposition of TMAE vapor is undoubtedly free radical in nature. It is also reasonably certain that the overall mechanism of the reaction is more complicated than the detected products reported in Table III suggest. A plausible mechanism can be written, however, to account for the predominant products of the pyrolysis:



The justifications for the proposed mechanisms are as follows. If one compares the bond dissociation energies of various amines,¹⁰ it is seen that the energy of the CH₃-N bond is decreased when the nitrogen is also bonded to a π -bonded system. In TMAE, where all the nitrogens are partially involved in the π bond of ethylene, the CH₃-N bonds are undoubtedly the weakest. This would tend to favor reaction 5 as the initial step over the elimination of a DMA radical. From an energetics standpoint, reactions 6-9 appear to be the most plausible ones to account for the formation of the two major products, CH₄ and DMA. The postulated product molecules in steps 6 and 8 are admittedly somewhat speculative and must be highly transitive. The compounds indicated, however, have been postulated by Urry,⁹ based on NMR analyses, as intermediates in the reaction of TMAE with methyl iodide in dioxane.

If one applies the usual steady-state approximations to the postulated mechanism it can be readily shown that

$$[\text{CH}_3]_{\text{ss}} = (k_5 k_8 / k_7 k_{10})^{1/2} \quad (11)$$

and

$$[(\text{CH}_3)_2\dot{\text{N}}]_{\text{ss}} = k_5 / k_9 \quad (12)$$

The rate of disappearance of TMAE is then found to be

$$-d[\text{TMAE}]/dt = \left[2k_5 + \left(\frac{k_5 k_7 k_8}{k_{10}} \right)^{1/2} \right] [\text{TMAE}] \quad (13)$$

Thus, the rate of decomposition of TMAE is seen to be first order, in agreement with that observed experimentally.

There is support for the fact that methane and dimethylamine are produced predominantly by only one reaction, such as that proposed in steps 7 and 9. If one takes the ratios of the Arrhenius parameters for the formation of CH₄ and DMA, it can be seen from eq 3 and 4

$$\frac{k_{\text{CH}_4}}{k_{\text{DMA}}} = \frac{4.3 \times 10^{11} e^{-39300/RT} \text{ s}^{-1}}{2.5 \times 10^{10} e^{-36500/RT} \text{ s}^{-1}} = 17.20 e^{-2800/RT} \quad (14)$$

that $E_9 - E_7 = 2.8$ kcal/mol. This represents the increase in activation energy required for a (CH₃)₂ $\dot{\text{N}}$ radical to abstract a hydrogen from TMAE over that required for a $\dot{\text{C}}\text{H}_3$ radical to remove a similar H atom. If one assumes $E_7 = 7.2$ kcal/mol as an average value for the abstraction of an H atom from amines¹¹ by a methyl radical, then the activation energy for a similar abstraction by a (CH₃)₂ $\dot{\text{N}}$ radical, E_9 , becomes 10.0 kcal/mol.

Further, if one refers to the data in Table IV at 323 °C, it is seen that the ratio CH₄/DMA = 1.6. At this temperature, the ratio of $k_{\text{CH}_4}/k_{\text{DMA}}$ is found by eq 14 to be 1.6. This excellent agreement between the observed and calculated values for the CH₄/DMA ratios provides additional support to the argument that these compounds are each the product of a single step reaction.

Acknowledgment. The authors wish to thank Professor S. R. Smith of this Department for his helpful suggestions and advice during the course of this research and preparation of this paper.

References and Notes

- (1) R. L. Pruett, J. T. Barr, K. E. Rapp, C. T. Bahner, J. D. Gibson, and R. H. Laffety, Jr., *J. Am. Chem. Soc.*, **72**, 3646 (1950).
- (2) H. E. Winberg, J. R. Downing, and D. D. Coffman, *J. Am. Chem. Soc.*, **87**, 2054 (1965).
- (3) N. Wiberg and J. W. Buchler, *Angew. Chem., Int. Ed. Engl.*, **1**, 406 (1962).
- (4) A. N. Fletcher and C. A. Heller, *J. Catal.*, **6**, 263 (1966).
- (5) A. N. Fletcher and C. A. Heller, *J. Phys. Chem.*, **71**, 1507 (1967).
- (6) W. H. Urry and J. Sheets, *Photochem. Photobiol.*, **4**, 1067 (1965).
- (7) J. P. Paris, *Photochem. Photobiol.*, **4**, 1059 (1965).
- (8) T. H. McGee and C. E. Waring, *J. Phys. Chem.*, **73**, 2838 (1969).
- (9) W. H. Urry, private communication.
- (10) J. A. Kerr, *Chem. Rev.*, **66**, 465 (1966).
- (11) "Tables of Biomolecular Reactions", *Natl. Stand. Ref. Data Ser., Natl. Bur. Stand.*, **No. 9** (1967).

COMMUNICATIONS TO THE EDITOR

Evidence for Superficial Reduction of NH₄Y Zeolite Silicon upon Pyridine Adsorption at 150 °C

Sir: A number of studies of zeolites by x-ray photoelectron spectroscopy (XPS) have recently been published,¹⁻⁴ but none so far has been concerned with adsorption phenomena of organic bases by zeolites. In particular, this problem constitutes a very interesting field to explore the potentialities of XPS for the characterization of surface acidity, a problem of major interest in catalysis. Some preliminary results⁵ have shown that the position of the N_{1s} line of aniline adsorbed at room temperature depends on the activation temperature. It seemed interesting, therefore, to investigate this problem further by using other substances, e.g.,

pyridine. In infrared spectroscopy studies especially, the adsorption of pyridine has very often been carried out at 150 °C to prevent physisorption of the adsorbing molecule. For the sake of comparison, we have conducted some experiments involving the adsorption of pyridine at 150 °C. We report here the results obtained in this case. An unexpected experimental result brings a new complication in the study of surface acidity by XPS of adsorbed probe molecules.

The procedure includes an outgassing of the NH₄Y zeolite (Union Carbide no. 3606-385, Si/Al molar ratio: 2.2, exchange level: 72%) up to 300 °C at a very slow rate (<100 °C h⁻¹) under 10⁻⁵ to 10⁻⁶ Torr; the final temperature is maintained for another 5 h before cooling the sample to 150

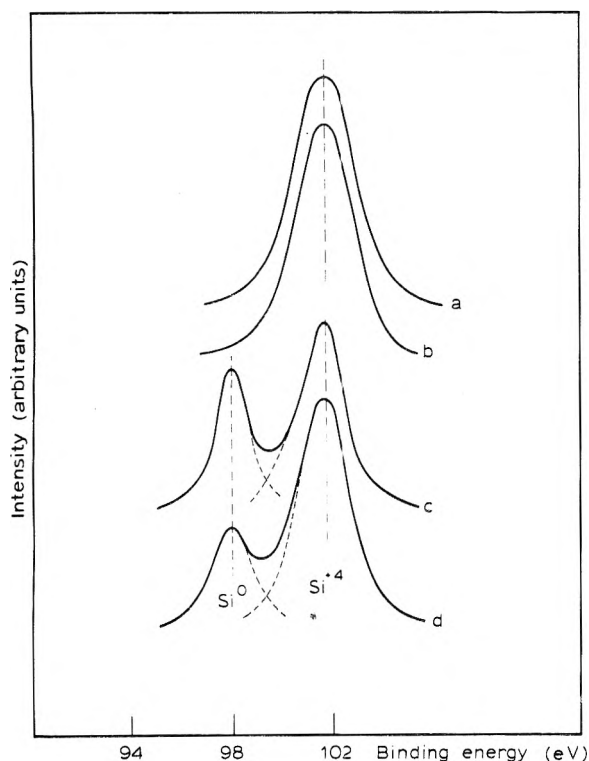


Figure 1. Si $2p_{1/2,3/2}$ profiles for NH_4Y zeolite activated at 300°C : (a) with no pyridine adsorption; (b) upon pyridine adsorption at room temperature; (c) upon pyridine adsorption at 150°C ; (d) upon ethylene adsorption at 150°C . The signal/noise ratio is $\sim 30/1$. Reference C_{1s} has a BE value of 283.5 eV .

$^\circ\text{C}$. Pyridine (distilled, outgassed thoroughly, and stored on a 5 \AA molecular sieve) is admitted under its own vapor pressure at room temperature for 0.5 h. After a further outgassing at the adsorption temperature, the sample is sealed off and kept in liquid nitrogen overnight. The cell is broken inside a drybox hermetically connected to the sample preparation chamber of a Vacuum Generators ESCA 2, and the powder is sprinkled on a polished gold backing.

Figure 1 shows the Si $2p_{1/2,3/2}$ profiles for different samples. In all cases, the probe is maintained at -50°C to minimize the carbon contamination of the surface.⁶ From these spectra, it is clear that a second Si $2p_{1/2,3/2}$ line appears after adsorption of pyridine at 150°C (c), which neither exists for the simply outgassed zeolite (a) nor for the sample exposed to pyridine at room temperature (b). Moreover, if the zeolite exposed to pyridine at room temperature is slowly outgassed further at 150°C for 1 h, the Si $2p_{1/2,3/2}$ line of higher binding energy (BE) is unique (similar to (b), not shown). Therefore it is concluded that the adsorption at 150°C is a necessary condition for the apparition of the second silicon species shifted to lower binding energies with respect to the position of the Si $2p_{1/2,3/2}$ line obtained in cases a and b. A similar experiment using C_2H_4 instead of $\text{C}_5\text{H}_5\text{N}$ gives the same result (d), except for the intensity ratio. Thus, the new species cannot be attributed to a specific interaction between pyridine and the zeolite, nor to a phenomenon induced by x-ray bombardment under vacuum, since it is not observed in cases a and b. The separation in two lines cannot be attributed to a charging effect because only the silicon XPS spectrum is modified by adsorption. Neither the Al_{2s} nor the O_{1s} lines are splitted by exposure to organic molecules.

The peak separation is nearly 4 eV , similar to the difference in binding energy between silicon in quartz and elemental silicon.^{7,8} We therefore conclude that some elemental silicon (Si^0) has been formed on the external zeolitic surface. This effect would be similar, although involving a much more surprising reduction (i.e., that of silicon), to those observed when adsorbing various hydrocarbon vapors on other oxides (e.g., Bi_2O_3).⁹

The difference in binding energy between the two peaks is too large for ascribing the left-hand side peak to some only partially reduced silicon. The hypothesis that some Si^0 is formed on the surface is also consistent with the fact that water exposure inside the preparation chamber of the machine followed by subsequent analysis leads to the observation of a third silicon species situated at -2.7 eV relative to the original position. This new peak may correspond to a partially reoxidized silicon. This fact rules out the possible explanation of the Si $2p$ line splitting by formation of a superficial silicon carbide because if Si C species were present at the surface, they would be more stable and would probably not react with H_2O . Moreover, it is difficult to admit a relaxation effect as an alternative explanation; this would assume a strong shielding of the Si atoms that would also very likely affect the O_{1s} and Al_{2s} line shape. Moreover the C/Si intensity ratios for samples c and d do not seem to be enhanced with respect to that of samples a and b. Nevertheless, because of the existence of a carbon contamination overlayer, their precision is not sufficient to rule out definitely this last hypothesis.

In spite of the possible interference of other contaminating gases, and the subsequent difficulties of correlating with certainty the decrease of the line attributed to Si^0 with the presence of a small amount of oxidizing gases, control experiments indicate that the latter line disappears in the presence of traces of O_2 . In addition, the line attributed to Si^0 tends to disappear over long periods of x-ray exposure at room temperature, probably by a diffusion into the bulk. Nevertheless, a possible reoxidation because of the poor quality of the vacuum cannot be excluded. This fact would reinforce the "surface" character of the reduced silicon. In view of this surface character, the reduction of the silicon atoms may only affect the very thin amorphous gangue surrounding the crystallites of the zeolite which may be mainly constituted of silica, as it has been shown by XPS that the superficial composition of this material is twice as rich in silicon atoms as the mass composition.^{4,10}

The results reported above suggest that previous studies on pyridine adsorption at 150°C on NH_4Y zeolites should be reexamined with consideration of our findings. Our results show that a strong reduction of the near surface atoms can occur. It is difficult to discern to which extent this sort of effect could modify the acidic properties of the surface. Moreover, we think that most methods are not sensitive enough to be perturbed by the effect which we have detected.

References and Notes

- W. N. Delgass, T. R. Hughes, and C. S. Fadley, *Catal. Rev.*, **4**, 179 (1970).
- Kh. M. Minachev, G. V. Antoshin, E. S. Shpiro, and T. A. Navruzov, *Izv. Akad. Nauk. SSSR Otd. Khim. Nauk.*, 2131 (1973).
- Kh. M. Minachev, G. V. Antoshin, E. S. Shpiro, and T. A. Navruzov, *Izv. Akad. Nauk. SSSR Otd. Khim. Nauk.*, 2134 (1973).
- J. F. Tempere, D. Delafosse, and J. P. Contour, *Chem. Phys. Lett.*, **33**, 95 (1975).
- C. Defosse and P. Canesson, *React. Kinet. Catal. Lett.*, **3**, 161 (1975).
- C. Defosse, R. M. Friedman, and J. J. Fripiat, *Bull. Soc. Chim. Fr.*, 1513 (1975).

- (7) R. Norberg, H. Brecht, R. G. Albridge, A. Fahlman, and J. R. Van Wazer, *Inorg. Chem.*, **9**, 2469 (1970).
(8) G. Hollinger and Tran Minh Duc, *Actual. Chim.*, **9**, 15 (1975).
(9) F. E. Massoth and D. A. Scarpiello, *J. Catal.*, **21**, 225 (1971).
(10) C. Defosse and P. Canesson, *J. Chem. Soc., Faraday Trans. 1*, submitted for publication.
(11) Aspirant du Fonds National de la Recherche Scientifique (Belgium).

*Groupe de Physico-Chimie
Minérale et de Catalyse
Université Catholique de Louvain
Louvain-la-neuve, Belgium*

C. Defossé¹¹
P. Canesson*
B. Delmon

Received November 21, 1975

PHYSICAL PHENOMENA

spectroscopy,
thermodynamics,
reaction kinetics,
and other areas
of experimental
and theoretical
physical chemistry
are covered
completely in

THE JOURNAL OF PHYSICAL CHEMISTRY

The biweekly JOURNAL OF PHYSICAL CHEMISTRY includes over 25 papers an issue of original research by many of the world's leading physical chemists. Articles, communications, and symposia cover new concepts, techniques, and interpretations. A "must" for those working in the field or interested in it, the JOURNAL OF PHYSICAL CHEMISTRY is essential for keeping current on this fast moving discipline. Complete and mail the coupon now to start your subscription to this important publication.

**The Journal of Physical Chemistry
American Chemical Society**

1976

1155 Sixteenth Street, N.W.
Washington, D.C. 20036

Yes, I would like to receive the JOURNAL OF PHYSICAL CHEMISTRY at the one-year rate checked below:

	U.S.	Canada**	Latin America**	Other Nations**
ACS Member One-Year Rate*	<input type="checkbox"/> \$24.00	<input type="checkbox"/> \$30.25	<input type="checkbox"/> \$29.75	<input type="checkbox"/> \$30.25
Nonmember	<input type="checkbox"/> \$96.00	<input type="checkbox"/> \$102.25	<input type="checkbox"/> \$101.75	<input type="checkbox"/> \$102.25

Bill me Bill company Payment enclosed

Air freight rates available on request.

Name _____

Street _____

Home
Business

City _____

State _____

Zip _____

Journal subscriptions start January '76

*NOTE: Subscriptions at ACS member rates are for personal use only. **Payment must be made in U.S. currency, by international money order, UNESCO coupons, U.S. bank draft, or order through your book dealer.

Tape Cassettes From The American Chemical Society Famous Scientists

ENERGY

- Energy & Industry**
A Waterland
Energy & Environment
Dr. S. Manahan
- Energy on the Shelf**
Dr. F. Kelhammer
H₂ and You
Dr. D. Gregory
- Green-Thumb Energy**
Dr. D. Klass
- Methane from Coalbeds**
Dr. R. Stefanek
- The Promise of Hydrogen**
Jack Russell
- Optical Communications**
J. Cook, B. DeLoach, A. D. Pearson
- Energy in the Future**
Dr. Paul Donovan
- Solar Homes for the Future**
- Coal's New Face**
Dr. Bernard Lee
- More Power, Less Pollution**
Dr. Daniel Benistock
- Cleaning A Dirty Fuel**
H. Feldman
From Wastes to Energy
Dr. Feldman
- Energy: A Critique**
Dr. Dean Abrahamson
- Puzzles of Air Pollution**
Arthur Levy
- Fusion: Prospects & Pitfalls—I**
Dr. H. Furth & Dr. H. Finsen
- Fusion: Prospects & Pitfalls—II**
Dr. H. Furth & Dr. H. Finsen
- Antidote to the Energy Crisis**
George Long
- Chemicals in the Environment**
Dr. Samuel Epstein
- Fusion and Fission: An Appraisal**
Dr. James L. Tuck
- The Prospects for Energy**
Dr. M. King Hubert

ENVIRONMENT

- The Spray Can Threat**
Dr. F. S. Rowland
- The Invisible Enemy**
Dr. R. Stewart
- Cities & Weather—I**
Dr. R. Brahm
- Cities & Weather—II**
Dr. R. Brahm
- Pure Oxygen for Polluted Water**
Dr. Jack McWhirter
- Mercury: Another Look—Part I**
Dr. John Wood
- Mercury: Another Look—Part II**
Dr. John Wood & D. G. Langley
- The Troubles with Water**
Dr. Daniel Okun
- Pure Oxygen for Polluted Water**
Dr. Jack McWhirter

CANCER RESEARCH

- Cancer & the Cell Membrane**
Dr. R. Barnett
- Interferon: From Colds to Cancer**
Dr. S. Baron
- Cancer & Chemicals—I**
Dr. Charles Heidelberger
- Cancer & Chemicals—II**
Dr. Charles Heidelberger
- Screening for Cancer Agents**
Dr. Bruce Ames
- Narcotics & the Brain**
Dr. Avram Goldstein
- Chemicals Combating Cancer**
Dr. David Grassetti
- Chemical Essence of Beer & Ale**
Dr. Rao Palamand
- Cancer Research I—Perspective & Progress**
Dr. Frank Rauscher
- Cancer Research II—Viruses**
Dr. R. Gallo & Dr. G. Todaro
- Cancer Research III—Chemotherapy**
Dr. C. Gordon Zubrod
- Cancer Research IV—Immunology**
Dr. Paul Levine
- Cancer Research V—Environmental Agents**
Dr. Umberto Saffiotti
- Cancer Research VI—NCI Roundtable**

BIO-MEDICAL

- Fighting Fat**
Dr. J. J. Marshall
- Tackling Tooth Decay**
Dr. J. Cassel
- Progress Against Diabetes**
Dr. D. Steiner
- The Sickie Cell Problem**
Dr. R. Jackson
- A New Look at Stroke**
Dr. R. Wurtman
- Chemical Look at Mental Illness**
Dr. S. Kety
- Nutrition & the Brain**
Dr. J. Fernstrom
- The Forgotten Nutrient**
Dr. J. Scala
- Remodeling the Body**
Dr. S. Carr
- Nuclear Medicine**
Dr. W. Wolf
- Putting Potatoes in Plastics**
Dr. Gerald Griffin
- Lead Poisoning in Children**
Dan Darrow
- New Look in Phosphorus Removal**
Dr. Gilbert Levin
- A Solution for Metals**
Thomas Chapman
- Turning Insects Against Themselves**
Daniel Lazare
- Updating Aluminum**
Dr. Allen Russell
- Energy and Environmental Thrift**
Dr. S. Berry
- Tracing the Skeleton's Image**
Dr. T. Raby
- Seafood From Waste**
J. Huguinin
- Underwater World of Communications**
Dr. J. Atema
- Water Supply of The Future**
Dr. J. Kugelmeier
- The Secrets of Salmon**
Dr. A. Hasler
- Cleaner Water Through Chemistry**
D. Parker
- Bromine Chloride: A Better Disinfectant**
Dr. J. Mills
- The Damaged Air—I**
- The Damaged Air—II**
- How Smells Shape Up**
Dr. John Amore
- Urban Auto Design**
- Tough Filaments of Fragile Liquid**
James Bacon
- Electricity from Rooftops**
Dr. Charles Backus
- The Struggle for Clean Water—I**
- The Struggle for Clean Water—II**
- The Oil Mystery**
Harold Bernard
- The Language of Odors**
Dr. Stanley Freeman
- The Lonely Atom**
Dr. Philip Skell
- How Green The Revolution**
Lester Brown
- Mercury: Another Look—Part I**
Dr. John Wood
- Mercury: Another Look—Part II**
Dr. John Wood & D. G. Langley
- The Troubles with Water**
Dr. Daniel Okun
- Pure Oxygen for Polluted Water**
Dr. Jack McWhirter

- Monitoring High Risk Pregnancies**
Dr. G. Sties & J. Hobbins
- Progress in Enzyme Replacement Therapy**
Dr. Roscoe Brady
- Safety for Premature Infants**
Dr. John Morrison
- Help for the Critically Ill**
Dr. Joseph Moilan
- Pinpointing Hepatitis Viruses**
Dr. Robert Purcell
- New Key to Heart Disease**
Dr. Antonio Gotto
- Nature's Own Toxicants in Foods Added, Not Intended**
Dr. H. Kraybill
- Seventy-Two Per Minute—I**
- Seventy-Two Per Minute—II**
Dr. L. Harmonson
- Two Drugs, More or Less**
Dr. K. Hussar
- Filling the Molar Gap**
Dr. J. Cassel
- A Tilt at Genetic Ills**
V. Apostian
- Binding the Catalysts of Life**
Dr. H. Garlinkel
- Early Prenatal Diagnosis of Genetic Disease**
Dr. M. J. Moss
- From Mother to Child**
Dr. M. Horning & Dr. R. Hill
- Insulin & Diabetes—I**
Dr. George Cahill
- Insulin & Diabetes—II**
Dr. George Cahill
- Stalking the Molecules of Memory**
Dr. Leslie Iverson
- Immunotherapy**
Dr. Kenneth Bagshawe
- Engineering Enzymes**
Dr. Victor Edwards
- Drugs, Plasticizers, & Mass Spec**
Dr. G. W. A. Milne
- Birth Control: Problems & Prospects**
Dr. Carl Diergass
- Hormones, Terpenes, & the German Air Force**
Dr. A. J. Birch
- Prospects for Implants**
Dr. Donald Lyman
- New Dimensions for Polymers**
Dr. Alan Michaels
- Fabricating Life**
An Essay Report
- New Ways to Better Food**
Dr. R. W. F. Hardy
- Chemistry of the Mind: Schizophrenia**
Dr. Larry Stein
- Chemistry of the Mind: Depression**
Dr. Joel Elkes
- The Molecules of Memory**
Dr. W. L. Byrne & Dr. A. M. Golub
- The Master with Memory**
Dr. J. McGaugh

- Dissonant Harmony**
Dr. Denham Harman
- Why We Grow Old**
Dr. Howard Curtis
- New Materials for Spare Parts**
Dr. V. Gott & Dr. A. Rubin
- Against Individuality**
Dr. R. Reisfeld & Dr. B. Kahan
- A Richness of Lipids**
Dr. Roscoe O. Brady
- Life: Origins to Quality**
Dr. Stanley Miller
- The Nitrogen Fixer**
Dr. Eugene van Tamelen
- Prostaglandins: A Potent Future**
Dr. E. J. Corey & Dr. S. Bergstrom
- Chemical Evolution**
Dr. Russell Doolittle
- An Evolving Engine**
Dr. R. E. Dickerson
- Dissonant Harmony**
Dr. Denham Harman
- Why We Grow Old**
Dr. Howard Curtis
- New Materials for Spare Parts**
Dr. V. Gott & Dr. A. Rubin
- Against Individuality**
Dr. R. Reisfeld & Dr. B. Kahan
- A Richness of Lipids**
Dr. Roscoe O. Brady
- Life: Origins to Quality**
Dr. Stanley Miller
- The Nitrogen Fixer**
Dr. Eugene van Tamelen
- Prostaglandins: A Potent Future**
Dr. E. J. Corey & Dr. S. Bergstrom
- Chemical Evolution**
Dr. Russell Doolittle
- An Evolving Engine**
Dr. R. E. Dickerson

- The View from Space**
Dr. R. Maddie & R. Anderson
- The Attraction of Magnets**
David Kelland
- Cosmic Ray Astronomy**
Dr. P. Meyer
- The Reactor Never Lies**
T. Raby
- Wine From Native American Grapes—I**
- Wine From Native American Grapes—II**
Dr. A. Rice
- Community Needs: New Emphasis in Research**
Dr. H. Guyford Stever
- Aspirin vs. Prostaglandins**
Dr. John Vane
- A Breakdown in Plastics—I**
Drs. J. Guillet & G. Scott
- A Breakdown in Plastics—II**
Drs. J. Guillet & G. Scott
- Protein: The Next Big Production?**
Dr. Steven Tannenbaum
- Clean Energy: A One-Way Dream**
Dr. J. R. Eaton
- Nitrosamines: A Reappraisal**
Dr. Phillip Issenberg
- The Emperor of Ice Cream**
Dr. Wendell Atbuckle
- Ethics and Genetics**
Dr. Robert F. Murray
- The American Diet: A Critique**
Dr. Arnold Schaefer
- Probing Creation**
Dr. Myron A. Coler
- New Directions in U.S. Science**
Dr. William McEnroy
- Aspirins, Enzymes, & Fragrant Redheads**
An Essay Report
- Vitamin D: A New Dimension**
Dr. Hector DeLuca
- Engineering Microbes**
Dr. Elmer Gaden
- Liquid Crystals: A Bright Promise**
Dr. George Heilmeyer
- Lively Xenon**
Dr. Neil Bartlett
- The Repressor Hunt**
Dr. Mark Ptashne

NOBEL PRIZE WINNERS

- Dr. Linus Pauling**
The Committed Scientist
- Dr. Jacob Bronowski**
Science and Man
- Dr. Glenn Seaborg**
The Atomic World of Glenn Seaborg
- Dr. George Wald**
Vision, Night Blindness, & Professor Wald
- Dr. Melvin Calvin**
The Search for Significance—Parts I & II

SCIENCE

- Tagging the Oceans**
Dr. O. Roels
- Davy Jones' Treasure**
Dr. S. Gerard
- The Need for Nitrogen**
Dr. R. Hardy
- Modifying Milk for Millions**
A. Rand & J. Hourigan
- The Seas in Motion**
Dr. Wallace Broecker
- Rumbles in the Earth**
Dr. Christopher Scholz
- Tagging the Oceans**
Dr. O. Roels
- Davy Jones' Treasure**
Dr. S. Gerard
- The Need for Nitrogen**
Dr. R. Hardy
- Modifying Milk for Millions**
A. Rand & J. Hourigan
- The Seas in Motion**
Dr. Wallace Broecker
- Rumbles in the Earth**
Dr. Christopher Scholz

ACS Members Nonmembers
Single cassette \$5.95 \$6.95
Any Eight cassettes \$4.95/cassette \$5.95/cassette
Any 20 or more cassettes to one address \$4.00/cassette
10% Discount if payment accompanies order

Name _____ Address _____
City _____ State _____ Zip _____
Order from: American Chemical Society, Dept. SH
1155 16th St., N.W., Wash., D.C. 20036
Allow 4 to 6 weeks for delivery